UNIVERSITY OF SANTIAGO DE COMPOSTELA

SCHOOL OF ENGINEERING

Department of Chemical Engineering

ABSORPTION OF CARBON DIOXIDE IN IONIC LIQUIDS AND THEIR MIXTURES

A thesis submitted by ALICIA M. PINTO CASTILLO for the degree of Doctor in Chemical and Environmental Engineering to the University of Santiago de Compostela

Santiago de Compostela, November 2013

Authorisation for submission by the thesis directors (in Galician)

Alberto Arce Arce e **Ana M. Soto Campos**, Catedráticos de Enxeñería Química, e **Héctor Rodríguez Martínez**, Investigador 'Ramón y Cajal', todos eles pertencentes ó Departamento de Enxeñería Química da Universidade de Santiago de Compostela,

INFORMAN:

Que a presente memoria, titulada *"Absorption of carbon dioxide in ionic liquids and their mixtures"*, que para optar ó grao de Doutora en Enxeñería Química e Ambiental presenta **Alicia María Pinto Castillo**, foi realizada baixo a nosa inmediata dirección no Departamento de Enxeñería Química da Universidade de Santiago de Compostela.

Considerando que constitúe traballo de Tese, autorizan a súa presentación ao Centro de Posgrao da Universidade de Santiago de Compostela.

E para que así conste, asinan o presente informe en Santiago de Compostela, a 2 de diciembre de 2013.

Alberto Arce Arce Ana M. Soto Campos Héctor Rodríguez Martínez

A mis padres Alfonso y Verónica,
mi hermano Alfonso y
mi abuela querida

Abstract

The potential application of some ionic liquids and of binary mixtures of them as absorbents for CO_2 has been investigated.

The CO_2 absorption capacity of these solvents has been experimentally determined in the low pressure range. Several mixtures of two CO_2-physisorbing ionic liquids, and of a CO_2-physisorbing ionic liquid with a CO_2-chemisorbing ionic liquid, have been analysed. Although their absorption capacities generally lie within those of the corresponding pure ionic liquids, different synergistic effects have been found. These effects are accompanied by the tuning of thermal behaviour and physical properties with variation of the composition of the mixtures. The results are discussed in terms of the mechanisms of absorption and the influence of the structural features of the ionic liquids. Suitable correlations of the experimental data for both the CO_2 absorption isotherms and the physical properties investigated (density, viscosity, and surface tension) have been carried out.

In a further aspect, the CO_2 absorption capacity of a highly viscous amino acid ionic liquid has been substantially improved, along with its thermal stability, by supporting it onto mesoporous silica.

Acknowledgements (in Spanish)

Todo el trabajo que se refleja en esta tesis ha sido un esfuerzo colectivo. Son muchas las personas e instituciones que, directa o indirectamente, me han ayudado en su desarrollo.

En primer lugar quiero agradecer al Ministerio de Asuntos Exteriores y Cooperación, quien a través de las Becas MAEC-AECID ha financiado el proceso para que todo esto se haya convertido en una realidad.

A mis directores de tesis, el profesor Alberto Arce, la profesora Ana Soto y el doctor Héctor Rodríguez, por haber confiado en mí, por su ayuda, por la motivación y todo el apoyo que me han entregado durante estos años. Especialmente porque me permitieron entrar en este pequeño grupo humano pero que es enorme en amistad, compañerismo y dedicación.

A los profesores Rasmus Fehrman y Anders Riisager, de la Universidad Técnica de Dinamarca (DTU), por haberme aceptado en su grupo de trabajo para la realización de mi estancia. Aunque fue corta en tiempo, fue una gran experiencia para mí pertenecer a su grupo.

A mis compañeros del laboratorio, los cuales hicieron mucho más agradables las horas de trabajo. Con su alegría y apoyo hicieron que mi estadía aquí se transformase en un recuerdo imborrable que me mantendrá eternamente unida a ustedes.

Debo hacer una mención especial a mis amigos Angélica, Lucia, Borja, Iago, Sara, Toño, Iria y David. Chicos, la verdad es que no sé cómo podré agradecerles todo este tiempo juntos. Han sido una parte muy importante de mi vida acá. Jamás podré olvidar todo lo que compartimos, las tonterías que hicimos, los consejos que me dieron, pero sobre todo nunca olvidaré lo querida y acogida que me hicieron sentir.

Y aunque todos mis amigos son importantes, hay una persona a la que siento que debo agradecer de forma particular. A mi amiga Dafne, tú sabes que sin ti probablemente esto nunca hubiese ocurrido. Gracias a ti por haberme arrastrado a tierras gallegas y haberme dado la oportunidad de vivir todo esto. Gracias por toda tu

paciencia, por cada palabra en el momento preciso, por tu compañía, pero sobre todo por formar parte de mi vida durante tantos años, tú sabes bien que más que mi amiga has sido como mi hermana.

Finalmente, y no por ello menos importante, me gustaría agradecer a mi familia. A mis padres Alfonso y Verónica, porque la distancia nunca ha sido un obstáculo para sentir su amor, su comprensión y su apoyo. Porque me han enseñado a ser fuerte y luchar cada día por lo que quiero, pero sobre todo porque sé que ustedes son y serán siempre el apoyo y la inspiración que necesito para construir mi vida. A mi hermano Alfonso por toda la preocupación y el interés que has puesto en mi carrera, aunque no te enteras de nada, y porque me demuestras cada día tu cariño y apoyo incondicional. Y finalmente a ti mi abuela querida porque tú fuiste la base de todo esto.

Contents

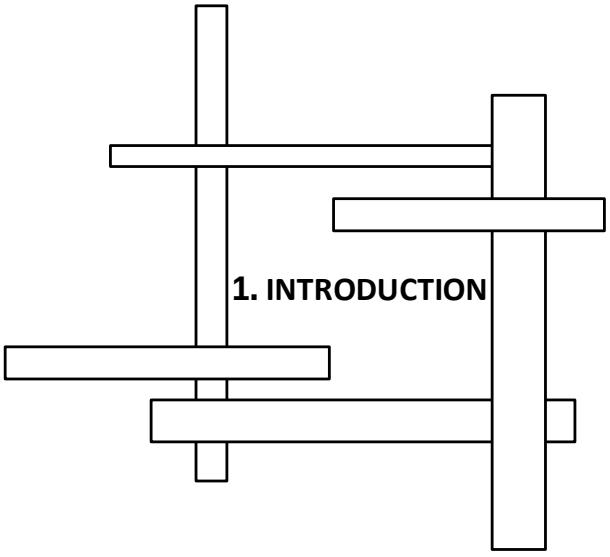

1. INTRODUCTION

1. INTRODUCTION

1.1 The problem of carbon dioxide emissions

The increase in emissions of greenhouse gases resulting from anthropogenic activities has become a global environmental concern in the last decades (Metz *et al*., 2005).

After the discovery of the ozone hole in Antarctica in late 1985, numerous treaties, conventions and institutions arose in order to curb the greenhouse gas emissions. That same year, 28 countries signed the "Vienna Convention" (United Nations Enviroment Programme, 1985). This was the first international treaty seeking protection of the ozone layer to avoid adverse effects on the health of people and the environment. This treaty laid the foundations for the "Montreal Protocol", signed two years later by 46 countries, and seeking a reduction in the consumption and production of chlorofluorocarbons according to the level of development of the economies of the countries (United Nations Enviroment Programme, 1987). The following year, at the request of the World Meteorological Organization and the United Nations Environment Programme, the Intergovernmental Panel on Climate Change (IPCC) was created. This group analyses the scientific, technical and socioeconomic information relevant to the risk of climate change caused by human activity, and it looks for ways of mitigating such change. In 1990 they presented their first report, which stated that the land atmospheric warming was real, so that the international community asked them to take effective measures to prevent it. This led governments to create, in 1992, the United Nations Framework Convention on Climate Change (UNFCCC), trying to stabilise the concentration of greenhouse gases and prevent climate change. From the second IPCC report (1995), UNFCCC began to develop the "Kyoto Protocol on climate change". This protocol was signed in 1997, but did not come into force until 2005, when it was ratified by 187 countries. Its main objective was to reduce, at least by 5 % (below the levels in 1990), the emissions of six greenhouse gases that cause global warming (namely carbon dioxide (CO_2), methane (CH_4), nitrous oxide (N_2O), hydrofluorocarbons (HFCs), perfluorocarbons (PFCs), and

sulfur hexafluoride (SF_6)) before the end of 2012 (Figure 1.1) (United Nations Framework Convention on Climate Change, 1997).

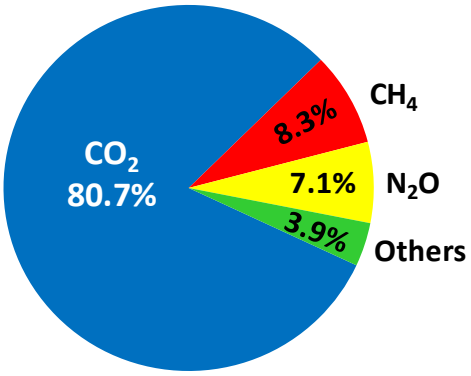

Figure 1.1: Proportional emissions of greenhouse gases to the atmosphere. Source: European environmental agency, web reference.

The European Union, as part of the UNFCCC, takes inventory of its emissions every year. In Figure 1.2 the latest data are shown. The decrease in total emissions between 1990 and 2011 was 18 %, of which 3 % was obtained in the last year (European Enviromental Agency, 2013). Undoubtedly, and as it can be seen in Figures 1.1 and 1.2, carbon dioxide is the main contributing gas to the total emissions.

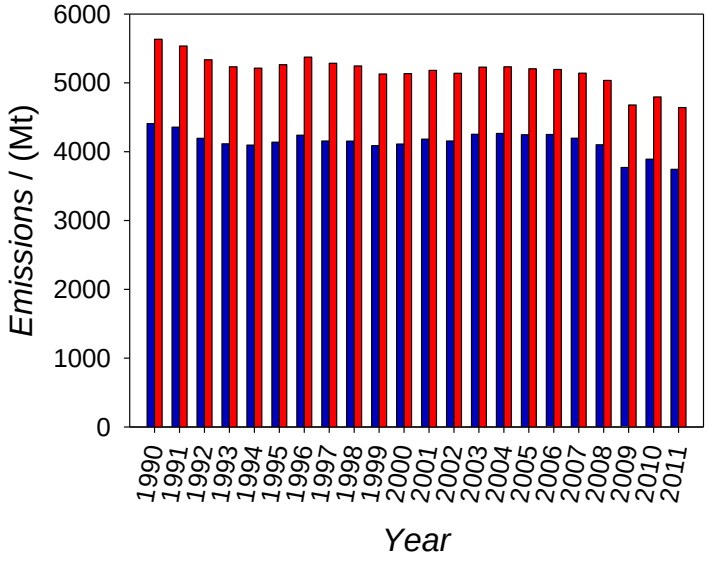

Figure 1.2: Evolution of greenhouse gas emissions in the European Union: carbon dioxide emissions (blue), and total greenhouse gas emissions (red). Source: European environmental agency, web reference.

Carbon dioxide (CO_2) is the main greenhouse gas, and its most important origin in anthropogenic activities is the combustion of fossil fuels for power generation (Figure 1.3) (Metz *et al*., 2005). A possible way to reduce its emissions is therefore the use of renewable energies. Although the latter are increasingly used, they are still far from being able to meet the whole world energy demand (Wall, 2007). It is known that none of the existing technologies, on their own, can reduce the emissions to the desired level. Thus, the development of new technologies, more economical and efficient, has become a focus of worldwide interest (Hasib-ur-Rahman *et al*., 2010). Among the alternatives to reduce the emission produced by fossil fuels, the following can be cited: improvement of the efficiency of the production plants, replacement of coal with gas, and improvement of the mechanisms for capture and storage of CO_2 (Metz *et al*., 2005; Wall, 2007). The increase of the process efficiency is certainly an inescapable target, but it is also true that good processes for CO_2 capture and storage are absolutely necessary in the present context.

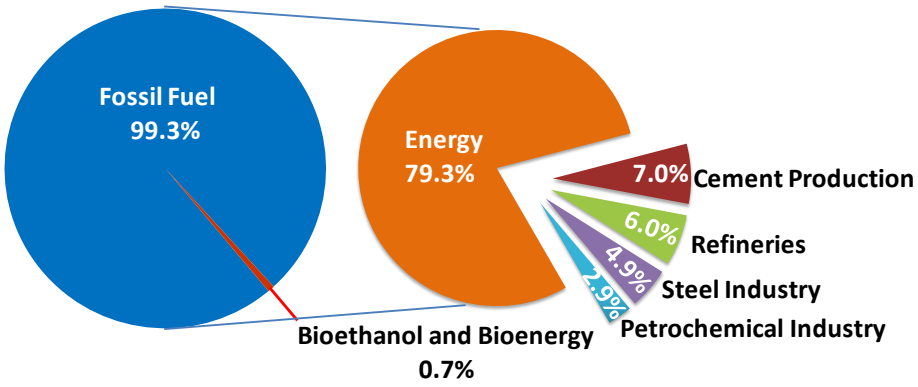

Figure 1.3: Distribution of annual CO_2 emissions from industrial activities with CO_2 production over 0.1 Mt/year (adapted from Metz *et al*., 2005).

1.2. Carbon dioxide absorption technologies

When developing a CO_2 capture process, several aspects must be taken into account: the possibility of using renewable chemicals, reliability of supply to avoid stockouts, and the increasing cost of raw materials (D'Alessandro *et al*., 2010). Furthermore, some physicochemical properties of CO_2 can help simplify the conception and design of the process (Freeman and Rhudy, 2007):

- It is a weak acid that can be absorbed by alkaline solvents.
- It can be adsorbed onto microporous structures and physical adsorbents.
- It may react with simple plants and be fixed as biomass.
- It can be removed via a freezing procedure.

The CO_2 produced in power generation plants is captured mainly through three different types of processes (Figueroa *et al.*, 2008): oxy-combustion, pre-combustion, and post-combustion (Figure 1.4).

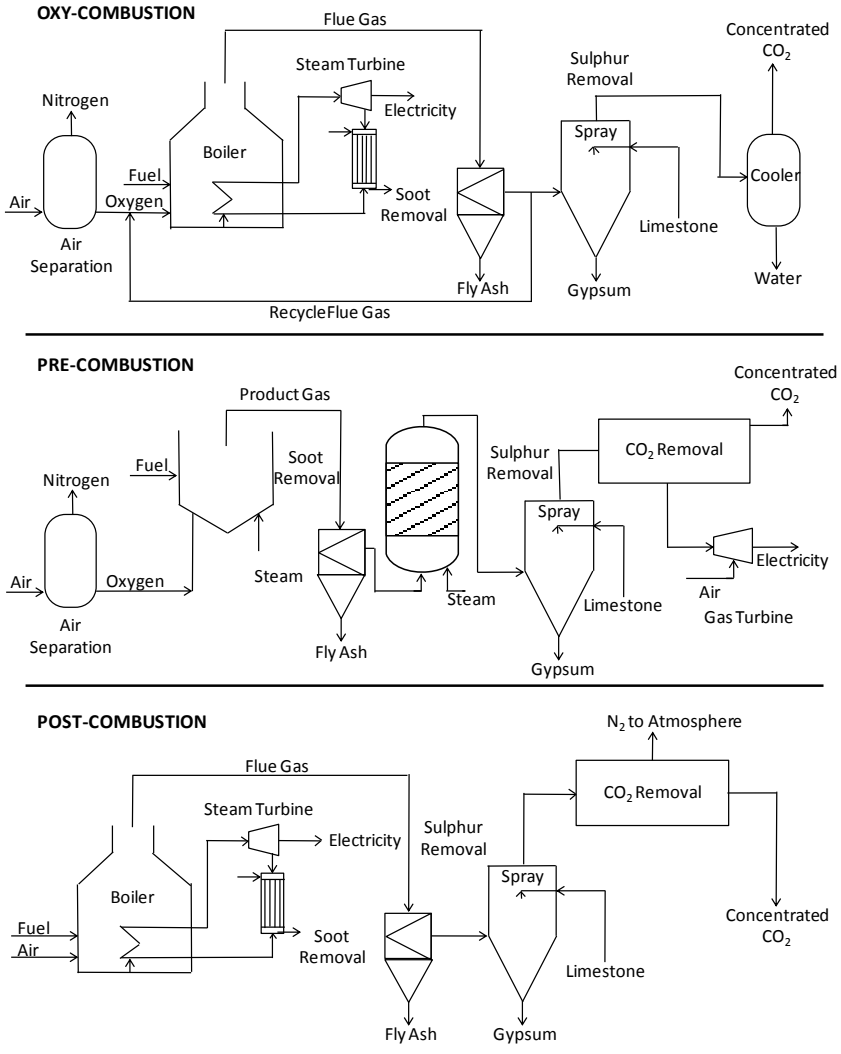

Figure 1.4: Carbon dioxide capture technologies (adapted from Figueroa *et al.*, 2008).

Oxy-combustion is the most widely used process in the glass industry. In this strategy, the fuel is burned with purified oxygen (O_2) mixed with recycled CO_2, coming from previous combustion (Wall, 2007). The flue gas (water and CO_2) is then cooled to condense and remove water, and to get the CO_2, that will be partially recycled (Ciferno *et al*., 2011).

Pre-combustion is a method applied in natural gas plants, where capture occurs at high pressures. The CO_2 is recovered from a stream before burning the fuel. In this process, the fuel is gasified in the presence of O_2 and water vapour to produce synthesis gas. This is a mixture of carbon monoxide and hydrogen (H_2), which is fed into a reactor where it is mixed with steam to produce H_2 and CO_2. The latter is recovered, and the H_2 is burned in a gas turbine to produce electricity and heat (Figueroa *et al*., 2008).

The post-combustion process is mainly applied to CO_2 produced in power stations from coal (Figueroa *et al*., 2008). Usually the flue gas is at atmospheric pressure, at high temperature, saturated with water vapour, and containing 15 % of CO_2, along with other gases (Table 1.1) (Freeman and Rhudy, 2007; D'Alessandro *et al*., 2010). Thus, a post-combustion process must be highly selective for CO_2 and should be able to perform at low pressures (Ramdin *et al*., 2012).

Table 1.1: Typical gas composition (in a mass basis) for post-combustion processes at 313-348 K and atmospheric pressure.

Compound	Composition
CO_2	10-15 %
H_2O	5-10 %
O_2	3-4 %
CO	20 ppm
N_2	70-75 %
NO_x	<800 ppm
SO_x	<500 ppm

The most commonly used post-combustion process is the absorption with aqueous amines. At industrial level, the most used amines for CO_2 removal are the primary amines monoethanolamina (MEA) and diglycolamine (DGA), the secondary

amines diethanolamine (DEA) and diisopropanolamine (DIPA), and the tertiary amines methyldiethanolamine (MDEA) and triethanolamine (TEA) (Kohl and Nielsen, 1997). The absorption is achieved by forcing the gas stream with the CO_2 to flow in countercurrent through the aqueous solution of amine, at about 40 °C (Huttenhuis *et al*., 2007). Primary and secondary amines react rapidly, with a 1:2 stoichiometry, through a zwitterion mechanism to form the corresponding carbamate (Figure 1.5). However, the high amount of energy required to revert the carbamate formation and recover the gas increases substantially the cost of the process (Vaidya and Kenig, 2007; D'Alessandro *et al*., 2010).

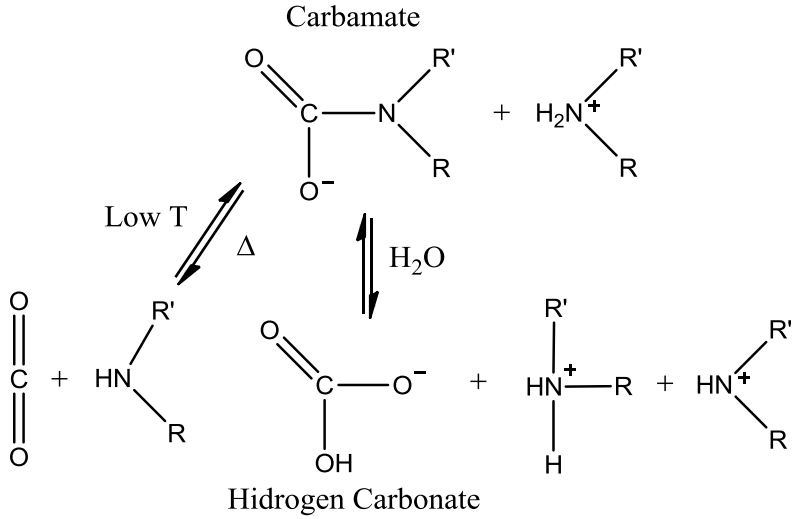

Figure 1.5: Reaction scheme for primary and secondary amines with CO_2.

In contrast to the above, tertiary amines have no hydrogen attached to their central nitrogen atom, so the reaction for formation of the carbamate cannot be carried out. The actual reaction occurring in this case is described as a base-catalysed hydration of CO_2, and consists of a hydrolysis reaction to form bicarbonate (Figure 1.6). It is known that these tertiary amines are less reactive towards CO_2 than the primary and secondary amines, but in turn they result in a better reaction stoichiometry (1:1). The energy required to break the bicarbonate bonds is less than that required for the carbamate, and therefore the costs associated with the regeneration step are also lower (Vaidya and Kenig, 2007; D'Alessandro *et al*., 2010).

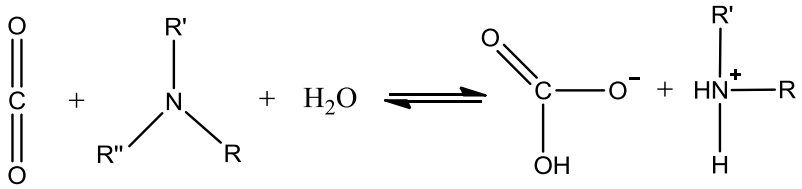

Figure 1.6: Reaction scheme for tertiary amines with CO_2.

In spite of representing the main state of the art, the use of these amine-based processes involves several important drawbacks:

- High operating costs due to the energy requirements of the desorption step (Rolker and Arlt, 2006).
- Amines are highly corrosive; so, their concentration in the aqueous solution has to be kept low. In addition, corrosion inhibitors must be used (Chinn *et al*., 2005; D'Alessandro *et al*., 2010).
- Amines are susceptible of undergoing thermal and chemical degradation.
- Due to their volatility, amines are partially lost during the process by evaporation, affecting the costs of the process and having a strong environmental impact assessment (Forsyth *et al*., 2004).

An emerging technology for post-combustion processes is based on the use of ionic liquids as absorbents (Figueroa *et al*., 2008). Ionic liquids are a family of substances that do typically have a good affinity for CO_2, and their appealing properties have made them a good alternative to replace volatile organic compounds used in some existing technologies (Seddon and Stark, 2007).

1.3. Ionic liquids

1.3.1. Context and definition

The growing concern about the impact of industrial processes on the environment has led scientists to seek, reduce or eliminate the use or generation of hazardous substances to human health and the environment. This involves a significant investment of time, money and effort, as well as a need to look for new products and processes more environmentally friendly. In this context, ionic liquids have attracted

great interest as a result of their characteristic set of properties and of the numerous choices that they offer.

Ionic liquids are generally formed by an inorganic or organic anion (Welton, 2004), and an organic, bulky, usually asymmetric cation, which may or may not have a cyclic structure to which alkyl chains of different lengths may be appended (Cadena *et al.,* 2004) (Figure 1.7). Strictly speaking from a lexical point of view, ionic liquid would be any substance formed by ions and in the liquid state. However, the current utilisation of the 'ionic liquid' term restricts its definition, with a quite general consensus, to organic salts or eutectic mixtures between organic and inorganic salts with a melting point lower than 373 K (Freemantle, 2010).

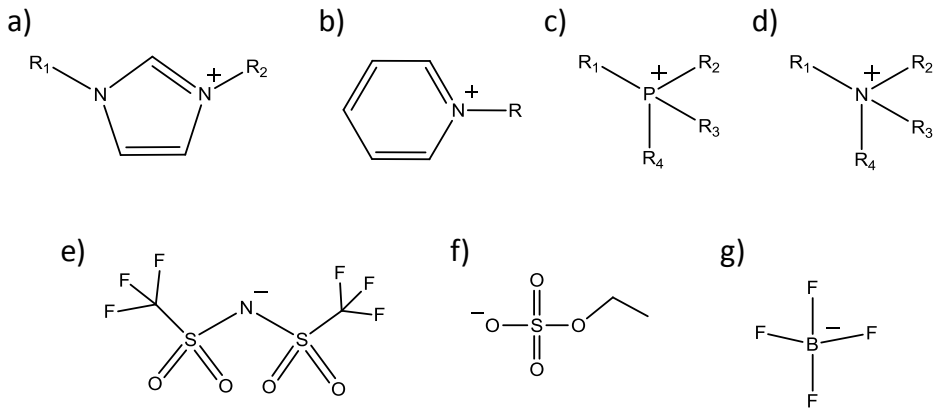

Figure 1.7: Some representative constituent cations and anions of ionic liquids ("R_1", "R_2", "R_3" and "R_4" represent linear or substituted alkyl chains, with our without functional groups). Cations: a) 1,3-dialkylimidazolium, b) 1-alkylpyridinium, c) tetraalkylphosphonium, d) tetraalkylammonium. Anions: e) bis(trifluoromethylsulfonyl)amide, f) ethylsulfate; g) tetrafluoroborate.

A 'first generation' of ionic liquids consisted of bulky cations (1,3-dialkylimidazolium, 1-alkylpyridinium...) and anions mainly based on haloaluminates. These ionic liquids have an easily tunable Lewis acidity, but they are highly sensitive to water or even environmental humidity (Seddon and Stark, 2007), which is a killing flaw for many purposes. This issue was overcome by the development, in the last decade of the 20th century, of a 'second generation' of ionic liquids, more stable to air and water (Wilkes and Zaworotko, 1992). At the same time, these ionic liquids have provided a basis for the further development of ionic liquids functionalised for use in specific applications, constituting a 'third generation' of ionic liquids (Seddon and Stark, 2007).

1.3.2. Features and properties

The properties of ionic liquids are obviously dependent on their constitutive ions. The wide variety of possible cation-anion combinations enables the 'tailoring' of ionic liquids for a specific application purpose. Together with a series of appealing properties for their use as solvents, this has led to the coinage of the term "designer solvents" (Freemantle, 1998). In fact, Holbrey and Seddon (1999) estimated that about one million combinations of cation and anion could give rise to an ionic liquid.

As a result of this tunability, there exists a wide variation of properties in ionic liquids. For example, they may be acidic, basic or neutral; they can be hydrophilic or hydrophobic; they have different degrees of toxicity and stability; etc. (Freemantle, 2010). The most attractive single property is probably their extremely low volatility under normal operation conditions. Thus, the ionic liquid can be easily recovered by evaporation of the volatile substances mixed with it; it increases the safety of the working environment due to the absence of flammable vapours; and it can also improve the environmental friendliness of a process by avoiding the release of vapours to the atmosphere.

Regarding thermophysical properties, density is the most investigated one in ionic liquids, and is a critical piece of information for the appropriate design of most processes. In the literature, most of the data available correspond to ionic liquids containing an imidazolium cation, reporting values generally in the range 1.0-1.6 $g \cdot cm^{-3}$ (Marsh *et al*., 2004; Freemantle, 2010). Nevertheless, there are denser and less dense ionic liquids; for example, some phosphonium ionic liquids have been reported with a density lower than that of water (Kilaru *et al*., 2007).

Other important property is the viscosity. In general, the viscosity of ionic liquids depends on Van der Waals forces and hydrogen bonds present in the ionic liquid (Bônhote *et al*., 1996), and is typically higher (even by some order of magnitude) than in molecular solvents (Mantz and Trulove, 2008; Marsh *et al*., 2004). Although many of them behave as Newtonian fluids, ionic liquids with long alkyl chains tend to behave as non-Newtonian (Huddleston *et al*., 2001; Jacquemin *et al*., 2006; Seddon and Stark, 2007).

The surface tension is a property scarcely investigated in ionic liquids, but critical in the design of many operation units. In general, the surface tension of ionic

liquids is lower than for water and other inorganic salt melts, but higher or close to the values of other organic liquids (Martino *et al*., 2006; Freemantle, 2010). Its magnitude is governed by interactions between the ions present (Freire *et al*., 2007).

Thermal stability conditions the applicability of an ionic liquid to a process (Freemantle, 2010). The maximum temperature limit which can be used, as a result of the practically negligible vapour pressure of ionic liquids, is given by their decomposition temperature (Huddleston *et al*., 2001; Holbrey and Rogers, 2008). The thermal stability of ionic liquids is limited by the strength of their heteroatom-carbon and heteroatom-hydrogen bond (Wasserchеid and Keim, 2000). At the other end of the commonly wide liquid range of ionic liquids is the melting (or crystallisation) temperature (Seddon and Stark, 2007), which is the minimum recommended for operation in a process if solidification of the ionic liquid is to be avoided. The thermal behaviour of ionic liquids in this regard is complex: solidification kinetics is slow, and the ionic liquid can crystallise or can form a glass (below its glass transition temperature) (Easteal and Angell, 1970; Seddon and Stark, 2007).

1.3.3. Mixtures of ionic liquids

The ability to 'design' an ionic liquid for a specific application is a great advantage for application at industrial level. However, sometimes an ion pair will not be sufficient to obtain the optimal fluid properties for the target application. In this case, an alternative to expand the range of property sets achievable is the use of mixtures of ionic liquids (Canongia Lopes *et al*., 2005; Navia *et al*., 2007; Niedermeyer *et al*., 2012). Mixtures of two 'pure' ionic liquids, for example, can have up to four different ions, or can be made with two ionic liquids with common cation or with common anion. In any of the cases, there will be extra interactions among the ions, as compared to the case of a 'pure' ionic liquid with just a single type of cation and a single type of anion; and this will result in new properties for the mixture, that are not observable when using any of the 'pure' ionic liquids that constitute it (Aparicio and Antilhan, 2012).

The available literature on mixtures of ionic liquids focuses mainly on the study of their properties, in particular as a function of the composition of the mixtures, to see if these are behaving or not as an ideal solution. In properties such as molar volume, which is related to the chemical potential, this ideal behaviour would

correspond to a linear variation with composition (Niedermeyer *et al*., 2012). In mixtures of ionic liquids with common or similar ions, a behaviour close to ideal could be observed (Aparicio and Antilhan, 2012; Niedermeyer *et al*., 2012). However, more complex behaviours are also possible, with important deviations from the ideal one. Nonetheless, studies are inconclusive as to the magnitude and direction to which the deviations are produced (Canongia Lopes *et al*., 2005; Navia *et al*., 2007). In those cases with behaviour close to ideal, properties such as density and viscosity of the mixtures of ionic liquids have been fairly well predicted through mixing rules as a first approximation (Canongia Lopes *et al*., 2005; Niedermeyer *et al*., 2012). On the contrary, prediction of the properties of the mixture from the properties of the constituent 'pure' ionic liquids becomes more challenging in the case of mixtures with large difference in ion sizes (and less ideal behaviour) (Canongia Lopes *et al*., 2005),

With the increase of studies performed on the behaviour of the mixtures, there is also a growing number of applications for which they are proposed. Most uses correspond to their utilisation as improved solvents for chemical synthesis, as in the improved Difasol™ process (Chauvin *et al*., 1995; Niedermeyer *et al*., 2012), in the production of highly valuable chemicals from cellulose (Long *et al*., 2011), or in the esterification catalysed by glucose lipase (Lee *et al*., 2008). However, mixtures of ionic liquids have also been proposed for other potential applications; for example as electrolytes in batteries (Sugimoto *et al*., 2008, 2009), as stationary phase in gas chromatography (Baltazar *et al*., 2008), or as heat transfer and energy storage fluids in solar energy applications (Raade and Padowitz, 2011).

1.3.4. Supported ionic liquid phases (SILPs)

A supported ionic liquid phase (SILP) consists of an ionic liquid immobilised on a solid support with high surface area (Figure 1.8). In this way, a combination of advantages of ionic liquids and of heterogeneous support materials is possible (Valkenberg *et al*., 2002). The immobilisation can be carried out via either the cation or the anion of the ionic liquid, and the SILP may be prepared by different procedures according to the interaction intended to occur between the ionic liquid and the support (Valkenberg *et al*., 2002; Mehnert, 2005). Two main general strategies have been described (Mehnert, 2005; Riisager *et al*., 2006): a first one in which the ionic liquid is covalently bound to the support; and a second one in which the ionic liquid is just deposited on

the support. Some of the supports used are: zirconium dioxide (ZrO_2), titanium oxide (TiO_2), silica (SiO_2), alumina (Al_2O_3), etc., which will have different ability to act as supports depending on the specific characteristics of the ionic liquid (Menhert, 2005).

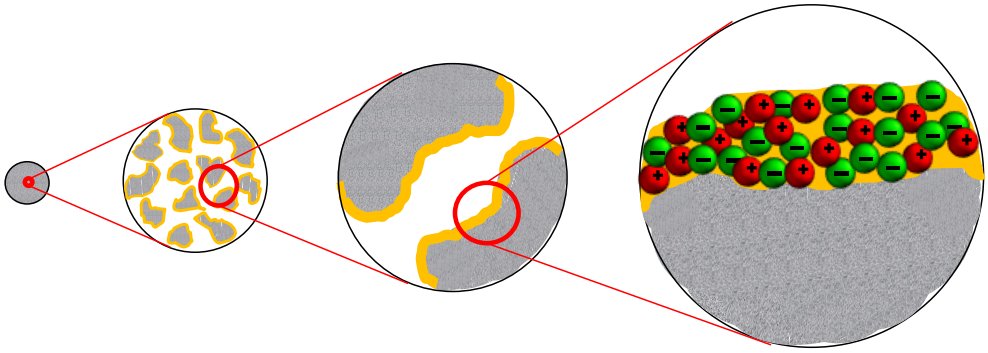

Figure 1.8: Scheme of a SILP (adapted from Riisager *et al.*, 2006).

An example that can be taken as a precursor of the concept of SILP was reported by Rao and Datta (1988). This was a eutectic mixture of palladium chloride with copper chloride supported on silica, to investigate its application in the partial oxidation of olefin. Although the result was not as expected, it was the basis for further research. The SILP term was coined 15 years later, derived from studies by Riisager *et al*. (2003) on the application of ionic liquids in catalysis. Indeed, the main application investigated to date for SILPs has been catalysis in chemical reactions (Riisager *et al*., 2003, 2005, 2006; Menhert *et al*., 2005; Virtanen *et al*., 2009; Werner *et al*., 2010), in particular with regard to the possibility of utilising fixed bed reactors (Mehnert, 2005; Riisager *et al*., 2005; Haumann and Riisager, 2008). Other potential applications of SILPs relate to separations (Riisager *et al.*, 2006). Although an important body of research has been carried out, some issues still remain; for example, their long-term stability and their recyclability (Selvam *et al*., 2012).

1.4. Carbon dioxide solubility in ionic liquids

The first studies involving ionic liquids and carbon dioxide were conducted by Blanchard *et al*. (1999), who used supercritical CO_2 to extract non-volatile organic compounds dissolved in an ionic liquid, without cross-contamination due to the non-solubilisation of the ionic liquid in the CO_2. Furthermore, the absorbed gas could be

fully recovered by simply lowering the pressure. Following this seminal paper, an increasing interest evolved on the connection between CO_2 and ionic liquids, giving rise to many studies on solubility, selectivity, interactions, etc.

It has been shown that the CO_2 absorption capacity of ionic liquids is superior to that of other organic compounds, although it typically remains below those obtained with solvents such as amines (Wilhelm and Battino, 1973; Bermejo and Martin, 2011). Interestingly, the solubility of CO_2 in ionic liquids is much higher than that of other gases such as ethylene, ethane, methane, oxygen, etc. (Anthony *et al*., 2002, 2005). The variation of the solubility with temperature is also different: whereas it increases for gases such as N_2 or H_2 with increasing temperature, it decreases for CO_2 (Finotello *et al*., 2008a).

The CO_2 absorption capacity of ionic liquids, like many of their properties, is substantially sensitive to their water content (Seddon *et al*., 2000; Huddleston *et al*., 2001; Blanchard *et al*., 2001). This is not a problem circumscribed to hydrophilic ionic liquids. In hydrophobic ionic liquids, huge differences in absorption capacity have been observed between 'dry' and water-saturated samples (Blanchard *et al*., 2001; Husson *et al*., 2010). The presence of water can even produce chemical instability of the ionic liquid, causing it to decompose (Swatloski *et al*., 2003; Van Valkenburg *et al*., 2005; Ficke *et al*., 2008). However, there are cases where the mixing of the ionic liquid with water improves the level of absorption, in particular in some ionic liquids with a too high viscosity in dry state (Feng *et al*., 2010; Zhang *et al*., 2013). This absorption capacity can even be boosted when combining some specific ionic liquids with water in a certain proportion (Atkins *et al*., 2011)

The following list summarises the main advantages that have been identified for ionic liquids as absorbents in CO_2 capture processing:

- The amount of energy needed is lower than that required when using amines (particularly in the CO_2 recovery stage), in those cases in which the absorption of CO_2 in the ionic liquid is of physical type (Huang and Rüther, 2009).
- Due to sufficient chemical and thermal stability, they can be typically used in a wide temperature range (Forsyth *et al*., 2004).

- They have a practically negligible vapour pressure, which prevents loss of the absorbent or contamination of the gaseous effluent (Anthony *et al*., 2002).
- Since its physicochemical properties are dependent on the chemical structure, the ionic liquid can be conveniently designed for the specific process (Freemantle, 2010).

The latter is a key aspect in the development of ionic liquids for CO_2 capture: their tunability. The mechanism by which an ionic liquid will absorb the gas, and the extent of such absorption, will be modified with variation of the chemical structure of the constituent ions of the ionic liquid.

1.4.1. Physical absorption

Physical absorption, or physisorption, is the mechanism by which most ionic liquids investigated to date do absorb CO_2 (Ramdin *et al*., 2012). This mechanism is dominated by entropic effects (Carvalho and Coutinho, 2010), and is based on weak links between CO_2 and the ionic liquid (Kolding *et al*., 2012). No chemical reaction occurs.

In a typical physisorption isotherm, the amount of CO_2 absorbed increases with the system pressure. The gas fills the free spaces in the ionic liquid, interacting with its ions (Cadena *et al*., 2004), without significantly affecting the structure of the ionic liquid (Jutz *et al*., 2011).

The main advantage of the physical absorption is the low enthalpy of sorption, which implies a low energy requirement to recover the absorbed gas. For this desorption, either a moderate increase in temperature or a decrease of pressure would suffice (Yu *et al*., 2012). This method would be economically competitive with high concentrations of CO_2 in the stream to be treated (Kolh and Nielsen, 1997), even when the maximum absorption capacity is not competitive with the processes currently applied (Anderson *et al*., 2007; Huang and Rüther, 2009).

In physical absorption of CO_2 in ionic liquids, the anion typically has a stronger influence. Spectroscopic data (Cadena *et al*., 2004) and *ab initio* calculations (Raveendran and Wallen, 2002) have indicated that the anion and CO_2 interact as a

Lewis acid-base pair, with the anion giving electrons and the oxygen atom of CO_2 receiving them (Raveendran and Wallen, 2003). However, Van der Waals interactions (Anthony *et al*., 2005), electrostatic interactions (Raveendran and Wallen, 2002; Supasitmongkol and Styring, 2010) and, to a lesser degree, the contribution of hydrogen bonds (Palomar *et al*., 2011), have also been identified.

Ionic liquids with a fluorinated anion have been usually found to lead to greater CO_2 absorption capacities (Aki *et al*., 2004; Muldoon *et al*., 2007; Jalili *et al*., 2010; Manic *et al*., 2012a; Yim and Lim, 2013). The electronegativity of the fluorine atoms is much higher than that of the hydrogen atoms, and therefore the C-F bond can interact with the carbon atom of the CO_2 much better than the C-H bond (Raveendran and Wallen, 2003; Kolding *et al*., 2012). However, it must be noted that these fluorinated ionic liquids present the drawback, at least, of a higher cost.

A simple variation of the nature of the core of the cation does not produce a significant variation in the solubility of CO_2 (Muldoon *et al*., 2007; Scovazzo *et al*., 2004; Anthony *et al*., 2005). However, this should not be generalised, since some cations with the capacity to establish hydrogen bonding with the anion can lead to a decrease of the solubility (Muldoon *et al*., 2007). The most widely studied ionic liquids for absorption of CO_2 to date have been those with an imidazolium cation (Blanchard *et al*., 2001; Anthony *et al*., 2005; Hong *et al*., 2007; Muldoon *et al*., 2007; Supasitmongkol and Styring, 2010; Chen *et al*., 2011), most specifically those with a 1,3-dialkylimidazolium cation. The latter type has a quite acidic hydrogen on the C2 ring position, which has been seen as a potential additional mechanism to interact with CO_2, through hydrogen bonding (Cadena *et al*., 2004; Ramdin *et al*., 2012). The experimental results demonstrate that the substitution of this hydrogen with a methyl group causes just a slight decrease in solubility at low pressures, with the difference being greater at higher pressures (Aki *et al*., 2004; Cadena *et al*., 2004).

In view of the good results obtained with fluorinated anions, some cations with fluorinated alkyl substituent chains were also studied, but the improvement achieved was lower than expected (Muldoon *et al*., 2007). Another alternative tested for improvement of the absorption capacity was the introduction of functional groups in the alkyl substituent chains, for instance ether groups (Aki *et al*., 2004; Muldoon *et*

al., 2007). This led to varied degrees of success, with an important influence of the cation core on the efficacy of the functional group substitution.

The solubility of CO_2 in ionic liquids can be associated with their free volume (Blanchard *et al*., 2001; Aki *et al*., 2004; Carvalho and Coutinho, 2010). An increase in the absorption capacity can be achieved by increasing the free volume of the ionic liquid. A common way of doing this is by adding alkyl substituent chains (optionally fluorinated), or increasing their length, in any of the constitutive ions (Kazarian *et al*., 1996; Beckman, 2004; Shariati and Peters, 2005; Hong *et al*., 2007; Muldoon *et al*., 2007; Manic *et al*., 2012a). An optimum length of the chains was found, regardless of being attached to the anion or to the cation (Raveendran and Wallen, 2003; Chen *et al*., 2011).

Interestingly, as opposed to organic compounds, the volume expansion of ionic liquids upon gas absorption is low due to the coulombic interactions present (Cadena *et al*., 2004; Huang and Rüther, 2009).

1.4.2. Chemical absorption

Chemical absorption, or chemisorption, is the mechanism typically present in capture of CO_2 by functionalised ionic liquids. A chemical bond is established between the CO_2 and the functional groups incorporated in the ionic liquid structure, forming a chemical complex (Yokozeki *et al.*, 2008; Huang and Rüther, 2009; Shunmugavel *et al*., 2010). The energy required to recover the CO_2 has to be enough to break the chemical bonds previously formed, thus requiring higher process temperatures than in the case of physical absorption (Bates *et al.*, 2002; Shiflett *et al.*, 2008; Yu *et al*., 2012).

The first studies of functionalised ionic liquids applied to CO_2 absorption were performed by Bates *et al*. (2002). They functionalised an imidazolium cation with a primary amine in one of its alkyl substituents. The absorption achieved was similar to the theoretical maximum obtained with amines through a reversible reaction. Thereafter, numerous researchers have studied these new ionic liquids. Galán Sánchez *et al*. (2007) functionalised another imidazolium cation with primary or tertiary amines, or a hydroxyl group, and observed that the primary amine functionalisation improves the absorption capacity more than the tertiary amine. Other chemical moieties used in the functionalisation of ionic liquids for absorption of

CO_2 were amino acids, which can act as anion, as cation, or as a substituent in any of them (Ohno and Fukumoto, 2007). The amino acid ionic liquids have a high absorption capacity, and are inexpensive and biodegradable, although they also present a very high viscosity.

New structures have been recently sought to improve the stoichiometry of the reaction, in order to make it more competitive. With the above mentioned ionic liquids, with amino group functionalisation in the substituent chains of the cation, the stoichiometry achieved is 1:2, like the one corresponding to the process based on amine solutions (Bates *et al*., 2002). The mechanism established is similar to aqueous solutions of amines to capture CO_2 (section 1.2):

$$*\sim NH_2 + CO_2 \rightleftharpoons *\sim NHCO_2H$$

$$*\sim NHCO_2H + *\sim NH_2 \rightleftharpoons *\sim NHCO_2^- + *\sim NH_3^+$$

Gurkan *et al*. (2010a) introduced the functionalisation in the anion. They used the ionic liquids trihexyl(tetradecyl)phosphonium prolinate and trihexyl(tetradecyl)phosphonium methioninate, with which a stoichiometry of 1:1 could be achieved as a result of only undergoing the first of the two indicated reactions. Previous studies by the same research team had previously established the relationship between the position of the amino group and the relative energies of the two chemical reactions through *ab initio* calculations. Their results showed that, when the amine is attached to the cation, the carbamate formation (second reaction) is favoured; whereas when bound to the anion, the formation of carbamic acid (first reaction) is the favoured one. The proposed mechanism was confirmed for the anion-functionalised ionic liquids by Fourier transform infrared (FTIR) spectroscopy.

Besides functionalisation via appendage of specific groups to the cation or the anion, some 'conventional' ionic liquids can also lead to chemical absorption of CO_2. This is the case, for example, or ionic liquids with an amino acid anion (Zhang *et al*., 2006), or of some ionic liquids with a sufficiently basic anion (Gurau *et al*., 2011). A paradigmatic case in the latter group is the one of 1,3-dialkylimidazolium acetates. The analysis of the behaviour of these ionic liquids in absorption of CO_2 has led to the proposal of different mechanisms. The first one was raised by Maginn (2005), after his study of the absorption of CO_2 in 1-butyl-3-methylimidazolium acetate

([C_4C_1im][OAc]) (Figure 1.7). This suggested mechanism consisted on the deprotonation of the imidazolium cation by the action of the acetate anion, thus enabling the CO_2 to easily bind to the carbene generated (Maginn, 2005). Although simple, this mechanism involved some aspects incompatible with experimental evidence, which could not be backed by any reasonable explanation.

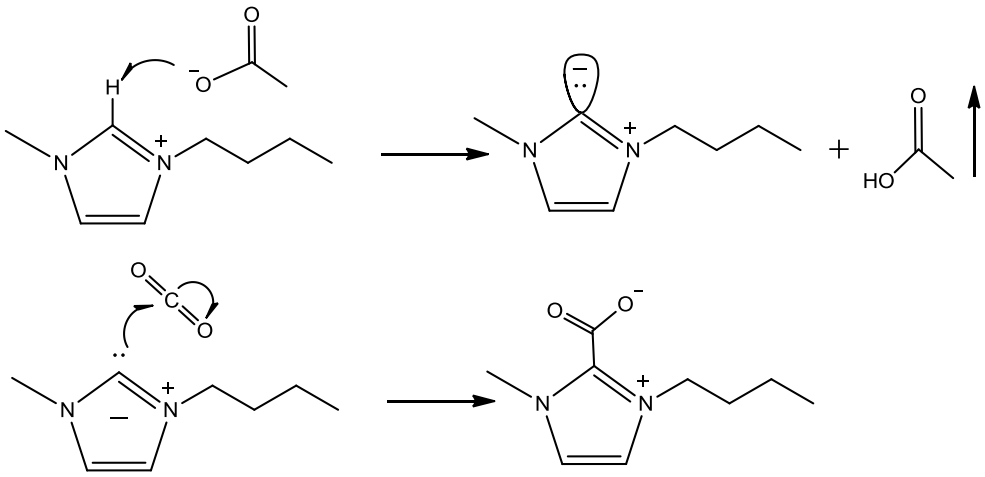

Figure 1.7: Mechanism of chemical absorption of CO_2 in [C_4C_1im][OAc] proposed by Maginn (2005).

Yokozeki *et al*. (2008) proposed a new mechanism where there were two types of chemical complexes, AB and AB_2, from the binary mixture A + B (A = CO_2; B = ionic liquid); however it was found that only the AB_2 complex is dominant in solution. Gurau *et al*. (2011) have later verified experimentally the presence of complex systems AB_2 in mixtures 1-ethyl-3-methylimidazolium acetate ([C_2C_1im][OAc]) + CO_2, and they have proposed a more solid mechanism involving the formation of a complex acetic acid-acetate ion (Figure 1.8).

For the above mechanism to take place, the existence of a sufficiently acidic proton in the cation is required. This is available in 1,3-dialkylimidazolium cations, but for example it is not in pyridinium cations, leading to substantial differences in absorption capacity of acetate ionic liquids (Chen *et al*., 2011).

Contrary to physical absorption, in a typical chemisorption isotherm two stages can be identified: at low pressures there is a rapid increase of the gas absorbed, due to the chemical absorption; subsequently there is a more gradual increase in the

amount absorbed with increasing pressure, where physical absorption becomes the predominant mechanism (Shiflett *et al.*, 2008; Gurkan *et al*., 2010b).

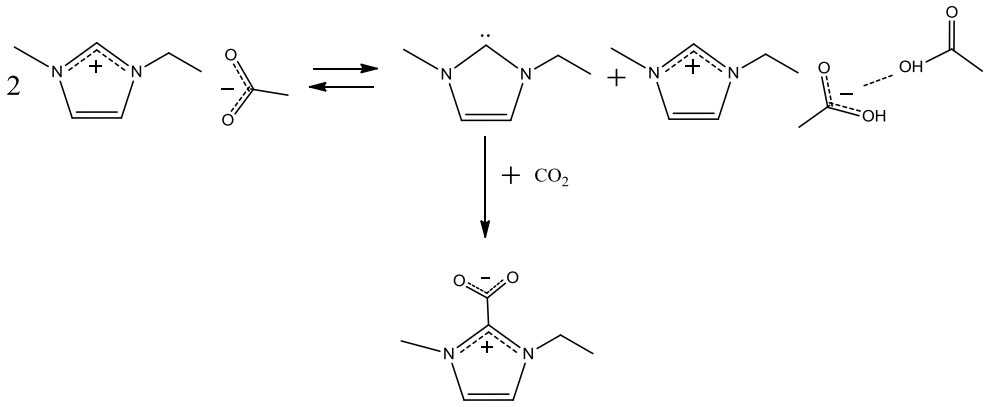

Figure 1.8: Mechanism of chemical absorption of CO_2 in [C_2mim][OAc] proposed by Gurau *et al.* (2011).

1.4.3. Alternative strategies for improvement of the capacity of ionic liquids to absorb CO_2

Works in the literature have mainly focused, to date, on modification of chemical structures of ionic liquids in order to improve their absorption capacity for CO_2. Besides this procedure, inherent to the characteristic tunability of ionic liquids, and in combination with it, other alternatives may be considered.

One option is the use of mixtures of ionic liquids. Studies on the CO_2 absorption capacity in mixtures of ionic liquids is rather limited, and basically circumscribed to mixtures of imidazolium ionic liquids (Finotello *et al*., 2008b; Shifflett and Yokozeki, 2009; Lei *et al*., 2012). Promising results were observed in the limited literature available, improving the absorption capacity of the ionic liquid with less capacity (Shifflett and Yokozeki, 2009; Lei *et al*., 2012) and even outperforming the capacity of the pure ionic liquid with higher absorption capacity (Finotello *et al*., 2008b).

Another alternative is the use of supported ionic liquids. Compared to pure ionic liquids in their bulk liquid state, immobilised ionic liquids may improve the kinetics of absorption. This aspect can be of particular importance in ionic liquids with relatively unfavourable transport properties. Some studies have been carried

out, to date, on the use of SILPs for absorption of gases, especially supporting amino acid ionic liquids on silica (Zhang *et al*., 2006, 2009; Shunmugavel *et al*., 2010; Kolding *et al*., 2012). In general, it was observed that the absorption was fast and reversible, with no significant loss of the absorption capacity after several absorption/desorption cycles. As a favourable side effect, an improved thermal stability was observed, enabling the utilisation of higher temperatures to achieve complete desorption.

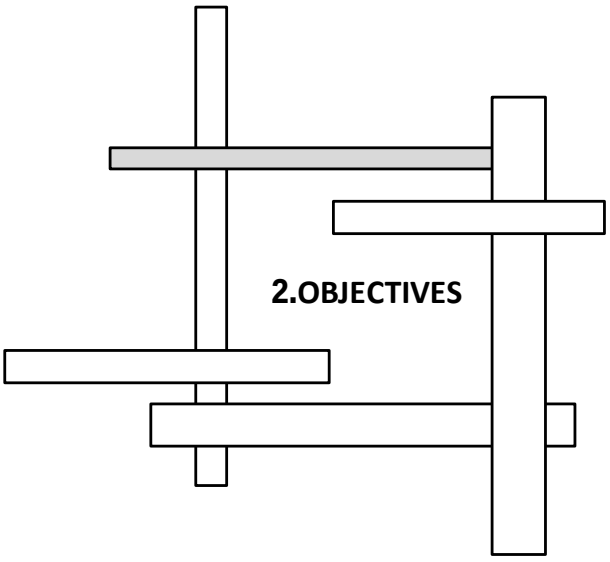

2.OBJECTIVES

2. OBJECTIVES

The overall objective of this Thesis is the generation of deeper knowledge on the possibilities of ionic liquids as the basis for improved technologies for carbon dioxide capture. The accomplishment of such objective will be accompanied by the set up of apparatus and the development of methods for the experimental determination of gas absorption in ionic liquid samples and their thermal behaviour.

Ionic liquids will be prepared and characterised, and their ability to absorb (and desorb) CO_2 will be analysed at different pressures and, in some cases, at different temperatures. Identification of the absorption mechanisms will be carried out. A relationship between the structural features of the constituent ions of the tested ionic liquids and their absorption capacity will be also sought.

With information available for the CO_2 absorption by individual ionic liquids, the possibility of obtaining synergistic effects by utilising mixtures of ionic liquids will be explored. Typically, an ionic liquid with a known good capacity for CO_2 absorption, but with some issues for its individual use (such as high cost, toxicity...), will be combined with an ionic liquid with a lower CO_2 absorption capacity, but with more favourable attributes from other perspectives. This investigation will emphasise both the absorption capacity and the thermal (liquid range, thermal stability) and physical (density, viscosity, surface tension) characteristics of the liquid absorbent formed by the mixed ionic liquids. A rigorous analysis of the latter, with the corresponding thermodynamic treatment, will allow a deeper insight on the interactions occurring in the mixture, and how they might affect the absorption capacity. Knowledge of the properties selected is needed for a suitable design of a real process for CO_2 capture with ionic liquids at an industrial level.

Attempts to model the CO_2 absorption isotherms by means of classical models of thermodynamic basis will also be carried out, for the case of single ionic liquids and for the mixed ionic liquid absorbents.

In a further approach, the option of utilising a porous support to deposit the ionic liquid on it as active absorbing agent will be also investigated, in particular with an ionic liquid presenting problems from the standpoint of transport properties.

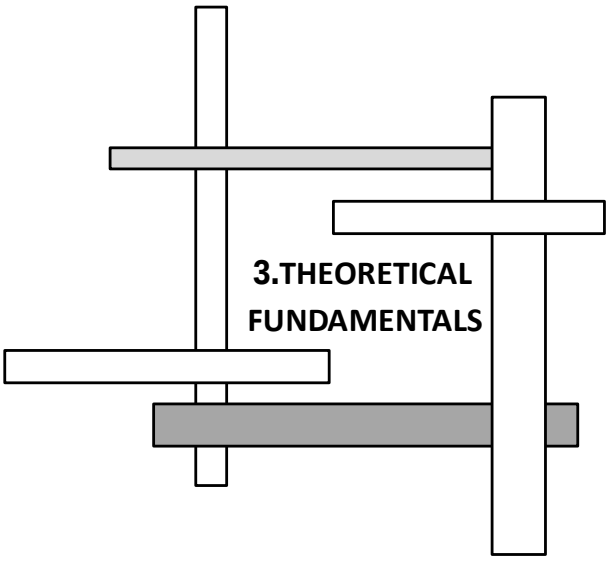

3.THEORETICAL FUNDAMENTALS

3. THEORETICAL FUNDAMENTALS

3.1. Absorption of gases

The absorption of gases in liquids depends on multiple variables, such as the nature of the components, the process conditions, the absorption mechanisms, etc. In the case of physisorption in non-volatile liquid sorbents, valuable information for the comparison of performances can be obtained via analysis of the Henry constants, which emanate from the so-called Henry's law.

The usefulness of the experimental pressure-composition data in absorption isotherms is enriched if they can be continuously described by a mathematical expression, which would allow reliable interpolation of data and a simplified computerised treatment. Among various models available in the literature, the one selected herein for data reduction was the Non-Random Two-Liquid (NRTL) model (Renon and Prausnitz, 1968).

Both Henry's law and the NRTL correlation derive from the fundamentals of thermodynamic equilibrium in physical systems. Thus, a brief introductory subsection to its basic aspects becomes necessary.

3.1.1. Fundamentals of physical thermodynamic equilibrium

A system in thermodynamic equilibrium is one in which no change, or tendency to change state, occurs. In a closed system at given temperature (T) and pressure (P) conditions, the equilibrium state will be the state in which the total Gibbs free energy (G) be a minimum with respect to all possible changes in the conditions (Smith *et al*., 2005).

In an open system with a single fluid phase, G can be written in terms of intensive properties:

$$dG = V \cdot dP - S \cdot dT + \sum_i (\mu_i \cdot dn_i) \tag{3.1}$$

where V and S are the volume and the entropy of the system, and n_i and μ_i are the numbers of moles and the chemical potential of component i, respectively. The chemical potential of component i can be defined as:

$$\mu_i = \left(\frac{dG}{dn_i} \right)_{P,T,n_j} \tag{3.2}$$

with subscript j indicating all the species in the system but the i-th.

In a closed system with multiple fluid phases, each of these phases can be considered as an open system that can transfer mass to the other(s). Therefore, equation 3.1 will be applicable to each phase. The sum of all of them determines the total variation of Gibbs free energy in the system (equation 3.3):

$$dG = V \cdot dP - S \cdot dT + \sum_k \sum_i \left(\mu_i^{(k)} \cdot dn_i^{(k)} \right) \tag{3.3}$$

where superscript k in parentheses denotes a generic phase. In a multiphasic system in equilibrium, both P and T will be uniform. From this, and taking into account that G has to be a minimum, it can be mathematically deduced that the chemical potential of each species has to be also uniform throughout the phases of the system:

$$\mu_i^{(1)} = \mu_i^{(2)} = ... = \mu_i^{(\phi)} \ , \quad i = 1,2,...,m \tag{3.4}$$

with ϕ and m being respectively the total number of phases and total number of components in the system. This expression constitutes a general criterion for phase equilibrium at constant pressure and temperature.

However the chemical potential does not have a direct 'physical' equivalent, and therefore it is preferred to express it in terms of another function with a clearer physical connection. To this aim, the concept of fugacity (f) is defined, for any isothermal change in any system, so that the following expression is met for each component i:

$$\mu_i = \mu_i^0 + R \cdot T \cdot \ln \frac{f_i}{f_i^0} \tag{3.5}$$

where superscript 0 indicates the standard state condition and R is the universal constant of gases. This equation can be applied to each phase in a multiphasic system. From this, it can be derived that, if the system is in equilibrium, the fugacities of each component in all the phases of the system have to be the same:

$$f_i^{(1)} = f_i^{(2)} = ... = f_i^{(\phi)} \ , \quad i = 1,2,...,m \tag{3.6}$$

In equation 3.5, the ratio of the fugacity to the standard state fugacity (f_i/f_i^0) is used. This term is known, by definition, as the activity of the component (a_i). It provides an idea of how 'active' a substance is in relation to its standard potential at the state of interest and that at its standard state (Prausnitz *et al.*, 1999). If the standard state for all phases is the same, and taking into account equation 3.6, it is easily inferred that the activity of a component has to be the same in all phases in the system if such system is at equilibrium:

$$a_i^{(1)} = a_i^{(2)} = ... = a_i^{(\phi)} \ , \quad i = 1,2,...,m \tag{3.7}$$

The activity coefficient for a substance i (γ_i) is defined as the ratio of its activity to its concentration (usually in molar fraction, x_i):

$$\gamma_i = \frac{a_i}{x_i} \tag{3.8}$$

By combining equations 3.7 and 3.8, a practical expression for the equilibrium criterion in a multiphasic system can be obtained:

$$(\gamma_i \cdot x_i)^{(1)} = (\gamma_i \cdot x_i)^{(2)} = ... = (\gamma_i \cdot x_i)^{(\phi)} \ , i = 1,2,..., \ m \tag{3.9}$$

Besides fugacity, in the description of the equilibrium in fluid systems the fugacity coefficients (φ_i) are also frequently utilised:

$$\varphi_i^L \equiv \frac{f_i^L}{x_i \cdot P} \tag{3.10}$$

$$\varphi_i^V \equiv \frac{f_i^V}{y_i \cdot P} \tag{3.11}$$

where superscripts *L* and *V* refer to the liquid and vapour phases respectively, and the molar fractions of component *i* in the liquid phase and the vapour phase are respectively represented by x_i and y_i.

3.1.2. Gas-liquid equilibrium. Henry's law

The determination of the solubility of a gas in a solvent, as a function of the temperature and pressure, is of particular importance for the design of gas separation processes. When the absorption process occurs via a physical mechanism, knowledge about the phase equilibrium behaviour is required. From equation 3.6, for a system composed of a liquid phase and a vapour phase, the steady state can be expressed as:

$$f_i^{(L)} = f_i^{(V)} \tag{3.12}$$

For non-ideal systems, there exist basically two methods for the characterisation of this equivalence of fugacities. In a first one, known as the *phi-phi method* (φ-φ), both phases are described by means of equations of state, and the fugacity coefficients are utilised:

$$x_i \cdot \varphi_i^L = y_i \cdot \varphi_i^V \tag{3.13}$$

with all symbols having been previously defined. In the second method, known as the *gamma-phi method* (γ-φ), a model is used to describe the non-ideal liquid phase and an equation of state is used for the vapour phase, and the mathematical expression is as follows:

$$x_i \cdot \gamma_i \cdot f_i^0 = y_i \cdot \varphi_i^V \cdot P \tag{3.14}$$

The first model is interesting when suitable equations of state and reliable mixing rules are available for the reliable calculation of the fugacity coefficients. The second model is a versatile approach that, however, presents a problem linked to the standard fugacity in the left hand side of equation 3.14. Usually, in vapour-liquid equilibrium, the fugacity of the pure liquid at the temperature and pressure of the system is used as standard fugacity. However, for solubilities of supercritical compounds, this standard cannot be used anymore. Henry constants are typically used instead, as standard fugacities (Gmehling *et al*., 2012).

In 1803, William Henry formulated a gas law which states that, at constant temperature, the amount of a given gas that dissolves in a particular type and volume of liquid is directly proportional to the partial pressure of this gas in equilibrium with the liquid (Smith *et al*., 2005). This law, known as Henry's law, is often used to describe the solubility of a gas solute *i* at low pressure, and is expressed as:

$$H_i(T,P) \equiv \lim_{x_i \to 0} \frac{f_i^L}{x_i} \tag{3.15}$$

where $H_i(T,P)$ is the Henry constant, x_i is the mole fraction of gas dissolved, and f_i^L is the fugacity of the gas dissolved (Smith and Harvey, 2007).

Henry's law may be applied to a variety of gases until equilibrium pressures of about 5 to 10 bar, as long as the solubility of the gas does not exceed a molar fraction of 0.3 (Prausnitz *et al*., 1999). If the solubility of the gas is notably lower, however, the validity of Henry's law may expand until pressures as high as 25 bar (Pray *et al*., 1952).

In the case of a gas absorbed in an ionic liquid, no ionic liquid will be present in the gas phase under usual pressure and temperature conditions, as a result of its negligible vapour pressure. Thus, it may be reasonable to assume that the behaviour of the gas phase is nearly ideal (*i.e.* the fugacity coefficient of the gas is close to the unity), and then the fugacity is practically equal to the gas pressure (P) above the ionic liquid sample with absorbed gas (Anderson *et al*., 2008). Therefore, Henry's law could be rewritten as follows:

$$H_i(T) = \lim_{x_i \to 0} \frac{P}{x_i} \tag{3.16}$$

which, for low solubilities, can be rearranged as:

$$P = H_i(T) \cdot x_i \tag{3.17}$$

This expression establishes a linear dependency of the molar fraction of gas solubilised with the total pressure of the system. It can be used in the case of absorption of a gas into non-volatile compounds, such as ionic liquids, and at low pressures (Anderson, 2008), as long as the solute be not dissociated, ionised or react with the solvent (Felder and Rousseau, 2005). Please note that equation 3.17 is a

particular case of equation 3.14 applied to the gas, with the assumption of γ_i and φ_i^V being the unity, and with $y_i = 1$ (the ionic liquid is non-volatile and does not enter the gas phase), in addition to the above mentioned replacement of f_i^0 with $H_i(T)$.

3.1.3. Correlation of equilibrium data. The Non-Random, Two-Liquid (NRTL) model

For application of the equilibrium data experimentally obtained, it is generally necessary to describe the behaviour of the system by means of a suitable correlation of the experimental data. Among the possible correlations to be used, we can distinguish between those correlating directly the experimental data measured (not allowing extrapolation of their parameters to other multicomponent mixtures), and those which, in principle, can extend their applicability to multicomponent mixtures through the use of just binary parameters. The latter group includes equations used for the correlation of the excess Gibbs energy (G^E), which is related to the activity coefficient as follows:

$$ln\gamma_i = \left[\frac{\partial}{\partial n_i}\left(\frac{G^E}{R\cdot T}\right)\right]_{T,P,n_j} \qquad (3.18)$$

where subscript *j* refers to all the species in the system but the *i*th, and all other symbols have been defined previously. A suitable model for G^E can be combined with equations 3.8 and 3.18 to yield models for the correlation of equilibrium experimental data. One of the most versatile and widely used models in this regard is the Non-Random, Two-Liquid (NRTL) model.

The NRTL model, developed by Renon and Prausnitz (1968), is a classical model for the correlation of equilibrium data. It has a semi-empirical nature and can be applied to completely or partially miscible systems. The NRTL model arises from the combination of a previous model for G^E (Wilson, 1964), which had introduced the concept of local composition, with the two-liquid theory by Scott (1956). An original innovation in the model is the introduction of an adjustable parameter characteristic of the non-randomness of the mixture. This non-randomness parameter, denoted as α_{ij}, represents the tendency of the molecules of components *i* and *j* to not mix in a random fashion. It can be interpreted as the inverse of the number of nearest

neighbours of a molecule in the mixture, and usually its value is in the range 0.1-0.3 (Newsham, 1992). Although a set of rules was devised by the authors of the model for theoretical estimation of the non-randomness parameter depending on the nature of the substances in the mixture, it is common practice to assign an empirical value to it, based on previous experiences in the correlation of experimental data of similar systems.

The NRTL model is applicable to multicomponent systems, using only binary interaction parameters as adjustable parameters. For a solution of *n* components, the NRTL equation for G^E is:

$$\frac{G^E}{R \cdot T} = \sum_{i=1}^{n} \left[x_i \cdot \frac{\sum_{j=1}^{n} x_j \cdot \tau_{ji} \cdot G_{ji}}{\sum_{k=1}^{n} x_k \cdot G_{ki}} \right] \tag{3.19}$$

where:

$$G_{ji} = exp(-\alpha_{ji} \cdot \tau_{ji}), \quad \alpha_{ji} = \alpha_{ij} \tag{3.20}$$

$$\tau_{ji} = \frac{g_{ji} - g_{ij}}{R \cdot T} \tag{3.21}$$

with $(g_{ji} - g_{ij}) = \Delta g_{ji}$ being the binary interaction parameters. These parameters have the same meaning as in the model by Wilson (1964); but in the NRTL model the α_{ji} parameter is added, complicating the calculations.

The following is the expression for the activity coefficient of component *i* in a mixture of *n* components for the NRTL model:

$$ln\,\gamma_i = \frac{\sum_{j=1}^{n} x_j \cdot \tau_{ji} \cdot G_{ji}}{\sum_{k=1}^{n} x_k \cdot G_{ki}} + \sum_{j=1}^{n} \left[\frac{x_j \cdot G_{ij}}{\sum_{k=1}^{n} x_k \cdot G_{kj}} \cdot \left(\tau_{ij} - \frac{\sum_{l=1}^{n} x_l \cdot \tau_{lj} \cdot G_{lj}}{\sum_{k=1}^{n} x_k \cdot G_{kj}} \right) \right] \tag{3.22}$$

The NRTL model was originally developed for systems with non-electrolyte components. Different modifications were developed later to make it suitable for systems containing electrolytes (for instance: Cruz and Renon (1978); Chen and Evans (1986)). However, in the case of systems involving ionic liquids, which are electrolytes by nature, the original NRTL model was found to provide suitable correlation of equilibrium data (particularly liquid-liquid equilibrium data) in

numerous occasions and for miscellaneous systems over the last decade (for instance: Crosthwaite *et al.*, 2006; Chen *et al.*, 2008; Simoni *et al.*, 2008; García *et al.*, 2011; and references therein). In this Thesis, the original NRTL model was used for correlation of gas-liquid systems composed on an ionic liquid and carbon dioxide. In particular, it was used to carry out the correlation of the experimental pressure-temperature-composition data. The correlation parameters are obtained using a computer program by Sørensen and Arlt (1980). This program optimises an objective function, defined in terms of the pressure variable, by means of a non-linear regression method based on the maximum likelihood principle. The ternary mixtures composed of CO_2 plus two ionic liquids were treated as a pseudo-binary system (*i.e.* with the mixture of ionic liquids taken as a single component), and given that no evaporation of the ionic liquid(s) occurs, the gas phase was assumed to have an ideal behaviour. In the correlation process, the saturation pressures P^{sat} for each *i*-th compound are calculated with Antoine's equation (Smith *et al.*, 2005):

$$\ln P_i^{sat} = A - \frac{B}{T + C} \tag{3.23}$$

where T is the absolute temperature, and A, B, and C are empirical parameters specific to each substance. In the case of CO_2, the values can be found in the literature (Shiflett and Yokozeki, 2006); however, for the ionic liquids these values are not easy to find, so fictional values are arbitrarily set to lead to negligible vapour pressures.

The non-randomness parameter of the model, α, is set beforehand to typical values 0.1, 0.2 and 0.3, and the interaction parameters, Δg_{12} and Δg_{21} are obtained for each system. These parameters are used to calculate the correlated pressures, and the root mean square deviations are determined from the data sets of experimental pressures and their corresponding correlated pressures.

3.2. Thermophysical properties

Knowledge and understanding of relevant thermophysical properties of a system are necessary for a suitable design of the corresponding process or operation unit. The influence of temperature on these properties responds to different patterns, and must be taken into account in process design. If working with mixtures, a further influence

to be analysed is that of composition. In both cases, the development of simple correlations for the continuous description of discrete experimental values with a small number of adjustable parameters is of high interest. In addition, a deeper insight on the interactions occurring in the system at a molecular level can be obtained. Ideally, an expression for prediction (with sufficient accuracy) of the properties of a mixture from properties of its pure components would be preferred, but this is only possible in a limited number of occasions.

3.2.1. Density, viscosity and surface tension

Density, viscosity and surface tension are among the properties of greatest importance in the design of processes involving fluid streams. In particular they are among the key properties for the design of critical parameters in absorption units, such as tray diameter, pressure drop, or pumping requirements.

Density (ρ) is probably the most useful physical property, including its utilisation in the calculation of many other properties (Riddick *et al.*, 1986). It is defined as the mass of a substance per unit volume. The molar volume (V) of a pure compound is related to its density, as follows:

$$V = \frac{MW}{\rho} \tag{3.24}$$

where MW stands for the molecular weight of the compound. For a mixture, a weighted average (in a molar basis) of the molecular weights of the compounds involved is used in the numerator of equation 3.24.

Dynamic viscosity (η), or simply viscosity, is a measurement of the resistance of a fluid to flow. Specifically, it corresponds to the force per unit area necessary to maintain a unit velocity gradient between two parallel planes a unit distance apart (Riddick *et al.*, 1986). It is defined via Newton's law of viscosity:

$$\tau_{yx} = -\eta \cdot \frac{\partial v_x}{\partial y} \tag{3.25}$$

where τ_{yx} is the force in the x direction on a unit area perpendicular to the y direction, v_x is the component in the x direction of the velocity vector of the fluid, and η acts as

the proportionality constant. Those fluids whose resistance to flow is well described by equation 3.25 are referred to as Newtonian fluids.

Surface tension (σ) is defined as the force exerted in the plane of the surface of a liquid per unit length. It is a result of the unequal forces acting upon the molecules at the boundary between a liquid phase and a gas phase (Poling *et al*., 2001; Freire *et al*., 2007).

3.2.2. Excess and deviation properties

Excess and deviation properties derived from thermophysical properties can provide valuable information on the behaviour of real mixtures.

For any property M, the property of change of mixing ΔM, or deviation property, in a solution is defined as:

$$\Delta M \equiv M - \sum_i x_i \cdot M_i \tag{3.26}$$

where M is the property of the solution, x_i is the molar fraction of the i-th component, and M_i is the property of the i-th component. For the particular cases of molar volume, viscosity and surface tension, the corresponding deviation properties can be written as:

$$\Delta V = V - \sum_i x_i \cdot V_i \tag{3.27}$$

$$\Delta \eta = \eta - \sum_i x_i \cdot \eta_i \tag{3.28}$$

$$\Delta \sigma = \sigma - \sum_i x_i \cdot \sigma_i \tag{3.29}$$

If M represents the molar (or specific) value of an extensive thermodynamic property (*e.g.* volume, internal energy, enthalpy, entropy, etc.), then the excess property M^E is defined as the difference between the real value of the property and the value that it would have if it behaved as an ideal solution at the same temperature, pressure and composition (Smith *et al*., 2005):

$$M^E \equiv M - M^{id} \tag{3.30}$$

where the superscript *id* indicates the value corresponding to the ideal solution behaviour. In the case of molar volume, the ideal solution molar volume is given by (Smith *et al*., 2005):

$$V^{id} = \sum_i x_i \cdot V_i \tag{3.31}$$

where x_i and V_i correspond to the molar fraction and the molar volume of the *i*-th substance. By combination of equations 3.30 and 3.31, an expression for the excess molar volume V^E is obtained:

$$V^E = V - \sum_i x_i \cdot V_i \tag{3.32}$$

The right-hand terms in equations 3.27 and 3.32 are the same, and therefore V^E is equal to ΔV.

Developing the summations in equations 3.28, 3.29 and 3.32 for the case of binary mixtures, the excess molar volume V^E, the viscosity deviation $\Delta\eta$, and the surface tension deviation $\Delta\sigma$ can be expressed as:

$$V^E = V - (x_1 \cdot V_1 + x_2 \cdot V_2) \tag{3.33}$$

$$\Delta\eta = \eta - (x_1 \cdot \eta_1 + x_2 \cdot \eta_2) \tag{3.34}$$

$$\Delta\sigma = \sigma - (x_1 \cdot \sigma_1 + x_2 \cdot \sigma_2) \tag{3.35}$$

3.2.3. Data correlation: influence of the temperature

In general, properties of liquids such as density, viscosity, or surface tension tend to decrease with increasing temperature. However, the way in which temperature influences this decrement may be starkly different.

For many liquids, the variation of density with temperature can be described, over a relatively broad range of temperatures, and with a reasonably good degree of accuracy, by means of a linear correlation. In some other situations, the fit to a polynomial expression of higher order may be preferred. For the density ρ of pure ionic liquids, either a linear fit (Gu and Brennecke, 2002; Jacquemin *et al*., 2008; Deng *et al*., 2011) or a second order polynomial fit (Gomes de Azevedo *et al*., 2005;

Jacquemin *et al.,* 2007; Hasse *et al*., 2009) are the solutions typically adopted for its correlation with temperature:

$$\rho = a + b \cdot T \tag{3.36}$$

$$\rho = a + b \cdot T + c \cdot T^2 \tag{3.37}$$

where T is the temperature, and a, b and c are fit parameters. In evaluating the quality of the fits provided by each of the equations, the standard deviation is a valuable comparative parameter, defined as follows:

$$\sigma = \frac{\sum_{i=1}^{m} \left(\rho_{i_{exp}} - \rho_{i_{calc}} \right)^2}{m - \nu} \tag{3.38}$$

where the subscripts *exp* and *calc* indicates experimental and calculated values obtained for the density, m represent the number of experimental data points, and ν the number of adjustable parameters.

The effect of temperature on the viscosity of liquids follows a clearly distinct pattern. The following Arrhenius-type equation (Andrade, 1930) does often constitute a good approximation for the viscosity of many liquids:

$$ln\ \eta = A + \frac{B}{T} \tag{3.39}$$

where η is the liquid viscosity, T the absolute temperature, and A and B the fit parameters. Rewriting this expression in a more conventional Arrhenius-like style, we get:

$$\eta = \eta_{\infty} \cdot exp\left(-\frac{E_a}{R \cdot T} \right) \tag{3.40}$$

where η_{∞} is the viscosity at infinite temperature, and E_a is an energy term ('activation energy'). This simple, 2-parameter approach fits acceptably well the viscosity of some ionic liquids. Nevertheless, for most ionic liquids, equation 3.40 does not provide an accurate description of the evolution of their viscosity with temperature (Seddon *et al.*, 2002; Okoturo and VanderNoot, 2004; Wilkes, 2004), and a significantly improved fit is obtained with a 3-parameter equation known as the Vogel-Fulcher-Tammann

equation (Vogel, 1921; Fulcher, 1925; Tammann and Hesse, 1926). This equation, traditionally used for glass-forming liquids, is expressed as follows in its modified version by Cohen and Turnbull (1959):

$$\eta = A \cdot T^{0.5} \cdot exp\left(\frac{k}{T - T_0}\right) \tag{3.41}$$

where A, k and T_0 are fitting parameters. As originally conceived, the equation was totally empirical, but the development of the free volume theory (Cohen and Turnbull, 1959) and the configurational entropy approach (Adam and Gibbs, 1965) provided it with some theoretical significance. In particular, in this semi-theoretical framework, T_0 is presented as the 'ideal glass transition temperature', below which the fluid behaves as an equilibrium glass where there is no mass transport (Angell and Moynihan, 1969). Due to kinetic limitation, this 'ideal glass transition temperature' can not be reached in a finite time scale experiment; instead, the experimental glass transition T_g is obtained, and should have a somewhat greater value (Gibbs and DiMarzio, 1958). No other theoretical meaning could be clearly inferred for the other two parameters A and k in equation 3.41, although it is known that their values are strongly dependent on the choice of the value of T_0 (Angell and Moynihan, 1969).

In a similar manner to what was mentioned above for density, the standard deviation would be an interesting parameter to establish a comparison of the quality of different fitting equations. Nevertheless, given that the viscosity values for a liquid can expand over one or several orders of magnitude in moderate temperature ranges, a relative standard deviation is preferred:

$$\sigma_r = \frac{\sum_{i=1}^{m}\left(\frac{\eta_{i_{exp}} - \eta_{i_{calc}}}{\eta_{i_{calc}}}\right)^2}{m - \nu} \tag{3.42}$$

where the subscripts *exp* and *calc* indicates experimental and calculated values obtained for the viscosity, m represent the number of experimental data points, and ν the number of adjustable parameters.

3.2.4. Data correlation: influence of the composition

In the work with mixtures, the influence of the composition on the physical properties is typically studied *via* analysis of their excess and deviation properties rather than directly on the physical properties. If the excess and deviation properties can be adequately correlated by any mathematical equation, the physical properties will be automatically correlated by means of the defining equations of excess and deviation properties.

One of the most commonly used equations for correlation of excess and deviation properties is the polynomial expansion proposed by Redlich and Kister (1948). This is an empirical algebraic expansion, fairly straightforward because it consists of polynomial terms of the molar fractions. For a binary system, the Redlich-Kister polynomial adopts the following form:

$$Q = x_1 \cdot x_2 \cdot \sum_{i=0}^{n} A_i \cdot (x_1 - x_2)^i \qquad (3.43)$$

where Q is the excess or deviation property, x_1 and x_2 are the molar fractions of component 1 and component 2 respectively, n is the degree of the polynomial expresion, and A_i are the fit coefficients of the polynomial.

The number of parameters needed in equation 3.43 to obtain a good correlation of the experimental data varies according to the complexity of the mixture, the number of experimental points, and the quality of these data (Prausnitz *et al*., 1999). The F-test is often used to determine the appropriate number of these parameters. The quality of the fitting obtained in each case can be evaluated by means of the root mean square deviation (rmsd), which is defined as:

$$rmsd = \sqrt{\frac{\sum_{i=1}^{m} (Q_{i_{exp}} - Q_{i_{calc}})^2}{m}} \qquad (3.44)$$

where subscripts *exp* and *calc* denote experimental and correlated values obtained for the property Q, and m represents the number of experimental data points.

3.2.5. Prediction of properties in binary mixtures

Beyond correlation, the possibility of predicting the properties of mixtures from information on the properties of the pure components is desirable.

Molar volume and density

From a volumetric property perspective, mixtures with an 'ideal behaviour' would be those with a molar volume corresponding to the weighted average of the molar volumes of the constituent compounds; *i.e.*, with an excess molar volume equal to zero. In practice, this does not occur. However, the magnitude of the excess molar volume is very much smaller than the molar volume itself. In such cases, although neglecting the excess molar volume implies the loss of important information that it provides of the liquid medium at a molecular level, quantitatively reasonable estimates of the molar volume could be obtained by direct weighted average of the molar volumes of the pure components. This rationale can be extended to the particular case of mixtures of ionic liquids (Canongia Lopes *et al.*, 2005). After estimation of the molar volume of the mixture, an approximated density is immediately calculable by means of equation 3.24.

Viscosity

For the viscosity of a mixture, estimation *via* a linearly weighted average of the viscosities of the pure components is not appropriate, since viscosity is a dynamic, non-molar property (Navia *et al.*, 2008). Current predictive estimation of the viscosity of mixtures is essentially based on mixing rules relating pure component viscosities to composition, where little theory is applicable (Poling *et al.*, 2001). One of the simplest equations used, for binary mixtures, is the so-called Arrhenius relation (Arrhenius, 1887):

$$\ln \eta = x_1 \cdot \ln \eta_1 + x_2 \cdot \ln \eta_2 \qquad (3.45)$$

where η is the viscosity of the mixture, η_1 and η_2 are the viscosities of the pure components 1 and 2 respectively, and x_1 and x_2 are the corresponding molar fractions. Grunberg and Nissan (1949) found that a better fit of experimental data could be achieved by introducing a binary interaction parameter. For a binary mixture, their equation adopts the form:

$$\ln\eta = x_1 \cdot \ln\eta_1 + x_2 \cdot \ln\eta_2 + x_1 \cdot x_2 \cdot G_{12} \qquad (3.46)$$

with G_{12} being the interaction parameter for species 1 and 2. This is currently one of the methods of reference for estimation of the viscosity of liquid mixtures (Poling *et al.*, 2001). One of its handicaps is the need to calculate G_{12}. Tabulated data have been generated for a series of functional groups, allowing easy calculation of G_{12}; however, this is more complicated for compounds containing groups not included in the tables. If the substances mixed are of similar nature, it may be assumed that G_{12} is going to be small. This can be the case of mixtures of similar ionic liquids. Taking G_{12} as zero, equation 3.46 transforms into equation 3.45.

There are also expressions with some theoretical basis for the prediction of viscosity of liquid mixtures. This is the case of the equation due to Katti and Chaudhri (1964), who introduced in its development the theoretical model by Eyring and co-workers for the viscosity of a pure liquid (Powell *et al.*, 1941). Its 'ideal' version (assuming that the molar free energy of flow is a linear function of the molar free energies of the pure components of the mixture) is independent of any parameter and takes the form:

$$\ln(\eta \cdot V) = x_1 \cdot \ln(\eta_1 \cdot V_1) + x_2 \cdot \ln(\eta_2 \cdot V_2) \qquad (3.47)$$

where η, V and x represent viscosity, molar volume and molar fraction, respectively, either for the mixture (if no subscript) or for any of the pure components (subscripts 1 and 2).

Surface tension

A series of methods have been proposed for the prediction of surface tension in mixtures. The Macleod-Sugden method (Poling *et al.*, 2001), one of the most popular methods, does also require, however, knowledge of the density for the specific mixture. The method proposed by Suárez *et al.* (1989) requires, for non-aqueous mixtures, knowledge of critical values. In the case of ionic liquids, these critical values are difficult to determine experimentally, and very limited information is available at present. Other methods are exclusively applicable to aqueous mixtures. Therefore, for mixtures of ionic liquids, and relying exclusively on properties of pure components, a possibility is to adapt equations 3.45 and 3.47, in a totally empirical

approach, to the case of surface tension instead of viscosity. This adaption yields the following expressions:

$$\ln\sigma = x_1 \cdot \ln\sigma_1 + x_2 \cdot \ln\sigma_2 \tag{3.48}$$

$$\ln(\sigma \cdot V) = x_1 \cdot \ln(\sigma_1 \cdot V_1) + x_2 \cdot \ln(\sigma_2 \cdot V_2) \tag{3.49}$$

Often, a general form like the following can also be chosen:

$$\sigma^r = \sum_i^n x_i \cdot \sigma_i^r \tag{3.50}$$

where, in mixtures with a non-linear behaviour, the exponent *r* does typically range between -1 and -3 (Poling *et al.*, 2001). Taking *r* = -1, for a binary mixture, equation 3.50 becomes:

$$\frac{1}{\sigma} = \frac{x_1}{\sigma_1} + \frac{x_2}{\sigma_2} \tag{3.51}$$

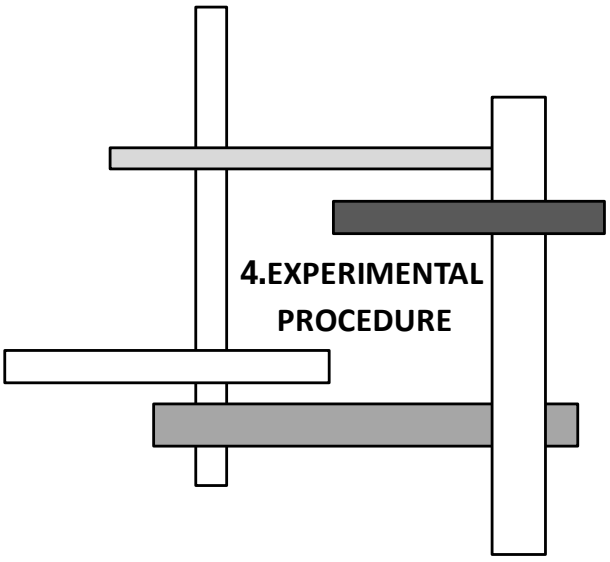

4.EXPERIMENTAL PROCEDURE

4. EXPERIMENTAL PROCEDURE

4.1 Chemicals

4.1.1. Carbon dioxide

Pure carbon dioxide with a nominal purity of 99.99 %, was supplied by Praxair as a liquefied gas cylinder at a pressure of 200 bar. A pressure regulator was coupled to this cylinder, to supply the gas at a moderate pressure to the experimental device (see section 4.2.1.1).

4.1.2. Ionic liquids

Most ionic liquids used in the experiments were synthesised and purified in-house. The only exception was 1-ethyl-3-methylimidazolium acetate ([C_2C_1im][OAc]), which was purchased from Iolitec, GmbH (Heilbronn, Germany), with a nominal purity greater than 95 %, and purified under high vacuum prior to use, as described below for the other ionic liquids. The chemical structures of all the ionic liquids involved in this work are shown in Figure 4.1.

4.1.2.1. Synthesis

1-Ethyl-3-methylimidazolium ethylsulfate ([C_2C_1im][$EtSO_4$]):

This ionic liquid was synthesised by direct alkylation of 1-methylimidazole (Aldrich, 99 %) with diethylsulfate (Fluka, ≥99 %) in absence of solvent, following the procedure reported by Ficke *et al.* (2008). A three-necked round-bottomed flask with 1-methylimidazole was placed in an ice bath, with magnetic stirring and a reflux condenser attached, under argon atmosphere (Praxair, 99.999 %). The experimental setup is shown in Figure 4.2. An equimolar amount of diethylsulfate was added into the flask slowly, to avoid a drastic increase in the system temperature due to the high exothermic character of the alkylation reaction. The mixture was stirred while

allowing the ice in the bath to melt and to reach room temperature. After that, the water bath was replaced with a silicon oil bath, and the temperature was gradually increased to 343 K. The mixture was kept at these conditions for 12 h, to ensure completion of the reaction.

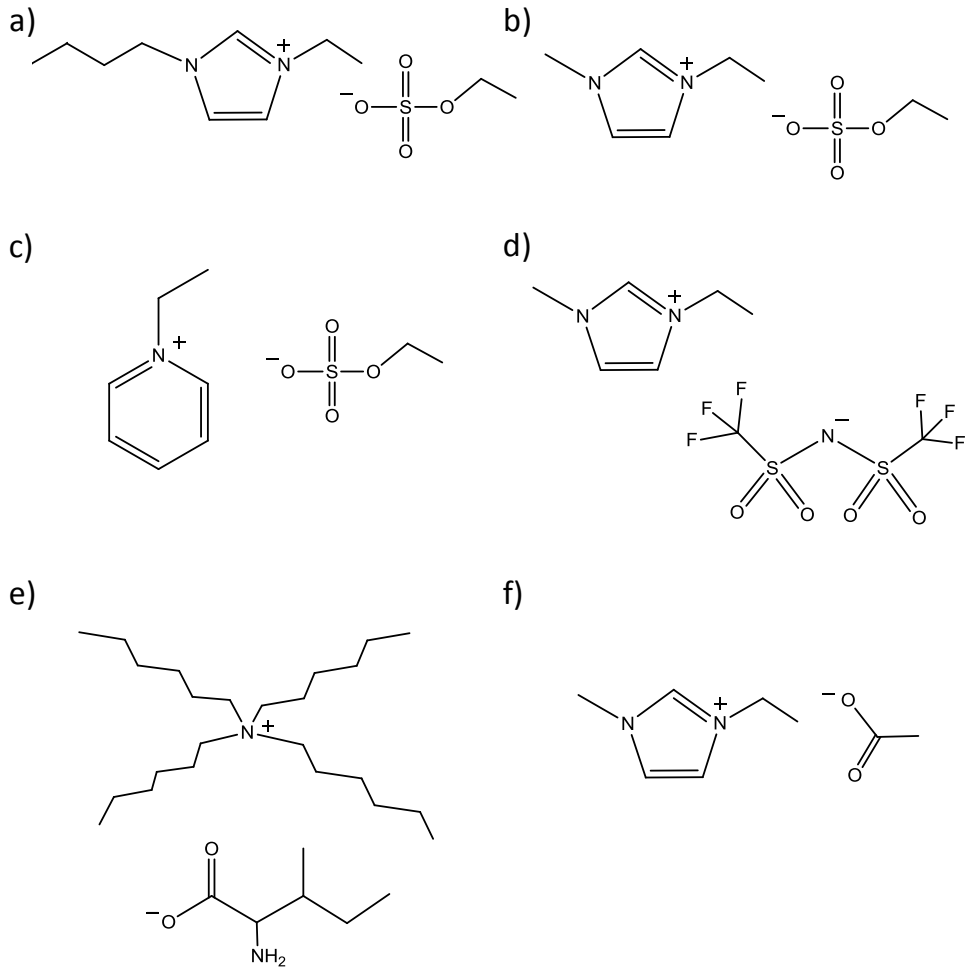

Figure 4.1: Chemical structures of ionic liquids: a) 1-butyl-3-ethylimidazolium ethylsulfate ($[C_4C_2im][EtSO_4]$); b) 1-ethyl-3-methylimidazolium ethylsulfate ($[C_2C_1im][EtSO_4]$); c) 1-ethylpyridinium ethylsulfate ($[C_2py][EtSO_4]$); d) 1-ethyl-3-methylimidazolium bis(trifluoromethylsulfonyl)amide ($[C_2C_1im][NTf_2]$); e) tetrahexylammonium isoleucine ($[N_{6666}][Ile]$); f) 1-ethyl-3-methylimidazolium acetate ($[C_2C_1im][OAc]$).

Figure 4.2: Typical experimental setup for in-house synthesis of ionic liquids.

The resulting liquid was subjected to soft vacuum distillation in a Büchi R-200 rotary evaporator (Figure 4.3a) for 4 h at 343 K, for preliminary elimination of residual volatile compounds. Then, it was placed in a high vacuum setup (Figure 4.3b), attached to an Edwards RV3 vacuum pump, for *ca*. 48 h while being stirred and heated at *ca.* 343 K, to complete the removal of unreacted starting materials and other volatile impurities that might be present. The vacuum pump provided a nominal vacuum of 10^{-3} mbar, but due to small losses throughout the setup, the vacuum to which the ionic liquid sample was exposed is estimated to be lower than 0.05 mbar (as verified with a portable Vacuubrand DCP 3000 vacuum meter).

Figure 4.3: Devices for the purification stages in the synthesis of ionic liquids: a) Büchi R-200 rotary evaporator; b) high vacuum purification setup.

1-Butyl-3-ethylimidazolium ethylsulfate ([C_4C_2im][$EtSO_4$]):

Its synthesis was completely analogous to that described above for [C_2C_1im][$EtSO_4$], but in this case alkylating 1-butylimidazole (Aldrich, 98 %) with diethylsulfate (Fluka, ≥99 %).

1-Ethylpyridinium ethylsulfate ([C_2py][$EtSO_4$]):

Its synthesis was completely analogous to that described above for [C_2C_1im][$EtSO_4$], but in this case alkylating pyridine (Riedel-de Haën, >99.5 %) with diethylsulfate (Fluka, ≥99 %).

1-Ethyl-3-methylimidazolium bis(trifluoromethylsulfonyl)amide ([C_2C_1im][NTf_2]):

The synthesis of [C_2C_1im][NTf_2] was performed in two steps. The first one consisted of the alkylation of 1-methylimidazole (Aldrich, 99 %) with an excess of bromoethane (Sigma-Aldrich, 98 %), in the absence of any external solvent, using the same procedure as in the synthesis of the ionic liquids previously described. In a second step, the 1-ethyl-3-methylimidazolium bromide thus formed was dissolved in water, and a metathetic reaction was carried out by mixing it with an aqueous solution of lithium bis(trifluoromethylsulfonyl)amide (Solvionic, +99 %) in a slight stoichiometric excess of *ca*. 5 %, at room temperature. The mixture was left to stir for up to 4 h, although formation of the desired hydrophobic ionic liquid was immediately noticeable upon mixing of the aqueous solutions. Dichloromethane (Fluka, ≥99.9 %) was added to facilitate the separation of [C_2C_1im][NTf_2] (in the organic phase) from the spectator ions Li^+ and Br^- (in the aqueous phase). The organic phase was washed with fresh water several times, until no precipitation was observed upon addition of some drops of aqueous solution of $AgNO_3$ (Fluka, ≥99.0 %) to the discarded washings. This guaranteed the absence of spectator ions in relevant concentrations in the final ionic liquid sample.

The washed organic phase was placed in a rotary evaporator for removal of the dichloromethane, and the purification was completed by connecting the ionic liquid under high vacuum, as previously described for [C_2C_1im][$EtSO_4$].

Tetrahexylammonium isoleucine ([N_{6666}][Ile]):

The synthesis of [N_{6666}][Ile] was carried out following the method described by Jiang *et al*. (2008). A *ca*. 40 % solution of tetrahexylammonium hydroxyde (Aldrich) was mixed at room temperature with a slight excess of the amino acid *L*-isoleucine (Sigma-Aldrich, ≥98 %) dissolved in water, to obtain the desired ionic liquid via a neutralisation reaction. The mixture was stirred for 4 h, and subsequently the water was removed first by rotary evaporation at 333 K and later under high vacuum (<0.05 mbar) for *ca.* 48 h while stirred and heated at *ca.* 333 K. The resulting liquid was dissolved in ethanol (Panreac, ≥99.8 %) to precipitate the amino acid in excess, which was filtered off. Finally, the ethanol was removed by rotary evaporation, and the purification was completed under high vacuum, as with the above ionic liquids.

4.1.2.2. Characterisation

The chemical identity and absence of relevant levels of impurities in the synthesised ionic liquids were confirmed by ^{1}H and ^{13}C nuclear magnetic resonance (NMR) spectroscopy (Figure 4.4a). The corresponding spectra are presented in Appendix A.

Water is a ubiquitous impurity in ionic liquids, which are inherently hygroscopic. The water content of an ionic liquid can critically affect its properties and performance (Seddon *et al*., 2000; Anthony *et al*., 2001; Blanchard *et al*., 2001; Cammarata *et al*., 2001; Menjoge *et al*., 2009; Husson *et al*., 2010; Zhao *et al*., 2010; Stevanovic *et al*., 2012). Therefore, it is important to work with ionic liquid samples with their water content well characterised and kept to a low level. The water content of the samples herein synthesised was measured by means of the Karl-Fischer titration method in a Metrohm 737 KF coulometer (Figure 4.4b). The values obtained were below in masss fraction of 0.04 in all cases, except for [C_2C_1im][OAc] and [N_{6666}][Ile], for which it was 0.09 (Table 4.1).

The ionic liquids were stored in desiccators under soft vacuum until use, to avoid moisture uptake from the ambient air. For further verification of the batches prepared, selected physical properties of the synthesised ionic liquids were experimentally measured at 298.15 K, as described in section 4.2.3, and compared

with selected values taken from the literature. The comparative values are reported in Table 4.1. A good match between the experimental and literature data sets is observed.

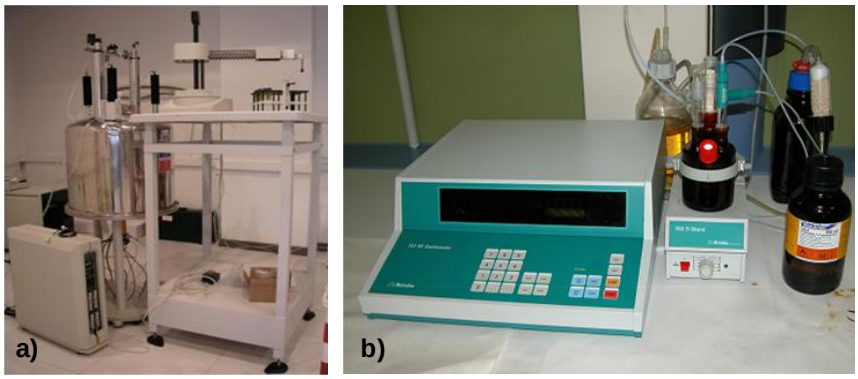

Figure 4.4: Equipment for the characterisation of ionic liquids: a) Varian Mercury 300 NMR spectrometer; b) Metrohm 737 KF coulometer.

Table 4.1: Water mass fraction (ω_{H2O}) and experimental density (ρ), viscosity (η), and surface tension (σ) for the ionic liquids used. A comparison of the experimental values of physical properties with literature data is provided.

Ionic liquid	ω_{H2O}	ρ / g·cm^{-3}		η / mPa·s		σ / mN·m^{-1}	
		Exp.	Lit.	Exp.	Lit.	Exp.	Lit.
$[C_2C_1im][EtSO_4]$	0.01	1.23893	1.2392[a,*] 1.2411[b] 1.23763[c] 1.2383[d]	100.6	101.4[a,*] 97.58[c]	48.6	45.43[b] 46.967[c]
$[C_4C_2im][EtSO_4]$	0.03	1.15188	---	255.2	---	38.8	---
$[C_2py][EtSO_4]$	0.02	1.26277	1.252[e]	143.0	126.3[f] 137[g]	50.0	---
$[C_2C_1im][NTf_2]$	0.01	1.51887	1.5178[a,*] 1.5187[b] 1.5193[h]	32.55	34.24[a,*] 32.46[h]	36.6	35.71[b] 36.68[i,**]
$[C_2C_1im][OAc]$	0.09	1.09904	1.09968[j] 1.0993[k] 1.100[l,*]	138.4	143.6[k] 144.4[l,*]	40.6	42.9[m]
$[N_{6666}][Ile]$	0.09	0.90623	---	---	---	---	---

[a] Jacquemin *et al.*, 2006; [b] Wandschneider *et al.*, 2008; [c] Gómez *et al.*, 2006; [d] Rilo *et al.*, 2012; [e] Gómez *et al.*, 2010; [f] González *et al.*, 2009; [g] Crosthwaite *et al.*, 2005; [h] Schreiner *et al.*, 2010; [i] Carvalho *et al.*, 2008; [j] Fröba *et al.*, 2010; [k] Freire *et al.*, 2011; [l] Stevanovic *et al.*, 2012; [m] Quijada-Maldonado *et al.*, 2012.

** Value calculated by means of a correlation equation presented in the referenced article.*

*** Value calculated by linear interpolation from the experimental data reported in the referenced article.*

4.1.3. Supported ionic liquids phase (SILP)

A solid-supported ionic liquid, or supported ionic liquid phase (SILP), was prepared with a 40 % load of the ionic liquid [N_{6666}][Ile], using mesoporous silica gel (Fluka, pore size 60 Å) as a solid support. The silica was previously calcined in a vacuum furnace at 873 K for 6 h.

The ionic liquid was placed in a round-bottomed flask and dissolved in acetonitrile (Sigma-Aldrich, 99.8 %), with constant stirring at room temperature. The silica was then added, and the heterogeneous mixture was thoroughly stirred for 24 h at room temperature. Subsequently, the solvent was primarily removed in a rotary evaporator, and purification was completed by eliminating residual volatile species under high vacuum (<0.05 mbar) for *ca.* 24 h at room temperature.

4.2. Equipment and procedure

4.2.1. Absorption of carbon dioxide

4.2.1.1. Magnetic suspension balance

The solubility of carbon dioxide was measured using a Rubotherm magnetic suspension balance, Metal model (Figure 4.5), which allows the determination of absorption-desorption isotherms of gases with continuous monitoring of the weight, pressure, and temperature of the system.

The fundamental part of this apparatus is a microbalance with an accuracy of ±10 μg. Its operation is based on having the sample hung from a permanent magnet, which is suspended by the action of another fixed electromagnet attached to the balance. Thus, the weight of the sample can be transmitted without mechanical contact between the measuring chamber (pressurised and/or at a specific set temperature) and the microbalance (at ambient pressure and temperature). A functioning scheme of the magnetic suspension balance, with particular attention to the microbalance and the measuring chamber, is shown in Figure 4.6.

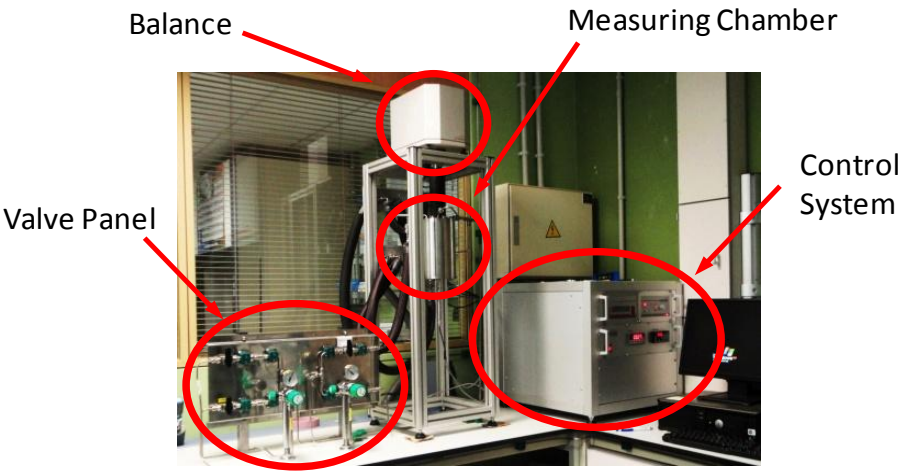

Figure 4.5: Rubotherm magnetic suspension balance, Metal model, installed in place for operation.

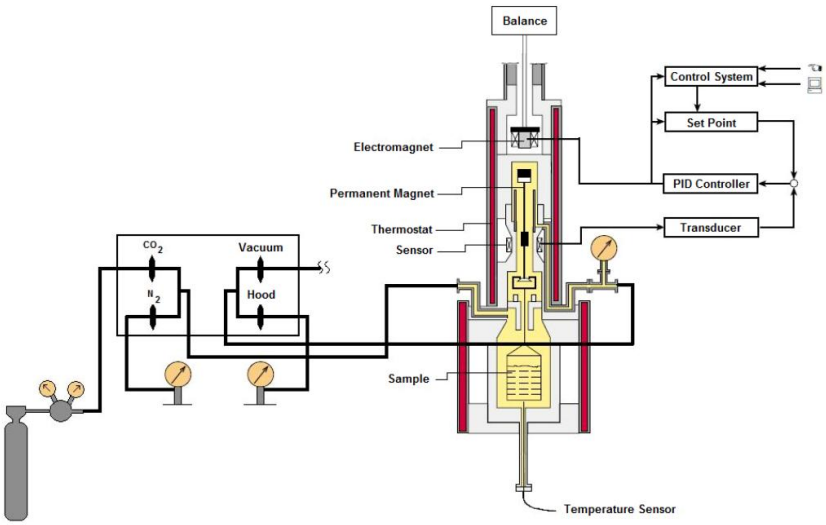

Figure 4.6: Functional diagram of the magnetic suspension balance.

The measuring chamber has a pressure-resistant jacketed metal cover which permits the maintenance of isothermal conditions during the solubility measurements. This was achieved by circulation, through the jacket, of water from a Huber Ministat 230 thermostat with heating and cooling capacity for a more efficient temperature control.

For determination of absorption/desorption isotherms with the magnetic suspension balance, the mass and volume of the small bucket where the sample is placed must be known. These values were obtained *via* a pseudo-absorption experiment, using the empty bucket, with no sample. Starting from vacuum, pressure was increased stepwise using an inert gas: nitrogen (Praxair, 99.995 %). At each step, and at a constant temperature of 298.2±0.3 K, the pressure and the mass measured by the balance at equilibrium (m_{bal}) were recorded. The equilibrium criterion used was a variation lower than 10 μg over a period of 10 min. The mass read by the balance is the difference between the real mass of the empty bucket (m_r) and the buoyancy acting on it. Since the buoyancy is the product of the bucket volume (V_r) and the density of the gaseous phase (ρ_{gas}), then the following expression can be written:

$$m_{bal} = m_r - \rho_{gas} \cdot V_r \qquad (4.1)$$

Therefore, the mass and volume of the sample bucket can be obtained by means of a linear fit of the plot of m_{bal} values against ρ_{gas} values. The density of the gas phase at each pressure-temperature conditions was obtained from the NIST Chemistry WebBook (web reference). Plotting the m_{bal} values against the density of nitrogen, the expected straight line with a negative slope was obtained (the mass read by the balance decreases with increasing gas pressure –or density– due to the buoyancy that acts on the sample bucket). By means of a least-squares linear regression, both m_r and V_r were obtained (from the intercept and from the slope of the linear fit, respectively).

To carry out the measurement of samples, a pre-conditioning was required. This consisted of flushing the measuring chamber with inert gas (nitrogen) once the sample was loaded. Then, the chamber was vacuumed and heated to 333 K for at least 4 h, to help in further removing any residual volatiles and stabilising the weight of the

sample. After this step, the chamber was cooled or heated to the temperature set for the experiment.

Following pre-treatment of each sample in the chamber, the absorption curve was determined. CO_2 was added stepwise, at constant temperature, gradually increasing the pressure of the chamber until reaching a maximum pressure of *ca*. 16 bar. At each step, time was allowed for the sample to absorb gas until reaching the equilibrium. The equipment monitors continuously (a reading every 20 s) the temperature and pressure of the system, as well as the mass in the balance. As in the case of the blank test with inert gas, the equilibrium criterion was taken as a variation lower than 10 μg in the recorded mass of the balance over a period of 10 min. It is important to correct the value of the mass of sample at equilibrium for the effect of buoyancy:

$$m_{corr} = m_{bal} + \rho_{CO_2} \cdot V_{r+s} \tag{4.2}$$

where m_{corr} represents the corrected sample mass, m_{bal} is the mass read by the balance, V_{r+s} corresponds to the volume of the sample and the bucket together, and ρ_{CO2} is the density of the gaseous CO_2. With the corrected value of the mass, the mass of the sample (*i.e.*, the ionic liquid, or SILP, plus the absorbed gas) can be calculated by simple subtraction of the mass of the empty bucket (m_r):

$$m = m_{corr} - m_r \tag{4.3}$$

where m is the mass of ionic liquid (or SILP) with absorbed gas. To obtain the mass of the absorbed gas at each step, the mass of the starting sample (pure ionic liquid or SILP) must be subtracted. By combination of equations 4.2 and 4.3, and taking into account that the mass of the starting sample used for calculations is measured by the equipment at time zero, the following expression is obtained after algebraic operations:

$$m_0 = \frac{m_{bal_0} + \rho_{CO_2} \cdot V_r - m_r}{1 - \dfrac{\rho_{CO_2}}{\rho_s}} \tag{4.4}$$

where m_0 is the initial mass of the ionic liquid (or SILP), m_{bal0} is the mass given by the equipment at time zero, and ρ_{CO2} and ρ_s correspond to the densities of gaseous CO_2 and of the sample (ionic liquid or SILP), respectively.

To determine the desorption curves, the temperature was kept constant and the pressure was decreased stepwise, in a similar fashion to the procedure for the determination of the absorption isotherm, allowing the absorbed gas to gradually desorb. The same equilibrium criterion was maintained.

Since it was not possible to monitor the variation of the volume of the sample with absorbed gas during the absorption experiments, it had to necessarily be assumed that no significant variation of the volume of the sample occurred upon absorption of the gas. Although not strictly true, this assumption is supported by previous works in the literature (Blanchard *et al*., 2001; Cadena *et al*., 2004; Huang *et al*., 2005), which found that the variation caused by absorbed gas in ionic liquids was typically much lower than that occurring in other liquid absorbents.

4.2.1.2. Thermogravimetric analyser

In addition to the magnetic suspension balance, a thermogravimetric analyser was also used in the case of the SILP to determine its CO_2 absorption capacity, specifically at atmospheric pressure. A Mettler Toledo TGA/DSC 1 STAR^e System thermogravimetric analyser (TGA) was utilised (Figure 4.7), with a weight precision of 1 μg, and with a GC 100 gas controller coupled. Approximately 15 mg of sample was placed in an alumina crucible for each run.

Figure 4.7: Mettler Toledo TGA/DSC 1 STAR^e System thermogravimetric analyser.

The measurement procedure comprised three stages: drying, absorption and desorption. In the first one, the samples were dried at 373.2 K in a nitrogen gas atmosphere for 4 h, verifying that no mass change was observed in the sample mass by the end of that period. Subsequently, the absorption cycle was carried out in a CO_2 atmosphere at 298.2 K and atmospheric pressure for 200 min, enough for the sample to reach the equilibrium. Total desorption for each sample was achieved by raising the system temperature to 353.2 K for 200 min in a nitrogen gas atmosphere. The Star^e software, version 11, was used for treatment of the generated data.

4.2.2. Thermal properties

4.2.2.1. Thermal stability

Decomposition temperatures of the ionic liquids and SILP were measured with a TA Instruments Q500 thermogravimetric analyser (TGA) with a weight precision of ±0.01 % (Figure 4.8). All runs were carried out under an inert atmosphere of nitrogen. Approximately 20 μg of sample was placed in an aluminium pan, and it was initially heated at a rate of 10 K/min from room temperature to 373 K, holding it at this temperature for 40 min to help in removing water and other volatile compounds that might be present. After that, the decomposition curve was performed by heating the sample at a rate of 5 K/min up to 823 K.

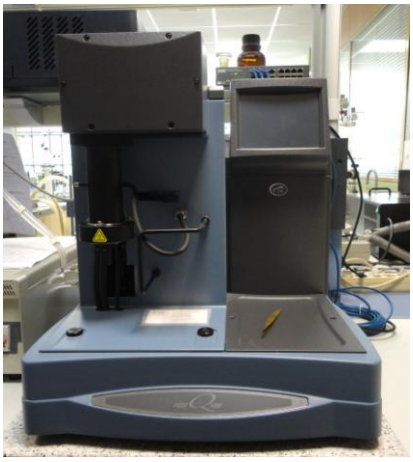

Figure 4.8: TA Instruments Q500 thermogravimetric analyser.

The TA Universal Analysis 2000 software, version 4.5A, was used for treatment of the generated thermograms. In plots of percent of sample mass versus temperature, the 5 % onset decomposition temperature was calculated (Figure 4.9) as the temperature at the intersection of the extrapolation of the original base line (after the isotherm at 373 K) and a tangent line to the point where a 5 % loss of the initial mass occurred (considering as initial mass the one right after the isothermal step at 373 K).

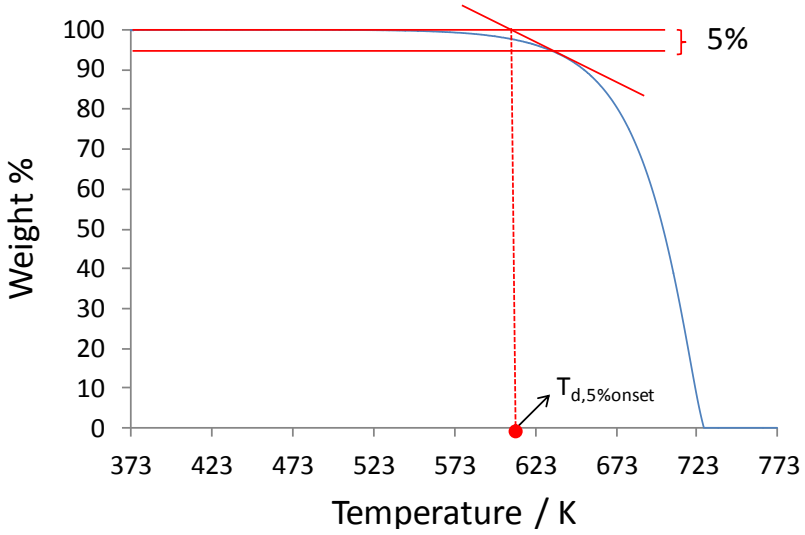

Figure 4.9: Schematic representation of the calculation of the 5% onset decomposition temperature on a TGA thermogram.

4.2.2.2. Phase transitions

Phase transitions in condensed phase were determined in a TA Instruments Q2000 differential scanning calorimeter (DSC), equipped with a TA Refrigerated Cooling System 90 unit, and with a temperature accuracy of ±1 K (Figure 4.10). A nitrogen atmosphere was used in all runs. Approximately 15 μg of sample was encapsulated in aluminium hermetic pans with lids of the same material, and loaded into the measuring chamber by means of an autosampler. Heating and cooling rates of 2 K/min were used, completing two full cycles, in the temperature range 183-293 K. Although the lower temperature limit in the ramps was 183 K, the baseline was observed to lose its stability below *ca*. 200 K, due to cooling limitations of the apparatus. Therefore, the portion of the thermograms below 200 K was

systematically disregarded in the identification of possible thermal events of the samples.

Figure 4.10: TA Instruments Q2000 differential scanning calorimeter.

The same software than for the TGA curves (see section 4.2.2.1) was used in evaluating the DSC curves. Due to the peculiar behaviour of ionic liquids, often showing widely spread peaks in the thermograms without a well defined onset, the reported melting and crystallisation temperatures were considered at the maxima of the peaks. A schematic representation of a typical DSC thermogram is presented in Figure 4.11.

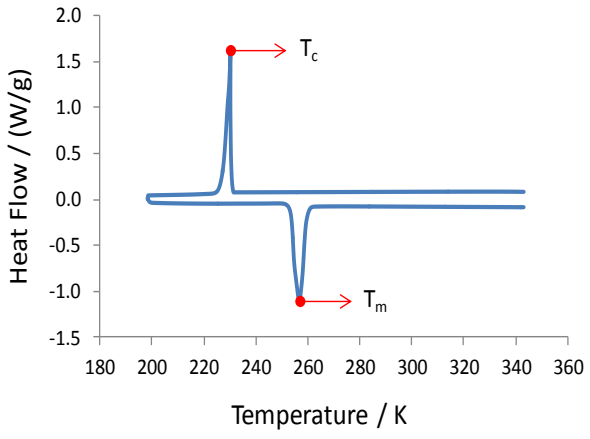

Figure 4.11: Schematic representation of a typical DSC curve (one cooling-heating complete cycle). T_c: crystallisation temperature; T_m: melting temperature.

4.2.3. Physical properties

4.2.3.1. Density

Density measurements were made in an Anton Paar DMA 5000 oscillating U-tube density meter, with an uncertainty of $\pm 3 \times 10^{-5}$ g·cm^{-3}, and with automatic correction for the viscosity of the sample (Figure 4.12). The temperature was controlled internally with high precision (±0.001 K), assisted by two integrated Pt 100 platinum thermometers. For calibration of the apparatus, air and degassed bidistilled water were used. To obtain each value, two measurements were performed with different samples, at atmospheric pressure. If the results did not agree within the uncertainty, new samples were prepared and measured.

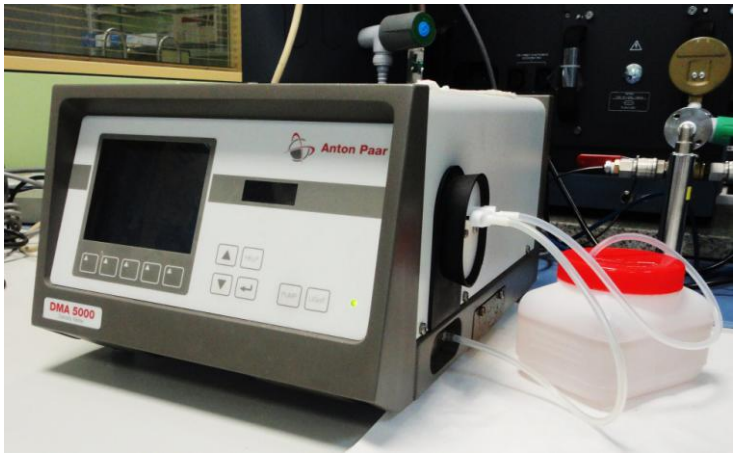

Figure 4.12: Anton Paar DMA 5000 density meter.

4.2.3.2. Viscosity

Kinematic viscosities were determined using micro-Ubbelohde capillary viscometers manufactured by Schott (Figure 4.13). Depending on the viscosity of the sample, capillaries of different diameters (from type I to type III according to the classification by the manufacturer) were used, in order to provide flow times of the samples in the specified range for each capillary. All capillaries were calibrated and certified by the manufacturer. Flow times were measured with a resolution of 0.01 s in a Lauda PVS1 Processor Viscosity system, which incorporates a photoelectric cell. The temperature

was kept constant during the measurements by means of a Lauda D20 KP clear view thermostat with a Lauda DLK 10 through-flow cooler attached (Figure 4.13).

Figure 4.13: Example of micro-Ubbelohde capillary viscometer (left), and PVS1 systems partially immersed in a Lauda D20 KP clear view thermostat with a Lauda DLK 10 through-flow cooler attached (right).

Measurements were repeated at least three times for each sample; or a fourth time if a standard deviation greater than 0.1 s was achieved, discarding the outlier value. An average flow time was concluded in each case, and the kinematic viscosity was obtained multiplying this value by the calibration constant of the capillary viscometer used. Dynamic viscosities (η) were finally calculated as:

$$\eta = \rho \cdot \nu \tag{4.5}$$

where ρ is the density, and ν is the kinematic viscosity. An uncertainty of ±0.5 % is estimated for the values of η. The viscosity of two different samples was determined, and the results were checked to meet the reported uncertainty; otherwise, new samples were prepared for additional measurements.

4.2.3.3. Surface tension

Surface tensions were measured in a Krüss K11 tensiometer by means of the Wilhelmy plate method (Figure 4.14). A platinum 'plate' folded in a cylindrical shape (Krüss accessory reference PL22), especially adapted to perform measurements with small amounts of sample, was used (Figure 4.14). The dimensions of the plate were

2.0 mm long × 1.0 mm height × 0.1 mm width. The sample containers were of cylindrical form, made of glass, with a diameter of 30 mm, sufficient to avoid influence of wall effects in the measurements. The temperature of the samples, monitored by a built-in thermometer with a resolution of 0.1 K, was kept constant by means of an oil bath controlled by circulating water from a Selecta Frigiterm cryogenic thermostat. The surface tension measurements were made for two different samples, and an uncertainty of 0.3 $mN \cdot m^{-1}$ was typically obtained.

Figure 4.14: Krüss K11 tensiometer (left) and platinum 'plate' folded in a cylindrical shape to perform measurements with smaller amounts of sample (right).

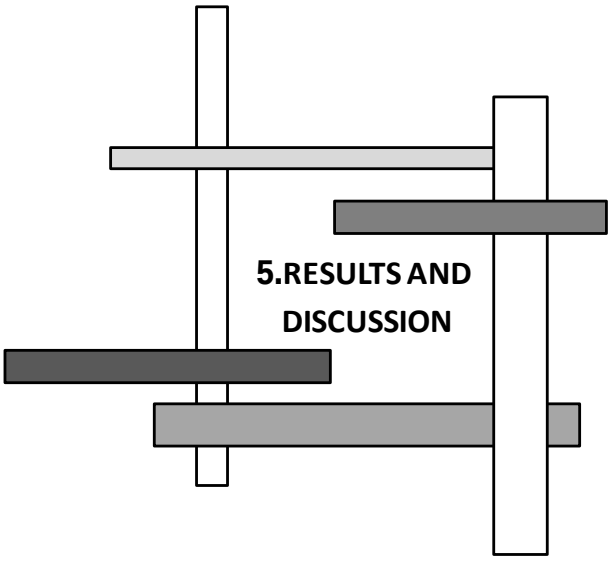

5.RESULTS AND DISCUSSION

5. RESULTS AND DISCUSSION

An important number of ionic liquids have been tested to date for their capacity to absorb carbon dioxide. Most studies on the matter have focused on individual ionic liquids in pure liquid state, establishing connections and trends between their constitutive ions (and associated structural features) and the mechanism and extent to which they can absorb CO_2. Still, there is substantial room for improvement of the knowledge on the tailoring of the structures of the constitutive ions of the ionic liquids to get enhanced absorbance of CO_2. Thus, in this Chapter, a first session is devoted to individual ionic liquids and the measurement of their CO_2 absorbance capacity.

Beyond the use of individual ionic liquids, alternative strategies are explored here. The second section in this Chapter is devoted to the use of mixtures of ionic liquids. Their absorption capacity as well as their thermal and physical properties are characterised as a function of composition, and in some case as a function of temperature. A final section investigates a preliminary attempt to use an amino acid-based ionic liquid supported on a mesoporous material to capture CO_2.

5.1. Pure ionic liquids

The absorption of carbon dioxide with ionic liquids has received significant attention from researchers over the last decade. Inherent advantages associated with the common characteristics of ionic liquids would be obvious for a gas absorption process in which they were used as absorbents, and they have been found to favourably absorb CO_2. Although many different ionic liquids have been tested so far, there is still an important lack of knowledge in this regard. In this Thesis, some ionic liquids were re-tested, in order to validate the technologies and experimental setups implemented; and additional ionic liquids were investigated, to expand knowledge on their behaviour and potentialities for CO_2 capture processes. The set of ionic liquids used herein comprises: $[C_2C_1im][NTf_2]$, $[C_2C_1im][EtSO_4]$, $[C_4C_2im][EtSO_4]$, $[C_2py][EtSO_4]$, and

[C_2C_1im][OAc]. This set allows analysis of the variation of the cation, of the anion, and of the absorption mechanism.

Absorption of CO_2 in all pure ionic liquids, at 298.2 K and as a function of pressure, is plotted in Figure 5.1 (the corresponding numerical data, in a molar basis, are listed in Table 5.1, and in a mass basis in Table B.1 in Appendix B). Two types of isotherm shapes are observed, as a result of the different mechanisms involved for the absorption of CO_2. For [C_2C_1im][OAc] a typical curve of chemical absorption is observed, with a rapid increase in the absorbed fraction of CO_2 at the initial pressures due to chemical absorption, followed by a strong decrease in the slope when physical absorption starts to prevail (Shiflett and Yokozeki, 2009; Stevanovic *et al*., 2012). In the case of the other ionic liquids investigated, typical curves of physical absorption are observed, with an approximately steady increment of the absorbed CO_2 with increasing pressure (Blanchard *et al*., 2001; Jalili *et al*., 2010).

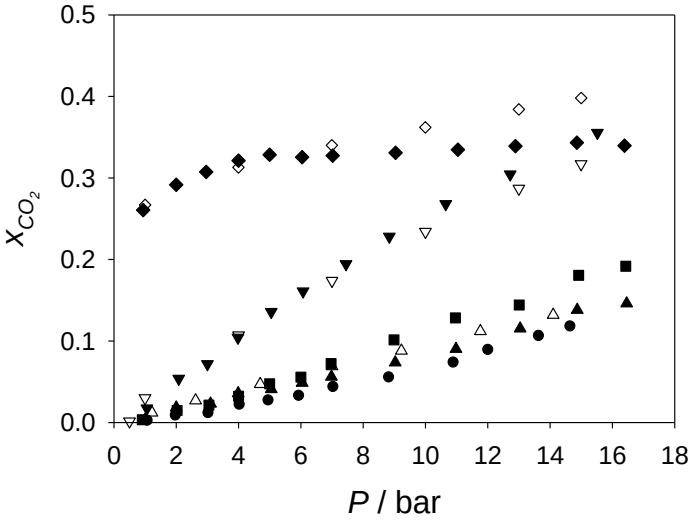

Figure 5.1: Molar fraction solubility of CO_2 (x_{CO2}), as a function of pressure (P), in pure ionic liquids at 298.2 K. Ionic liquid: ♦, [C_2C_1im][OAc], this work; ◊, [C_2C_1im][OAc] (Yokozeki *et al.*, 2008); ▼, [C_2C_1im][NTf_2], this work; ▽,[C_2C_1im][NTf_2], (Yokozeki *et al.*, 2008); ■, [C_4C_2im][$EtSO_4$], this work; ▲,[C_2C_1im][$EtSO_4$], this work; △, [C_2C_1im][$EtSO_4$], (Jalili *et al.*, 2010) (at 303 K); ●, [C_2py][$EtSO_4$], this work.

Among the ionic liquids that absorb CO_2 exclusively *via* a physical mechanism, the absorption values in the ionic liquids containing the $[EtSO_4]^-$ anion are notably lower than for [C_2C_1im][NTf_2]. The latter is a widely studied ionic liquid with a high

absorption capacity, which was chosen as a sort of benchmark ionic liquid in the construction of the mixtures of ionic liquids (see section 5.2 below). Its absorption capacity is higher as a result of having a fluorinated anion. However, it must be noted that, due to its higher molecular weight when compared to the [$EtSO_4$]-based ionic liquids, the difference in CO_2 solubility in a mass basis is not as large as it is in a molar basis.

Table 5.1: Numerical values for the absorption/desorption of CO_2 (in molar fraction, x_{CO2}) for pure ionic liquids, at 298.2 K.

[C_2C_1im][OAc]		[C_2C_1im][NTf_2]		[C_4C_2im][$EtSO_4$]		[C_2C_1im][$EtSO_4$]		[C_2py][$EtSO_4$]	
P / bar	x_{CO2}	P / bar	x_{CO2}	P / bar	x_{CO2}	P / bar	x_{CO2}	P / bar	x_{CO2}
Absorption process									
0.94	0.2606	1.06	0.0174	0.91	0.0035	1.00	0.0034	1.09	0.0019
2.00	0.2916	2.08	0.0538	2.03	0.0147	2.00	0.0182	1.99	0.0082
2.96	0.3075	3.00	0.0717	3.05	0.0214	3.10	0.0231	3.04	0.0113
4.00	0.3213	3.98	0.1043	4.00	0.0322	3.99	0.0358	4.04	0.0215
5.00	0.3284	5.05	0.1359	5.00	0.0475	5.05	0.0409	4.97	0.0268
6.04	0.3255	6.07	0.1609	6.00	0.0557	6.04	0.0486	5.95	0.0324
7.02	0.3273	7.45	0.1944	6.97	0.0723	6.98	0.0561	7.05	0.0432
9.04	0.3308	8.84	0.2282	8.99	0.1014	9.03	0.0737	8.84	0.0549
11.04	0.3347	10.65	0.2681	10.96	0.1284	10.98	0.0903	10.91	0.0732
12.89	0.3391	12.72	0.3044	13.01	0.1441	13.04	0.1152	12.02	0.0886
14.86	0.3432	15.52	0.3554	14.92	0.1806	14.87	0.1382	13.65	0.1059
16.39	0.3396			16.43	0.1917	16.46	0.1460	14.66	0.1174
Desorption process									
14.03	0.3468	13.89	0.3314	14.01	0.1889	14.05	0.1447	13.26	0.1086
12.00	0.3433	11.81	0.2962	12.12	0.1813	12.02	0.1396	11.68	0.1047
10.03	0.3397	9.87	0.2595	10.03	0.1566	9.82	0.1182	10.01	0.0964
8.01	0.3362	7.90	0.2191	8.02	0.1409	8.03	0.1019	8.02	0.0818
6.00	0.3324	6.00	0.1754	5.99	0.1116	6.08	0.0839	6.06	0.0662
4.98	0.3303	5.00	0.1514	5.00	0.1035	5.00	0.0757	4.96	0.0546
4.00	0.3281	4.01	0.1254	4.02	0.0913	4.00	0.0662	4.04	0.0474
2.99	0.3258	2.99	0.0978	3.02	0.0768	3.00	0.0546	3.00	0.0364
2.03	0.3228	2.00	0.0681	1.97	0.0666	2.01	0.0415	2.02	0.0265
1.02	0.3184	1.04	0.0383	1.02	0.0569	1.02	0.0359	1.02	0.0167

Regarding the comparative performance of the three [$EtSO_4$]-based ionic liquids, it can be seen that the ionic liquid with longer alkyl substituent chains in the cation, [C_4C_2im][$EtSO_4$], presents the highest absorption capacity. This result is in agreement with multiple studies which concluded that, for analogous ion cores, an increase in the length of the alkyl substituent leads to an increase in the CO_2 absorption capacity of the ionic liquid (Anderson *et al.*, 2007; Jacquemin *et al.*, 2007; Raeissi and Peters, 2009; Manic *et al.*, 2012a). The absorption capacity of [C_2py][$EtSO_4$] is just a little lower than that of [C_2C_1im][$EtSO_4$], and this small

difference is in agreement with the findings by other authors (Anderson *et al*., 2007; Muldoon *et al*., 2007; Supasitmongkol and Styring, 2010; Yunus *et al*., 2012). The slightly favourable capacity of $[C_2C_1im][EtSO_4]$ is possibly related to its greater steric effects with generation of a greater free volume, as a result of having two short alkyl substituents in the cation instead of the only cationic substituent of $[C_2py][EtSO_4]$. On the other hand, it must be noted that $[C_2py][EtSO_4]$ would be cheaper and more biodegradable than $[C_2C_1im][EtSO_4]$ (Docherty *et al*., 2007; Ramdin *et al*., 2012), which might compensate the difference in absorption capacity when implemented in a real, scaled-up CO_2 absorption process.

Figure 5.1 also shows comparative data from the literature for $[C_2C_1im][OAc]$, $[C_2C_1im][NTf_2]$ and $[C_2C_1im][EtSO_4]$ (Yokozeki *et al*., 2008; Jalili *et al*., 2010). There is a relatively good agreement between the data series in this work and the corresponding ones in the literature. The slight deviations observed in the case of $[C_2C_1im][NTf_2]$ and $[C_2C_1im][EtSO_4]$ can be attributed to different water content of the ionic liquid samples, or also different (although similar) temperature of the absorption experiment. However, in the case of $[C_2C_1im][OAc]$, the behaviour observed in this work is different than that described in the literature at the highest pressures. While in the work by Yokozeki *et al.* (2008) the CO_2 absorbed keeps growing with increasing pressure, in the experimental data corresponding to this Thesis, the CO_2 solubility reaches a plateau and no further increase is observed with increasing pressure. This characteristic behaviour is likely due to the formation of the solid product resulting from the chemical reaction between the gaseous CO_2 and the liquid $[C_2C_1im][OAc]$ (Figure 1.8 in section 1.4.2), which may hinder the ability to physically absorb CO_2 once the chemical reaction is nearly completed. This was previously reported by Gurau *et al.* (2011), who showed that the solidification of the product of reaction between $[C_2C_1im][OAc]$ and CO_2 depends on the water content present in the system (Figure 5.2). For the reaction at 20 bar, the resulting product was totally solidified up to water contents of 3 %. In the conditions of the experimental work carried out herein (at lower pressures of CO_2, but also at notably lower water contents below 0.2 %), probably a total solidification occurs, thus explaining the hindering of the absorption capacity above mentioned.

No previous data were found in the literature for comparison with $[C_2py][EtSO_4]$ and $[C_4C_2im][EtSO_4]$. The absorption of CO_2 in these ionic liquids is herein reported for the first time.

Figure 5.2: Resulting products from the reaction between $[C_2C_1im][OAc]$ and CO_2 at 20 bar, for various initial water contents (Gurau *et al.*, 2011). The numbers written in the vials indicate the corresponding water contents, in mass percentage.

5.2. Mixtures of ionic liquids

The CO_2 absorption capacity of the single ionic liquids investigated differs significantly. The acetate ionic liquid and the one with the fluorinated anion exhibit a good absorption capacity, whereas those based on the ethylsulfate anion have a poorer capacity. However, the latter present other advantages over the former, for example in terms of cost, toxicity, or prevention of solidification upon absorption of CO_2. Given this dichotomy, it was decided to explore combinations of ionic liquids, hoping to find some synergies from the two constitutive single ionic liquids of the mixtures. Mixtures of ionic liquids exhibiting only physical absorption of CO_2 were explored, as well as mixtures in which physical and chemical absorption of the gas are combined.

5.2.1. Mixtures with physical absorption of CO_2

The ionic liquid $[C_2C_1im][NTf_2]$ has a good absorption capacity for CO_2 among ionic liquids. Also, it presents some favourable thermal and physical properties, such as good thermal stability and relatively low viscosity. However, it also possesses a relatively high toxicity, and its cost is (and will likely remain) too high for practical application in a process at an industrial scale.

In searching for possible synergies to minimise its downsides, the investigation of the performance of mixtures of $[C_2C_1im][NTf_2]$ with different ethylsulfate ionic liquids (which do also absorb CO_2 physically) has been carried out. Ethylsulfate ionic liquids are much cheaper and less toxic (Holbrey *et al*., 2002). In particular, the following three mixtures have been explored: $[C_2C_1im][NTf_2]$ + $[C_2C_1im][EtSO_4]$, $[C_2C_1im][NTf_2]$ + $[C_4C_2im][EtSO_4]$, and $[C_2C_1im][NTf_2]$ + $[C_2py][EtSO_4]$. The performance of the mixtures has been evaluated both from the perspective of CO_2 absorption capacity and from the point of view of thermal and physical properties.

5.2.1.1. Analysis of the CO_2 absorption capacity

The absorption/desorption of CO_2 was investigated in the pure ionic liquids and in their mixtures at molar fractions (in a CO_2-free basis) of approximately 0.25, 0.50, and 0.75, at 298.2 K. The results obtained are shown in Figures 5.3 to 5.5, and the corresponding numerical data, in a molar basis, are listed in Tables 5.2 to 5.4 (the results in mass fraction are reported in Tables B.2 to B.4 in Appendix B).

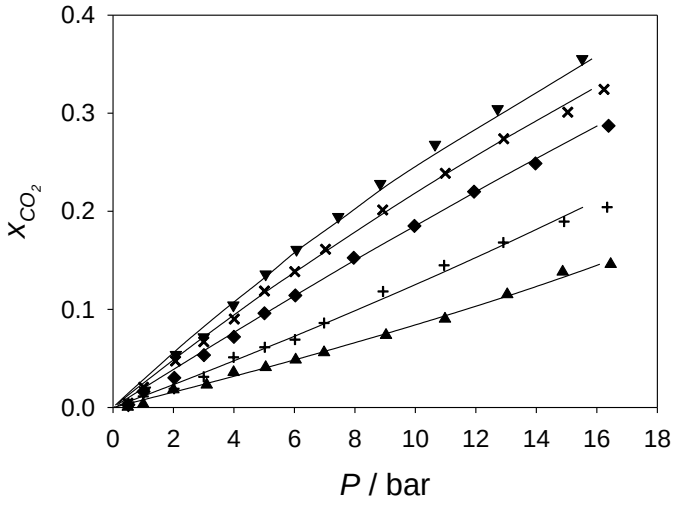

Figure 5.3: Carbon dioxide absorption (in molar fraction, x_{CO2}), at 298.2 K, in the mixture $[C_2C_1im][NTf_2]$ + $[C_2C_1im][EtSO_4]$ as a function of pressure, at different molar ratios: ▼, 100:0 (pure $[C_2C_1im][NTf_2]$); ×, 75:25; ♦, 49:51; +, 25:75; ▲, 0:100 (pure $[C_2C_1im][EtSO_4]$). Solid lines correspond to the NRTL correlation for each series.

Table 5.2: Numerical values for the absorption/desorption of CO_2 (in molar fraction, x_{CO2}) in the mixture $[C_2C_1im][NTf_2]$ + $[C_2C_1im][EtSO_4]$, at 298.2 K and as a function of the composition ratio (x'_1 stands for the molar fraction of $[C_2C_1im][NTf_2]$ in a CO_2-free basis).

$[C_2C_1im][NTf_2]$ (1) + $[C_2C_1im][EtSO_4]$ (2) + CO_2									
x'_1 = 0.0000		x'_1 = 0.2526		x'_1 = 0.4918		x'_1 = 0.7452		x'_1 = 1.0000	
P / bar	x_{CO2}	P / bar	x_{CO2}	P / bar	x_{CO2}	P / bar	x_{CO2}	P / bar	x_{CO2}
Absorption									
1.00	0.0034	1.00	0.0112	1.01	0.0162	1.01	0.0206	1.06	0.0174
2.00	0.0182	2.02	0.0190	2.03	0.0302	2.07	0.0474	2.08	0.0538
3.10	0.0231	3.00	0.0312	3.01	0.0533	3.00	0.0670	3.00	0.0717
3.99	0.0358	3.99	0.0511	4.00	0.0720	4.01	0.0901	3.98	0.1043
5.05	0.0409	5.02	0.0614	5.01	0.0960	5.01	0.1187	5.05	0.1359
6.04	0.0486	6.02	0.0692	6.03	0.1142	6.01	0.1385	6.07	0.1609
6.98	0.0561	6.98	0.0861	7.96	0.1526	7.03	0.1613	7.45	0.1944
9.03	0.0737	8.93	0.1183	9.97	0.1851	8.92	0.2014	8.84	0.2282
10.98	0.0903	10.95	0.1449	11.94	0.2200	10.99	0.2387	10.65	0.2681
13.04	0.1152	12.91	0.1682	13.97	0.2488	12.92	0.2740	12.72	0.3044
14.87	0.1382	14.92	0.1895	16.39	0.2872	15.04	0.3010	15.52	0.3554
16.46	0.1460	16.34	0.2042			16.24	0.3243		
Desorption									
14.05	0.1447	14.13	0.1929	13.02	0.2495	14.08	0.3003	13.89	0.3314
12.02	0.1396	12.02	0.1700	10.91	0.2214	12.07	0.2691	11.81	0.2962
9.82	0.1182	10.07	0.1485	9.05	0.1920	10.01	0.2355	9.87	0.2595
8.03	0.1019	8.09	0.1272	7.03	0.1611	7.99	0.1989	7.90	0.2191
6.08	0.0839	6.09	0.1023	6.01	0.1414	6.06	0.1603	6.00	0.1754
5.00	0.0757	5.01	0.0958	4.92	0.1220	5.01	0.1392	5.00	0.1514
4.00	0.0662	3.94	0.0753	4.00	0.1047	4.02	0.1168	4.01	0.1254
3.00	0.0546	3.03	0.0623	2.99	0.0852	3.00	0.0924	2.99	0.0978
2.01	0.0415	1.99	0.0487	2.01	0.0657	1.87	0.0654	2.00	0.0681
1.02	0.0359	1.04	0.0331	1.02	0.0460	1.04	0.0448	1.04	0.0383

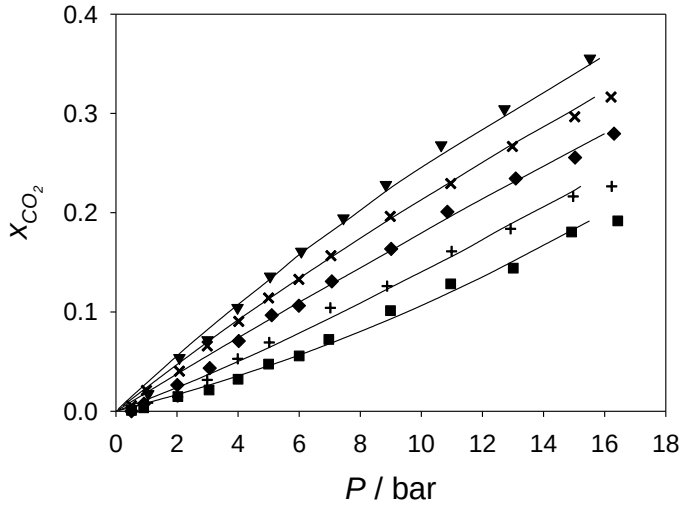

Figure 5.4: Carbon dioxide absorption (in molar fraction, x_{CO2}), at 298.2 K, in the mixture $[C_2C_1im][NTf_2]$ + $[C_4C_2im][EtSO_4]$ as a function of pressure, at different molar ratios: ▼, 100:0 (pure $[C_2C_1im][NTf_2]$); ×, 74:26; ♦, 49:51; +, 24:76; ■, 0:100 (pure $[C_4C_2im][EtSO_4]$). Solid lines correspond to the NRTL correlation for each series.

Table 5.3: Numerical values for the absorption/desorption of CO_2 (in molar fraction, x_{CO2}) in the mixture $[C_2C_1im][NTf_2]$ + $[C_4C_2im][EtSO_4]$, at 298.2 K and as a function of the composition ratio (x'_1 stands for the molar fraction of $[C_2C_1im][NTf_2]$ in a CO_2-free basis).

$[C_2C_1im][NTf_2]$ (1) + $[C_4C_2im][EtSO_4]$ (2) + CO_2									
x'_1 = 0.0000		x'_1 = 0.2361		x'_1 = 0.4885		x'_1 = 0.7434		x'_1 = 1.0000	
P / bar	x_{CO2}	P / bar	x_{CO2}	P / bar	x_{CO2}	P / bar	x_{CO2}	P / bar	x_{CO2}
Absorption									
0.91	0.0035	1.04	0.0085	0.92	0.0076	1.00	0.0209	1.06	0.0174
2.03	0.0147	2.02	0.0144	2.01	0.0264	2.08	0.0403	2.08	0.0538
3.05	0.0214	2.99	0.0316	3.07	0.0434	2.99	0.0657	3.00	0.0717
4.00	0.0322	3.99	0.0528	4.02	0.0707	4.02	0.0905	3.98	0.1043
5.00	0.0475	5.02	0.0693	5.10	0.0967	5.00	0.1141	5.05	0.1359
6.00	0.0557	7.02	0.1041	5.99	0.1063	5.99	0.1328	6.07	0.1609
6.97	0.0723	8.88	0.1260	7.07	0.1308	7.04	0.1566	7.45	0.1944
8.99	0.1014	10.99	0.1610	9.01	0.1636	8.98	0.1963	8.84	0.2282
10.96	0.1284	12.92	0.1837	10.85	0.2009	10.96	0.2294	10.65	0.2681
13.01	0.1441	14.97	0.2163	13.09	0.2344	12.98	0.2667	12.72	0.3044
14.92	0.1806	16.23	0.2266	15.03	0.2556	15.02	0.2967	15.52	0.3554
16.43	0.1917			16.31	0.2796	16.21	0.3165		
Desorption									
14.01	0.1889	14.07	0.2228	14.13	0.2626	14.14	0.2921	13.89	0.3314
12.12	0.1813	12.06	0.2001	12.29	0.2350	12.08	0.2616	11.81	0.2962
10.03	0.1566	10.04	0.1746	9.99	0.2004	10.08	0.2282	9.87	0.2595
8.02	0.1409	8.03	0.1512	8.15	0.1716	8.08	0.1925	7.90	0.2191
5.99	0.1116	6.05	0.1170	6.02	0.1331	6.06	0.1578	6.00	0.1754
5.00	0.1035	5.01	0.1012	4.96	0.1164	5.03	0.1330	5.00	0.1514
4.02	0.0913	3.99	0.0872	4.00	0.1004	4.04	0.1115	4.01	0.1254
3.02	0.0768	3.01	0.0688	2.98	0.0773	3.00	0.0882	2.99	0.0978
1.97	0.0666	2.01	0.0499	2.01	0.0574	2.00	0.0632	2.00	0.0681
1.02	0.0569	1.04	0.0325	1.03	0.0384	1.05	0.0418	1.04	0.0383

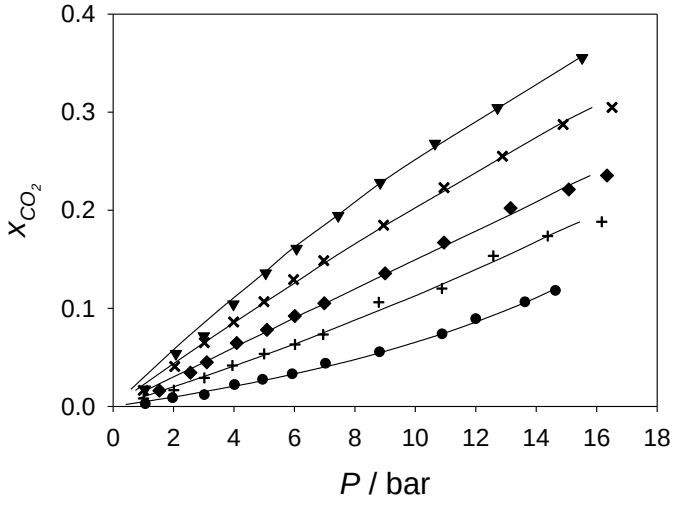

Figure 5.5: Carbon dioxide absorption (in molar fraction, x_{CO2}), at 298.2 K, in the mixture $[C_2C_1im][NTf_2]$ + $[C_2py][EtSO_4]$ as a function of pressure, at different molar ratios: ▼, 100:0 (pure $[C_2C_1im][NTf_2]$); ×, 74:26; ♦, 49:51; +, 25:75; ●, 0:100 (pure $[C_2py][EtSO_4]$). Solid lines correspond to the NRTL correlation for each series.

Table 5.4: Numerical values for the absorption/desorption of CO_2 (in molar fraction, x_{CO2}) in the mixture $[C_2C_1im][NTf_2]$ + $[C_2py][EtSO_4]$, at 298.2 K and as a function of the composition ratio (x'_1 stands for the molar fraction of $[C_2C_1im][NTf_2]$ in a CO_2-free basis).

$[C_2C_1im][NTf_2]$ (1) + $[C_2py][EtSO_4]$ (2) + CO_2									
x'_1 = 0.0000		x'_1 = 0.2505		x'_1 = 0.4894		x'_1 = 0.7441		x'_1 = 1.0000	
P / bar	x_{CO2}	P / bar	x_{CO2}	P / bar	x_{CO2}	P / bar	x_{CO2}	P / bar	x_{CO2}
Absorption									
1.09	0.0019	1.01	0.0081	1.53	0.0160	1.00	0.0163	1.06	0.0174
1.99	0.0082	2.01	0.0165	2.56	0.0343	2.04	0.0407	2.08	0.0538
3.04	0.0113	3.02	0.0291	3.10	0.0450	3.02	0.0650	3.00	0.0717
4.04	0.0215	3.95	0.0417	4.09	0.0646	3.99	0.0861	3.98	0.1043
4.97	0.0268	5.00	0.0536	5.09	0.0780	4.99	0.1068	5.05	0.1359
5.95	0.0324	6.02	0.0632	6.01	0.0921	5.97	0.1293	6.07	0.1609
7.05	0.0432	6.95	0.0733	6.99	0.1052	6.97	0.1486	7.45	0.1944
8.84	0.0549	8.79	0.1062	9.00	0.1357	8.95	0.1848	8.84	0.2282
10.91	0.0732	10.88	0.1202	10.95	0.1670	10.95	0.2230	10.65	0.2681
12.02	0.0886	12.58	0.1535	13.15	0.2021	12.88	0.2550	12.72	0.3044
13.65	0.1059	14.38	0.1737	15.08	0.2212	14.89	0.2875	15.52	0.3554
14.66	0.1174	16.17	0.1882	16.34	0.2354	16.51	0.3049		
Desorption									
13.26	0.1086	13.92	0.1801	15.31	0.2350	14.10	0.2821	13.89	0.3314
11.68	0.1047	12.01	0.1575	13.57	0.2218	12.2	0.2528	11.81	0.2962
10.01	0.0964	10.00	0.1415	11.62	0.1960	9.15	0.2045	9.87	0.2595
8.02	0.0818	7.94	0.1144	9.53	0.1676	7.96	0.1833	7.90	0.2191
6.06	0.0662	5.95	0.0889	7.55	0.1397	6.10	0.1479	6.00	0.1754
4.96	0.0546	4.99	0.0845	6.52	0.1240	5.00	0.1267	5.00	0.1514
4.04	0.0474	4.02	0.0657	5.51	0.1094	4.01	0.1052	4.01	0.1254
3.00	0.0364	3.00	0.0524	4.52	0.0928	3.00	0.0826	2.99	0.0978
2.02	0.0265	2.02	0.0376	2.48	0.0578	1.99	0.0586	2.00	0.0681
1.02	0.0167	1.02	0.0316	0.98	0.0319	1.04	0.0346	1.04	0.0383

In all three studied mixtures, an increase of the concentration of $[C_2C_1im][NTf_2]$ in the ionic liquid mixture causes an increase of its absorption capacity. Also, this capacity is increased with increasing pressure. In any case, none of the mixtures investigated exhibits a higher absorption capacity than pure $[C_2C_1im][NTf_2]$.

A quantitative analysis and useful insight for comparison is possible by means of the corresponding Henry constants (H) from the absorption isotherms. It was considered that, up to a pressure of *ca*. 10 bar, a fairly linear dependency of solubility with pressure (as presumed by Henry's law) could be reasonably assumed. Thus, the H values (Table 5.5) were calculated as the inverse of the slopes of the linear fits of the solubility-versus-pressure plots using the data points within the mentioned pressure range (equation 3.17).

Tabla 5.5: Henry constants (*H*) calculated from the CO_2 absorption data at 298.2 K in the mixture $[C_2C_1im][NTf_2]$ + [Cat][$EtSO_4$] (where $[Cat]^+$ = $[C_2C_1im]^+$, $[C_4C_2im]^+$, or $[C_2py]^+$), as a function of the composition of the ionic liquid mixture.

$[EtSO_4]^-$ ionic liquid	$x_{[C2C1im][NTf2]}$	*H* / bar
$[C_2C_1im][EtSO_4]$	0.0000	119
	0.2526	74.1
	0.4918	49.8
	0.7452	43.5
	1.0000	37.0
$[C_4C_2im][EtSO_4]$	0.0000	82.6
	0.2361	60.6
	0.4885	50.3
	0.7434	44.6
	1.0000	37.0
$[C_2py][EtSO_4]$	0.0000	145
	0.2505	81.3
	0.4894	62.9
	0.7441	46.9
	1.0000	37.0

As expected, the values for the Henry constants decrease as the concentration of $[C_2C_1im][NTf_2]$ increases, which is in agreement with the increase observed in the absorption capacity. A strong effect on the Henry constants is observed when replacing the anion $[NTf_2]^-$ by $[EtSO_4]^-$. The variation of the cation also has a influence, as well as the variation of the length of their alkyl substituent chains.

In Figure 5.6, the *H* values are plotted as a function of the composition of the binary mixtures. A synergistic effect on the absorption capacity of the intermediate compositions can be inferred from the nonlinear behaviour with a convex shape. The latter means that a larger amount of CO_2 can be solubilised than the amount corresponding to the 'ideal' linear average of the solubilities in the pure ionic liquids. Thus, the mixtures of ionic liquids, even though always having a lower CO_2 absorption capacity than the pure ionic liquid with the highest capacity of the two ($[C_2C_1im][NTf_2]$), might be a preferred absorbent in a real process if it led, simultaneously, to a better combination of sustainability and more favourable processing properties.

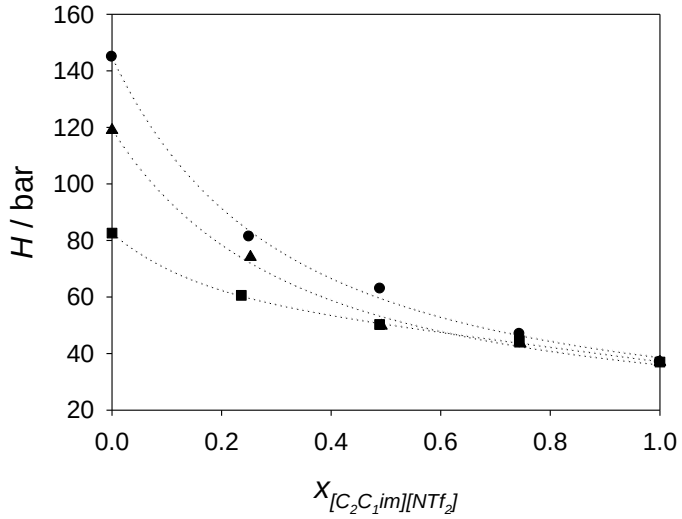

Figure 5.6: Henry constants, at 298.2 K, for CO_2 absorption in the mixtures of ionic liquids, as a function of the molar fraction of $[C_2C_1im][NTf_2]$. Ionic liquid mixtures: ●, $[C_2C_1im][NTf_2]$ +$[C_2py][EtSO_4]$; ▲, $[C_2C_1im][NTf_2]$ +$[C_2C_1im][EtSO_4]$; ■, $[C_2C_1im][NTf_2]$ +$[C_4C_2im][EtSO_4]$.

In the concentration range with predominance of the ethylsulfate ionic liquids, there is an appreciable difference between the values. The system with $[C_2py][EtSO_4]$ exhibits higher *H* values, in accordance with the poorer capacity of this ionic liquid to absorb CO_2. Interestingly, when the molar fraction of $[C_2C_1im][NTf_2]$ becomes greater than *ca*. 0.60, there is practically no difference among the calculated *H* values for the different systems at a given concentration.

Other relevant aspect to evaluate is the reversibility of the capture of the gas through regeneration of the solvent regeneration. For this, the desorption curves were performed at the same temperature condition and decreasing the pressure. Selected series (each pure ionic liquid, plus the 50:50 mixtures) of the systems are plotted in Figures 5.7 to 5.9.

At the end of each desorption series, the conservation of the chemical identities of the ions involved was verified by ^1H NMR and ^{13}C NMR spectroscopy. Thus, all ionic liquids (or the mixture of ionic liquids) were confirmed to be stable and not to undergo decomposition in the presence of CO_2, in particular at the conditions of temperature and pressure applied in the experiments reported herein.

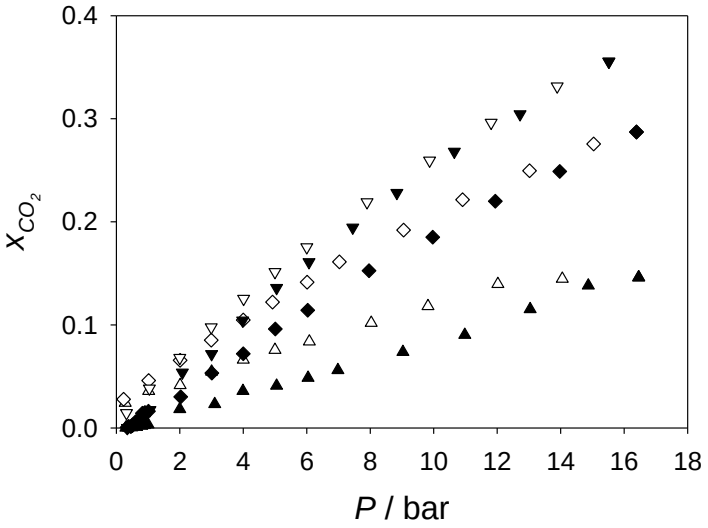

Figure 5.7: Comparison of absorption (solid symbols) and desorption (open symbols) isotherms for CO_2 in $[C_2C_1im][NTf_2]$ + $[C_2C_1im][EtSO_4]$. Solvent: ▼, pure $[C_2C_1im][NTf_2]$; ♦, 49:51 mixture in molar basis; ▲, pure $[C_2C_1im][EtSO_4]$.

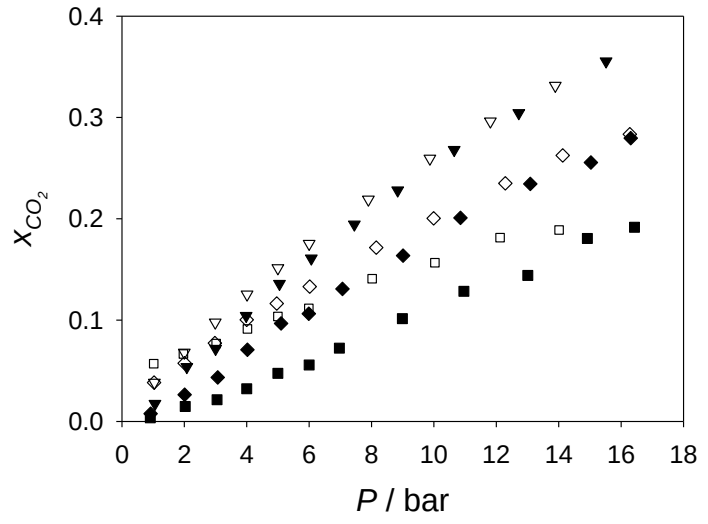

Figure 5.8: Comparison of absorption (solid symbols) and desorption (open symbols) isotherms for CO_2 in $[C_2C_1im][NTf_2]$ + $[C_4C_2im][EtSO_4]$. Solvent: ▼, pure $[C_2C_1im][NTf_2]$; ♦, 49:51 mixture in molar basis; ■, pure $[C_4C_2im][EtSO_4]$.

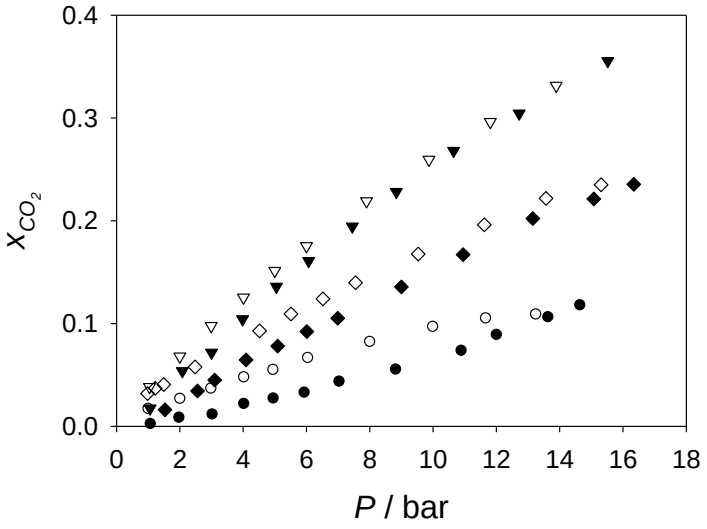

Figure 5.9: Comparison of absorption (solid symbols) and desorption (open symbols) isotherms for CO_2 in $[C_2C_1im][NTf_2]$ + $[C_2py][EtSO_4]$. Solvent: ▼, pure $[C_2C_1im][NTf_2]$; ♦, 49:51 mixture in molar basis; ●, pure $[C_2py][EtSO_4]$.

As can be seen in Figures 5.7 to 5.9, practically all the gas is desorbed upon lowering the pressure. In the case of the fluorinated ionic liquid, this desorption is complete; however, in ethylsulfate ionic liquids a small portion is retained in the ionic liquid (see numerical values in Table 5.2 to 5.4).

Not so favourable is that, for a given pressure, the solubility of CO_2 in the ionic liquid during the desorption process is higher than that of the absorption process. This occurs over the investigated range for all mixtures, including pure ionic liquids. The difference between the trajectories of the absorption and desorption isotherms varies with the composition of the mixture. Thus, for the ionic liquid with a higher absorption capacity ($[C_2C_1im][NTf_2]$), this difference is smaller and therefore the absorption and desorption paths are almost coincident. As the concentration of the $[EtSO_4]$-based ionic liquid is increased, however, such difference gets larger and larger, reaching the maximum difference for the pure $[C_4C_2im][EtSO_4]$ (Figure 5.8, square symbols).

As in the previous case, at the end of each desorption series, preservation of the chemical structure of the ionic liquids was verified by ^1H NMR and ^{13}C NMR.

The absorption data obtained were correlated by means of one of the most widely used thermodynamic models: the NRTL model (Renon and Prausnitz, 1968).

The binary mixture of ionic liquids was treated as a single pseudo-component, thus treating the system composed by CO_2 and the two ionic liquids as a pseudo-binary system. The correlation parameters were obtained using a computer program that runs a non-linear regression method to diminish deviations among experimental and correlated pressures (Sørensen and Arlt, 1980). The correlation was made using values of 0.1, 0.2 and 0.3 for the non-randomness parameter of the model, α. The best fit of the experimental data was achieved for α = 0.3. For each system, the corresponding binary interaction parameters (Δg_{12} and Δg_{21}) are reported in Table 5.6. The low values of the root mean square deviations are indicative of a good correlation of the experimental data, as it can be visually observed in Figures 5.3 to 5.5.

Table 5.6: Binary interaction parameters, Δg_{12} and Δg_{21}, of the NRTL model with α = 0.3 for correlation of the pressure-composition data at 298.2 K of the pseudo-binary system CO_2 (1) + ([C_2C_1im][NTf_2] + [Cat][$EtSO_4$]) (2), where [Cat]$^+$ = [C_2C_1im]$^+$, [C_4C_2im]$^+$, or [C_2py]$^+$. The root mean square deviations (rmsd) calculated from experimental and correlated pressure data are shown in the column on the right for each case.

[$EtSO_4$]$^-$ ionic liquid	$x_{[C2C1im][NTf2]}$	Δg_{12} / J·mol^{-1}	Δg_{21} / J·mol^{-1}	rmsd(P) / bar
[C_2C_1im][$EtSO_4$]	0.0000	1751.04	345.70	0.33
	0.2526	-320.20	1072.41	0.38
	0.4918	1761.76	-2007.87	0.26
	0.7452	2493.85	-3036.04	0.25
	1.0000	2866.34	-3676.93	0.24
[C_4C_2im][$EtSO_4$]	0.0000	-2305.28	4717.99	0.47
	0.2361	-2633.95	4387.15	0.50
	0.4885	1623.32	-1827.61	0.39
	0.7434	2339.62	-2840.74	0.23
	1.0000	2866.34	-3676.93	0.24
[C_2py][$EtSO_4$]	0.0000	-2138.33	5852.83	0.32
	0.2505	-1347.45	2751.85	0.35
	0.4894	2563.86	-1813.73	0.29
	0.7441	1130.77	-1896.21	0.24
	1.0000	2866.34	-3676.93	0.24

5.2.1.2. Thermal properties

The thermal phase transitions of the pure ionic liquids, as well as of their binary mixtures over the entire composition range, were determined from the DSC thermograms and are reported in Table 5.7 (see figures C.1 to C.3 in Appendix C). Although the samples were cooled down to 183 K in each cycle, the signal baseline lost

stability below *ca.* 200 K (due to limitation of the apparatus used). Thus, the portions of the thermograms below this temperature were systematically disregarded (even though some glass transitions seemed to lie there, which would be in accordance with literature data for the pure ionic liquids (Holbrey *et al*., 2002; Fredlake *et al*., 2004; Tokuda *et al*., 2005; Crosthwaite *et al*., 2005; Domańska *et al*., 2007; Domańska and Laskowska, 2008; Liu *et al*., 2010).

For the pure ionic liquid $[C_2C_1im][NTf_2]$, a crystallisation temperature of 232 K and a melting temperature of 257 K were found. This is in very good agreement with literature values for the melting temperature (Ngo *et al*., 2000; Fredlake *et al*., 2004; Tokuda *et al*., 2005), and in fair agreement with the (more erratic) crystallisation temperature (Ngo *et al*., 2000; Holbrey *et al*., 2002; Tokuda *et al*., 2005; Domańska *et al*., 2007; Domańska and Laskowska, 2008; Liu *et al*., 2010).

In the thermogram obtained for pure $[C_2C_1im][EtSO_4]$ no thermal event was identified, in accordance with literature data, where only a glass transition below the lower temperature limit for reliable measurements of our apparatus was reported (Domańska *et al*., 2007; Domańska and Laskowska, 2008). Nevertheless, in its mixtures with $[C_2C_1im][NTf_2]$, signals were observed in the samples with $[C_2C_1im][NTf_2]$ molar fractions of 0.90 (cold crystallisation at 232 K, and melting temperature 254 K) and of 0.80 (cold crystallisation at 243 K, and melting temperature 252 K). For all the other samples, with a $[C_2C_1im][NTf_2]$ molar fraction of 0.70 or lower, no thermal events were identified.

In the thermograms of mixtures of $[C_2C_1im][NTf_2]$ with $[C_4C_2im][EtSO_4]$, the melting and crystallisation peaks of pure $[C_2C_1im][NTf_2]$ were suppressed even for the sample with a $[C_2C_1im][NTf_2]$ molar fraction as high as 0.88. It must be noted, nevertheless, that a tiny 'melting peak' was consistently observed in all these samples, at *ca.* 242 K. Since its associated specific enthalpy was well below 1 J/g in all cases, and this was far much lower than 54 J/g found for pure $[C_2C_1im][NTf_2]$, we suspect that this tiny peak might be the result of some slight contamination of the $[C_4C_2im][EtSO_4]$ batch used in the preparation of the DSC samples. Because of this concern, we preferred not to display it in Table 5.7, where the melting and crystallisation temperatures of pure $[C_2C_1im][NTf_2]$ are the only reported transition temperatures of the entire $[C_2C_1im][NTf_2]$ + $[C_4C_2im][EtSO_4]$ system.

Table 5.7: Melting temperature (T_m) and crystallisation temperature (T_c) (determined by DSC at heating/ cooling rates of 2 K·min^{-1}, in the range 200-293 K), as well as decomposition temperatures at the 5 % onset ($T_{d,5\%onset}$) (determined at a heating rate of 5 K·min^{-1}), for binary mixtures of [C_2C_1im][NTf_2] + ([C_2C_1im][$EtSO_4$] or [C_4C_2im][$EtSO_4$] or [C_2py][$EtSO_4$]), at different molar fraction compositions of [C_2C_1im][NTf_2] (x_1). Cold crystallizations are indicated with an asterisk (*).

x_1	T_m (K)	T_c (K)	$T_{d,5\%onset}$ (K)
[C_2C_1im][NTf_2] (1) + [C_2C_1im][$EtSO_4$] (2)			
0.0000	-	-	438
0.1042	-	-	430
0.2008	-	-	428
0.2975	-	-	432
0.4356	-	-	431
0.4940	-	-	433
0.5982	-	-	431
0.6996	-	-	500
0.8000	252	243*	542
0.9025	254	232*	570
1.0000	257	232	597
[C_2C_1im][NTf_2] (1) + [C_4C_2im][$EtSO_4$] (2)			
0.0000	-	-	431
0.0917	-	-	424
0.1810	-	-	427
0.2981	-	-	421
0.3791	-	-	429
0.4755	-	-	433
0.5798	-	-	475
0.6746	-	-	517
0.7767	-	-	530
0.8829	-	-	560
1.0000	257	232	597
[C_2C_1im][NTf_2] (1) + [C_2py][$EtSO_4$] (2)			
0.0000	289	245*, 258*	419
0.1024	241		415
0.1981	242		418
0.2987	247		417
0.4002	245		429
0.5001	245		462
0.6034	244		511
0.7060	243		519
0.8195	243		548
0.9169	249	226*	569
1.0000	257	232	597

In the case of the $[C_2C_1im][NTf_2]$ + $[C_2py][EtSO_4]$ system, $[C_2py][EtSO_4]$ was found to have a relatively high melting point (289 K) if compared with similar ionic liquids such as $[C_2C_1im][EtSO_4]$, which shows a glass transition at 187 K (or 208 K) (Holbrey *et al.*, 2002; Domańska *et al.*, 2007), or 1-ethyl-3-methylpyridinium ethylsulfate ($[C_2C_1py][EtSO_4]$), whose glass transition occurs at 202 K (Crosthwaite *et al.*, 2005). The higher degree of symmetry of the $[C_2py]^+$ cation, with respect to $[C_4C_2im]^+$ and $[C_2C_1im]^+$, is likely the reason for such a substantial increase in the liquefaction temperature (Bonhôte *et al.*, 1996; Ngo *et al.*, 2000). Interestingly, however, all studied mixtures of $[C_2py][EtSO_4]$ with $[C_2C_1im][NTf_2]$ have a lower melting point than either of the pure ionic liquids. Although no clear trend is observed, it can be speculated that this could be indicative of a eutectic behaviour. In any case, it is remarkable how the observed melting temperature drops by near 50 K by addition of 10 mol% $[C_2C_1im][NTf_2]$ to the ionic liquid $[C_2py][EtSO_4]$, thus enabling its use as a fluid in engineering processes in a notably wider temperature range.

In addition to the melting point at 289 K, two cold crystallisation peaks were registered for $[C_2py][EtSO_4]$ at the measuring conditions used. Crystallisation temperatures for the mixtures of $[C_2py][EtSO_4]$ and $[C_2C_1im][NTf_2]$ were only observed for the most concentrated one in $[C_2C_1im][NTf_2]$ (90 mol%), during the DSC heating ramps; *i.e.*, as cold crystallisation. For all other mixtures studied, no crystallisation peak appeared in the thermograms.

The DSC results described are indicative that, for any of the systems studied, the addition of the ethylsulfate ionic liquids in small to moderate amounts to $[C_2C_1im][NTf_2]$ causes the mixture to remain liquid at temperatures well below the melting temperature of pure $[C_2C_1im][NTf_2]$, even lower than 200 K.

Table 5.7 also includes the decomposition temperatures for the onset at a 5 wt% decomposition ($T_{d,5\%onset}$). The values obtained for the pure ionic liquids are more conservative than others available in the literature (Ngo *et al.*, 2000; Holbrey *et al.*, 2002; Domańska and Laskowska, 2008; Liu *et al.*, 2010). It must be taken into account that $T_{d,5\%onset}$ is reported herein, instead of the simple onset decomposition temperature. Also, in this work a heating rate of 5 K·min^{-1} was used, which is lower than the more usual rate of 10 K·min^{-1} used in most literature references to date.

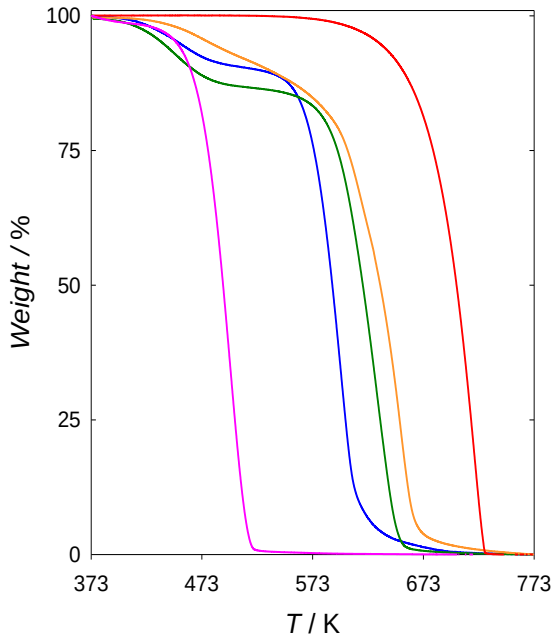

Figure 5.10: TGA plots for pure ionic liquids (from right to left, at a 50% decomposition): $[C_2C_1im][NTf_2]$ (red), $[C_2C_1im][EtSO_4]$ (orange), $[C_4C_2im][EtSO_4]$ (green), $[C_2py][EtSO_4]$ (blue), and $[C_2C_1im][OAc]$ (purple).

The analysis of the evolution of the sample weight with temperature in the TGA thermograms of the pure ionic liquids (Figure 5.10) highlights the influence of the anion in the ionic liquid stability. For example, $[C_2C_1im][NTf_2]$ is thermally stable up to a temperature 150 K higher than $[C_2C_1im][EtSO_4]$ (Table 5.7), in a similar way to what was previously reported by Ngo *et al*. (2000). Analogously, the increase of the alkyl substituent chains in the cation improves the thermal stability of the ionic liquid (as deduced from the comparison of $[C_2C_1im][EtSO_4]$ and $[C_4C_2im][EtSO_4]$), although not as markedly as in the previous case with variation of the anion.

A detailed analysis of the thermograms in Figure 5.10 reveals a 2-step decomposition for the ionic liquids with the ethylsulfate anion. Typically, a first step with little degradation is apparent, while most of the degradation happens in a second, much more prominent step.

The experimental decomposition temperatures for the three binary mixtures of ionic liquids are plotted as a function of molar fraction of $[C_2C_1im][NTf_2]$ in Figure 5.11 (the TGA plots are plotted in Figures C.5 to C.7 in Appendix C). The thermal stability of the samples rich in the ethylsulfate ionic liquid remains quite constant

($T_{d,5\%onset}$ in the range 420-440 K), up to $[C_2C_1im][NTf_2]$ molar fractions of *ca.* 0.5-0.6. With further enrichment in $[C_2C_1im][NTf_2]$, the mixtures become increasingly stable, up to the almost 600 K that correspond to the pure $[C_2C_1im][NTf_2]$.

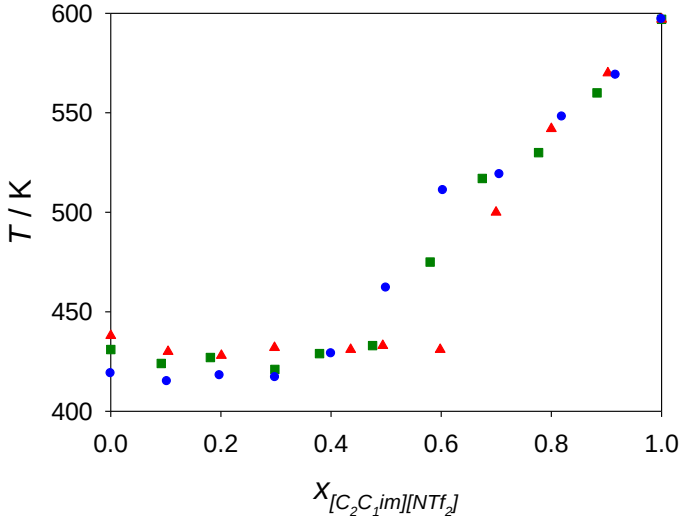

Figure 5.10: Decomposition temperatures of the mixtures $[C_2C_1im][NTf_2]$ + $[C_2C_1im][EtSO_4]$ (▲), $[C_2C_1im][NTf_2]$ + $[C_4C_2im][EtSO_4]$ (■), and $[C_2C_1im][NTf_2]$ + $[C_2py][EtSO_4]$ (●), as a function of the molar fraction of $[C_2C_1im][NTf_2]$ in the mixture, as determined by TGA.

From the curves in Figures C.5 and C.7 in Appendix C, it can be observed that the onset temperatures for the two steps of decomposition of the ethylsulfate ionic liquids in the mixtures do not remain constant and equal to those of each pure ionic liquid, as it would be likely to happen if both ionic liquids in the mixture were decomposing separately (Niedermeyer *et al.*, 2012).

5.2.1.3. Physical properties

Density, viscosity and surface tension were determined, at 298.2 K and atmospheric pressure, for all the mixtures over the entire compositional range (Table 5.8). The experimental results for density are shown in Figure 5.12. With an increase in the molar fraction of $[C_2C_1im][NTf_2]$, and since it is denser than the ethylsulfate ionic liquids, the density of the mixtures increases in all cases. Only a small difference is observed between the values of the $[C_2C_1im][NTf_2]$ + $[C_2py][EtSO_4]$ and the $[C_2C_1im][NTf_2]$ + $[C_2C_1im][EtSO_4]$ mixtures, with the latter having a slightly lower

density. This may be possibly connected with the greater number (two versus one) of alkyl substituent chains in the cation of the ethylsulfate ionic liquid. A stronger difference in density is observed with the $[C_2C_1im][NTf_2]$ + $[C_4C_2im][EtSO_4]$ mixture. By comparison of the latter with the mixture comprising the $[C_2C_1im][EtSO_4]$ ionic liquid, it can be deduced that, for these systems, the density decreases as the length of the alkyl substituent chains increase, as reported by other researchers (Huddleston *et al.*, 2001; Fredlake *et al.*, 2004; Jacquemin *et al.*, 2008).

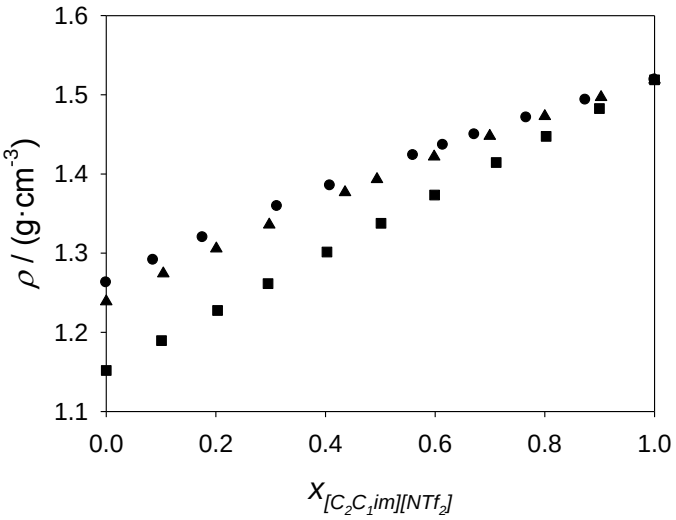

Figure 5.12: Density (ρ) of mixtures of ionic liquids, at 298.15 K, as a function of the molar fraction of $[C_2C_1im][NTf_2]$. Ionic liquid mixtures: ▲, $[C_2C_1im][NTf_2]$ + $[C_2C_1im][EtSO_4]$; ■, $[C_2C_1im][NTf_2]$ + $[C_4C_2im][EtSO_4]$; ●, $[C_2C_1im][NTf_2]$ + $[C_2py][EtSO_4]$.

In Figure 5.13, the variation of viscosity of the mixtures of ionic liquids with the molar fraction of $[C_2C_1im][NTf_2]$ is shown. The viscosity of the pure ethylsulfate ionic liquids increases in the order: $[C_2C_1im][EtSO_4]$ < $[C_2py][EtSO_4]$ < $[C_4C_2im][EtSO_4]$; and so does the viscosity of the corresponding mixtures that comprise them, in particular when the mixtures are richer in the ethylsulfate ionic liquid. At molar fractions of $[C_2C_1im][NTf_2]$ above *ca.* 0.50, there is practically no difference between the viscosity of the mixtures of $[C_2C_1im][NTf_2]$ + $[C_4C_2im][EtSO_4]$ and $[C_2C_1im][NTf_2]$ + $[C_2py][EtSO_4]$; and the difference of these with the mixture of $[C_2C_1im][NTf_2]$ + $[C_2C_1im][EtSO_4]$ becomes also negligible above $[C_2C_1im][NTf_2]$ molar fractions of *ca.* 0.70. For all three mixtures, the viscosity decreases with an increase of the concentration of $[C_2C_1im][NTf_2]$, which is less viscous than any of the ethylsulfate ionic liquids with which it has been mixed.

Table 5.8: Density (ρ), viscosity (η) and surface tension (σ) for the binary systems $[C_2C_1im][NTf_2]$ + $[C_2C_1im][EtSO_4]$, $[C_2C_1im][NTf_2]$ + $[C_4C_2im][EtSO_4]$, and $[C_2C_1im][NTf_2]$ + $[C_2py][EtSO_4]$, at 298.15 K and atmospheric pressure, for different molar fractions of $[C_2C_1im][NTf_2]$ ($x_{[C2C1im][NTf2]}$).

$x_{[C2C1im][NTf2]}$	ρ (g·cm^{-3})	η (mPa·s)	σ (mN·m^{-1})
	$[C_2C_1im][NTf_2]$ + $[C_2C_1im][EtSO_4]$		
0.0000	1.23893	100.6	48.6
0.1042	1.27418	95.64	43.1
0.2008	1.30567	90.59	41.7
0.2975	1.33588	84.09	40.7
0.4356	1.37683	72.51	39.5
0.4940	1.39328	67.82	39.0
0.5982	1.42177	58.31	38.5
0.6996	1.44801	50.07	37.8
0.8000	1.47287	43.24	37.4
0.9025	1.49692	37.67	37.1
1.0000	1.51887	32.55	36.6
	$[C_2C_1im][NTf_2]$ + $[C_4C_2im][EtSO_4]$		
0.0000	1.15188	255.2	38.8
0.1009	1.18955	212.4	37.7
0.2031	1.22758	172.4	37.0
0.2951	1.26158	139.9	36.4
0.4027	1.30145	109.3	36.0
0.5013	1.33766	87.58	35.9
0.5989	1.37349	69.65	35.9
0.7113	1.41449	57.11	36.0
0.8024	1.44748	47.55	36.0
0.8996	1.48263	39.59	36.2
1.0000	1.51887	32.55	36.6
	$[C_2C_1im][NTf_2]$ + $[C_2py][EtSO_4]$		
0.0000	1.26277	143.0	50.0
0.0859	1.29124	141.2	45.4
0.1761	1.31985	130.0	42.9
0.3119	1.35919	111.4	41.1
0.4084	1.38523	96.44	39.8
0.5599	1.42348	74.90	39.3
0.6145	1.43655	67.81	38.9
0.6717	1.44980	60.42	38.7
0.7665	1.47110	50.78	38.1
0.8742	1.49356	41.09	37.4
1.0000	1.51887	32.55	36.6

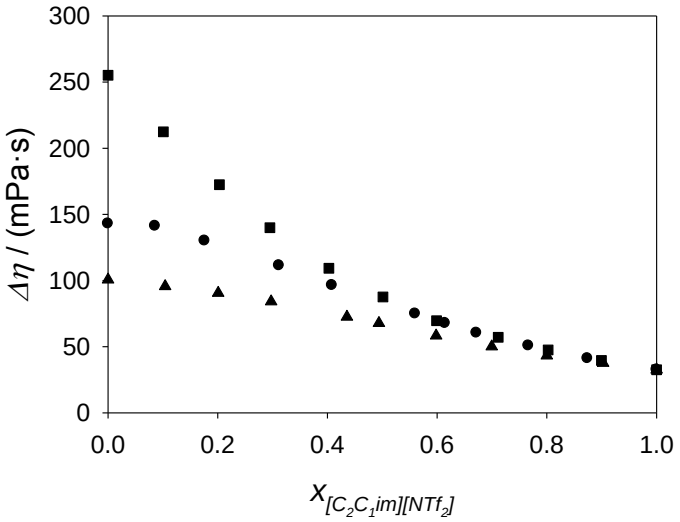

Figure 5.13: Viscosity (η) of mixtures, at 298.15 K, as a function of the molar fraction of $[C_2C_1im][NTf_2]$. Ionic liquid mixtures: ▲, $[C_2C_1im][NTf_2]$ + $[C_2C_1im][EtSO_4]$; ■, $[C_2C_1im][NTf_2]$ + $[C_4C_2im][EtSO_4]$; ●, $[C_2C_1im][NTf_2]$ + $[C_2py][EtSO_4]$.

Surface tension values for the three mixtures of ionic liquids studied are plotted in Figure 5.14 as a function of composition. For the mixtures of $[C_2C_1im][NTf_2]$ + $[C_2C_1im][EtSO_4]$ and $[C_2C_1im][NTf_2]$ + $[C_2py][EtSO_4]$, the surface tension decreases with an increase in the concentration of $[C_2C_1im][NTf_2]$. This is consistent with the fact of $[C_2C_1im][NTf_2]$ having a lower surface tension. For the mixture of $[C_2C_1im][NTf_2]$ + $[C_4C_2im][EtSO_4]$, interestingly, the series presents intermediate compositions for which the surface tension is lower than any of the pure constituent ionic liquids of the mixture. The surface tension of $[C_4C_2im][EtSO_4]$ is notably lower than that of $[C_2C_1im][EtSO_4]$ or $[C_2py][EtSO_4]$, due to its longer alkyl side chains (Law and Watson, 2001; Freire *et al*., 2007; Kilaru *et al*., 2007; Freemantle, 2010); and therefore the difference between the surface tension of pure ionic liquids is smaller in the mixture of $[C_2C_1im][NTf_2]$ and $[C_4C_2im][EtSO_4]$ than in the other two.

A more detailed analysis of the mixing effect on these physical properties was carried out by examining the excess molar volume, the viscosity deviation, and the surface tension deviation, as explained in section 3.2.2.

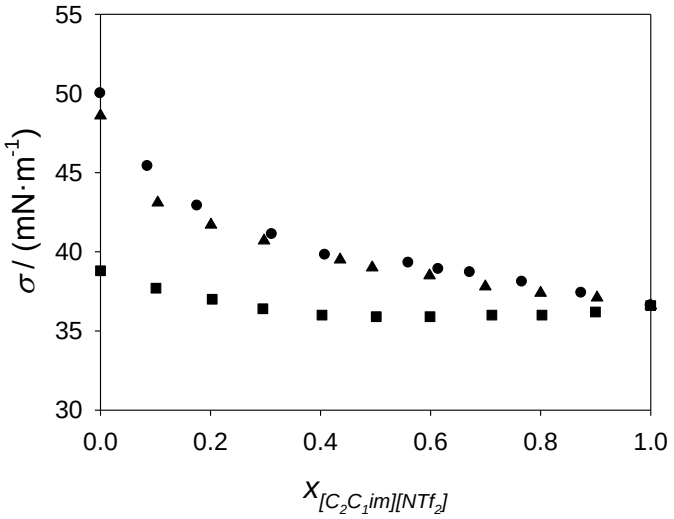

Figure 5.14: Surface tension (σ) of mixtures, at 298.2 K, as a function of the molar fraction of $[C_2C_1im][NTf_2]$. Ionic liquid mixtures: ▲, $[C_2C_1im][NTf_2]$ + $[C_2C_1im][EtSO_4]$; ■, $[C_2C_1im][NTf_2]$ + $[C_4C_2im][EtSO_4]$●, $[C_2C_1im][NTf_2]$ + $[C_2py][EtSO_4]$.

The excess molar volume, V^E, is the difference between the observed and the ideal volume of a mixture and it is calculated with equation 3.33. The values obtained for the studied systems are relatively large in the context of typical values for excess molar volumes (Table 5.9). However, even for the longest molar volumes, such values are lower than 1 $cm^3 \cdot mol^{-1}$, and therefore much smaller in absolute terms than the molar volumes V of the mixtures (calculated as the quotient of the composition-weighted average formula weight divided by the density). The excess volume is positive over the entire composition range, with a maximum between 0.3-0.6 $[C_2C_1im][NTf_2]$ molar fraction (Figure 5.15). This is indicative of a lower level of attractive interaction in the mixed ionic liquids, compared to the interactions occurring in the pure ionic liquids. This causes an increase of the free volume upon mixing of the pure ionic liquids. Since the free volume has been connected in the literature with the capacity of an ionic liquid for the physical absorption of CO_2 (Anderson *et al*., 2007; Blanchard *et al*., 2001), the positive excess molar volume may be, at least in part, a reason for the synergistic absorption capacity effect described in section 5.2.1.1 (see Figure 5.6). In the case of the mixture with the pyridinium ionic liquid, the absolute values of V^E are less than 0.50 $cm^3 \cdot mol^{-1}$. This is probably due to the $[C_2py]^+$ cation having only one alkyl substituent versus the two alkyl substituents

of the $[C_2mim]^+$, and therefore $[C_2py]^+$ contributing less to the generation of free volume within the mixture (Canongia Lopes *et al.*, 2005; Niedermeyer *et al.*, 2012).

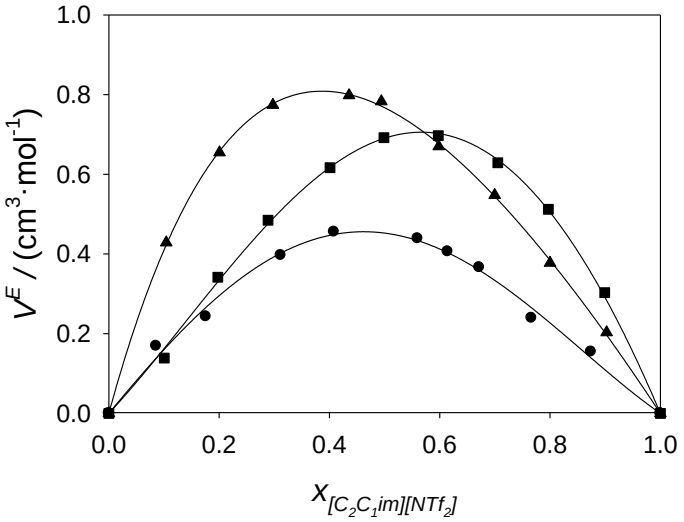

Figure 5.15: Excess molar volume (V^E) of mixtures, at 298.15 K, as a function of the molar fraction of $[C_2C_1im][NTf_2]$. Ionic liquid mixtures: ▲, $[C_2C_1im][NTf_2]$ + $[C_2C_1im][EtSO_4]$; ■, $[C_2C_1im][NTf_2]$ + $[C_4C_2im][EtSO_4]$; ●, $[C_2C_1im][NTf_2]$ + $[C_2py][EtSO_4]$.

The viscosity deviation for the mixtures is reported as a function of the composition in Table 5.9. In the mixtures of $[C_2py][EtSO_4]$ and of $[C_2C_1im][EtSO_4]$ with $[C_2C_1im][NTf_2]$, the $\Delta\eta$ values switch from positive to negative at a $[C_2C_1im][NTf_2]$ molar fraction of 0.4-0.6, approximately (Figure 5.16). However the system with $[C_4C_2im][EtSO_4]$ exhibits much larger viscosity deviations (in absolute value), and always negative. This is consistent with the reports by Navia *et al.* (2008), who stated that the largest deviations are obtained for those mixtures of ionic liquids with more dissimilar structures, particularly in terms of lengths of alkyl substituent chains. An absolute maximum viscosity deviation of almost 60 mPa·s is achieved in this system for a molar fraction of $[C_2C_1im][NTf_2]$ of 0.5-0.6, which accounts for more than 40 % deviation of the value that would results from the weighted average of the viscosities of the individual ionic liquids constituting the mixture.

The viscosity deviations of lowest magnitude in absolute value correspond to the system $[C_2C_1im][NTf_2]$ + $[C_2C_1im][EtSO_4]$, likely due to the fact of both ionic liquids sharing exactly the same cation. This is in contrast with the mixture of $[C_2C_1im][NTf_2]$

+ $[C_2py][EtSO_4]$, where, although the $[C_2py]^+$ cation has a similar size to $[C_2C_1im]^+$, there are four different ions involved.

Table 5.9: Excess molar volume (V^E), viscosity deviation ($\Delta\eta$) and surface tension deviation ($\Delta\sigma$) for the binary systems $[C_2C_1im][NTf_2]$ + $[C_2C_1im][EtSO_4]$, $[C_2C_1im][NTf_2]$ + $[C_4C_2im][EtSO_4]$, and $[C_2C_1im][NTf_2]$ + $[C_2py][EtSO_4]$, at 298.15 K and atmospheric pressure, for different molar fractions of $[C_2C_1im][NTf_2]$ ($x_{[C2C1im][NTf2]}$).

$[EtSO_4]^-$ ionic liquid	$x_{[C2C1im][NTf2]}$	V^E/ $cm^3 \cdot mol^{-1}$	$\Delta\eta$/ mPa·s	$\Delta\sigma$/ $mN \cdot m^{-1}$
$[C_2C_1im][EtSO_4]$	0.0000	0.000	0.00	0.0
	0.1042	0.429	2.15	-4.2
	0.2008	0.655	3.67	-4.5
	0.2975	0.774	3.75	-4.3
	0.4356	0.798	1.56	-3.8
	0.4940	0.783	0.85	-3.7
	0.5982	0.670	-1.58	-2.9
	0.6996	0.548	-2.92	-2.4
	0.8000	0.377	-2.92	-1.6
	0.9025	0.203	-1.51	-0.7
	1.0000	0.000	0.00	0.0
$[C_4C_2im][EtSO_4]$	0.0000	0.000	0.00	0.0
	0.1009	0.315	-20.4	-0.9
	0.2031	0.537	-37.7	-1.4
	0.2951	0.691	-49.6	-1.8
	0.4027	0.747	-56.3	-1.9
	0.5013	0.754	-56.0	-1.8
	0.5989	0.691	-52.2	-1.6
	0.7113	0.573	-39.7	-1.3
	0.8024	0.441	-29.0	-1.0
	0.8996	0.250	-15.3	-0.6
	1.0000	0.000	0.00	0.0
$[C_2py][EtSO_4]$	0.0000	0.000	0.00	0.0
	0.0859	0.169	7.65	-3.4
	0.1761	0.243	6.50	-4.8
	0.3119	0.397	2.88	-4.8
	0.4084	0.455	-1.37	-4.8
	0.5599	0.439	-6.14	-3.3
	0.6145	0.406	-7.17	-2.9
	0.6717	0.366	-8.23	-2.5
	0.7665	0.239	-7.38	-1.8
	0.8743	0.155	-5.14	-1.0
	1.0000	0.000	0.00	0.0

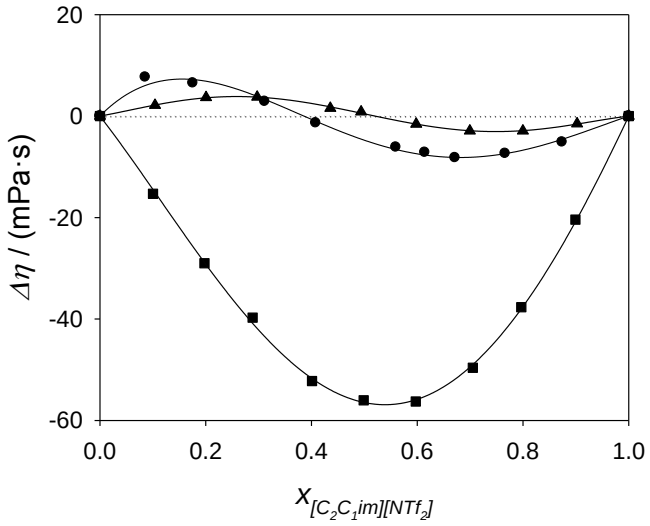

Figure 5.16: Viscosity deviation ($\Delta\eta$) of mixtures, at 298.15 K, as a function of the molar fraction of $[C_2C_1im][NTf_2]$. Ionic liquid mixtures: ▲, $[C_2C_1im][NTf_2]$ + $[C_2C_1im][EtSO_4]$; ■, $[C_2C_1im][NTf_2]$ + $[C_4C_2im][EtSO_4]$; ●, $[C_2C_1im][NTf_2]$ + $[C_2py][EtSO_4]$.

A similar analysis was established for surface tension. The surface tension deviation of the mixtures was calculated using equation 3.35, and the numerical values obtained are reported in Table 5.9. For the entire compositional range, negative surface tension deviations were systematically obtained (Figure 5.17). This can be taken as an indication of a preferential enrichment of the surface in the ionic liquid with the lower surface tension (or in one of its ions mainly responsible for the low value of surface tension). In this case, the ionic liquid with the lower surface tension is $[C_2C_1im][NTf_2]$; so probably the surface of the mixtures is proportionally richer in the $[NTf_2]^-$ anion than the bulk.

A minimum is found approximately in the range of 0.2-0.4 molar fraction of $[C_2C_1im][NTf_2]$ for the mixtures of $[C_2C_1im][NTf_2]$ + $[C_2py][EtSO_4]$ and $[C_2C_1im][NTf_2]$ + $[C_2C_1im][EtSO_4]$. However, in the case of mixture of $[C_2C_1im][NTf_2]$ + $[C_4C_2im][EtSO_4]$ the minimum is around a $[C_2C_1im][NTf_2]$ molar fraction of 0.6. The impressive coincidence of the surface tension deviation of the $[C_2C_1im][NTf_2]$ + $[C_2py][EtSO_4]$ mixture with the $[C_2C_1im][NTf_2]$ + $[C_2C_1im][EtSO_4]$ mixture can also be observed in Figure 5.17. The only variation of the $[C_2py]^+/[C_2mim]^+$ cations has a very small effect on the surface activity of the mixture.

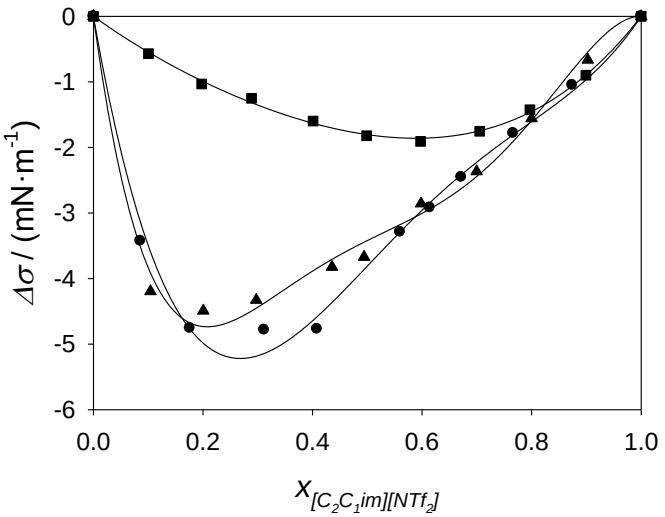

Figure 5.17: Surface tension deviation ($\Delta\sigma$) of mixtures, at 298.15 K, as a function of the molar fraction of $[C_2C_1im][NTf_2]$. Ionic liquid mixtures: ▲, $[C_2C_1im][NTf_2]$ + $[C_2C_1im][EtSO_4]$; ■, $[C_2C_1im][NTf_2]$ + $[C_4C_2im][EtSO_4]$; ●, $[C_2C_1im][NTf_2]$ + $[C_2py][EtSO_4]$.

Data correlation

The excess and deviation properties could be correlated by means of Redlich-Kister polynomial expansions (Redlich and Kister, 1948), with the form of the mathematical expression in equation 3.43. The fit parameters and the corresponding root mean square deviations (rmsd) (equation 3.44) are summarised in Table 5.10. Also, the correlation polynomials are plotted in Figures 5.15 to 5.17.

Acceptably good correlations were obtained for all three properties with a second-degree polynomial for the mixtures $[C_2C_1im][NTf_2]$ + $[C_2py][EtSO_4]$ and $[C_2C_1im][NTf_2]$ + $[C_4C_2im][EtSO_4]$, and with a third-degree polynomial for the mixture $[C_2C_1im][NTf_2]$ + $[C_2C_1im][EtSO_4]$.

Data prediction

Beyond correlation, the possibility of predicting the properties of the mixture of ionic liquids merely from information on the properties of the pure ionic liquids would be desirable and very welcome from an application perspective. For density, a first estimate can be obtained by a weighted average of the molar volumes of the pure components (Canongia Lopes *et al.*, 2005; Navia *et al.*, 2007). The results are very

similar to the experimental data, with deviations less than 0.5 % (Figure 5.18). Nevertheless, it is important to note that this approach neglects the excess molar volume of the mixture, and the valuable information that it provides of the liquid medium at a molecular level.

Table 5.10: Coefficients A_i of the Redlich-Kister polynomials for the correlation of the excess molar volume (V^E), viscosity deviation ($\Delta\eta$) and surface tension deviation ($\Delta\sigma$), for the mixtures [C_2C_1im][NTf_2] + [C_2C_1im][$EtSO_4$], [C_2C_1im][NTf_2] + [C_4C_2im][$EtSO_4$] and [C_2C_1im][NTf_2] + [C_2py][$EtSO_4$], at 298.15 K and atmospheric pressure. The coefficients and the corresponding root mean square deviations (shown in the column on the right) are expressed in $cm^3 \cdot mol^{-1}$, mPa·s and $mN \cdot m^{-1}$ for V^E, $\Delta\eta$ and $\Delta\sigma$, respectively.

Solvent	A_0	A_1	A_2	A_3	rmsd
Excess molar volume (V^E)					
[C_2C_1im][NTf_2]+[C_2C_1im][$EtSO_4$]	3.0686	-1.3839	0.5118	-0.0989	0.006
[C_2C_1im][NTf_2]+[C_4C_2im][$EtSO_4$]	3.0038	-0.5195	0.1857	–	0.007
[C_2C_1im][NTf_2]+[C_2py][$EtSO_4$]	1.8098	-0.3559	-0.4943	–	0.015
Viscosity deviation ($\Delta\eta$)					
[C_2C_1im][NTf_2]+[C_2C_1im][$EtSO_4$]	1.788	-43.92	1.402	28.42	0.12
[C_2C_1im][NTf_2]+[C_4C_2im][$EtSO_4$]	-225.8	43.53	48.06	–	0.54
[C_2C_1im][NTf_2]+[C_2py][$EtSO_4$]	-19.01	-70.85	54.29	–	0.62
Surface tension deviation ($\Delta\sigma$)					
[C_2C_1im][NTf_2]+[C_2C_1im][$EtSO_4$]	-13.7	8.28	-16.8	22.5	0.2
[C_2C_1im][NTf_2]+[C_4C_2im][$EtSO_4$]	-7.22	-2.40	-1.17	–	0.0
[C_2C_1im][NTf_2]+[C_2py][$EtSO_4$]	-15.2	17.6	-14.9	–	0.2

For the prediction of the viscosity of a binary mixture, there exist some well known mixing laws, among which those expressed by means of equations 3.45 and 3.47 have been reportedly used with mixtures of two ionic liquids (Navia *et al*., 2008). Application of both equations to the prediction of the viscosity of the mixtures yielded similar results. However, the best predictions were obtained for the system [C_2C_1im][NTf_2] + [C_4C_2im][$EtSO_4$], with root mean square deviations below 3.0 mPa·s. In the other mixtures, the results obtained were higher, leading to deviations as large as *ca.* 20 % for some of the data points (Figure 5.19). With such degree of deviation, these predictive methods would not be too useful for most design purposes.

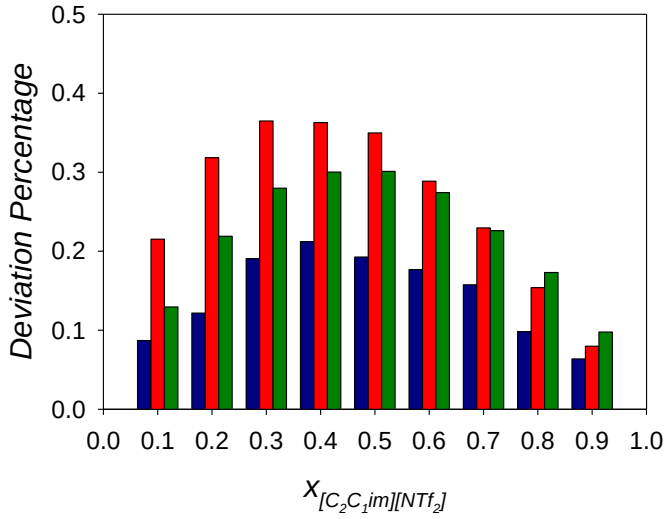

Figure 5.18: Deviation percentage for the prediction of molar volume of the ionic liquid mixtures, at 298.15 K, as a function of the molar fraction of $[C_2C_1im][NTf_2]$. Ionic liquid mixtures: red, $[C_2C_1im][NTf_2]$ + $[C_2C_1im][EtSO_4]$; green, $[C_2C_1im][NTf_2]$ + $[C_4C_2im][EtSO_4]$; blue, $[C_2C_1im][NTf_2]$ + $[C_2py][EtSO_4]$.

Equivalent expressions to equations 3.45 and 3.47 can be written for surface tension instead of viscosity, yielding equations 3.48 and 3.49. Application of such mixing laws for the case of surface tension in the studied mixtures led to predictions with maximum deviations as high as *ca.* 10 % for some of the experimental data points (Figure 5.20). Although this is relatively low in percentage (as it would be expected in any case, due to the similarity of the surface tension values of the pure ionic liquids), it must be noticed that the predicted values did not provide a good qualitative description of the variation of the surface tension with composition.

The use of equation 3.51 predicts surface tension values that lead to intermediate deviation percentages if compared to those obtained with equations 3.48 and 3.49. Given this intermediate character, the values obtained with equation 3.51 are not included in Figure 5.20, to facilitate its reading.

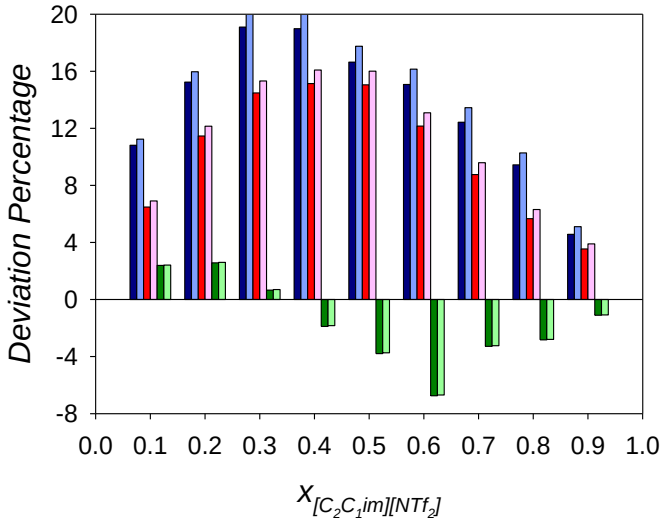

Figure 5.19: Deviation percentage for the prediction of the viscosity of the ionic liquid mixtures, at 298.15 K, as a function of the molar fraction of $[C_2C_1im][NTf_2]$. Ionic liquid mixtures: blue, $[C_2C_1im][NTf_2]$ + $[C_2py][EtSO_4]$; red, $[C_2C_1im][NTf_2]$ + $[C_2C_1im][EtSO_4]$; green, $[C_2C_1im][NTf_2]$ + $[C_4C_2im][EtSO_4]$. For each mixture, the dark colour represents the deviation percentages obtained from equation 3.45, and the light colour those obtained from equation 3.47.

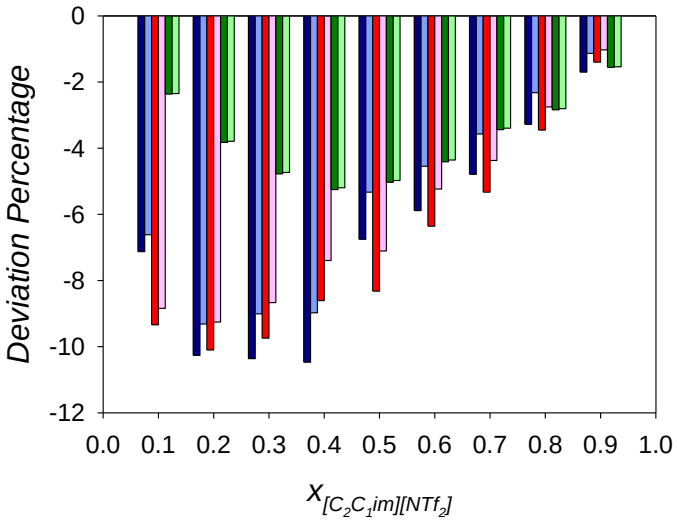

Figure 5.20: Deviation percentage for the prediction of the surface tension of the ionic liquid mixtures, at 298.2 K, as a function of the molar fraction of $[C_2C_1im][NTf_2]$. Ionic liquid mixtures: blue, $[C_2C_1im][NTf_2]$ + $[C_2py][EtSO_4]$; red, $[C_2C_1im][NTf_2]$ + $[C_2C_1im][EtSO_4]$; green, $[C_2C_1im][NTf_2]$ + $[C_4C_2im][EtSO_4]$. For each mixture, the dark colour represents the deviation percentages obtained from equation 3.48, and the light colour those obtained from equation 3.49.

5.2.2. Combined physical and chemical absorption

In the section 5.1, interesting features were observed by mixing two ionic liquids with the capacity to absorb CO_2 by means of a physical mechanism. Nevertheless, the absolute absorption values achieved are lower than those corresponding to typical chemical absorption procedures. In trying to combine the advantages of both physical and chemical mechanisms, and a possible enhancement of such advantages via the use of a mixture of ionic liquids, in this section the CO_2 absorption capacity and thermal and physical properties are studied for a mixture of an ionic liquid that absorbs CO_2 physically and another ionic liquid that absorbs it chemically. In particular, the mixture $[C_2C_1im][OAc]$ + $[C_2C_1im][EtSO_4]$ is investigated.

Table 5.11: Pressure-composition data for the absorption/desorption of CO_2 in $[C_2C_1im][EtSO_4]$ at different temperatures. The solubility of CO_2 is expressed as molar fraction (x_{CO2}).

$[C_2C_1im][EtSO_4]$ + CO_2							
T = 298.2 K		T = 318.2 K		T = 338.2 K		T = 358.2 K	
P / bar	x_{CO2}	P / bar	x_{CO2}	P / bar	x_{CO2}	P / bar	x_{CO2}
Absorption							
1.00	0.0034	1.03	0.0042	1.04	0.0012	1.04	0.0004
2.00	0.0182	2.04	0.0042	2.01	0.0046	2.05	0.0024
3.10	0.0231	3.02	0.0148	3.00	0.0087	3.08	0.0055
3.99	0.0358	4.04	0.0214	4.02	0.0156	4.00	0.0084
5.05	0.0409	4.96	0.0301	5.03	0.0191	5.01	0.0143
6.04	0.0486	6.00	0.0372	6.00	0.0247	6.00	0.0169
6.98	0.0561	6.93	0.0450	6.94	0.0334	7.03	0.0193
9.03	0.0737	8.90	0.0553	9.02	0.0412	8.98	0.0268
10.98	0.0903	10.89	0.0661	10.91	0.0507	11.00	0.0379
13.04	0.1152	12.34	0.0862	12.67	0.0629	12.98	0.0409
14.87	0.1382	14.89	0.0935	14.48	0.0745	15.00	0.0492
16.46	0.1460	16.02	0.1024	16.06	0.0750	16.36	0.0504
Desorption							
14.05	0.1447	14.01	0.1044	13.92	0.0745	14.01	0.0514
12.02	0.1396	11.99	0.0974	11.93	0.0693	12.01	0.0483
9.82	0.1182	9.92	0.0806	9.96	0.0606	9.94	0.0425
8.03	0.1019	8.02	0.0697	7.97	0.0520	7.99	0.0333
6.08	0.0839	6.03	0.0536	5.98	0.0387	6.02	0.0249
5.00	0.0757	5.00	0.0474	4.98	0.0325	5.00	0.0208
4.00	0.0662	3.99	0.0405	3.94	0.0309	4.02	0.0174
3.00	0.0546	2.98	0.0332	3.01	0.0229	2.99	0.0136
2.01	0.0415	1.98	0.0244	1.99	0.0159	2.01	0.0100
1.02	0.0359	1.01	0.0191	1.00	0.0081	1.01	0.0049

5.2.2.1. Analysis of the CO_2 absorption capacity

The ionic liquid $[C_2C_1im][OAc]$ absorbs CO_2 chemically (Shiflett and Yokozeki, 2009; Stevanovic *et al*., 2012), whereas $[C_2C_1im][EtSO_4]$ absorbs it physically, as discussed before. The absorption/desorption of CO_2 by pure $[C_2C_1im][OAc]$ and by its mixture with $[C_2C_1im][EtSO_4]$ (which was previously studied in pure state in section 5.2.1) was investigated, in the pressure range up to *ca.* 16 bar, at several isotherms from 298.2 K to 358.2 K. The mixtures of these two ionic liquids were prepared at approximate molar fractions of 0.25, 0.50, and 0.75. The results in molar basis are summarised in Tables 5.11 to 5.14, and in mass fraction in Tables B.5 to B.8 in Appendix B.

Table 5.12: Pressure-composition data for the absorption/desorption of CO_2 in $[C_2C_1im][OAc]$ at different temperatures. The solubility of CO_2 is expressed as molar fraction (x_{CO2}).

$[C_2C_1im][OAc] + CO_2$							
T = 298.2 K		T = 318.2 K		T = 338.2 K		T = 358.2 K	
P / bar	x_{CO2}	P / bar	x_{CO2}	P / bar	x_{CO2}	P / bar	x_{CO2}
Absorption							
0.94	0.2606	0.95	0.2223	0.92	0.1621	0.98	0.1624
2.00	0.2916	2.01	0.2574	1.92	0.2441	1.96	0.2006
2.96	0.3075	3.03	0.2732	3.04	0.2642	3.11	0.2218
4.00	0.3213	3.98	0.2819	4.00	0.2697	4.00	0.2325
5.00	0.3284	4.99	0.2927	5.02	0.2845	5.01	0.2448
6.04	0.3255	6.03	0.3030	5.98	0.2922	5.97	0.2528
7.02	0.3273	7.30	0.3097	7.00	0.2974	7.02	0.2591
9.04	0.3308	8.95	0.3227	9.01	0.3112	9.10	0.2720
11.04	0.3347	10.99	0.3346	10.97	0.3218	11.02	0.2832
12.89	0.3391	12.98	0.3452	12.96	0.3290	13.01	0.2922
14.86	0.3432	14.93	0.3555	14.96	0.3379	14.98	0.3002
16.39	0.3396	16.44	0.3614	16.33	0.3425	16.30	0.3050
Desorption							
14.03	0.3468	14.03	0.3591	14.03	0.3412	13.99	0.3027
12.00	0.3433	12.01	0.3508	11.97	0.3377	11.97	0.2954
10.03	0.3397	10.02	0.3456	10.04	0.3337	10.04	0.2896
8.01	0.3362	8.02	0.3368	8.00	0.3254	7.95	0.2771
6.00	0.3324	6.05	0.3209	6.11	0.3049	6.00	0.2654
4.98	0.3303	5.03	0.3122	4.99	0.2991	5.00	0.2625
4.00	0.3281	4.02	0.3082	4.02	0.2899	4.04	0.2518
2.99	0.3258	2.99	0.2920	2.99	0.2825	2.98	0.2395
2.03	0.3228	1.98	0.2838	2.00	0.2706	2.01	0.2309
1.02	0.3184	1.01	0.2698	1.04	0.2582	1.06	0.2046

Table 5.13: Pressure-composition data for the absorption/desorption of CO_2 in the binary mixture [C_2C_1im][OAc] + [C_2C_1im][$EtSO_4$], at 298.2 K and as a function of the composition ratio of the two ionic liquids (x'_1 stands for the molar fraction of [C_2C_1im][OAc] in a CO_2-free basis). The solubility of CO_2 is expressed as molar fraction (x_{CO2}).

[C_2C_1im][OAc] (1) + [C_2C_1im][$EtSO_4$] (2) + CO_2									
x'_1 = 0.0000		x'_1 = 0.2516		x'_1 = 0.4919		x'_1 = 0.7503		x'_1 = 1.0000	
P / bar	x_{CO2}	P / bar	x_{CO2}	P / bar	x_{CO2}	P / bar	x_{CO2}	P / bar	x_{CO2}
Absorption									
1.00	0.0034	0.99	0.0790	0.98	0.1344	0.98	0.1956	0.94	0.2606
2.00	0.0182	2.03	0.1042	1.98	0.1640	1.99	0.2174	2.00	0.2916
3.10	0.0231	3.02	0.1168	2.91	0.1821	3.03	0.2356	2.96	0.3075
3.99	0.0358	4.04	0.1294	3.93	0.1936	4.06	0.2485	4.00	0.3213
5.05	0.0409	5.00	0.1360	4.91	0.2035	5.00	0.2538	5.00	0.3284
6.04	0.0486	5.99	0.1524	6.00	0.2093	5.98	0.2673	6.04	0.3255
6.98	0.0561	6.97	0.1619	6.74	0.2244	7.05	0.2794	7.02	0.3273
9.03	0.0737	8.95	0.1811	8.71	0.2404	8.96	0.2952	9.04	0.3308
10.98	0.0903	10.98	0.1970	10.89	0.2540	10.98	0.3074	11.04	0.3347
13.04	0.1152	12.95	0.2141	12.46	0.2711	12.90	0.3200	12.89	0.3391
14.87	0.1382	15.04	0.2283	14.39	0.2862	15.03	0.3369	14.86	0.3432
16.46	0.1460	16.02	0.2402	16.02	0.2971	16.39	0.3456	16.39	0.3396
Desorption									
14.05	0.1447	13.97	0.2399	13.04	0.2857	13.98	0.3427	14.03	0.3468
12.02	0.1396	12.03	0.2264	11.98	0.2839	12.10	0.3339	12.00	0.3433
9.82	0.1182	10.04	0.2104	9.78	0.2680	10.05	0.3189	10.03	0.3397
8.03	0.1019	8.01	0.1957	7.90	0.2607	8.06	0.3135	8.01	0.3362
6.08	0.0839	6.03	0.1802	5.70	0.2351	6.00	0.2912	6.00	0.3324
5.00	0.0757	5.00	0.1706	4.97	0.2285	5.01	0.2826	4.98	0.3303
4.00	0.0662	4.02	0.1545	3.98	0.2231	3.99	0.2791	4.00	0.3281
3.00	0.0546	2.97	0.1498	2.98	0.2083	2.99	0.2673	2.99	0.3258
2.01	0.0415	2.00	0.1424	2.01	0.1988	2.00	0.2650	2.03	0.3228
1.02	0.0359	1.02	0.1251	1.04	0.1899	1.05	0.2494	1.02	0.3184

Several authors have reported that the absorption capacity of ionic liquids decreases with increasing temperature (Anthony *et al.*, 2002; Chen *et al.*, 2006; Deng *et al.*, 2011; Manic *et al.*, 2012a, 2012b). This is mostly in agreement with the experiments performed herein with each of the ionic liquids (Figure 5.21). The only exception to that trend is observed for pure [C_2C_1im][OAc] at high pressures within the range studied: the absorption capacity at 298.2 K is approximately equivalent or lower than the absorption capacities obtained at 318.2 and 338.2 K. This peculiar behaviour is likely due to the formation of the solid product of reaction between [C_2C_1im][OAc] and CO_2, as explained in section 5.1, which may limit the ability to physically absorb CO_2 once the chemical reaction is nearly completed. For the other investigated temperatures, the sample with absorbed gas remains liquid, thus not undergoing such limitation.

Table 5.14: Pressure-composition data for the absorption/desorption of CO_2 in the binary mixture $[C_2C_1im][OAc]$ + $[C_2C_1im][EtSO_4]$, at 358.2 K and as a function of the composition ratio of the two ionic liquids (x'_1 stands for the molar fraction of $[C_2C_1im][OAc]$ in a CO_2-free basis). The solubility of CO_2 is expressed as molar fraction (x_{CO2}).

$[C_2C_1im][OAc]$ (1) + $[C_2C_1im][EtSO_4]$ (2) + CO_2									
x'_1 = 0.0000		x'_1 = 0.2516		x'_1 = 0.4919		x'_1 = 0.7503		x'_1 = 1.0000	
P / bar	x_{CO2}	P / bar	x_{CO2}	P / bar	x_{CO2}	P / bar	x_{CO2}	P / bar	x_{CO2}
Absorption									
1.04	0.0004	1.06	0.0397	1.01	0.0835	1.00	0.0952	0.98	0.1624
2.05	0.0024	2.06	0.0560	2.02	0.1071	1.99	0.1263	1.96	0.2006
3.08	0.0055	3.01	0.0669	3.04	0.1212	3.08	0.1439	3.11	0.2218
4.00	0.0084	4.01	0.0771	4.02	0.1309	4.07	0.1539	4.00	0.2325
5.01	0.0143	5.02	0.0836	5.03	0.1400	5.02	0.1635	5.01	0.2448
6.00	0.0169	5.99	0.0892	5.99	0.1479	6.03	0.1726	5.97	0.2528
7.03	0.0193	7.02	0.0981	7.03	0.1545	7.03	0.1793	7.02	0.2591
8.98	0.0268	9.02	0.1042	8.98	0.1653	8.97	0.1915	9.10	0.2720
11.00	0.0379	10.93	0.1164	10.95	0.1753	11.05	0.2028	11.02	0.2832
12.98	0.0409	12.98	0.1258	13.02	0.1850	12.94	0.2128	13.01	0.2922
15.00	0.0492	15.00	0.1368	14.93	0.1941	15.00	0.2201	14.98	0.3002
16.36	0.0504	16.37	0.1380	16.48	0.1996	16.14	0.2251	16.30	0.3050
Desorption									
14.01	0.0514	14.01	0.1341	13.99	0.1981	14.00	0.2233	13.99	0.3027
12.01	0.0483	11.98	0.1260	12.03	0.1882	11.94	0.2145	11.97	0.2954
9.94	0.0425	9.97	0.1173	9.99	0.1784	10.04	0.2061	10.04	0.2896
7.99	0.0333	7.99	0.1086	8.01	0.1692	8.02	0.2004	7.95	0.2771
6.02	0.0249	6.02	0.0984	6.00	0.1588	5.95	0.1833	6.00	0.2654
5.00	0.0208	5.00	0.0917	4.98	0.1505	5.02	0.1776	5.00	0.2625
4.02	0.0174	4.02	0.0868	3.92	0.1404	4.00	0.1678	4.04	0.2518
2.99	0.0136	2.99	0.0801	2.98	0.1311	3.00	0.1557	2.98	0.2395
2.01	0.0100	1.99	0.0694	1.99	0.1222	2.00	0.1431	2.01	0.2309
1.01	0.0049	1.02	0.0591	1.04	0.1023	1.04	0.1257	1.06	0.2046

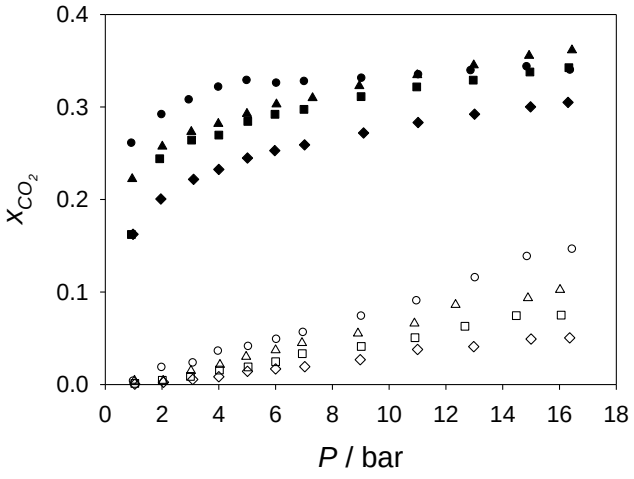

Figure 5.21: Molar fraction solubility of CO_2 (x_{CO2}), as a function of pressure (P), in pure $[C_2C_1im][OAc]$ (solid symbols) and pure $[C_2C_1im][EtSO_4]$ (open symbols) at several temperatures: 298.2 K (circles), 318.2 K (triangles), 338.2 K (squares), and 358.2 K (diamonds).

Figure 5.21 also provides a direct visual comparison of the CO_2 absorption capacities of $[C_2C_1im][OAc]$ and of $[C_2C_1im][EtSO_4]$. As expected, the absorption capacity of $[C_2C_1im][OAc]$, with chemisorption of CO_2 accompanied by physical absorption, is much higher than that of $[C_2C_1im][EtSO_4]$, with only physisorption of CO_2; for the entire temperature range explored herein.

The absorption capacity of mixtures of $[C_2C_1im][OAc]$ and $[C_2C_1im][EtSO_4]$ were investigated at the lowest and highest temperature for which the absorption capacity of the constituent pure ionic liquids was determined – namely 298.2 K and 358.2 K. The numerical values are presented in Tables 5.13 and 5.14. In Figure 5.22, a graphical visualisation is provided of how the absorption varies with pressure for the different series of constant composition. For both temperatures, a change in the shape of the curve and an increment of the absorption capacity are observed with an increase of the concentration of $[C_2C_1im][OAc]$ in the mixture of ionic liquids. In general, the solubility of CO_2 in the blends lies within those of the pure ionic liquids for any given pressure. However, at 298.2 K, the CO_2 absorption achieved by the mixture with a $[C_2C_1im][OAc]$ molar fraction of 0.75 is comparable and even slightly higher than that of pure $[C_2C_1im][OAc]$ at the highest pressures investigated. This is possibly due, again, to the solidification occurring exclusively with pure $[C_2C_1im][OAc]$ at 298.2 K, as mentioned above.

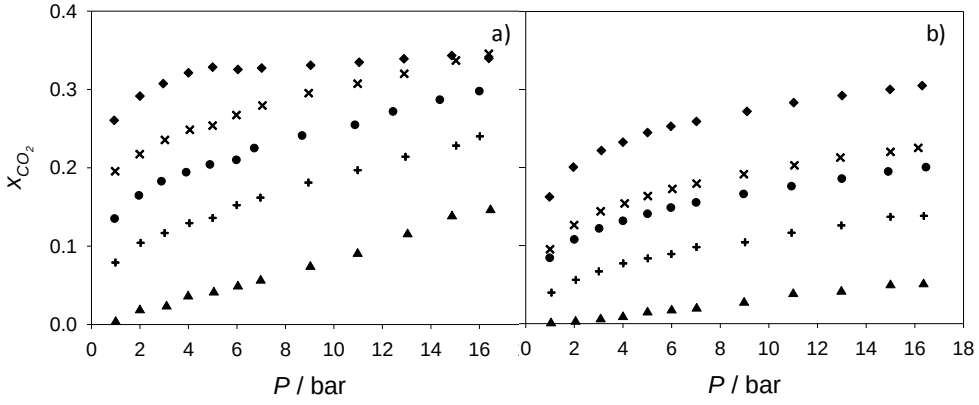

Figure 5.22: Comparison of carbon dioxide absorption (in molar fraction, x_{CO2}) in the mixture $[C_2C_1im][OAc]$ + $[C_2C_1im][EtSO_4]$ at 298.2 K (a) and 358.2 K (b), as a function of pressure and at different molar ratios of the mixture of ionic liquids: ♦, 100:0 (pure $[C_2C_1im][OAc]$); ×, 75:25; ●, 49:51; +, 25:75; ▲, 0:100 (pure $[C_2C_1im][EtSO_4]$).

Regarding desorption, it is observed in Figure 5.23 that the mechanism by which the gas is absorbed has a strong influence on the desorption ability under isothermal conditions. In the case of $[C_2C_1im][EtSO_4]$, most of the absorbed CO_2 can be desorbed by simply lowering the pressure. However, with $[C_2C_1im][OAc]$ this is not enough: the covalent bonds formed between CO_2 and $[C_2C_1im][OAc]$ in chemical absorption are stronger, so a greater input of energy (for example an increase in temperature) will be required to recover the CO_2.

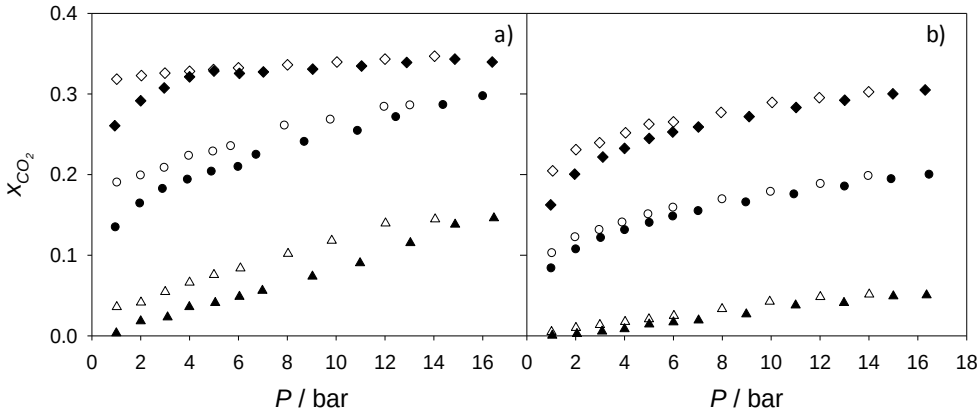

Figure 5.23: Comparison of absorption (solid symbols) and desorption (open symbols) isotherms for CO_2 in $[C_2C_1im][OAc]$ + $[C_2C_1im][EtSO_4]$ at 298.2 K (a) and 358.2 K(b), at different molar ratios of the mixture of ionic liquids: ♦, 100:0 (pure $[C_2C_1im][OAc]$); ●, 49:51; ▲, 0:100 (pure $[C_2C_1im][EtSO_4]$).

5.2.2.2. Thermal properties

DSC analyses were carried out to identify the phase transitions in the system $[C_2C_1im][OAc]$ + $[C_2C_1im][EtSO_4]$ over the entire composition range. In the reliable temperature range analysed, only cold crystallisation peaks were observed in the thermograms of the mixtures with a $[C_2C_1im][OAc]$ molar fraction between 0.20 and 0.90 (see Figure C.4 in appendix C). The numerical values obtained are reported in Table 5.15. It is unclear why these cold crystallisations occur practically at a constant temperature (*ca.* 250 K), regardless of the composition. In any case, all mixtures are clearly liquid well below the common ranges of operation temperature in CO_2 capture processes. For the pure ionic liquids no phase transitions were observed, in agreement with the literature (Bonhôte *et al.*, 1996; Domańska *et al.*, 2007; Troshenkova *et al.*, 2010a), where glass transitions below 200 K and no melting temperatures are reported for these ionic liquids.

Table 5.15 also includes the numerical values of the decomposition temperatures of the mixture at a 5 wt% onset ($T_{d,5\%onset}$), as determined by TGA (see TGA thermograms in Figure C.8 in Appendix C). Both ionic liquids have similar $T_{d,5\%onset}$ values (438 K for $[C_2C_1im][EtSO_4]$ and 426 K for $[C_2C_1im][OAc]$), which in turn result in their mixtures also having thermal stabilities that do not differ significantly. The decomposition temperatures obtained in this work for the pure ionic liquids are lower than those previously reported in the literature (Holbrey *et al.*, 2002; Fernández *et al.*, 2007; Troshenkova *et al.*, 2010b; Almeida *et al.*, 2012), as a result of considering the $T_{d,5\%onset}$ value instead of the regular onset decomposition temperature (thus providing a better approach to the valid temperature upper limit for practical applications). In addition, a relatively low heating rate of 5 K/min was used in this work, also contributing to lowering the reported values and improving their practical significance.

Table 5.15: Melting temperature (T_m) and crystallisation temperature (T_c) (determined by DSC at heating/cooling rates of 2 K·min^{-1}, in the range 200-293 K), as well as decomposition temperatures at the 5 % onset ($T_{d,5\%onset}$) (determined at a heating rate of 5 K·min^{-1}), for binary mixtures at different molar fraction compositions. All crystallisation temperatures reported correspond to a cold crystallisation

$x_{[C2C1im][OAc]}$	T_m (K)	T_c (K)	$T_{d,5\%onset}$ (K)
0.0000	-	-	438
0.0993	-	-	427
0.2011	-	249	404
0.2973	-	251	402
0.3917	-	250	411
0.5069	-	251	428
0.5988	-	251	423
0.7050	-	251	419
0.8012	-	251	411
0.9007	-	246	407
1.0000	-	-	426

By analysing the TGA plots of weight versus temperature (Figure 5.24) in a similar manner to that carried out for the systems of section 5.2.1, it is observed that $[C_2C_1im][EtSO_4]$ exhibits a 2-step decomposition (Fernández *et al.*, 2007); unlike $[C_2C_1im][OAc]$, for which only one step is observed (Troshenkova *et al.*, 2010b). These distinct patterns of the pure constituent ionic liquids influence the thermal decomposition behaviour of the mixtures. Thus, with an increase in the concentration

of $[C_2C_1im][OAc]$, the 2-step decomposition from $[C_2C_1im][EtSO_4]$ is gradually shifted until it finally disappears. These observations are in good agreement with previous reports that indicate that, in a mixture of ionic liquids, each ionic liquid can decompose independently (Niedermeyer *et al.*, 2012). This is particularly suited for the mixture studied herein, where the ionic liquids mixed have a common cation, and therefore there is no possibility of 'crossed pairs' formation.

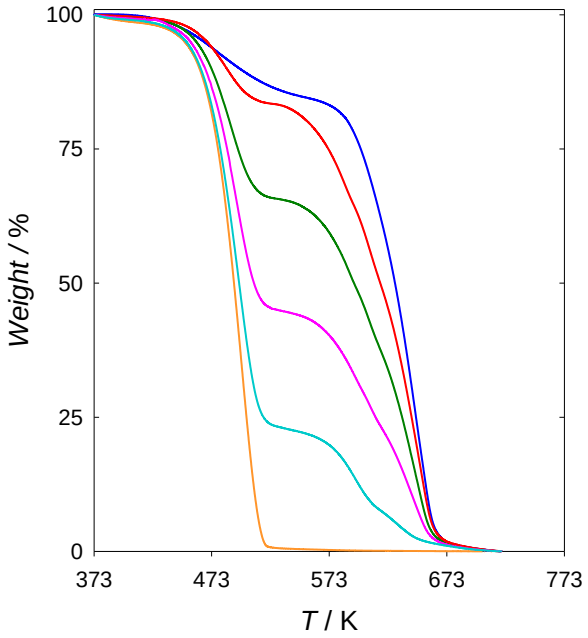

Figure 5.24: TGA thermograms (weight versus temperature) for selected compositions of the mixture of $[C_2C_1im][OAc]$ and $[C_2C_1im][EtSO_4]$. From top to bottom: 0:100 mixture (pure $[C_2C_1im][EtSO_4]$) (blue), 20:80 mixture (red), 39:61 mixture (green), 60:40 mixture (purple), 80:20 mixture (light blue), and 100:0 mixture (pure $[C_2C_1im][OAc]$). (Ratios provided in a molar basis.)

5.2.2.3. Physical properties

Two critical properties in the design of processes involving fluids are the density and viscosity. In this section, density and viscosity values were experimentally determined for the binary system $[C_2C_1im][OAc]$+$[C_2C_1im][EtSO_4]$, in the temperature range 298.15-358.15 K and at atmospheric pressure. The numerical values are reported in Table 5.16.

Both properties decrease with increasing temperature, while they follow different trends with the variation of the composition. The specific patterns of variation of the studied properties with these variables are discussed below.

Table 5.16: Density (ρ) and viscosity (η) for the binary system [C_2C_1im][OAc] (1) + [C_2C_1im][$EtSO_4$] (2) at different temperatures and atmospheric pressure, for different molar fraction compositions of [C_2C_1im][OAc] ($x_{[C2C1im][OAc]}$).

	Temperature (K)						
$x_{[C2C1im][OAc]}$	298.15	308.15	318.15	328.15	338.15	348.15	358.15
				ρ (g/cm^3)			
0.0000	1.23868	1.23192	1.22520	1.21851	1.21188	1.20819	1.19875
0.0993	1.22662	1.21990	1.21321	1.20659	1.20001	1.19634	1.18700
0.2011	1.21423	1.20750	1.20090	1.19433	1.18779	1.18412	1.17489
0.2973	1.20211	1.19548	1.18892	1.18238	1.17591	1.17227	1.16313
0.3917	1.18985	1.18326	1.17676	1.17026	1.16385	1.16023	1.15118
0.5069	1.17426	1.16773	1.16131	1.15488	1.14854	1.14494	1.13603
0.5988	1.16136	1.15486	1.14850	1.14213	1.13586	1.13229	1.12347
0.7050	1.14581	1.13950	1.13315	1.12687	1.12068	1.11712	1.10841
0.8012	1.13113	1.12487	1.11865	1.11255	1.10635	1.10278	1.09415
0.9007	1.11550	1.10930	1.10314	1.09701	1.09093	1.08739	1.07894
1.0000	1.09904	1.09295	1.08688	1.08086	1.07486	1.07137	1.06303
				η (mPa·s)			
0.0000	96.62	60.41	39.95	28.91	20.63	15.66	12.23
0.0993	97.20	61.11	40.47	29.06	20.70	15.63	12.57
0.2011	99.93	61.27	41.05	29.19	20.78	15.58	12.80
0.2973	101.8	62.35	41.59	29.32	20.84	15.50	12.95
0.3917	105.2	63.63	42.12	29.44	20.89	15.39	12.93
0.5069	110.1	65.47	41.77	29.58	20.92	15.24	12.90
0.5988	114.1	66.99	43.30	29.69	20.92	15.10	12.81
0.7050	120.1	69.07	43.93	29.81	20.89	14.91	12.70
0.8012	125.8	71.01	44.55	29.91	20.86	14.72	12.47
0.9007	131.0	73.40	45.24	30.00	20.84	14.51	12.17
1.0000	138.4	76.10	45.90	30.10	20.80	14.28	11.53

Figure 5.25 shows the density plotted as a function of temperature, for selected series at constant composition. A decrease of density occurs with increasing temperature, as well as with decreasing the concentration of [C_2C_1im][OAc] (the less dense ionic liquid of the two ionic liquids constituting the mixture). For the evolution with temperature, a linear behaviour was concluded, on the basis of analyses made by the statistical *F*-test method (Devore, 2000), which indicated that the quadratic term in the correlation of the data by a second-degree polynomial fit was not statistically

significant. Therefore, the density ρ for each specific composition of the mixture of ionic liquids was fit to the following expression:

$$\rho = a + b \cdot T \tag{3.36}$$

where T is the absolute temperature, and a and b are the fit parameters. These parameters are summarised in Table 5.17.

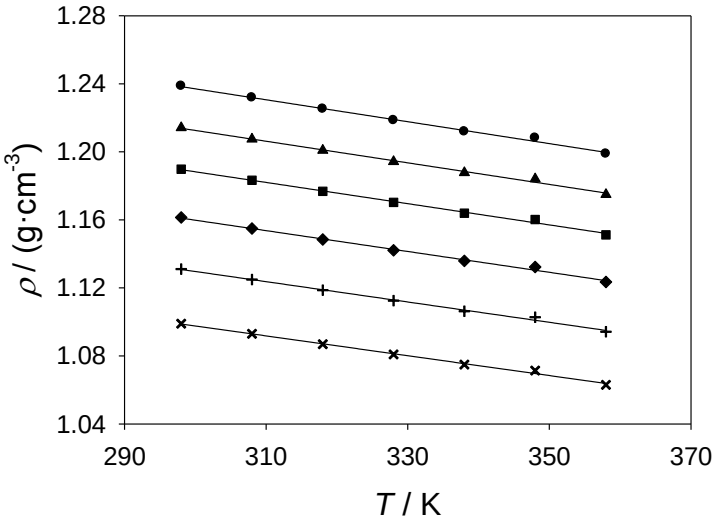

Figure 5.25: Density (ρ) of mixtures of $[C_2C_1im][OAc]$ + $[C_2C_1im][EtSO_4]$ as a function of temperature (T), for different molar fraction ratios (selected series): ●, 0:100 (pure $[C_2C_1im][EtSO_4]$); ▲, 20:80; ■, 39:61; ♦, 60:40; +, 80:20; ×, 100:0 (pure $[C_2C_1im][OAc]$). Solid lines correspond to linear fits (equation 3.36).

The excess molar volume (V^E) provides an approach to the nature of the forces existing at a molecular level in a liquid mixture. This property can be directly calculated from experimental composition and density values, according to equation 3.33. The numerical values obtained for the mixture of $[C_2C_1im][OAc]$ and $[C_2C_1im][EtSO_4]$ are reported in Table 5.18. Their graphical representation as a function of the composition of the mixture, for selected series at constant temperature, is provided in Figure 5.26. In all cases, positive values are obtained for V^E, indicating that the interionic forces existing within the mixture of ionic liquids are less attractive than those existing within the individual ionic liquids. It is postulated that the presence of two different anions in the mixture introduces a certain degree of disruption, as compared to the more ordered structuring in the pure ionic liquids, thus weakening the attraction among ions. A maximum was observed, at each given

temperature, for nearly equimolar mixtures. With increasing temperature, the values of V^E increase, probably in connection with a weakening of the attractive forces. The influence of temperature is greater at lower temperature.

Table 5.17: Fit parameters of equation 3.36 for the correlation of the density of mixtures $[C_2C_1im][OAc]+[C_2C_1im][EtSO_4]$ as a function of temperature, for different molar compositions of $[C_2C_1im][OAc]$ ($x_{[C2C1im][OAc]}$). The corresponding standard deviations (σ) (equation 3.38) are shown in the column on the right.

$x_{[C2C1im][OAc]}$	a / (g·cm^{-3})	b / (10^{-5} g·cm^{-3}·K^{-1})	σ / (g·cm^{-3})
0.0000	1.43051	-6.4437	0.002
0.0993	1.41705	-6.3974	0.001
0.2011	1.40317	-6.3483	0.002
0.2973	1.38972	-6.3023	0.001
0.3917	1.37547	-6.2446	0.002
0.5069	1.35841	-6.1862	0.001
0.5988	1.34371	-6.1261	0.001
0.7050	1.32600	-6.0520	0.002
0.8012	1.30908	-5.9768	0.001
0.9007	1.29180	-5.9219	0.001
1.0000	1.27265	-5.8305	0.001

Table 5.18: Excess molar volume (V^E) for the binary system $[C_2C_1im][OAc]$ (1) + $[C_2C_1im][EtSO_4]$ (2) at different temperatures and atmospheric pressure, for different molar fraction compositions of $[C_2C_1im][OAc]$($x_{[C2C1im][OAc]}$).

	Temperature (K)						
$x_{[C2C1im][OAc]}$	298.15	308.15	318.15	328.15	338.15	348.15	358.15
0.0000	0.000	0.000	0.000	0.000	0.000	0.000	0.000
0.0993	0.088	0.092	0.097	0.096	0.096	0.097	0.098
0.2011	0.112	0.128	0.126	0.126	0.130	0.132	0.133
0.2973	0.129	0.137	0.139	0.144	0.145	0.146	0.146
0.3917	0.132	0.143	0.145	0.151	0.151	0.153	0.153
0.5069	0.130	0.143	0.143	0.152	0.152	0.152	0.151
0.5988	0.119	0.136	0.137	0.144	0.143	0.143	0.143
0.7050	0.105	0.105	0.114	0.120	0.116	0.117	0.118
0.8012	0.086	0.088	0.089	0.078	0.087	0.092	0.098
0.9007	0.034	0.038	0.039	0.044	0.045	0.049	0.048
1.0000	0.000	0.000	0.000	0.000	0.000	0.000	0.000

The excess molar volumes were adequately correlated by Redlich-Kister polynomial expansions. For each series at constant temperature, a third-order polynomial expansion was found to suitably correlate the results in this work. The obtained fit parameters, along with the corresponding root mean square deviations (equation 3.44), are shown in Table 5.19. For selected isotherms, the correlations are graphically depicted in Figure 5.26.

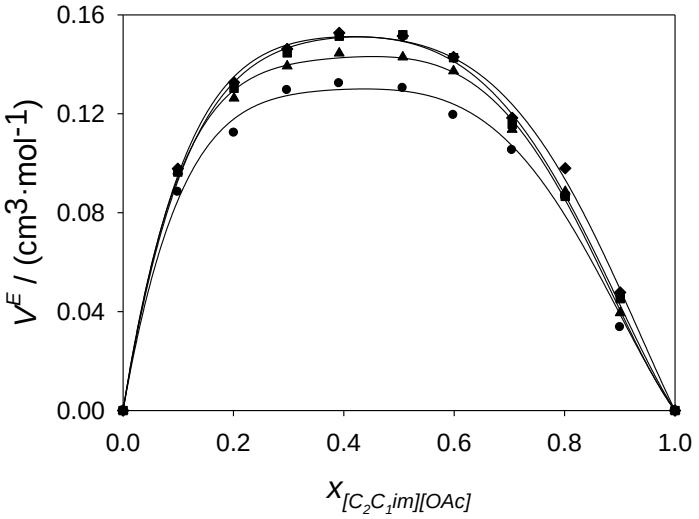

Figure 5.26: Excess molar volume (V^E) of mixtures of $[C_2C_1im][OAc]$ and $[C_2C_1im][EtSO_4]$ as a function of the molar fraction of $[C_2C_1im][OAc]$ ($x_{[C2C1im][OAc]}$) in the mixture, for different temperatures (selected series): ●, 298.2 K; ▲, 318.2 K; ■, 338.2 K; ♦, 358.2 K. Solid lines correspond to the correlations with Redlich-Kister polynomials.

Table 5.19: Coefficients A_i of the Redlich-Kister polynomials, in cm^3·mol^{-1}, for the fit of the excess molar volume (V^E) of the binary system $[C_2C_1im][OAc]+[C_2C_1im][EtSO_4]$, at different temperatures and atmospheric pressure. The corresponding root mean square deviations (rmsd) are also reported.

	Temperature (K)						
A_i, rmsd	298.15	308.15	318.15	328.15	338.15	348.15	358.15
A_0	0.5175	0.5654	0.5707	0.6031	0.5983	0.5984	0.5988
A_1	-0.0463	-0.0771	-0.0433	-0.0655	-0.0865	-0.0933	-0.0758
A_2	0.2717	0.2553	0.2807	0.1913	0.2475	0.2980	0.3205
A_3	-0.4301	-0.4367	-0.5130	-0.4754	-0.4116	-0.3549	-0.3822
rmsd	0.004	0.003	0.002	0.003	0.002	0.002	0.003

Figure 5.27 shows the influence of temperature in viscosity, for series of constant composition. A strong decrease of absolute viscosity is observed with increasing temperature in the low temperature range. Also in this temperature range,

the influence of the composition on the absolute viscosity is more pronounced than at the highest temperatures, with viscosity increasing as the $[C_2C_1im][OAc]$ concentration increases. The latter effect is probably a result of the higher basicity of the acetate anion, which causes an increase of the intermolecular forces (Hasse *et al*., 2009).

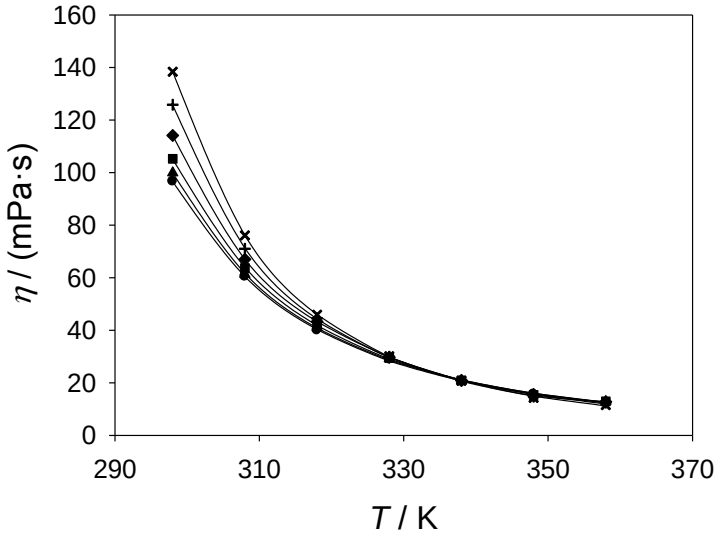

Figure 5.27: Viscosity (η) of mixtures of $[C_2C_1im][OAc]$ + $[C_2C_1im][EtSO_4]$ as a function of temperature (T), for different molar fraction ratios: ●, 0:100 (pure $[C_2C_1im][EtSO_4]$); ▲, 20:80; ■, 39:61; ♦, 60:40; +, 80:20; ×, 100:0 (pure $[C_2C_1im][OAc]$). Solid lines correspond to fits by means of the VFT equation.

The VFT equation, in the modified version of Cohen and Turnbull (equation 3.40), was used for correlation of the viscosity η as a function of the absolute temperature T. The fits for selected series, at constant composition, are plotted in Figure 5.27 along with the experimental data. The values of the fit parameters for all series are reported in Table 5.20.

The viscosity deviation can provide an additional insight into the interactions occurring within the mixture of ionic liquids at a molecular level. This viscosity deviation was calculated by equation 3.34. The values of $\Delta\eta$ thus calculated are reported in Table 5.21, and a selection of them is graphically plotted as a function of the mixture composition at different temperatures in Figure 5.28. At low temperatures, a strong negative deviation is observed. As the temperature increases, the deviation obtained decreases in absolute value, and it switches to positive values,

but much smaller in magnitude than those obtained at lower temperatures. For all isothermal series, a maximum/minimum at approximately equimolar compositions was observed, as in the case of the excess molar volume previously commented. This equimolar composition seems to be, again, the one causing the strongest disruption of forces at molecular level with respect to any of the pure ionic liquids.

Table 5.21: Viscosity deviation ($\Delta\eta$) for the binary system [C_2C_1im][OAc] (1) + [C_2C_1im][$EtSO_4$] (2) at different temperatures and atmospheric pressure, for different molar fraction compositions of [C_2C_1im][OAc] ($x_{[C2C1im][OAc]}$).

	Temperature (K)						
$x_{[C2C1im][OAc]}$	298.15	308.15	318.15	328.15	338.15	348.15	358.15
0.0000	0.00	0.00	0.00	0.00	0.00	0.00	0.00
0.0993	-3.56	-0.86	-0.07	0.03	0.06	0.11	0.41
0.2011	-5.09	-2.29	-0.10	0.04	0.12	0.21	0.71
0.2973	-7.24	-2.73	-0.13	0.05	0.16	0.25	0.93
0.3917	-7.76	-2.92	-0.16	0.06	0.20	0.27	0.98
0.5069	-7.69	-2.89	-0.19	0.07	0.21	0.29	1.03
0.5988	-7.49	-2.81	-0.22	0.07	0.20	0.27	1.01
0.7050	-5.96	-2.40	-0.22	0.06	0.15	0.23	0.96
0.8012	-4.27	-1.97	-0.17	0.04	0.10	0.17	0.81
0.9007	-3.25	-1.14	-0.07	0.02	0.06	0.10	0.57
1.0000	0.00	0.00	0.00	0.00	0.00	0.00	0.00

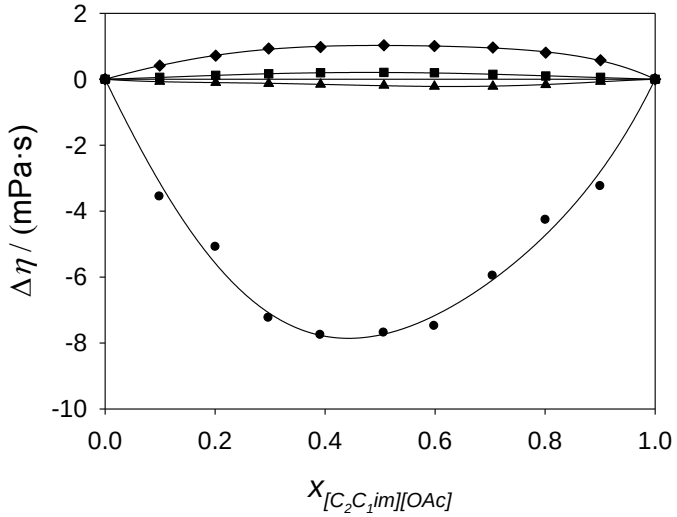

Figure 5.28: Viscosity deviation ($\Delta\eta$) of mixtures of [C_2C_1im][OAc] and [C_2C_1im][$EtSO_4$] as a function of the molar fraction of [C_2C_1im][OAc] in the mixture, for different temperatures: ●, 298.2 K; ▲, 318.2 K; ■, 338.2 K; ♦, 358.2 K. Solid lines correspond to the correlations with Redlich-Kister polynomials.

The viscosity deviation was satisfactorily correlated by the Redlich-Kister equation, using a third-order polynomial expansion. The obtained fit parameters, along with the corresponding root mean square deviations, are shown in Table 5.22. The quality of the fit can be visually verified in Figure 5.28, where the correlation lines were plotted for selected series along with the corresponding experimental data.

Table 5.22: Coefficients A_i of the Redlich-Kister polynomials, in mPa·s, for the fit of the viscosity deviation ($\Delta\eta$) of the binary system [C_2C_1im][OAc]+[C_2C_1im][$EtSO_4$] at different temperatures and atmospheric pressure. The corresponding root mean square deviations (rmsd) are also reported.

	Temperature (K)						
A_i, rmsd	298.15	308.15	318.15	328.15	338.15	348.15	358.15
A_0	-31.03	-11.95	-0.779	0.268	0.823	1.163	4.101
A_1	6.887	3.061	-0.673	0.026	-0.099	-0.103	-0.031
A_2	-3.305	-1.402	-0.111	0.006	-0.365	0.037	2.095
A_3	-6.975	-6.569	1.005	-0.188	0.106	-0.022	1.684
rmsd	0.30	0.11	0.01	0.00	0.00	0.01	0.01

5.3. Supported-ionic liquid phases (SILPs)

Amino acid ionic liquids constitute an interesting option in the absorption of CO_2 with ionic liquid absorbents. Their high absorption capacity via a chemical mechanism has been explored in an increasing number of publications. However, a major disadvantage for their application is the high viscosity that they typically exhibit. This limits the mass transfer, strongly lowering the pace at which the absorption process occurs. In order to improve the mass transfer, as well as the thermal stability of the ionic liquid, it was decided to use a supported-ionic liquid phase (SILP) approach, by supporting the ionic liquid in a mesoporous solid support. Namely, the ionic liquid investigated in this section was [N_{6666}][Ile], supported on mesoporous silica with an average pore size of 60 Å (SiO_2-60Å).

The TGA thermograms for thermal stability of the pure silica, the pure ionic liquid, and the SILP (with a 40 % ionic liquid loading) are shown in Figure 5.29. As expected, the silica is perfectly stable in the temperature range screened. On the other hand, an initial loss of mass is observed in both the pure ionic liquid and the SILP at near-ambient temperatures. This mass loss can be attributed, in the first instance, to

evaporation of water contained in the samples due to the strong hygroscopic character of $[N_{6666}][Ile]$. Therefore, for calculation of the decomposition temperatures, the inflexion point of the thermogram curve following the initial mass loss was taken as the starting point for determination of the onset. A $T_{d,5\%onset}$ value of 347 K was calculated for $[N_{6666}][Ile]$; whereas the corresponding $[N_{6666}][Ile]$-SiO_2 SILP led to an increase of its thermal stability, with a $T_{d,5\%onset}$ value of 401 K (*i.e.* an increase of 16 %) for a 40 % ionic liquid loading.

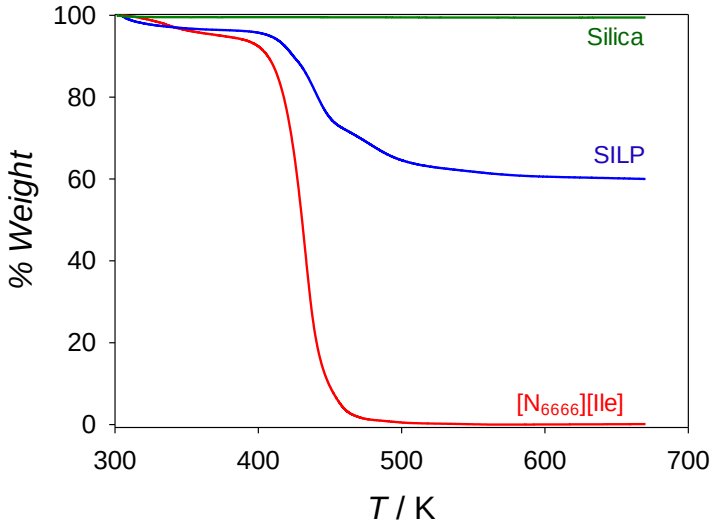

Figure 5.29: TGA plots (with a heating rate of 5 K·min^{-1}) for SiO_2-60Å (green); $[N_{6666}][Ile]$-SiO_2 SILP with 40 % load of ionic liquid (blue); and pure $[N_{6666}][Ile]$ (red).

A first set of studies on the absorption of CO_2 by the SILP was carried out in a TGA apparatus, at 298.2 K and atmospheric pressure, with the SILP as 'sample' and CO_2 as the gas flowing through. The flow of gas in the measuring chamber of the apparatus is horizontal, in parallel to the balance arm. Given this geometric layout, it can be presumed in principle that buoyancy effects will not be relevant. To verify this negligible buoyancy, firstly some experiments were conducted at different CO_2 flows. The results obtained are shown in Figure 5.30 (the first hours of the runs, comprising conditioning steps in the TGA method, are not shown). The two runs with the highest CO_2 flows (25 and 45 mL/min) gave very close results, whereas the experiment with a low flow (5 mL/min) led to a lower value. From these results it was assumed that, at sufficiently high CO_2 flows (>25 mL/min), the buoyancy of the measurements would be negligible; in particular at the atmospheric pressure at which the experiments were

carried out. Therefore, a gas flowrate of 45 mL/min was set for all subsequent experiments in the apparatus.

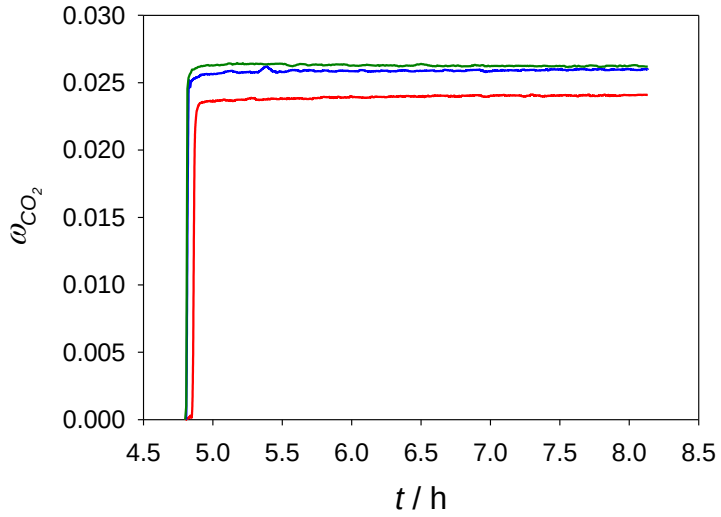

Figure 5.30: Mass fraction of CO_2 (ω_{CO2}) absorbed in $[N_{6666}][Ile]$-SiO_2 SILP at 298.2 K and atmospheric pressure, as determined by TGA, for different circulating flowrates of CO_2 (from bottom to top): 5 mL/min (red), 25 mL/min (blue), 45 mL/min (green).

The absorption of N_2 in the solid support was also tested, given that this gas was intended to be used as inert gas in the experiments. Runs were carried out with a sample of SiO_2-60Å, circulating either CO_2 or N_2. Figure 5.31 shows that the mesoporous support has the ability to absorb both gases, although to a very different extent: the concentration of absorbed N_2 attainable is much lower than that of CO_2 (as expected). The capacity of the silica to absorb N_2 was taken into account to correct the CO_2 absorption measurements.

To analyse the capacity of the SILP for absorption/desorption of CO_2, successive cycles were carried out consecutively with the same sample, without unloading it from the apparatus. The absorption steps were carried out with a flow of CO_2 of 45 mL/min. Reproducible cycles were obtained (although a systematic decay of the weights recorded by the balance was observed, probably due to problems with the calibration of the equipment for long term experiments). The maximum absorption capacity (the net absorption corresponding to each absorption step) remained practically constant, with just a slight decrease after each cycle (Table 5.23).

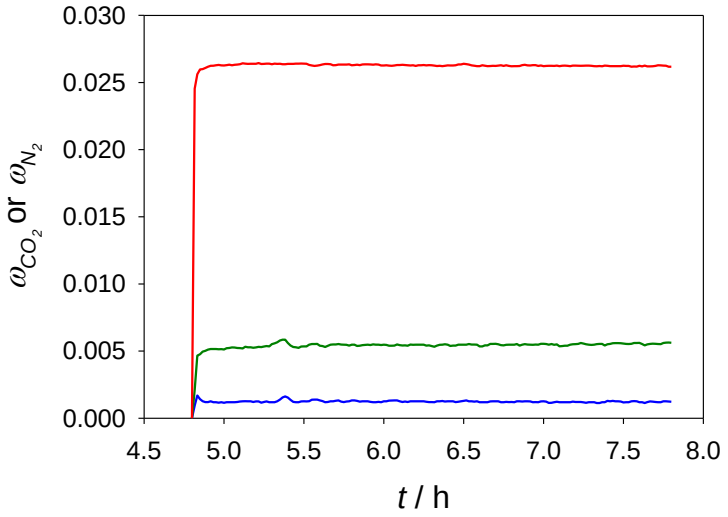

Figure 5.31: Mass fraction of CO_2 (ω_{CO2}) or of N_2 (ω_{N2}) absorbed in SiO_2-60Å or in the SILP at 298.2 K and atmospheric pressure, as determined by TGA, at a circulating flowrate of 45 mL/min. Gas and absorbent (from top to bottom): CO_2 in SILP (red), CO_2 in SiO_2-60Å (green), N_2 in SiO_2-60Å (blue).

Table 5.23: Concentration of CO_2 (in mass fraction) calculated after completion of the absorption step and of the desorption step in each cycle of CO_2 absorption/desorption in TGA experiments for the $[N_{6666}][Ile]$-SiO_2 SILP with a 40% loading of the ionic liquid.

cycle	ω_{CO2}	
	Absorption	Desorption
1	0.0238	0.0008
2	0.0231	0.0007
3	0.0227	0.0005
4	0.0224	0.0002

In a different set of experiments, the effect of pressure on the absorption capacity of $[N_{6666}][Ile]$ and of the SILP was analysed, using a magnetic suspension balance. Due to the high viscosity of the neat ionic liquid, the equilibrium criterion was enhanced with respect to the one used in previous experiments (see sections 5.1 and 5.2). Thus, instead of a mass variation of less than 10 μg in 10 min, a time period of 30 min was used in this case. Figure 5.32 shows the results obtained. In the case of pure $[N_{6666}][Ile]$, the amount of CO_2 absorbed at the maximum pressure tested was still below the one corresponding to the theoretical maximum for the 1:1 chemical reaction with CO_2 (ω_{CO2} = 0.083). Regarding the SILP, a much higher absorption is achieved, in part due to the absorption capacity of the silica, and in part due likely to

the facilitation of the access of the CO_2 molecules to the ionic liquid in the SILP configuration.

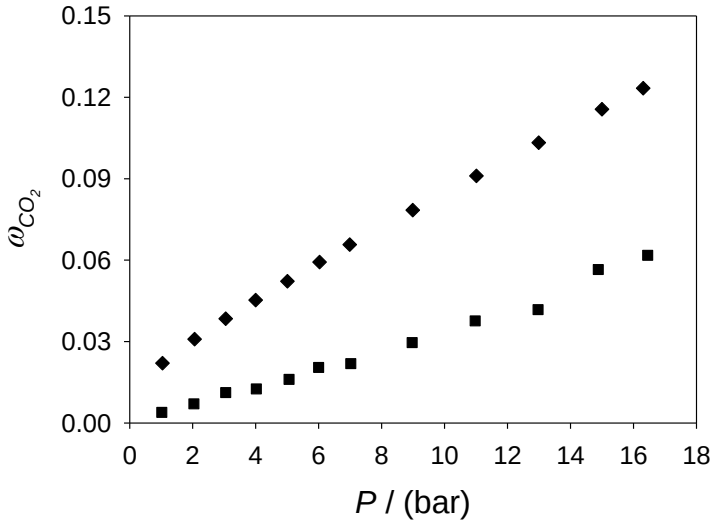

Figure 5.32: Absorption of CO_2 (in mass fraction), at 298.2 K and as a function of pressure, in pure $[N_{6666}][Ile]$ (■) and in the $[N_{6666}][Ile]$-SiO_2 SILP with a 40 % loading of the ionic liquid (♦).

As in the TGA experiments previously described in this section, the stability of the SILP was also tested in the magnetic suspension balance by means of successive cycles of absorption and desorption. However, in this case the desorbing stage was performed by lowering the pressure instead of by increasing the temperature. As shown in Figure 5.33, a total desorption is achieved in each cycle. A slight decrease in maximum and minimum values of absorbed CO_2 is observed with increasing the number of cycles. This might be partially due to a small drift of the baseline of the apparatus in long-time experimental runs. The net CO_2 absorption capacities for each cycle in the pressure range tested are numerically shown in Table 5.24.

Finally, it is interesting to note that there is a good agreement between the results obtained at atmospheric pressure by both techniques utilised in the experiments in this section: TGA and magnetic suspension balance.

Table 5.24: Concentration of CO_2 (in mass fraction) calculated after completion of the absorption step and of the desorption step in each cycle of CO_2 absorption/desorption in the magnetic suspension balance for the $[N_{6666}][Ile]$-SiO_2 SILP with a 40% loading of the ionic liquid, at 298.2 K.

cycle	ω_{CO2}	
	Absorption	Desorption
1	0.1225	0.0201
2	0.1174	0.0164
3	0.1131	0.0140
4	0.1122	0.0126
5	0.1115	0.0119

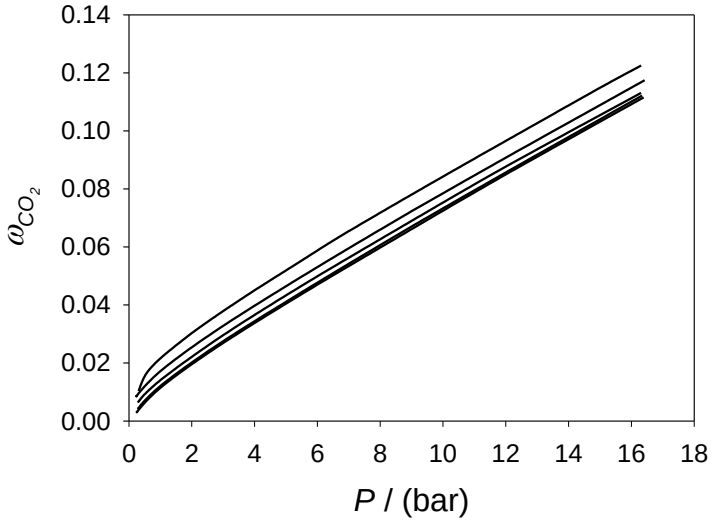

Figure 5.33: Absorption isotherms for consecutive cycles of absorption/desorption of CO_2, at 298.2 K and up to a pressure of *ca.* 16 bar, in the $[N_{6666}][Ile]$-SiO_2 SILP with a 40% loading of ionic liquid.

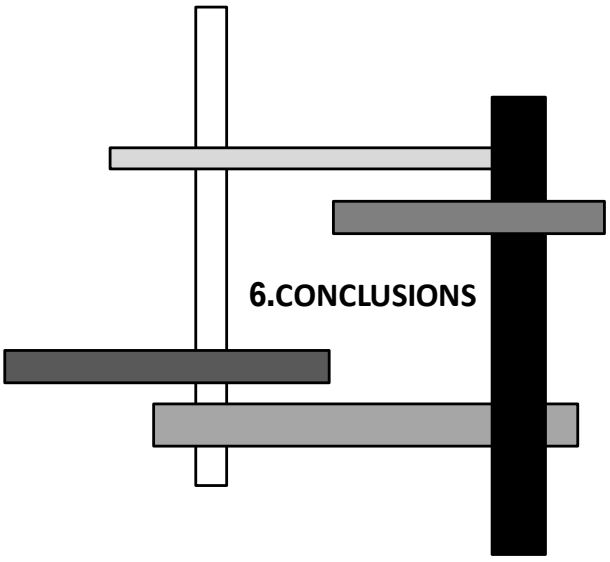

6.CONCLUSIONS

6. CONCLUSIONS

The CO_2 absorption capacity of a series of ionic liquids was studied. Namely, these ionic liquids were: $[C_2C_1im][NTf_2]$, $[C_2py][EtSO_4]$, $[C_2C_1im][EtSO_4]$, $[C_4C_2im][EtSO_4]$, $[C_2C_1im][OAc]$, and $[N_{6666}][Ile]$. In all cases, CO_2 solubilities were tested as a function of pressure in the pressure range up to *ca.* 17 bar. In some cases, investigation of the influence of temperature, or of supporting the ionic liquid on a mesoporous support, was also carried out. The variation of cations and anions of the ionic liquids allowed the analysis of the influence of features of their chemical structure on the CO_2 absorption capacity. Thus, it was found that the ionic liquids with the $[NTf_2]^-$ or the $[EtSO_4]^-$ anions absorbed CO_2 exclusively through a physical mechanism; whereas the ionic liquids containing anions with a basic character, namely $[OAc]^-$ and $[Ile]^-$, undergo a chemical reaction with CO_2, and therefore both chemical and physical absorption mechanisms may be present. Among the ionic liquids with just physisorption, $[C_2C_1im][NTf_2]$ exhibited a higher absorption capacity than any of the ionic liquids containing the $[EtSO_4]^-$ anion, regardless of the nature of the cation. Some influence of the cation was identified when comparing the absorption isotherms of all three ethylsulfate-containing ionic liquids, with the ion with longer alkyl substituent chains ($[C_4C_2im]^+$) leading to a greater absorption than the other two ($[C_2C_1im]^+$ or $[C_2py]^+$), in a molar basis. In any case, higher absorption levels could be achieved with ionic liquids involving chemical absorption. Nevertheless, this higher absorption capacity would come associated with a higher energy cost in the step of solvent recovery in a continuous CO_2 absorption unit.

The experimental methods used for the determination of the CO_2 absorption and the thermal properties were validated by checking the good agreement in the comparison of the results herein obtained for some of the individual ionic liquids with those results reported by other authors in the literature.

The use of binary mixtures of ionic liquids was explored, searching for possible synergies with respect to the utilisation of single ionic liquids. In a first instance, a series of mixtures of ionic liquids with only physical absorption of CO_2

were investigated, with one of the constituting ionic liquids being $[C_2C_1im][NTf_2]$ and the other one of the ethylsulfate ionic liquids: $[C_2py][EtSO_4]$, $[C_2C_1im][EtSO_4]$, or $[C_4C_2im][EtSO_4]$. The entire composition range was screened, both in terms of CO_2 absorption and from the point of view of a series of important thermal and physical properties, at 298.2 K. None of the intermediate compositions was found to have an absorption capacity greater than that of pure $[C_2C_1im][NTf_2]$, in the pressure range up to 16 bar. Nevertheless a slight synergistic effect was identified, by means of analysis of the Henry constants, for the absorption capacity of the mixtures when compared to linearly weighted averages, in a molar basis, of the pure ionic liquid components. This effect may be partially due to a positive excess molar volume in the mixtures, as derived from density measurements, which may be related to an increment of the free volume of the liquid solvent. In all three mixtures investigated in this section, a positive excess volume was found over the entire composition range. In addition to density and molar volume, other thermophysical properties of interest can be tuned with the mixture of two ionic liquids. For instance, viscosity and surface tension of the mixture do typically vary between the extreme limit values of the two constituent single ionic liquids, but interestingly they do not follow a linear variation with composition. Instead, relevant viscosity deviations and surface tension deviations are observed. In the case of viscosity, a pronouncedly negative deviation in viscosity occurs for the mixture $[C_2C_1im][NTf_2]$ + $[C_4C_2im][EtSO_4]$; whereas for the mixtures $[C_2C_1im][NTf_2]$ + $[C_2C_1im][EtSO_4]$ and $[C_2C_1im][NTf_2]$ + $[C_2py][EtSO_4]$ both positive and negative deviations are observed, depending on the concentration range, and in a smaller absolute magnitude. In terms of surface tension, a negative surface tension deviation is observed for all three systems studied, indicating a preferential concentration of the ionic liquid with a lower surface tension ($[C_2C_1im][NTf_2]$) at the surface of the liquid mixture. All mixtures remained liquid down to temperatures well below room temperature, and up to decomposition temperatures ($T_{d,5\%\ onset}$) above 373 K.

An acceptably good correlation of the experimental data of the CO_2 absorption isotherms, using ionic liquids and their mixtures which only implied a physical absorption mechanism, was obtained by means of the classical NRTL model. Redlich-Kister polynomial expansions were found to adequately describe the excess molar volume, viscosity deviation, and surface tension deviation as a function of the

composition of the binary mixtures. Predictive mixing laws for the estimation of viscosity and surface tension of mixtures of the ionic liquids only from data of the pure constituents were tested; but they failed to provide a prediction sufficiently accurate for most engineering purposes.

The mixture of a physisorbing ionic liquid and a chemisorbing ionic liquid was also investigated. Specifically, the absorption of CO_2 in the mixture of $[C_2C_1im][EtSO_4]$ + $[C_2C_1im][OAc]$ was studied at 298.2 K and 353.2 K, up to pressures of 16 bar. The absorption capacity was higher at the lowest temperature tested. At this temperature, the presence of $[C_2C_1im][EtSO_4]$ in the solvent prevented the solidification of the product resulting from the chemical reaction between CO_2 and $[C_2C_1im][OAc]$, improving the gas absorption capacity by facilitating physical absorption after the completion of the chemical reaction. In addition, a notably negative viscosity deviation was observed for the mixture at low temperatures. The maximum deviation of the viscosity from the linearly averaged behaviour of the pure ionic liquids occurs at an approximately equimolar composition, where also the maximum excess molar volume is observed. Both densities and viscosities for this system could be correlated as a function of temperature by means of a quadratic polynomial and of the VFT equation, respectively. Third-order Redlich-Kister polynomial were sufficient to provide an acceptable correlation of the excess molar volumes and viscosity deviations as a function of the composition of the ionic liquid mixture at the different temperatures. Thermal stability was not worse in the mixture than for the less stable ionic liquid, and the lower end of the liquidus range was also well preserved.

In general terms, it can be said that mixtures of ionic liquids can offer some improvements with regard to single ionic liquids with just one type of cation and one type of anion. On the one hand, relatively better absorption capacities can be obtained; and on the other, a greater flexibility in the tailoring of their properties is achieved. Moreover, other beneficial effects can be obtained by mixing ionic liquids in CO2 capture processes, as it was exemplified herein in the prevention of the solidification of the product of a chemical absorption reaction.

In a last approach, a SILP was investigated as absorbent. The absorption capacity obtained for neat $[N_{6666}][Ile]$ was very similar to that obtained with $[C_2C_1im][NTf_2]$, in a mass basis. However, the absorption values for the former are

probably limited by its high viscosity, not corresponding to the theoretical maximum capacity. A substantial improvement was observed when supporting the $[N_{6666}][Ile]$ onto mesoporous silica (configuring a SILP), achieving a CO_2 mass fraction equivalent to that for neat $[C_2C_1im][OAc]$. This improvement was accompanied by a higher thermal stability of the SILP. However, this stability might still be relatively too low as to be used in a real gas absorption unit. Exploration of other supports or tailoring of the structure of the amino acid ionic liquid could help in overcoming this aspect.

List of symbols

List of symbols

A	empirical fit parameter in the Antoine equation (3.23)
A	fit parameter in the Arrhenius-type equation for viscosity (3.39)
A	fit parameter in the Redlich-Kister equation (3.43)
A	fit parameter in the VFT equation (3.41)
a	activity
a	empirical fit parameter in equation for density (3.36 and 3.37)
B	empirical fit parameter in the Antoine equation (3.23)
B	fit parameter in the Arrhenius-type equation for viscosity (3.39)
b	empirical fit parameter in equation for density (3.36 and 3.37)
C	empirical fit parameter in the Antoine equation (3.23)
c	empirical fit parameter in equation for density (3.37)
E_a	'activation' energy; fit parameter in the Arrhenius-type equation for viscosity (3.40)
f	fugacity
G	Gibbs free energy
G	interaction parameters in the Grunberg and Nissan equation (3.46)
g_{ij}	binary interaction parameter in the NRTL model
H	Henry constant
k	fit parameter in the VFT equation (3.41)
M	generic property
m	number of experimental datapoints
m	number of components

m	mass
m	mass of liquid with absorbed gas
MW	molecular weight
n	degree of polynomial expansion
n	number of components
n	number of moles
P	pressure
Q	generic property
R	universal constant of gases
r	empirical exponent in equation 3.50
$rmsd$	root mean square deviation (3.44)
S	entropy
T	temperature
T_0	ideal glass transition temperature; fit parameter in the VFT equation (3.40)
V	volume
V	molar volume
v	velocity
x	molar fraction in the liquid phase
x	spatial direction
y	molar fraction in the vapour phase
y	spatial direction

Subscripts

bal	value measured by the balance at equilibrium
calc	calculated value

corr	corrected value
CO2	carbon dioxide
exp	experimental value
gas	gaseous phase
i	component
j	component
m	mixture
r	sample bucket
s	sample
x	vector component in the x direction
0	value at the initial time

Superscripts

E	excess property
id	ideal solution property
k	generic phase
L	liquid phase
sat	saturation value (3.23)
V	vapour phase
0	standard state

Greek letters

α	non-randomness parameter in the NRTL model
γ	activity coefficient
Δ	variation of property

η	dynamic viscosity
η_∞	dynamic viscosity at infinite temperature; fit parameter in the Arrhenius-type equation for viscosity (3.40)
μ	chemical potential
ν	kinematic viscosity
ρ	density
σ	surface tension
σ	standard deviation (3.38)
σ_r	relative standard deviation (3.41)
τ_{ij}	parameter in the NRTL model
τ_{yx}	shear stress in the x direction on a unit area perpendicular to the y direction
ϕ	number of phases
φ	fugacity coefficient
ω	mass fraction

References

References

A

Adam, G.; Gibbs, J. H. **1965**. On the Temperature Dependence of Cooperative Relaxation Properties in Glass-Forming Liquids. *J. Chem. Phys.*, 43, 139.

Aki, S. N. V. K.; Mellein, B. R.; Saurer, E. M.; Brennecke, J. F. **2004**. High-Pressure Phase Behavior of Carbon Dioxide with Imidazolium-Based Ionic Liquids. *J. Phys. Chem. B*, 108, 20355.

Almeida, H. F. D.; Passos, H.; Lopes-da-Silva, J. A.; Fernandes, A. M.; Freire, M. G.; Coutinho, J. A. P. **2012**. Thermophysical Properties of Five Acetate-Based Ionic Liquids. *J. Chem. Eng. Data*, 57, 3005.

Anderson, J. L. **2008**. Tunable Ionic Liquids for Gas Separation: Solubility Studies for Thermodynamics Analysis. Ph.D. Thesis, University of Notre Dame, South Bend, IN (USA).

Anderson, J. L.; Anthony, J. L.; Brennecke, J. F.; Maginn, E. J. **2008**. Gas Solubilities in Ionic Liquids, in *Ionic Liquids in Synthesis* (editors: Wasserscheid, P.; Welton, T.), 2nd edition, Wiley-VCH, Weinheim (Germany).

Anderson, J. L.; Dixon, J. K.; Brennecke, J. F. **2007**. Solubility of CO_2, CH_4, C_2H_6, C_2H_4, O_2 and N_2 in 1-Hexyl-3-methylpyridinium Bis(trifluoromethylsulfonyl)imide: Comparison to Other Ionic Liquids. *Acc. Chem. Res.*, 40, 1208.

Andrade, E. N. da C. **1930**. The viscosity of liquids. *Nature*, 125, 309.

Angell, C. A.; Moynihan, C. T. **1969**. Transport Processes in Low-Melting Molten Salt Systems, in *Molten Salts. Characterization and Analysis* (editor: G. Mamantov), 1st edition, Marcel Dekker, New York (USA).

Anthony, J. L.; Anderson, J. L.; Maginn, E. J.; Brennecke, J. F. **2005**. Anion Effects on Gas Solubility in Ionic Liquids. *J. Phys. Chem. B*, 109, 6366.

Anthony, J. L.; Maginn, E. J.; Brennecke, J. F. **2001**. Solution Thermodynamics of Imidazolium-Based Ionic Liquids and Water. *J. Phys. Chem. B*, 105, 10942.

Anthony, J. L.; Maginn, E. J.; Brennecke, J. F. **2002**. Solubilities and Thermodynamic Properties of Gases in the Ionic Liquid 1-*n*-Butyl-3-methylimidazolium Hexafluorophosphate. *J. Phys. Chem. B*, 106, 7315.

Aparicio, S.; Atilhan, M. **2012**. Mixed Ionic Liquids: The Case of Pyridinium-Based Fluids. *J. Phys. Chem. B*, 116, 2526.

Arrhenius, S. **1887**. Viscosity of dilute aqueous solutions. *Z. Phys. Chem., Stöch. Ve.*, 1, 285.

Atkins, M.; Kuah, Y. C.; Estager, J.; NG, S.; Oliferenko, A.; Plechkova, N.; Puga, A.; Seddon, K.; Wassell, D. **2011**. Removal of carbon dioxide from a gas stream by using aqueous ionic liquids. PCT patent WO2011/114168.

B

Baltazar, Q. Q.; Leininger, S. K.; Anderson, J. L. **2008**. Binary ionic liquid mixtures as gas chromatography stationary phases for improving the separation selectivity of alcohols and aromatic compounds. *J. Chromatogr. A*, 1182, 119.

Bates, E. D.; Mayton, R. D.; Ntai, I.; Davis Jr., J. H. **2002**. CO_2 Capture by a Task-Specific Ionic Liquid. *J. Am. Chem. Soc.*, 124, 926.

Beckman, E. J. **2004**. A challenge for green chemistry: designing molecules that readily dissolve in carbon dioxide. *Chem. Commun.*, 1885.

Bermejo, M. D.; Martín, A. **2011**. Solubility of gases in ionic liquids. *Global J. Phys. Chem.*, 2, 324.

Blanchard, L. A.; Gu, Z.; Brennecke, J. F. **2001**. High-Pressure Phase Behavior of Ionic Liquid/CO_2 Systems. *J. Phys. Chem. B*, 105, 2437.

Blanchard, L. A.; Hancu, D.; Beckman, E. J.; Brennecke, J. F. **1999**. Green processing using ionic liquids and CO_2. *Nature*, 399, 28.

Bonhôte, P.; Dias, A.-P.; Armand, M.; Papageorgiou, N.; Kalyanasundaram, K.; Grätzel, M. **1996**. Hydrophobic, Highly Conductive Ambient-Temperature Molten Salts. *Inorg. Chem.*, 35, 1168. [Erratum: **1998**, *Inorg. Chem.*, 37, 166.]

C

Cadena, C.; Anthony, J. L.; Shah, J. K.; Morrow, T. I.; Brennecke, J. F.; Maginn, E. J. **2004**. Why Is CO_2 So Soluble in Imidazolium-Based Ionic Liquids?. *J. Am. Chem. Soc.*, 126, 5300.

Cammarata, L.; Kazarian, S. G.; Salter, P. A.; Welton, T. **2001**. Molecular states of water in room temperature ionic liquids. *Phys. Chem. Chem. Phys.*, 3, 5192.

Canongia Lopes, J. N.; Cordeiro, T. C.; Esperança, J. M. S. S.; Guedes, H. J. R.; Huq, S.; Rebelo, L. P. N.; Seddon, K. R. **2005**. Deviations from Ideality in Mixtures of Two Ionic Liquids Containing a Common Ion. *J. Phys. Chem. B*, 109, 3519.

Carvalho, P.; Coutinho, J. A. P. **2010**. On the Nonideality of CO_2 Solutions in Ionic Liquids and Other Low Volatile Solvents. *J. Phys. Chem. Lett.*, 1, 774.

Carvalho, P. J.; Freire, M. G.; Marrucho, I. M.; Queimada, A. J.; Coutinho, J. A. P. **2008**. Surface Tensions for the 1-Alkyl-3-methylimidazolium Bis(trifluoromethylsulfonyl)imide Ionic Liquids. *J. Chem. Eng. Data*, 53, 1346.

Chauvin, Y.; Einloft, S.; Olivier, H. **1995**. Catalytic Dimerization of Propene by Nickel-Phosphine Complexes in 1-Butyl-3-methylimidazolium Chloride/$AlEt_xCl_{3-x}$ (x = 0, 1) Ionic Liquids. *Ind. Eng. Chem. Res.*, 34, 1149.

Chen, C.-C.; Evans, L. B. **1986.** A Local Composition Model for the Excess Gibbs Energy of Aqueous Electrolyte Systems. *AIChE J.*, 32, 444.

Chen, C.-C.; Simoni, L. D; Brennecke, J. F; Stadtherr, M. A. **2008**. Correlation and Prediction of Phase Behavior of Organic Compound in Ionic Liquids Using the Nonrandom Two-Liquid Segment Activity Coefficient Model. *Ind. Eng. Chem. Res.*, 47, 7081.

Chen, Y.; Han, J.; Wang, T.; Mu, T. **2011**. Determination of Absorption Rate and Capacity of CO_2 in Ionic Liquids at Atmospheric Pressure by Thermogravimetric Analysis. *Energy Fuels*, 25, 5810.

Chen, Y.; Zhang, S.; Yuan, X.; Zhang, Y.; Zhang, X.; Dai, W.; Mori, R. **2006**. Solubility of CO_2 in imidazolium-based tetrafluoroborate ionic liquids. *Thermochim. Acta*, 441, 42.

Chinn, D.; Vu, D.; Driver, M. S.; Boudreau, L. C. **2005**. Carbon dioxide removal from gas using ionic liquid absorbents. US Patent 2005/0129598.

Ciferno, J.; Litynski, J.; Brickett, L; Murphy, J.; Munson, R.; Zaemsky, C.; Marano, J.; Strock, J. **2011**. Advanced CO_2 Capture R&D Program: Technology Update. DOE/NETL. Available at the website: http://www.netl.doe.gov/technologies/ coalpower/ewr/pubs/ CO2CaptureTechUpdate051711.pdf (accessed: November 2013).

Cohen, M. H.; Turnbull, D. **1959**. Molecular Transport in Liquids and Glasses. *J. Chem. Phys.*, 31, 1164.

Crosthwaite, J. M.; Muldoon, M. J.; Aki, S. N. V. K.; Maginn, E. J.; Brennecke, J. F. **2006**. Liquid Phase Behavior of Ionic Liquids with alcohols: Experimental Studies and Modeling. *J. Phys. Chem.B*, 110, 9354.

Crosthwaite, J. M.; Muldoon, M. J.; Dixon, J. K.; Anderson, J. L.; Brennecke, J. F. **2005**. Phase transition and decomposition temperatures, heat capacities and viscosities of pyridinium ionic liquids. *J. Chem. Thermodyn.*, 37, 559.

Cruz, J. L.; Renon, H. **1978**. A New Thermodynamic Representation of Binary Electrolyte Solutions Nonideality in the Whole Range of Concentrations. *AIChE J.*, 24, 817.

D

D'Alessandro, D. M.; Smit, B.; Long, J. R. **2010**. Carbon Dioxide Capture: Prospects for New Materials. *Angew. Chem. Int. Ed.*, 49, 6058.

Deng, Y.; Husson, P.; Delort, A.-M.; Besse-Hoggan, P.; Sancelme, M.; Costa Gomes, M. F. **2011**. Influence of an Oxygen Functionalization on the Physicochemical Properties of Ionic Liquids: Density, Viscosity, and Carbon Dioxide Solubility as a Function of Temperature. *J. Chem. Eng. Data*, 56, 4194.

Devore, J. L. **2000**. *Probability and Statistics for Engineering and the Sciences*, 4th edition, Duxbury, Pacific Grove, CA (USA).

Docherty, K. M.; Dixon, J. K.; Kulpa Jr., C. F. **2007**. Biodegradability of imidazolium and pyridinium ionic liquids by an activated sludge microbial community. *Biodegradation*, 18, 481.

Domańska, U.; Laskowska, M. **2008**. Phase Equilibria and Volumetric Properties of (1-Ethyl-3-Methylimidazolium Ethylsulfate + Alcohol or Water) Binary Systems. *J. Solution Chem.*, 37, 1271.

Domańska, U.; Żołek-Tryznowska, Z.; Królikowski, M. **2007**. Thermodynamic Phase Behavior of Ionic Liquids. *J. Chem. Eng. Data*, 52, 1872.

E

Easteal, A. J.; Angell, C. A. **1970**. Phase Equilibria, Electrical Conductance, and Density in the Glass-Forming System Zinc Chloride + Pyridinium Chloride. A Detailed Low-Temperature Analog of the Silicon Dioxide + Sodium Oxide System. *J. Phys. Chem.*, 74, 3987.

European environmental agency. **2013**. Annual European Union greenhouse gas inventory 1990-2011 and inventory report 2013. Available at the website: http://www.eea.europa.eu/publications/european-union-greenhouse-gas-inventory-2013 (accessed: November 2013).

European environmental agency. Available at the website: http://www.eea.europa.eu/data-and-maps/data/data-viewers/greenhouse-gases-viewer (accessed: November 2013).

F

Felder, R. M.; Rousseau, R. W. **2005**. *Elementary principles of chemical processes*. 3rd edition, Wiley, Hoboken, NJ (USA).

Feng, Z.; Cheng-Gang, F.; You-Ting, W.; Yuan-Tao, W.; Ai-Min, L.; Zhi-Bing, Z. **2010**. Absorption of CO_2 in the aqueous solutions of functionalized ionic liquids and MDEA. *Chem. Eng. J.*, 160, 691.

Fernández, A.; Torrecilla, J. S; García, J.; Rodríguez, F. **2007**. Thermophysical Properties of 1-Ethyl-3-methylimidazolium Ethylsulfate and 1-Butyl-3-methylimidazolium Methylsulfate Ionic Liquids. *J. Chem. Eng. Data*, 52, 1979.

Ficke, L. E.; Rodríguez, H.; Brennecke, J. F. **2008**. Heat Capacities and Excess Enthalpies of 1-Ethyl-3-methylimidazolium-Based Ionic Liquids and Water *J. Chem. Eng. Data*, 53, 2112.

Figueroa, J. D.; Fout, T.; Plasynski, S.; McIlvried, H.; Srivastava, R. D. **2008**. Advances in CO_2 capture technology – The U.S. Department of Energy's Carbon Sequestration Program. *Int. J. Greenhouse Gas Control*, 2, 9.

Finotello, A.; Bara, J. E.; Camper, D.; Noble, R. D. **2008a**. Room-Temperature Ionic Liquids: Temperature Dependence of Gas Solubility Selectivity. *Ind. Eng. Chem. Res.*, 47, 3453.

Finotello, A.; Bara, J. E.; Narayan, S.; Camper, D.; Noble, R. D. **2008b**. Ideal Gas Solubility Selectivities in a Binary Mixture of Room-Temperature Ionic Liquids. *J. Phys. Chem. B*, 112, 2335.

Forsyth, S. A.; Pringle, J. M.; MacFarlane, D. R. **2004**. Ionic Liquids – An Overview. *Aust. J. Chem.*, 57, 113.

Fredlake, C. P.; Crosthwaite, J. M.; Hert, D. G.; Aki, S. N. V. K.; Brennecke, J. F. **2004.** Thermophysical Properties of Imidazolium-Based Ionic Liquids. *J. Chem. Eng. Data*, *49*, 954.

Freeman, B.; Rhudy, R. **2007**. Assessment of Post-Combustion Capture Technology Developments. Electric Power Research Institute, Palo Alto, CA (USA). Available at the website: http://www.epri.com/search/Pages/results.aspx?k=Assessment%20of%20Post-Combustion%20Capture%20Technology%20Developments (accessed: November 2013).

Freemantle, M. **1998**. Designer solvents – Ionic liquids may boost clean technology development. *Chem. Eng. News*, 76 [30th March issue], 32.

Freemantle, M. **2010**. *An Introduction to Ionic Liquids*, 1st edition, Royal Society of Chemistry, Cambridge (UK).

Freire, M. G.; Carvalho, P. J.; Fernandes, A. M.; Marrucho, I. M.; Queimada, A. J.; Coutinho, J. A. P. **2007**. Surface tension of imidazolium based ionic liquids: Anion, cation, temperature and water effect. *J. Colloid Interface Sci.*, 314, 621.

Freire, M. G.; Teles, A. R. R.; Rocha, M. A. A.; Schröder, B.; Neves, C. M. S. S.; Carvalho, P. J.; Evtuguin, D. V.; Santos, L. M. N. B. F.; Coutinho, J. A. P. **2011**. Thermophysical Characterization of Ionic liquids Able to Dissolve Biomass. *J. Chem. Eng. Data*, 56, 4813.

Fröba, A. P.; Rausch, M. H.; Krzeminski, K.; Assenbaum, D.; Wasserscheid, P.; Leipertz, A. **2010**. Thermal Conductivity of Ionic Liquids: Measurement and Prediction. *Int. J. Thermophys.*, 31, 2059.

Fulcher, G. S. **1925**. Analysis of Recent Measurements of the Viscosity of Glasses. *J. Am. Ceram. Soc.*, 8, 339.

G

Galán Sánchez, L. M.; Meindersma, G. W.; de Haan, A. B. **2007**. Solvent Properties of Functionalized Ionic Liquids for CO_2 Absorption. *Chem. Eng. Res. Des.*, 85, 31.

García, J.; García, S.; Torrecilla, J. S.; Rodríguez, F. **2011**. *N*-butylpyridinium bis-(trifluoromethylsulfonyl)imide ionic liquids as solvents for the liquid-liquid extraction of aromatics from their mixture with alkanes: Isomeric effect of the cation. *Fluid Phase Equilib.*, 301, 62.

Gibbs, J. H.; DiMarzio, E. A. **1958**. Nature of the Glass Transition and the Glassy State. *J. Chem. Phys.*, 28, 373.

Gmehling, J.; Kolbe, B.; Kleiber, M.; Rarey, J. **2012**. *Chemical Thermodynamics for Process Simulation*, 1st edition, Wiley-VCH, Weinheim (Germany).

Gomes de Azevedo, R.; Esperança, J. M. S. S.; Szydlowski, J.; Visak, Z. P.; Pires, P. F.; Guedes, H. J. R.; Rebelo, L. P. N. **2005**. Thermophysical and thermodynamic properties of ionic liquids over an extended pressure range: [bmim][NTf_2] and [hmim][NTf_2]. *J. Chem. Thermodyn.*, 37, 888.

Gómez, E.; Domínguez, I.; González, B.; Domínguez, Á. **2010**. Liquid-Liquid Equilibria of the Ternary Systems of Alkane + Aromatic + 1-Ethylpyridinium Ethylsulfate Ionic Liquid at T = (283.15 and 298.15) K. *J. Chem. Eng. Data*, 55, 5169.

Gómez, E.; González, B.; Calvar, N.; Tojo, E.; Domínguez, Á. **2006.** Physical Properties of Pure 1-Ethyl-3-methylimidazolium Ethylsulfate and Its Binary Mixtures with Ethanol and Water at Several Temperatures. *J. Chem. Eng. Data*, 51, 2096.

González, B.; Calvar, N.; Gómez, E.; Domínguez, I.; Domínguez, Á. **2009**. Synthesis and Physical Properties of 1-Ethylpyridinium Ethylsulfate and its Binary Mixture with Ethanol and 1-Propanol at Several Temperatures. *J. Chem. Eng. Data*, 54, 1353.

Grunberg, L.; Nissan, A. H. **1949**. Mixture law for viscosity. *Nature*, 164, 799.

Gu, Z.; Brennecke, J. F. **2002**. Volume Expansivities and Isothermal Compressibilities of Imidazolium and Pyridinium-Based Ionic Liquids. *J. Chem. Eng. Data*, 47, 339.

Gurau, G.; Rodríguez, H.; Kelley, S. P.; Janiczek, P.; Kalb, R. S.; Rogers, R. D. **2011**. Demostration of Chemisorption of Carbon Dioxide in 1,3-Dialkylimidazolium Acetate Ionic Liquids. *Angew. Chem. Int. Ed.*, 50, 12024.

Gurkan, B. E.; de la Fuente, J. C.; Mindrup, E. M.; Ficke, L. E.; Goodrich, B. F.; Price, E. A.; Schneider, W. F.; Brennecke, J. F. **2010a**. Equimolar CO_2 Absorption by Anion-Functionalized Ionic Liquids. *J. Am. Chem. Soc.*, 132, 2116.

Gurkan, B.; Goodrich, B. F.; Mindrup, E. M.; Ficke, L. E.; Massel, M.; Seo, S.; Senftle, T. P.; Wu, H.; Glaser, M. F.; Shah, J. K.; Maginn, E. J.; Brennecke, J. F.; Schneider, W. F. **2010b**. Molecular Design of High Capacity, Low Viscosity, Chemically Tunable Ionic Liquids for CO_2 Capture. *J. Phys. Chem. Lett.*, 1, 3494.

H

Hasib-ur-Rahman, M.; Siaj, M.; Larachi, F. **2010**. Ionic liquids for CO_2 capture – Development and progress. *Chem. Eng. Process.*, 49, 313.

Hasse, B.; Lehmann, J.; Assenbaum, D.; Wassercheid, P.; Leipertz, A.; Fröba, A. P. **2009**. Viscosity, Interfacial Tension, Density, and Refractive Index of Ionic Liquids [EMIM][$MeSO_3$], [EMIM][$MeOHPO_2$], [EMIM][$OcSO_4$], and [BBIM][NTf_2] in

Dependence on Temperature at Atmospheric Pressure. *J. Chem. Eng. Data*, 54, 2576.

Haumann, M.; Riisager, A. **2008**. Hydroformylation in Room Temperature Ionic Liquids (RTILs): Catalyst and Process Developments. *Chem. Rev.*, 108, 1474.

Holbrey, J. D.; Reichert, W. M.; Swatloski, R. P.; Broker, G. A.; Pitner, W. R.; Seddon, K. R.; Rogers, R.D. **2002**. Efficient, halide free synthesis of new, low cost ionic liquids: 1,3-dialkylimidazolium salts containing methyl- and ethyl-sulfate anions. *Green Chem.*, 4, 407.

Holbrey, J. D.; Rogers, R. D. **2008**. Physicochemical Properties of Ionic Liquids: Melting Point and Phase Diagrams, in *Ionic Liquids in Synthesis* (editors: Wasserscheid, P.; Welton, T.), 2nd edition, Wiley-VCH, Weinheim (Germany).

Holbrey, J. D.; Seddon, K. R. **1999**. Ionic Liquids. *Clean Prod. Proc.*, 1**,** 223.

Hong, G.; Jacquemin, J.; Deetlefs, M.; Hardacre, C.; Husson, P.; Costa Gomes, M. F. **2007**. Solubility of carbon dioxide and ethane in three ionic liquid based on the bis{(trifluoromethyl)sulfonyl}imide anion. *Fluid Phase Equilib.*, 257, 27.

Huang, J.; Rüther, T. **2009**. Why are Ionic Liquids Attractive for CO_2 Absorption? An Overview. *Aust. J. Chem.*, 62, 298.

Huang, X.; Margulis, C. J.; Li, Y.; Berne, B. J. **2005**. Why Is The Partial Molar Volume of CO_2 So Small When Dissolved in a Room Temperature Ionic Liquid? Structure and Dynamics of CO_2 Dissolved in [$Bmim^+$][$PF6^-$]. *J. Am. Chem. Soc.*, 127, 17842.

Huddleston, J. G.; Visser, A. E.; Reichert, W. M.; Willauer, H. D.; Broker, G. A.; Rogers, R. D. **2001**. Characterization and comparison of hydrophilic and hydrophobic room temperature ionic liquids incorporating the imidazolium cation. *Green Chem.*, 3, 156.

Husson, P.; Pison, L.; Jacquemin, J.; Costa Gomes, M. F. **2010**. Influence of water on the carbon dioxide absorption by 1-ethyl-3-methylimidazolium bis(trifluoromethylsulfonyl)amide. *Fluid Phase Equilib.*, 294, 98.

Huttenhuis, P. J. G.; Agrawal, N. J.; Hogendoorn, J. A.; Versteeg, G. F. **2007**. Gas solubility of H_2S and CO_2 in aqueous solutions of *N*-methyldiethanolamine. *J. Petrol. Sci. Eng.*, 55, 122.

J

Jacquemin, J.; Husson, P.; Majer, V.; Padua, A. A. H.; Costa Gomes, M. F. **2008**. Thermophysical properties, low pressure solubilities and thermodynamics of solvation of carbon dioxide and hydrogen in two ionic liquids based on the alkylsulfate anion. *Green Chem.*, 10, 944.

Jacquemin, J.; Husson, P.; Mayer, V.; Cibulka, I. **2007**. High-Pressure Volumetric Properties of Imidazolium-Based Ionic Liquids: Effect of the anion. *J. Chem. Eng. Data*, 52, 2204.

Jacquemin, J.; Husson, P.; Padua, A. A. H.; Majer, V. **2006**. Density and viscosity of several pure and water-satured ionic liquids. *Green Chem.*, 8, 172.

Jalili, A. H.; Mehdizadeh, A.; Shokouhi, M.; Sakhaeinia, H.; Taghikhani, V. **2010**. Solubility of CO_2 in 1-(2-hydroxyethyl)-3-methylimidazolium ionic liquids with different anions. *J. Chem. Thermodyn.*, 42, 787.

Jiang, Y.-Y.; Wang, G.-N.; Zhou, Z.; Wu, Y.-T.; Geng, J.; Zhang, Z.-B. **2008**. Tetraalkylammonium amino acids as functionalized ionic liquids of low viscosity. *Chem. Commun.*, 505.

Jutz, F.; Andanson, J.-M.; Baiker, A. **2011**. Ionic Liquids and Dense Carbon Dioxide: A Beneficial Biphasic System for Catalysis. *Chem. Rev.*, 111, 322.

K

Katti, P. K.; Chaudhri, M. M. **1964**. Viscosities of binary mixtures of benzyl acetate with dioxane, aniline, and m-cresol. *J. Chem. Eng. Data*, 9, 442.

Kazarian, S. G.; Vincent, M. F.; Bright, F. V.; Liotta, C. L.; Eckert, C. A. **1996**. Specific Intermolecular Interaction of Carbon Dioxide with Polymers. *J. Am. Chem. Soc.*, 118, 1729.

Kilaru, P.; Baker, G. A.; Scovazzo, P. **2007**. Density and Surface Tension Measurements of Imidazolium-, Quaternary Phosphonium-, and Ammonium-Based Room Temperature Ionic Liquids: Data and Correlations. *J. Chem. Eng. Data*, 52, 2306.

Kohl, A. L.; Nielsen, R. B. **1997**. *Gas Purification*, 5th edition, Gulf Publishing Company, Houston, TX (USA).

Kolding, H.; Fehrmann, R.; Riisager, A. **2012**. CO_2 Capture technologies: Current status and new directions using supported ionic liquid phase (SILP) absorbers. *Sci. China Chem.*, 55, 1648.

L

Law, G.; Watson, P. R. **2001**. Surface Tension Measurements of *N*-Alkylimidazolium Ionic Liquids. *Langmuir*, 17, 6138.

Lee, S. H.; Ha, S. H.; Hiep, N. M.; Chang, W. J.; Koo, Y. M. **2008**. Lipase-catalyzed synthesis of glucose fatty acid ester using ionic liquids mixtures. *J. Biotechnol.*, 133, 486.

Lei, Z.; Han, J.; Zhang, B.; Li, Q.; Zhu, J.; Chen, B. **2012**. Solubility of CO_2 in Binary Mixture of Room-Temperature Ionic Liquids at High Pressures. *J. Chem. Eng. Data*, 57, 2153.

Liu, K.; Zhou, Y.-X.; Han, H.-B.; Zhou, S.-S.; Feng, W.-F.; Nie, J.; Li, H.; Huang, X.-J.; Armand, M.; Zhou, Z.-B. **2010**. Ionic liquids based on (fluorosulfonyl)(pentafluoroethanesulfonyl)imide with various oniums. *Electrochim. Acta*, 55, 7145.

Long, J.; Guo, B.; Li, X.; Jiang, Y.; Wang, F.; Tsang, S. C.; Wang, L.; Yu, K. M. K. **2011**. One step catalytic conversion of cellulose to sustainable chemicals utilizing cooperative ionic liquid pairs. *Green Chem.*, 13, 2334.

M

Maginn, E. J. **2005**. Design and Evaluation of Ionic Liquids as Novel CO_2 Absorbent. *Quarterly Technical Report to DOE*. Available at the website: http://www.netl.doe.gov/technologies/coalpower/ewr/co2/pubs/42122%20U.%20Notre%20Dame%20ionic%20liquids%20Final%20Report%20Sep%202007.pdf (accessed: November 2013).

Manic, M. S.; Macedo, E. A.; Najdanovic-Visak, V. **2012b**. Trihexyl(tetradecyl)phosphonium bromide: Liquid density, surface tension and solubility of carbon dioxide. *Fluid Phase Equilib.*, 324, 8.

Manic, M. S.; Queimada, A. J.; Macedo, E. A.; Najdanovic-Visak, V. **2012a**. High-pressure solubilities of carbon dioxide in ionic liquids based on bis(trifluoromethylsulfonyl)imide and chloride. *J. Supercrit. Fluids*, 65, 1.

Mantz, R. A.; Trulove, P. C. **2008**. Viscosity and Density of Ionic Liquids, in *Ionic Liquids in Synthesis* (editors: Wasserscheid, P.; Welton, T.), 2nd edition, Wiley-VCH, Weinheim (Germany).

Marsh, K. N.; Boxall, J. A.; Lichtenthaler, R. **2004**. Room temperature ionic liquids and their mixtures – a review. *Fluid Phase Equilib.*, 219, 93.

Martino, W.; Fernandez de la Mora, J.; Yoshida, Y.; Saito, G.; Wilkes, J. **2006**. Surface tension measurements of highly conducting ionic liquids. *Green Chem.*, 8, 390.

Mehnert, C. P. **2005**. Supported Ionic Liquid Catalysis. *Chem. Eur. J.*, 11, 50.

Menjoge, A.; Dixon, J.; Brennecke, J. F.; Maginn, E. J.; Vasenkov, S. **2009**. Influence of Water on Diffusion in Imidazolium-Based Ionic Liquids: A Pulsed Field Gradient NMR study. *J. Phys. Chem. B*, 113, 6353.

Metz, B.; Davidson, O.; De Coninck, H. C.; Loos, M.; Meyer, L. A. **2005**. IPCC Special Report on Carbon Dioxide Capture and Storage, prepared by Working Group III of the Intergovernmental Panel on Climate Change, Cambridge University Press, New York (USA). Available at the website: http://www.ipcc-wg3.de/special-reports/special-report-on-carbon-dioxide-capture-and-storage (accessed: November 2013).

Muldoon, M. J.; Aki, S. N. V. K.; Anderson, J. L.; Dixon, J. K.; Brennecke, J. F. **2007**. Improving Carbon Dioxide Solubility in Ionic Liquids. *J. Phys. Chem. B*, 111, 9001.

N

Navia, P.; Troncoso, J.; Romaní, L. **2007**. Excess Magnitudes for Ionic Liquid Binary Mixtures with a Common Ion. *J. Chem. Eng. Data*, 52, 1369. [Erratum: **2007**. *J. Chem. Eng. Data,* 52, 2542].

Navia, P.; Troncoso, J.; Romaní, L. **2008**. Viscosities for Ionic Liquid Binary Mixtures with a Common Ion. *J. Solution Chem.*, 37, 677.

Newsham, D. M. T. **1992**. Liquid-liquid equilibria, in *Science and Practice of Liquid-Liquid Extraction* (editor: J. D. Thornton), vol. 1, Clarendon Press, Oxford (UK).

Ngo, H. L.; LeCompte, K.; Hargens, L.; McEwen, A. B. **2000**. Thermal properties of imidazolium ionic liquids. *Thermochim. Acta*, 357-358, 97.

Niedermeyer, H.; Hallet, J. P.; Villar-Garcia, I. J.; Hunt, P. A.; Welton, T. **2012**. Mixtures of ionic liquids. *Chem. Soc. Rev.*, 41, 7780.

NIST Chemistry WebBook. Available at the website: http://webbook.nist.gov/chemistry/ (accessed: November 2013).

O

Ohno, H.; Fukumoto, K. **2007**. Amino Acid Ionic Liquids. *Acc. Chem. Res.*, 40, 1122.

Okoturo, O. O.; VanderNoot, T. J. **2004**. Temperature dependence of viscosity for room temperature ionic liquids. *J. Electroanal. Chem.*, 568, 167.

P

Palomar, J.; Gonzalez-Miquel, M.; Polo, A.; Rodriguez, F. **2011**. Understanding the Physical Absorption of CO_2 in Ionic Liquids Using the COSMO-RS Method. *Ind. Eng. Chem. Res.*, 50, 3452.

Poling, B. E.; Prausnitz, J. M.; O'Connell, J. P. **2001**. *The Properties of Gases and Liquids*, 5th edition, McGraw-Hill, New York (USA).

Powell, R. E.; Roseveare, W. E.; Eyring, H. **1941**. Diffusion, Thermal Conductivity, and Viscous Flow of Liquids. *Ind. Eng. Chem.*, 33, 430.

Prausnitz, J. M.; Lichtenthaler, R. N.; Gomes de Azevedo, E. **1999**. *Molecular Thermodynamics of Fluid-Phase Equilibria*. 3th edition, Prentice Hall, Upper Saddle River, NJ (USA).

Pray, H. A.; Schweickert, C. C.; Minnich, B. H. **1952**. Solubility of Hydrogen, Oxygen, Nitrogen, and Helium in Water at Elevated Temperatures. *Ind. Eng. Chem.*, 44, 1146.

Q

Quijada-Maldonado, E.; van der Boogaart, S.; Lijbers, J. H.; Meindersma, G. W.; de Haan, A. B. **2012**. Experimental densities, dynamic viscosities and surface tensions of the ionic liquids series 1-ethyl-3-methylimidazolium acetate and dicyanamide and their binary and ternary mixtures with water and ethanol at T = (298.15 to 343.15 K). *J. Chem. Thermodyn.*, 51, 51.

R

Raade, J. W.; Padowitz, D. **2011**. Development of Molten Salt Heat Transfer Fluid with Low Melting Point and High Thermal Stability. *J. Sol. Energy Eng.*, 133, 031013.

Raeissi, S.; Peters, C. J. **2009**. Carbon Dioxide Solubility in the Homologous 1-Alkyl-3-methylimidazolium Bis(trifluoromethylsulfonyl)imide Family. *J. Chem. Eng. Data*, 54, 382.

Ramdin, M.; de Loos, T. W.; Vlugt, T. J. H. **2012**. State-of-the-Art of CO_2 Capture with Ionic Liquids. *Ind. Eng. Chem. Res.*, 51, 8149.

Rao, V.; Datta, R. **1988**. Development of a supported molten-salt Wacker catalyst for the oxidation of ethylene to acetaldehyde. *J. Catal.*, 114, 377.

Raveendran, P.; Wallen, S. L. **2002**. Cooperative C-H···O Hydrogen Bonding in CO_2-Lewis Base Complexes: Implications for Solvation in Supercritical CO_2. *J. Am. Chem. Soc.*, 124, 12590.

Raveendran, P.; Wallen, S. L. **2003**. Exploring CO_2-Philicity: Effects of Stepwise Fluorination. *J. Phys. Chem. B*, 107, 1473.

Redlich, O.; Kister, A. T. **1948**. Thermodynamics of Nonelectrolyte Solutions. Algebraic Representation of Thermodynamic Properties and the Classification of Solutions. *Ind. Eng. Chem.*, 40, 345.

Renon, H.; Prausnitz, J. M. **1968**. Local Compositions in Thermodynamic Excess Functions for Liquid Mixtures. *AIChE J.*, 14, 135.

Riddick, J. A.; Bunger, W. B.; Sakano, T. K. **1986**. *Organic Solvent – Physical Properties and Methods of Purification*, 4th edition, Wiley, New York (USA).

Riisager, A.; Eriksen, K. M.; Wasserscheid, P.; Fehrmann, R. **2003**. Propene and 1-octene hydroformylation with silica-supported, ionic liquid-phase (SILP) Rh-phosphine catalysts in continuous fixed-bed mode. *Catal. Lett.*, 90, 149.

Riisager, A.; Fehrmann, R.; Flicker, S.; van Hal, R.; Haumann, M.; Wasserscheid, P. **2005**. Very Stable and Highly Regioselective Supported Ionic-Liquid-Phase (SILP) Catalysis: Continuous Flow Fixed-Bed Hydroformylation of Propene. *Angew. Chem. Int. Ed.*, 44, 815.

Riisager, A.; Fehrmann, R.; Haumann, M.; Wasserscheid, P. **2006**. Supported ionic liquids: versatile reaction and separation media. *Top. Catal.*, 40, 91.

Rilo, E.; Varela, L. M.; Cabeza, O. **2012**. Density and Derived Thermodynamic Properties of 1-Ethyl-3-methylimidazolium Alkyl Sulfate Ionic Liquid Binary Mixtures with Water and with Ethanol from 288 K to 318 K. *J. Chem. Eng. Data*, 57, 2136.

Rolker, J.; Arlt, W. **2006**. Abtrennung von Kohlendioxid aus Rauchgasen mittels Absorption. *Chem. Ing. Tech.,* 78**,** 416.

S

Schreiner, C.; Zugmann, S.; Hartl, R.; Gores, H. J. **2010**. Fractional Walden Rule for Ionic Liquids: Examples from Recent Measurements and a Critique of the So-Called Ideal KCl Line for the Walden Plot. *J. Chem. Eng. Data*, 55, 1784.

Scott, R. L. **1956**. Corresponding States Treatment of Nonelectrolyte Solutions. *J. Chem. Phys.*, 25, 193.

Scovazzo, P.; Camper, D.; Kieft, J.; Poshusta, J.; Koval, C.; Noble, R. **2004**. Regular Solution Theory and CO_2 Gas Solubility in Room-Temperature Ionic Liquids. *Ind. Eng. Chem. Res.*, 43, 6855.

Seddon, K. R.; Stark, A. **2007**. Ionic Liquids., in *Kirk-Othmer Encyclopedia of Chemical Technology* (editor: A. Seidel), vol. 26, 5th edition, Wiley, Hoboken, NJ (USA).

Seddon, K. R.; Stark, A.; Torres, M. J. **2000**. Influence of Chloride, Water, and Organic Solvents on the Physical Properties of Ionic Liquids. *Pure Appl. Chem.*, 72, 2275.

Seddon, K. R.; Stark, A.; Torres, M.-J. **2002**. Viscosity and Density of 1-Alkyl-3-Methylimidazolium Ionic Liquids, in *Clean Solvents: Alternative Media for Chemical Reactions and Processing* (editors: Abraham, M. A.; Moens, L.), ACS Symposium Series, vol. 819, pp. 34-49, American Chemical Society, Washington, DC (USA).

Selvam, T.; Machoke, A.; Schwieger, W. **2012**. Supported ionic liquids on non-porous and porous inorganic materials – A topical review. *Appl. Catal. A*, 445-446, 92.

Shariati, A.; Peters, C. J. **2005**. High-pressure phase equilibria of systems with ionic liquids. *J. Supercrit. Fluids*, 34, 171.

Shiflett, M. B.; Kasprzak, D. J.; Junk, C. P.; Yokozeki, A. **2008**. Phase behaviour of {carbon dioxide + [bmim][Ac]} mixtures. *J. Chem. Thermodyn.*, 40, 25.

Shiflett, M. B.; Yokozeki, A. **2006**. Solubility and diffusivity of hydrofluorocarbons in room-temperature ionic liquids. *AIChE J.*, *52*, 1205.

Shiflett, M. B.; Yokozeki, A. **2009**. Phase Behavior of Carbon Dioxide in Ionic Liquids: [emim][Acetate], [emim][Trifluoroacetate], and [emim][Acetate] + [emim][Trifluoroacetate] Mixtures. *J. Chem. Eng. Data*, 54, 108.

Shunmugavel, S.; Kegnæs, S.; Due-Hansen, J.; Gretasdottir, T. A.; Riisager, A.; Fehrmann, R. **2010**. Selective Gas Absorption by Ionic Liquids. *ECS Trans.*, 7, 117.

Simoni, L. D.; Lin, Y.; Brennecke, J. F.; Stadtherr, M. A. **2008**. Modeling Liquid-Liquid Equilibrium of Ionic Liquid Systems with NRTL, Electrolyte-NRTL, and UNIQUAC. *Ind. Eng. Chem. Res.*, 47, 256.

Smith, F. L.; Harvey, A. H. **2007**. Avoid Common Pitfalls When Using Henry's Law. *Chem. Eng. Process* [September issue], 33.

Smith, J. M.; Van Ness, H. C.; Abbott, M. M. **2005**. *Introduction to Chemical Engineering Thermodynamics*. 7th edition, McGraw-Hill, New York (USA).

Sørensen, J. M.; Arlt, W. **1980**. *Liquid-Liquid Equilibrium Data Collection*. DECHEMA Chemistry Data Series, Frankfurt (Germany).

Stevanovic, S.; Podgoršek, A.; Pádua, A. A. H.; Costa Gomes, M. F. **2012**. Effect of Water on the Carbon Dioxide Absorption by 1-Alkyl-3-methylimidazolium Acetate Ionic Liquids. *J. Phys. Chem. B*, 116, 14416.

Súarez, J. T.; Torres-Marchal, C.; Rasmussen, P. **1989**. Prediction of surface tensions of nonelectrolyte solutions. *Chem. Eng. Sci.*, 44, 782.

Sugimoto, T.; Atsumi, Y.; Kikuta, M.; Ishiko, E.; Kono, M.; Ishikawa, M. **2009**. Ionic liquid electrolyte systems based on bis(fluorosulfonyl)imide for lithium-ion batteries. *J. Power Sources*, 189, 802.

Sugimoto, T.; Kikuta, M.; Ishiko, E.; Kono, M.; Ishikawa, M. **2008**. Ionic liquid electrolytes compatible with graphitized carbon negative without additive and their effects on interfacial properties. *J. Power Sources*, 183, 436.

Supasitmongkol, S.; Styring, P. **2010**. High CO_2 solubility in ionic liquids and a tetraalkylammonium-based poly(ionic liquid). *Energy Environ. Sci.*, 3, 1961.

Swatloski, R. P.; Holbrey, J. D.; Rogers, R. D. **2003**. Ionic liquids are not always green: hydrolysis of 1-butyl-3-methylimidazolium hexafluorophosphate. *Green Chem.*, 5, 361.

T

Tammann, G.; Hesse, W. **1926**. Die Abhängigkeit der Viscosität von der Temperatur bei unterkühlten Flüssigkeiten. *Z. anorg. allg. Chem.*, 156, 245.

Tokuda, H.; Hayamizu, K.; Ishii, K.; Abu Bin Hasan Susan, M.; Watanabe, M. **2005.** Physicochemical Properties and Structures of Room Temperature Ionic Liquids. 2. Variation of Alkyl Chain Length in Imidazolium Cation. *J. Phys. Chem. B*, 109, 6103.

Troshenkova, S. V.; Sashina, E. S.; Novoselov, N. P.; Arndt, K.-F. **2010a**. Structure of ionic liquids on the basis of imidazole and their mixtures with water. *Russ. J. Gen. Chem*., 80, 106.

Troshenkova, S. V.; Sashina, E. S.; Novoselov, N. P.; Arndt, K.-F. **2010b**. Light scattering in diluted solutions of cellulose and hydroxypropylcellulose in 1-ethyl-3-methylimidazolium acetate. *Russ. J. Gen. Chem*., 80, 501.

U

United Nations Environment Programme. **1985**. Vienna Convention. Avaliable at the website: http://ozone.unep.org/new_site/en/vienna_convention.php (accessed: November 2013).

United Nations Environment Programme. **1987**. Montreal Protocol. Avaliable at the website: http://ozone.unep.org/new_site/en/montreal_protocol.php (accessed November 2013).

United Nations Framework Convention on Climate Change. **1997**. Kyoto Protocol. Avaliable at the website: http://unfccc.int/resource/docs/convkp/kpeng.pdf (accessed November 2013).

V

Vaidya, P. D.; Kenig, E. Y. **2007**. CO_2-Alkanolamine Reaction Kinetics: A Review of Recent Studies. *Chem. Eng. Technol.*, 30, 1467.

Valkenberg, M. H.; de Castro, C.; Hölderich, W. F. **2002**. Inmobilisation of ionic liquids on solid supports. *Green Chem.*, 4, 88.

Van Valkenburg, M. E.; Vaughn, R. L.; Williams, M.; Wilkes, J. S. **2005**. Thermochemistry of ionic liquid heat-transfer fluids. *Thermochim. Acta*, 425, 181.

Virtanen, P.; Mikkola, J.-P.; Toukoniitty, E.; Karhu, H.; Kordas, K.; Eränen, K. **2009**. Supported ionic liquid catalysts – From batch to continuous operation in preparation of fine chemicals. *Catal. Today*, 147, S144.

Vogel, H. **1921**. Das Temperatur-abhängigkeitsgesetz der Viskosität von Flüssigkeiten. *Phys. Z.*, 22, 645.

W

Wall, T. F. **2007**. Combustion processes for carbon capture. *P. Combust. Inst.*, 31, 31.

Wandschneider, A.; Lehmann, J. K.; Heintz, A. **2008**. Surface Tension and Density of Pure Ionic Liquids and Some Binary Mixture with 1-Propanol and 1-Butanol. *J. Chem. Eng. Data*, 53, 596.

Wasserscheid, P.; Keim, W. **2000**. Ionic Liquids–New "Solutions" for Transition Metal Catalysis. *Angew. Chem. Int. Ed.*, 39,3772.

Welton, T. **2004**. Ionic liquids in catalysis. *Coord. Chem. Rev.*, 248, 2459.

Werner, S.; Szesni, N.; Bittermann, A.; Schneider, M. J.; Härter, P.; Haumann, M.; Wasserscheid, P. **2010**. Screening of Supported Ionic Liquid Phase (SILP) catalysts for the very low temperature water-gas-shift reaction. *Appl. Catal. A*, 377, 70.

Wilhem, E.; Battinno, R. **1973**. Thermodynamics Functions of the Solubilities of Gases in Liquids at 25°C. *Chem. Rev.*, 73, 1.

Wilkes, J. S. **2004**. Properties of ionic liquids solvents for catalysis. *J. Mol. Catal. A*, 214, 11.

Wilkes, J. S.; Zaworotko, M. J. **1992**. Air and water stable 1-ethyl-3-methylimidazolium based ionic liquids. *Chem. Commun.*, 965.

Wilson, G. M. **1964**. Vapor-Liquid Equilibrium. XI. A New Expression for the Excess Free Energy of Mixing. *J. Am. Chem. Soc.*, 86, 127.

Y

Yim, J.-H.; Lim, J. S. **2013**. CO_2 solubility measurement in 1-hexyl-3-methylimidazolium ([HMIM]) cation based ionic liquids. *Fluid Phase Equilib.*, 352, 67.

Yokozeki, A.; Shiflett, M. B.; Junk, C. P.; Grieco, L. M.; Foo, T. **2008**. Physical and Chemical Absorptions of Carbon Dioxide in Room-Temperature Ionic Liquids. *J. Phys. Chem. B*, 112, 16654.

Yu, C.-H.; Huang, C.-H.; Tan, C.-S. **2012**. A review of CO_2 Capture by Absorption and Adsorption. *Aerosol Air Qual. Res.*, 12, 745.

Yunus, N. M.; Mutalib, M. I. A.; Man, Z.; Bustam, M. A.; Murugesan, T. **2012**. Solubility of CO_2 in pyridinium based ionic liquids. *Chem. Eng. J.*, 189-190, 94.

Z

Zhang, J.; Zhang, S.; Dong, K.; Zhang, Y.; Shen, Y.; Lv, X. **2006**. Supported Absorption of CO_2 by Tetrabutylphosphonium Amino Acid Ionic Liquids. *Chem. Eur. J.*, 12, 4021.

Zhang, Y.; Yu, P.; Luo, Y. **2013**. Absorption of CO_2 by amino acid-functionalized and traditional dicationic ionic liquids: Properties, Henry's law constants and mechanisms. *Chem. Eng. J.*, 214, 355.

Zhang, Y.; Zhang, S.; Lu, X.; Zhou, Q.; Fan, W.; Zhang, X. **2009**. Dual Amino-Functionalised Phosphonium Ionic Liquids for CO_2 Capture. *Chem. Eur. J.*, 15, 3003.

Zhao, W.; He, G.; Zhang, L.; Ju, J.; Dou, H.; Nie, F.; Li, C.; Liu, H. **2010**. Effect of water in ionic liquid on the separation performance of supported ionic liquid membrane for CO_2/N_2. *J. Membr. Sci.*, 350, 279.

APPENDIX A:

^{1}H and ^{13}C NMR spectra of the ionic liquids

Appendix A:

^{1}H and ^{13}C NMR spectra of the ionic liquids

In this Appendix, the ^{1}H and ^{13}C NMR spectra of the ionic liquids used in this Thesis are presented. Most of them were synthesised in-house, whereas $[C_2C_1im][OAc]$ was purchased from a vendor and purified in-house prior to use (see Chapter 4 for details).

The alphabetically-ordered list of ionic liquids, with full names and the corresponding abbreviations, is shown in Table A.1. For each of them, the ^{1}H NMR spectrum is presented first, followed by the ^{13}C NMR spectrum, in the following pages.

Table A.1. Full names and abbreviations of the ionic liquids involved in the experimental work of this Thesis, and whose ^{1}H and ^{13}C NMR spectra are collected in this Appendix.

Name	Abbreviation
1-Butyl-3-ethylimidazolium ethylsulfate	$[C_4C_2im][EtSO_4]$
1-Ethyl-3-methylimidazolium acetate	$[C_2C_1im][OAc]$
1-Ethyl-3-methylimidazolium bis(trifluoromethylsulfonyl)amide	$[C_2C_1im][NTf_2]$
1-Ethyl-3-methylimidazolium ethylsulfate	$[C_2C_1im][EtSO_4]$
1-Ethylpyridinium ethylsulfate	$[C_2py][EtSO_4]$
Tetrahexylammonium isoleucine	$[N_{6666}][Ile]$

1-Butyl-3-ethylimidazolium ethylsulfate ($[C_4C_2im][EtSO_4]$)

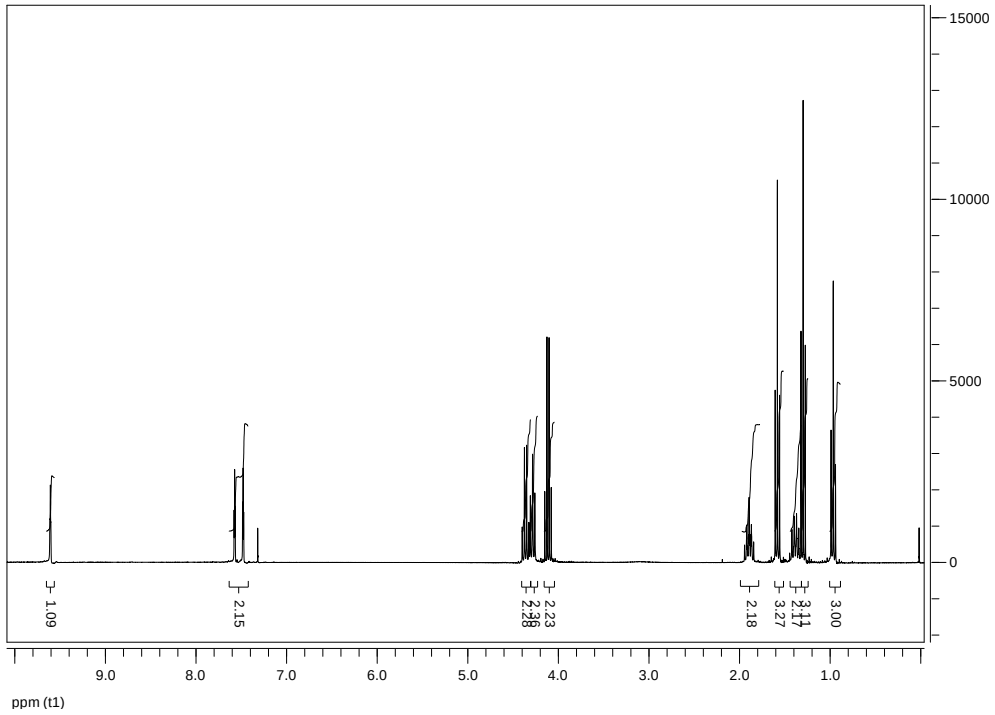

^{1}H NMR, δ_H ($CDCl_3$, 300 MHz): 0.95 (t, J = 7.4 Hz, 3H, $NCH_2CH_2CH_2C\underline{H}_3$), 1.28 (t, J = 7.1 Hz, 3H, $OCH_2C\underline{H}_3$), 1.38 (m, J = 7.5 Hz, 2H, $NCH_2CH_2C\underline{H}_2$), 1.57 (t, J = 7.4 Hz, 3H, $NCH_2C\underline{H}_3$), 1.88 (m, J = 7.6 Hz, 2H, $NCH_2C\underline{H}_2$), 4.10 (q, J = 7.1 Hz, 2H, OCH_2),4.27 (t, J = 7.4 Hz, 2H, $NC\underline{H}_2CH_2$), 4.35 (q, J = 7.4 Hz, 2H, $NC\underline{H}_2CH_3$), 7.46-7.57 (m, unresolved, 2H, C(5)H and C(4)H), 9.60 (1H, s, C(2)H).

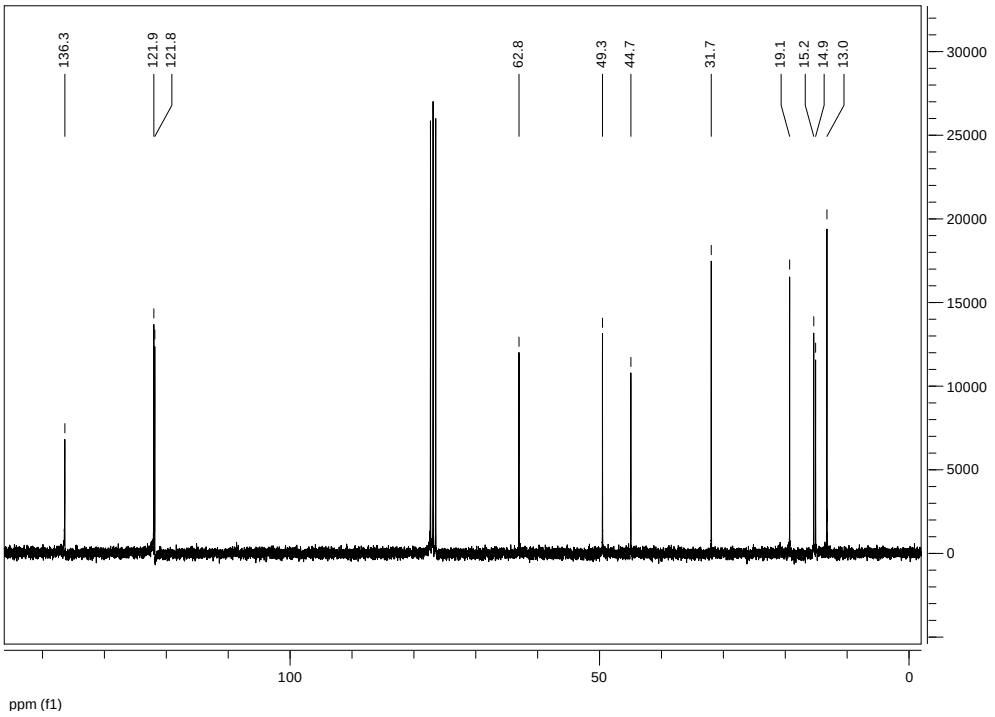

^{13}C NMR, δ_C ($CDCl_3$, 75.4 MHz): 13.0 ($NCH_2CH_2CH_2\underline{C}H_3$), 14.9 ($OCH_2\underline{C}H_3$), 15.2 ($NCH_2\underline{C}H_3$), 19.1 ($NCH_2CH_2\underline{C}H_2$), 31.7 ($NCH_2\underline{C}H_2$), 44.7 ($O\underline{C}H_2$), 49.3 ($N\underline{C}H_2CH_2$), 62.8 ($N\underline{C}H_2CH_3$), 121.8(C(4)H), 121.9 (C(5)H), 136.3 (C(2)H).

1-Ethyl-3-methylimidazolium acetate ([C_2C_1im][OAc])

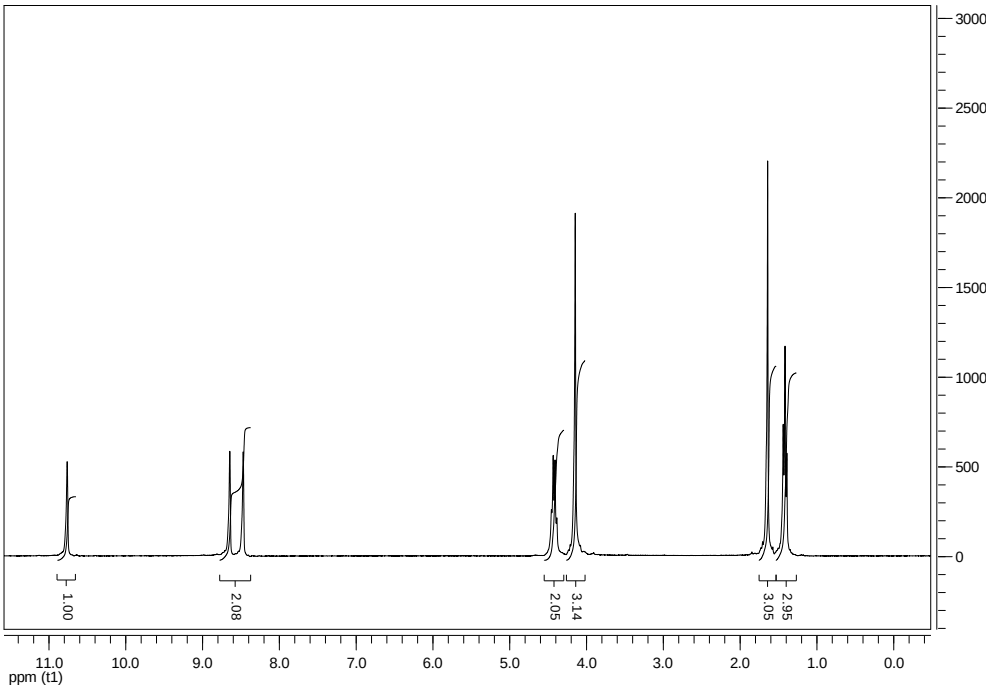

^{1}H NMR, δ_H ($CDCl_3$, 300 MHz): 1.40 (t, J = 7.2 Hz, 3H, $NCH_2C\underline{H}_3$), 1.62 (s, = 7.4 Hz, 3H, $COOC\underline{H}_3$), 4.13 (s, 3H, NCH_3), 4.4 (q, J = 7.0 Hz, 2H, NCH_2), 8.40-8.80 (m, unresolved,2H, C(5)H and C(4)H), 10.76 (1H, s, C(2)H).

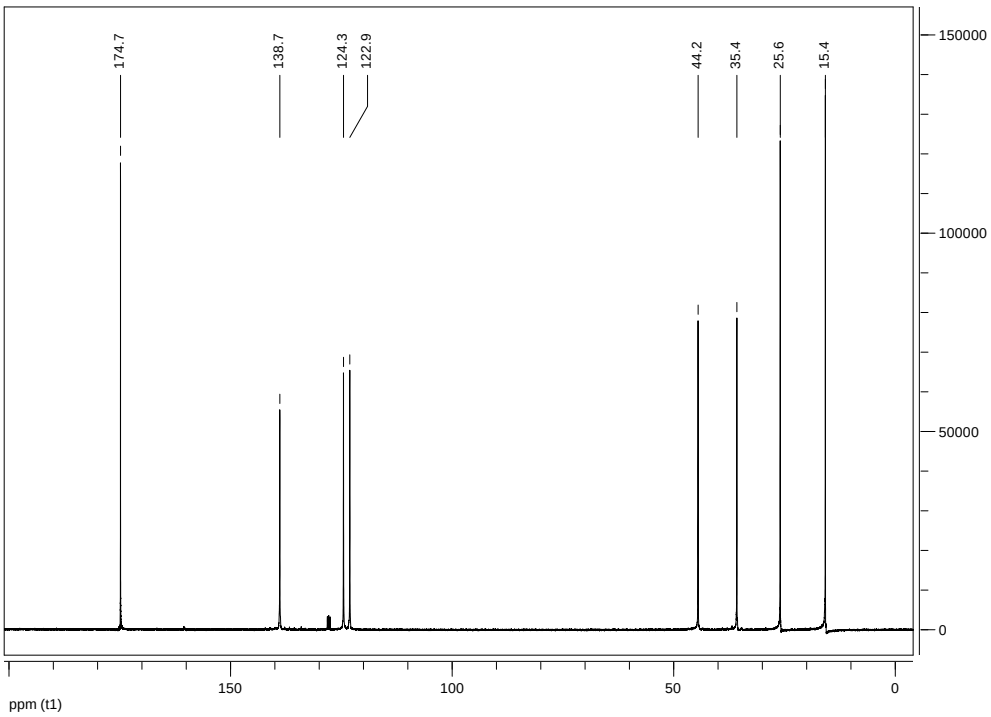

^{13}C NMR, δ_C ($CDCl_3$, 75.4 MHz): 15.4 ($NCH_2\underline{C}H_3$), 25.6 ($COO\underline{C}H_3$), 32.4 (NCH_3), 44.2 (NCH_2), 122.9 (C(4)H), 124.3 (C(5)H), 138.7 (C(2)H),174.7 ($\underline{C}OOCH_3$).

1-Ethyl-3-methylimidazolium bis(trifluoromethylsulfonyl)amide ($[C_2C_1im][NTf_2]$)

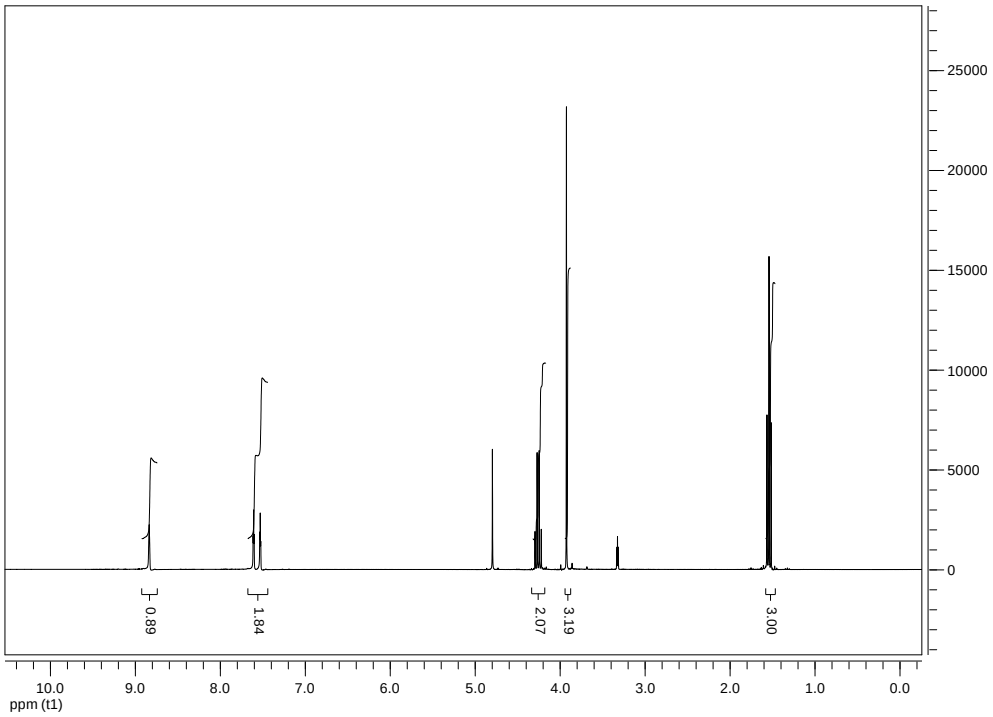

^{1}H NMR, δ_H (CD_3OD, 300 MHz): 1.52 (t, J = 7.4 Hz, 3H, $NCH_2C\underline{H}_3$), 3.91 (s, 3H, NCH_3), 4.25 (q, J = 7.4 Hz, 2H, NCH_2), 7.52-7.61 (m, unresolved, 2H, C(5)H and C(4)H), 8.83 (s, 1H, C(2)H).

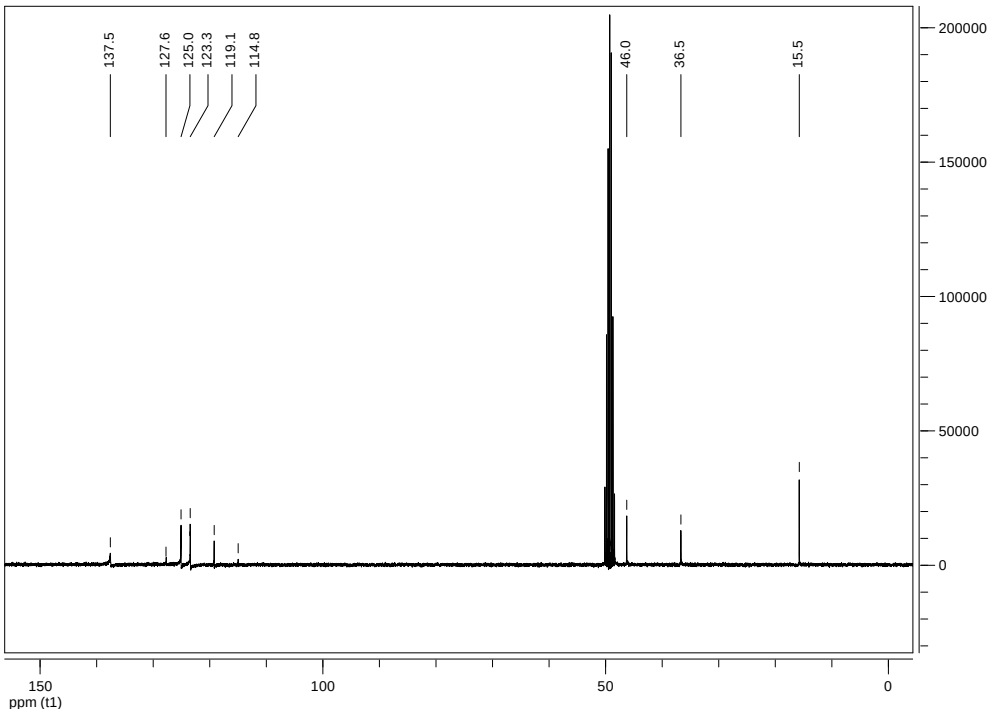

^{13}C NMR, δ_C (CD_3OD, 75.4 MHz): 15.5 ($NCH_2\underline{C}H_3$), 36.5 (NCH_3), 46.0 (NCH_2), 121.2 (q, $J_{C\text{-}F}$ = 322 Hz, 2 × CF_3), 125.0 (C(4)H), 127.6 (C(5)H), 137.5 (C(2)H).

1-Ethyl-3-methylimidazolium ethylsulfate ($[C_2C_1im][EtSO_4]$)

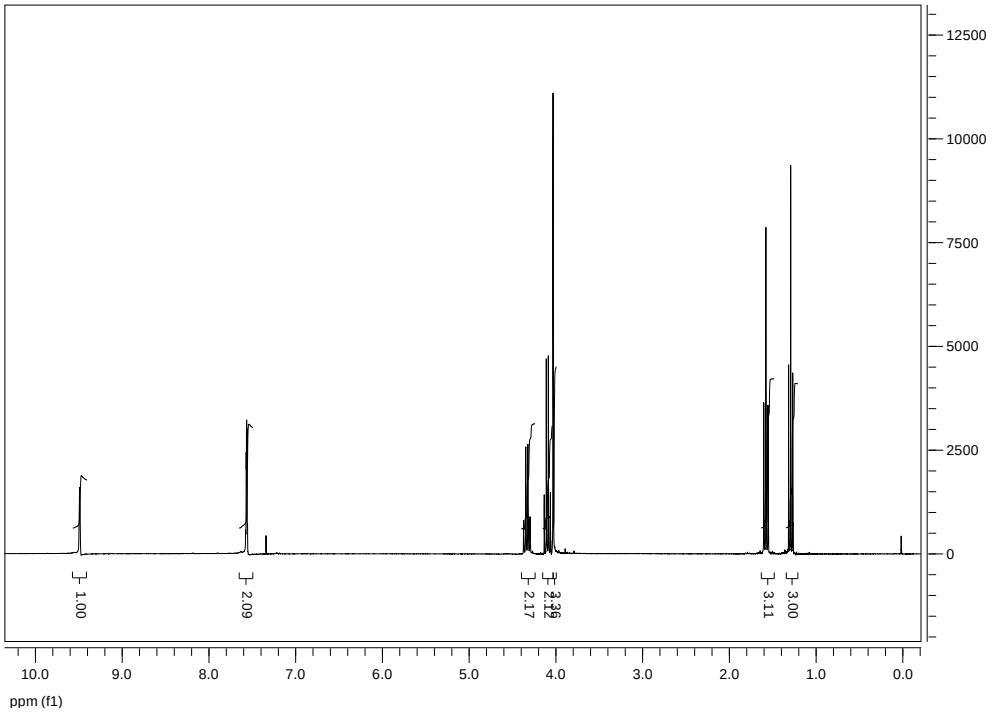

^{1}H NMR, δ_H ($CDCl_3$, 300 MHz): 1.28 (t, J = 7.1 Hz, 3H, $OCH_2C\underline{H}_3$), 1.56 (t, J = 7.4 Hz, 3H, $NCH_2C\underline{H}_3$), 4.02 (s, 3H, NCH_3), 4.09 (q, J = 7.1 Hz, 2H, OCH_2), 4.32 (q, J = 7.4 Hz, 2H, NCH_2), 7.50-7.70 (m, unresolved,2H, C(5)H and C(4)H), 9.48 (1H, s, C(2)H).

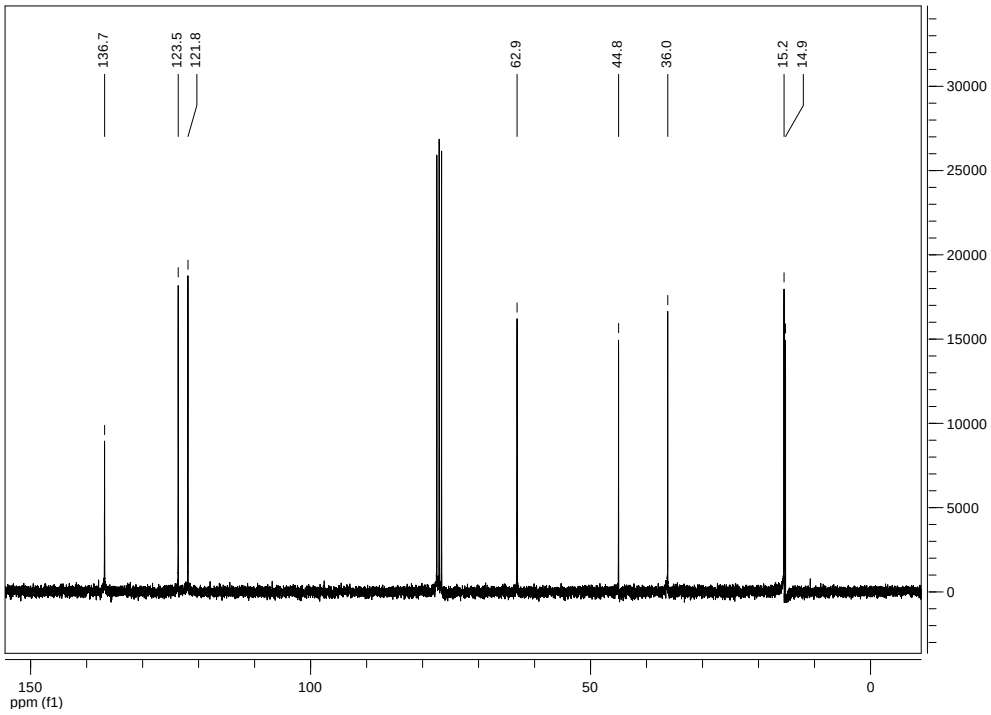

^{13}C NMR, δ_C ($CDCl_3$, 75.4 MHz): 14.9 ($OCH_2\underline{C}H_3$), 15.2 ($NCH_2\underline{C}H_3$), 36.0 (NCH_3), 44.8 (OCH_3), 62.9 (NCH_2), 121.8 (C(4)H), 123.5 (C(5)H), 136.7 (C(2)H).

1-Ethylpyridinium ethylsulfate ([C_2py][EtSO_4])

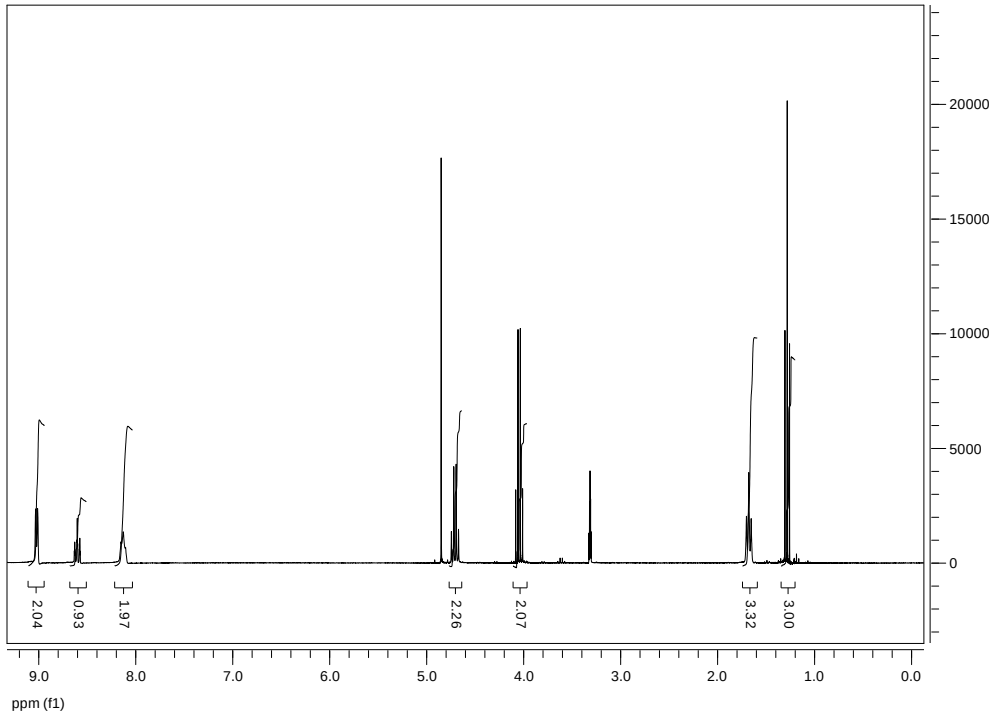

^{1}H NMR, δ_H (CD_3OD, 300 MHz): 1.27 (t, J = 7.1 Hz, 3H, $OCH_2C\underline{H}_3$), 1.66 (t, J = 7.4 Hz, 3H, $NCH_2C\underline{H}_3$), 4.04 (q, J = 7.1 Hz, 2H, OCH_2), 4.70 (q, J = 7.4 Hz, 2H, NCH_2), 8.13 (br s, J = 7.0 Hz, 2H, C(3)H and C(5)H), 8.60 (t, J = 7.8 Hz, 1H, C(4)H), 9.02 (d, J = 5.6 Hz, 2H, C(2)H y C(6)H).

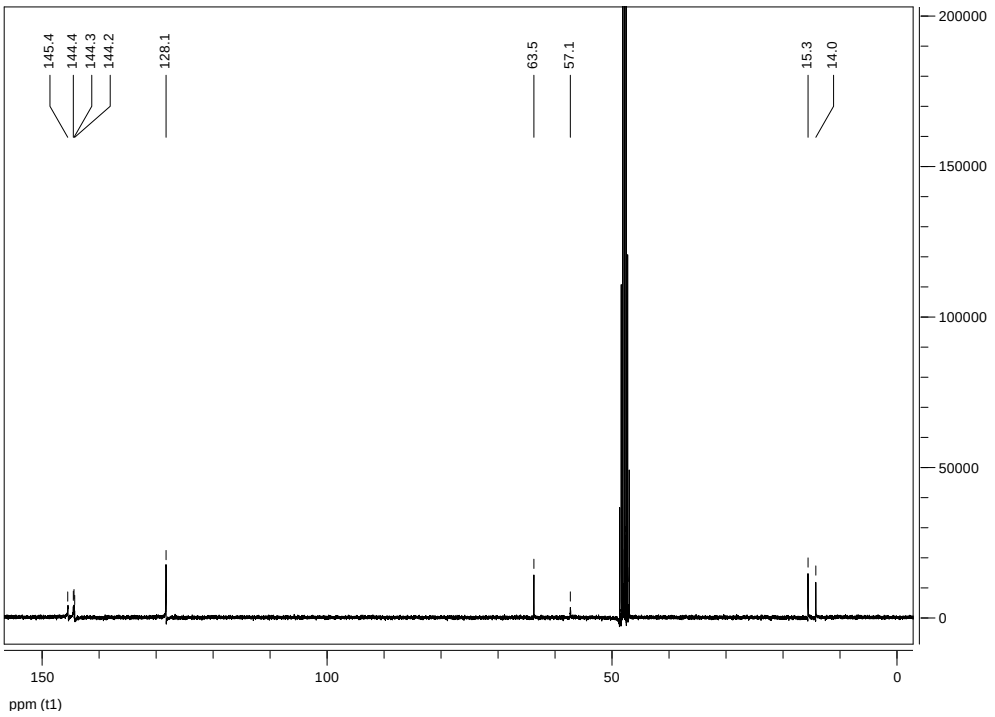

^{13}C NMR, δ_C (CD_3OD, 75.4 MHz): 14.0 ($OCH_2\underline{C}H_3$), 15.3 ($NCH_2\underline{C}H_3$), 57.1 (NCH_2), 63.5 (OCH_2), 128.1 (C(4)H), 144.3 (t, J = 18 Hz, C(3)H and C(5)H), 145.4 (s, C(2)H and C(6)H).

Tetrahexylammonium isoleucine ([N_{6666}][Ile])

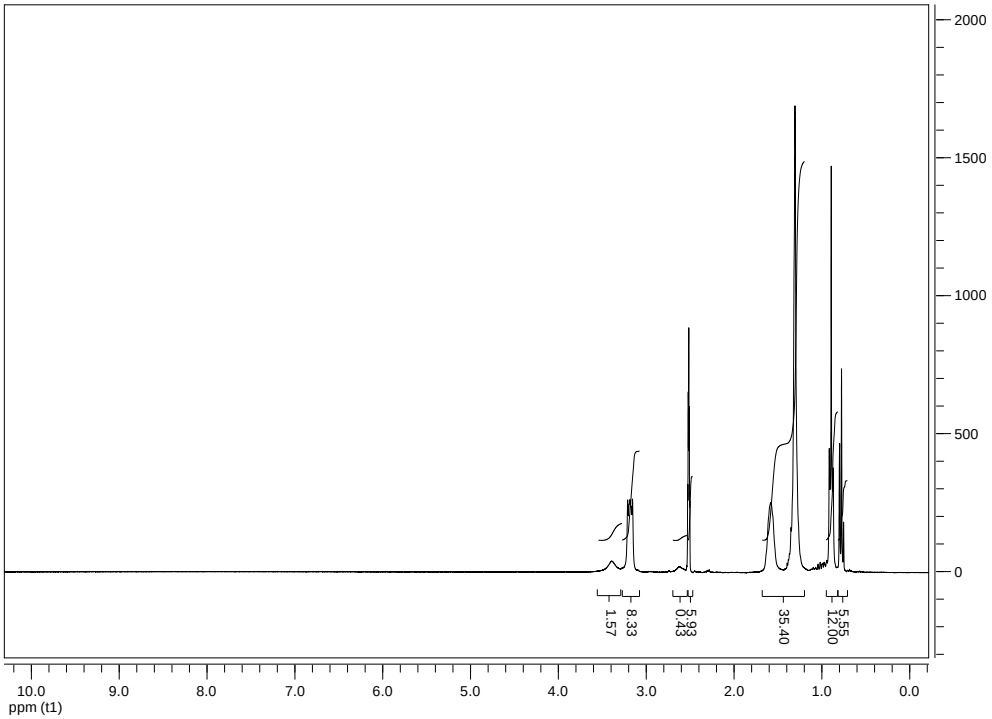

^{1}H NMR, δ_H ($(CD_3)_2SO$, 300 MHz): 0.71-0.80 (m, unresolved, 6H, $CHCH_2C\underline{H}_3$ + $CHC\underline{H}_3$), 0.88 (t, J = 7 Hz, 12H, 4 × $N(CH_2)_5C\underline{H}_3$), 1.14-1.68 (m, unresolved, 34H, 4 × $NCH_2(C\underline{H}_2)_4CH_3$ + $CHC\underline{H}_2CH_3$), 2.60 (br s, 1H, $C\underline{H}CH_2CH_3$), 3.17 (br, unresolved, 8H, 4 × NCH_2), 3.38 (br s, 1H, COOCH). The protons in the amino group of the anion are not observed.

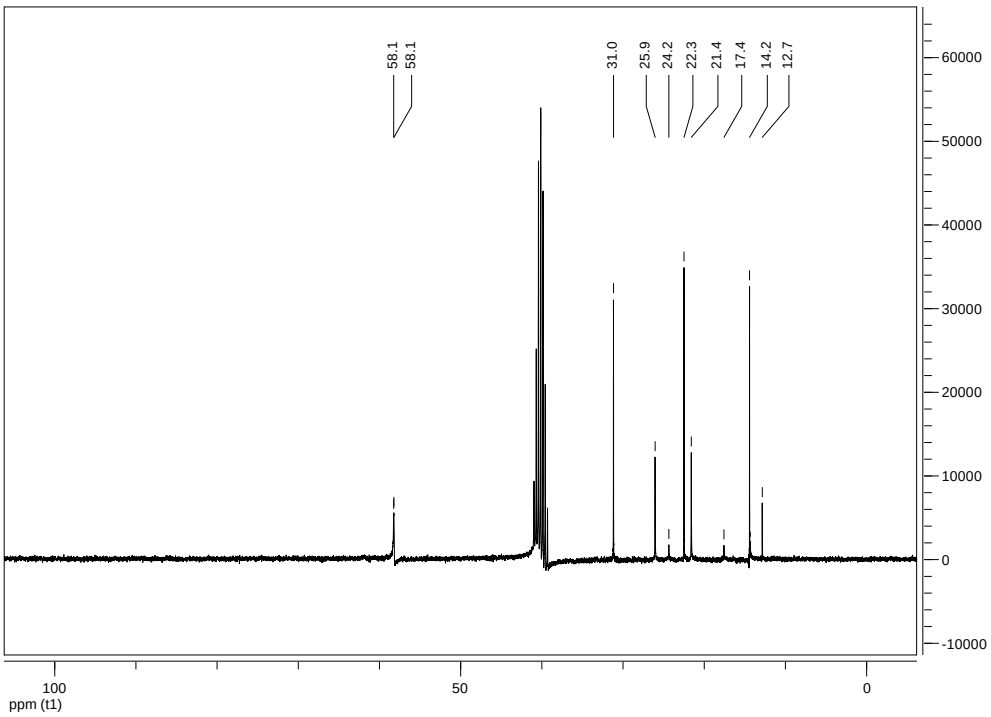

^{13}C NMR, δ_C ($(CD_3)_2SO$, 75.4 MHz): 12.1 ($CHCH_2\underline{C}H_3$), 13.7 ($4 \times N(CH_2)_5\underline{C}H_3$), 16.8 ($CH\underline{C}H_2CH_3$), 20.9 ($4 \times N(CH_2)_4\underline{C}H_2$), 21.8 ($4 \times N(CH_2)_3\underline{C}H_2$), 23.6 ($4 \times N(CH_2)_2\underline{C}H_2$), 25.3 ($CH\underline{C}H_3$), 30.5 ($4 \times NCH_2\underline{C}H_2$), 57.5 ($4 \times NCH_2$), 57.6 ($COO\underline{C}H$). The peak corresponding to the carbon in the β position is hidden by the signal of the deuteriated solvent (at *ca.* 38.6 ppm). The peak corresponding to the carbon in the carboxylate group could not be observed, likely due to low concentration of the NMR sample.

APPENDIX B:

Carbon dioxide absorption data in a mass basis

Appendix B:

Carbon dioxide absorption data in a mass basis

The tables in this Appendix summarise results of the experiments on absorption and desorption of CO_2 in pure ionic liquids and in mixtures of ionic liquids. These tables are equivalent to Tables 5.1 to 5.4 and 5.11 to 5.14; but with the CO_2 solubility expressed as a mass fraction instead of a molar fraction.

Table B.1: Pressure-composition data for the absorption/desorption of CO_2 in the pure ionic liquids at 298.2 K. The solubility of CO_2 is expressed as mass fraction (ω_{CO2}).

[C_2C_1im][OAc]		[C_2C_1im][NTf_2]		[C_4C_2im][$EtSO_4$]		[C_2C_1im][$EtSO_4$]		[C_2py][$EtSO_4$]	
P / bar	ω_{CO2}	P / bar	ω_{CO2}	P / bar	ω_{CO2}	P / bar	ω_{CO2}	P / bar	ω_{CO2}
Absorption									
0.94	0.0835	1.06	0.0020	0.91	0.0005	1.00	0.0006	1.09	0.0004
2.00	0.0962	2.08	0.0064	2.03	0.0024	2.00	0.0034	1.99	0.0016
2.96	0.1030	3.00	0.0086	3.05	0.0034	3.10	0.0044	3.04	0.0021
4.00	0.1090	3.98	0.0129	4.00	0.0052	3.99	0.0069	4.04	0.0041
5.00	0.1123	5.05	0.0174	5.00	0.0078	5.05	0.0079	4.97	0.0052
6.04	0.1109	6.07	0.0211	6.00	0.0092	6.04	0.0094	5.95	0.0063
7.02	0.1117	7.45	0.0264	6.97	0.0122	6.98	0.0109	7.05	0.0084
9.04	0.1134	8.84	0.0322	8.99	0.0175	9.03	0.0146	8.84	0.0108
11.04	0.1151	10.65	0.0396	10.96	0.0228	10.98	0.0181	10.91	0.0147
12.89	0.1171	12.72	0.0469	13.01	0.0259	13.04	0.0237	12.02	0.0180
14.86	0.1190	15.52	0.0584	14.92	0.0337	14.87	0.0290	13.65	0.0218
16.39	0.1174			16.43	0.0362	16.46	0.0309	14.66	0.0245
Desorption									
14.03	0.1207	13.89	0.0528	14.01	0.0355	14.05	0.0305	13.26	0.0225
12.00	0.1191	11.81	0.0452	12.12	0.0338	12.02	0.0293	11.68	0.0216
10.03	0.1174	9.87	0.0379	10.03	0.0285	9.82	0.0244	10.01	0.0197
8.01	0.1158	7.90	0.0306	8.02	0.0253	8.03	0.0207	8.02	0.0165
6.00	0.1141	6.00	0.0234	5.99	0.0195	6.08	0.0168	6.06	0.0132
4.98	0.1131	5.00	0.0197	5.00	0.0179	5.00	0.0150	4.96	0.0108
4.00	0.1121	4.01	0.0159	4.02	0.0156	4.00	0.0130	4.04	0.0093
2.99	0.1111	2.99	0.0120	3.02	0.0130	3.00	0.0106	3.00	0.0071
2.03	0.1097	2.00	0.0081	1.97	0.0112	2.01	0.0080	2.02	0.0051
1.02	0.1078	1.04	0.0045	1.02	0.0095	1.02	0.0069	1.02	0.0032

Table B.2: Pressure-composition data for the absorption/desorption of CO_2 in the mixture $[C_2C_1im][NTf_2]$ + $[C_2C_1im][EtSO_4]$ at 298.2 K. The solubility of CO_2 is expressed as mass fraction (ω_{CO2}).

$[C_2C_1im][NTf_2]$ (1) + $[C_2C_1im][EtSO_4]$ (2) + CO_2									
ω'_1 = 0.0000		ω'_1 = 0.3589		ω'_1 = 0.6158		ω'_1 = 0.8289		ω'_1 = 1.0000	
P / bar	ω_{CO2}	P / bar	ω_{CO2}	P / bar	ω_{CO2}	P / bar	ω_{CO2}	P / bar	ω_{CO2}
Absorption									
1.00	0.0006	1.00	0.0018	1.01	0.0023	1.01	0.0026	1.06	0.0020
2.00	0.0034	2.02	0.0031	2.03	0.0044	2.07	0.0062	2.08	0.0064
3.10	0.0044	3.00	0.0051	3.01	0.0079	3.00	0.0089	3.00	0.0086
3.99	0.0069	3.99	0.0085	4.00	0.0108	4.01	0.0122	3.98	0.0129
5.05	0.0079	5.02	0.0103	5.01	0.0147	5.01	0.0166	5.05	0.0174
6.04	0.0094	6.02	0.0117	6.03	0.0178	6.01	0.0197	6.07	0.0211
6.98	0.0109	6.98	0.0148	7.96	0.0247	7.03	0.0235	7.45	0.0264
9.03	0.0146	8.93	0.0210	9.97	0.0310	8.92	0.0306	8.84	0.0322
10.98	0.0181	10.95	0.0264	11.94	0.0382	10.99	0.0377	10.65	0.0396
13.04	0.0237	12.91	0.0313	13.97	0.0446	12.92	0.0451	12.72	0.0469
14.87	0.0290	14.92	0.0360	16.39	0.0537	15.04	0.0511	15.52	0.0584
16.46	0.0309	16.34	0.0394			16.24	0.0566		
Desorption									
14.05	0.0305	14.13	0.0368	13.02	0.0447	14.08	0.0510	13.89	0.0528
12.02	0.0293	12.02	0.0317	10.91	0.0385	12.07	0.0440	11.81	0.0452
9.82	0.0244	10.07	0.0271	9.05	0.0324	10.01	0.0371	9.87	0.0379
8.03	0.0207	8.09	0.0228	7.03	0.0263	7.99	0.0301	7.90	0.0306
6.08	0.0168	6.09	0.0179	6.01	0.0227	6.06	0.0233	6.00	0.0234
5.00	0.0150	5.01	0.0166	4.92	0.0192	5.01	0.0198	5.00	0.0197
4.00	0.0130	3.94	0.0129	4.00	0.0162	4.02	0.0163	4.01	0.0159
3.00	0.0106	3.03	0.0105	2.99	0.0130	3.00	0.0126	2.99	0.0120
2.01	0.0080	1.99	0.0081	2.01	0.0098	1.87	0.0087	2.00	0.0081
1.02	0.0069	1.04	0.0054	1.02	0.0067	1.04	0.0058	1.04	0.0045

Table B.3: Pressure-composition data for the absorption/desorption of CO_2 in the mixture $[C_2C_1im][NTf_2]$ + $[C_4C_2im][EtSO_4]$ at 298.2 K. The solubility of CO_2 is expressed as mass fraction (ω_{CO2}).

$[C_2C_1im][NTf_2]$ (1) + $[C_4C_2im][EtSO_4]$ (2) + CO_2									
ω'_1 = 0.0000		ω'_1 = 0.3029		ω'_1 = 0.5731		ω'_1 = 0.8028		ω'_1 = 1.0000	
P / bar	ω_{CO2}	P / bar	ω_{CO2}	P / bar	ω_{CO2}	P / bar	ω_{CO2}	P / bar	ω_{CO2}
Absorption									
0.91	0.0005	1.04	0.0012	0.92	0.0010	1.00	0.0026	1.06	0.0020
2.03	0.0024	2.02	0.0021	2.01	0.0036	2.08	0.0051	2.08	0.0064
3.05	0.0034	2.99	0.0047	3.07	0.0059	2.99	0.0085	3.00	0.0086
4.00	0.0052	3.99	0.0080	4.02	0.0099	4.02	0.0119	3.98	0.0129
5.00	0.0078	5.02	0.0106	5.10	0.0139	5.00	0.0154	5.05	0.0174
6.00	0.0092	7.02	0.0165	5.99	0.0155	5.99	0.0183	6.07	0.0211
6.97	0.0122	8.88	0.0204	7.07	0.0195	7.04	0.0221	7.45	0.0264
8.99	0.0175	10.99	0.0269	9.01	0.0252	8.98	0.0288	8.84	0.0322
10.96	0.0228	12.92	0.0314	10.85	0.0321	10.96	0.0349	10.65	0.0396
13.01	0.0259	14.97	0.0383	13.09	0.0388	12.98	0.0423	12.72	0.0469
14.92	0.0337	16.23	0.0406	15.03	0.0433	15.02	0.0487	15.52	0.0584
16.43	0.0362			16.31	0.0487	16.21	0.0532		
Desorption									
14.01	0.0355	14.07	0.0397	14.13	0.0496	14.14	0.0477	13.89	0.0528
12.12	0.0338	12.06	0.0348	12.29	0.0449	12.08	0.0413	11.81	0.0452
10.03	0.0285	10.04	0.0296	9.99	0.0390	10.08	0.0347	9.87	0.0379
8.02	0.0253	8.03	0.0251	8.15	0.0320	8.08	0.0281	7.90	0.0306
5.99	0.0195	6.05	0.0188	6.02	0.0266	6.06	0.0222	6.00	0.0234
5.00	0.0179	5.01	0.0160	4.96	0.0199	5.03	0.0183	5.00	0.0197
4.02	0.0156	3.99	0.0136	4.00	0.0171	4.04	0.0150	4.01	0.0159
3.02	0.0130	3.01	0.0105	2.98	0.0145	3.00	0.0116	2.99	0.0120
1.97	0.0112	2.01	0.0075	2.01	0.0109	2.00	0.0081	2.00	0.0081
1.02	0.0095	1.04	0.0048	1.03	0.0080	1.05	0.0053	1.04	0.0045

Table B.4: Pressure-composition data for the absorption/desorption of CO_2 in the mixture $[C_2C_1im][NTf_2]$ + $[C_2py][EtSO_4]$ at 298.2 K. The solubility of CO_2 is expressed as mass fraction (ω_{CO2}).

$[C_2C_1im][NTf_2]$ (1) + $[C_2py][EtSO_4]$ (2) + CO_2									
ω'_1 = 0.0000		ω'_1 = 0.3592		ω'_1 = 0.6165		ω'_1 = 0.8298		ω'_1 = 1.0000	
P / bar	ω_{CO2}	P / bar	ω_{CO2}	P / bar	ω_{CO2}	P / bar	ω_{CO2}	P / bar	ω_{CO2}
Absorption									
1.09	0.0004	1.01	0.0013	1.53	0.0023	1.00	0.0021	1.06	0.0020
1.99	0.0016	2.01	0.0027	2.56	0.0050	2.04	0.0053	2.08	0.0064
3.04	0.0021	3.02	0.0048	3.10	0.0066	3.02	0.0086	3.00	0.0086
4.04	0.0041	3.95	0.0070	4.09	0.0097	3.99	0.0117	3.98	0.0129
4.97	0.0052	5.00	0.0091	5.09	0.0118	4.99	0.0148	5.05	0.0174
5.95	0.0063	6.02	0.0108	6.01	0.0142	5.97	0.0183	6.07	0.0211
7.05	0.0084	6.95	0.0126	6.99	0.0164	6.97	0.0214	7.45	0.0264
8.84	0.0108	8.79	0.0188	9.00	0.0218	8.95	0.0276	8.84	0.0322
10.91	0.0147	10.88	0.0216	10.95	0.0276	10.95	0.0347	10.65	0.0396
12.02	0.0180	12.58	0.0284	13.15	0.0346	12.88	0.0412	12.72	0.0469
13.65	0.0218	14.38	0.0328	15.08	0.0387	14.89	0.0482	15.52	0.0584
14.66	0.0245	16.17	0.0360	16.34	0.0418	16.51	0.0521		
Desorption									
13.26	0.0225	13.92	0.0342	15.31	0.0417	14.10	0.0470	13.89	0.0528
11.68	0.0216	12.01	0.0293	13.57	0.0388	12.2	0.0407	11.81	0.0452
10.01	0.0197	10.00	0.0259	11.62	0.0334	9.15	0.0312	9.87	0.0379
8.02	0.0165	7.94	0.0204	9.53	0.0277	7.96	0.0274	7.90	0.0306
6.06	0.0132	5.95	0.0155	7.55	0.0225	6.10	0.0213	6.00	0.0234
4.96	0.0108	4.99	0.0147	6.52	0.0197	5.00	0.0179	5.00	0.0197
4.04	0.0093	4.02	0.0112	5.51	0.0171	4.01	0.0145	4.01	0.0159
3.00	0.0071	3.00	0.0088	4.52	0.0143	3.00	0.0112	2.99	0.0120
2.02	0.0051	2.02	0.0063	2.48	0.0086	1.99	0.0077	2.00	0.0081
1.02	0.0032	1.02	0.0052	0.98	0.0046	1.04	0.0045	1.04	0.0045

Table B.5: Pressure-composition data for the absorption/desorption of CO_2 in $[C_2C_1im][EtSO_4]$ at different temperatures. The solubility of CO_2 is expressed as mass fraction (ω_{CO2}).

$[C_2C_1im][EtSO_4] + CO_2$							
T = 298.2 K		T = 318.2 K		T = 338.2 K		T = 358.2 K	
P / bar	ω_{CO2}	P / bar	ω_{CO2}	P / bar	ω_{CO2}	P / bar	ω_{CO2}
Absorption							
1.00	0.0006	1.03	0.0008	1.04	0.0002	1.04	0.0001
2.00	0.0034	2.04	0.0008	2.01	0.0009	2.05	0.0004
3.10	0.0044	3.02	0.0028	3.00	0.0016	3.08	0.0010
3.99	0.0069	4.04	0.0040	4.02	0.0029	4.00	0.0016
5.05	0.0079	4.96	0.0057	5.03	0.0036	5.01	0.0027
6.04	0.0094	6.00	0.0071	6.00	0.0047	6.00	0.0032
6.98	0.0109	6.93	0.0087	6.94	0.0064	7.03	0.0036
9.03	0.0146	8.90	0.0108	9.02	0.0079	8.98	0.0051
10.98	0.0181	10.89	0.0130	10.91	0.0098	11.00	0.0073
13.04	0.0237	12.34	0.0173	12.67	0.0124	12.98	0.0079
14.87	0.0290	14.89	0.0189	14.48	0.0148	15.00	0.0095
16.46	0.0309	16.02	0.0208	16.06	0.0149	16.36	0.0098
Desorption							
14.05	0.0305	14.01	0.0212	13.92	0.0148	14.01	0.0100
12.02	0.0293	11.99	0.0197	11.93	0.0137	12.01	0.0094
9.82	0.0244	9.92	0.0161	9.96	0.0119	9.94	0.0082
8.03	0.0207	8.02	0.0138	7.97	0.0101	7.99	0.0064
6.08	0.0168	6.03	0.0104	5.98	0.0074	6.02	0.0047
5.00	0.0150	5.00	0.0092	4.98	0.0062	5.00	0.0039
4.00	0.0130	3.99	0.0078	3.94	0.0059	4.02	0.0033
3.00	0.0106	2.98	0.0064	3.01	0.0043	2.99	0.0026
2.01	0.0080	1.98	0.0046	1.99	0.0030	2.01	0.0019
1.02	0.0069	1.01	0.0036	1.00	0.0015	1.01	0.0009

Table B.6: Pressure-composition data for the absorption/desorption of CO_2 in [C_2C_1im][OAc] at different temperatures. The solubility of CO_2 is expressed as mass fraction (ω_{CO2}).

[C_2C_1im][OAc] + CO_2							
T = 298.2 K		T = 318.2 K		T = 338.2 K		T = 358.2 K	
P / bar	ω_{CO2}	P / bar	ω_{CO2}	P / bar	ω_{CO2}	P / bar	ω_{CO2}
Absorption							
0.94	0.0835	0.95	0.0688	0.92	0.0477	0.98	0.0477
2.00	0.0962	2.01	0.0823	1.92	0.0771	1.96	0.0609
2.96	0.1030	3.03	0.0886	3.04	0.0850	3.11	0.0686
4.00	0.1090	3.98	0.0921	4.00	0.0872	4.00	0.0726
5.00	0.1123	4.99	0.0966	5.02	0.0932	5.01	0.0773
6.04	0.1109	6.03	0.1010	5.98	0.0964	5.97	0.0804
7.02	0.1117	7.30	0.1040	7.00	0.0987	7.02	0.0829
9.04	0.1134	8.95	0.1097	9.01	0.1046	9.10	0.0881
11.04	0.1151	10.99	0.1151	10.97	0.1093	11.02	0.0927
12.89	0.1171	12.98	0.1200	12.96	0.1125	13.01	0.0965
14.86	0.1190	14.93	0.1248	14.96	0.1166	14.98	0.0998
16.39	0.1174	16.44	0.1277	16.33	0.1187	16.30	0.1019
Desorption							
14.03	0.1207	14.03	0.1265	14.03	0.1181	13.99	0.1009
12.00	0.1191	12.01	0.1226	11.97	0.1165	11.97	0.0978
10.03	0.1174	10.02	0.1201	10.04	0.1147	10.04	0.0953
8.01	0.1158	8.02	0.1161	8.00	0.1109	7.95	0.0902
6.00	0.1141	6.05	0.1089	6.11	0.1019	6.00	0.0854
4.98	0.1131	5.03	0.1050	4.99	0.0994	5.00	0.0843
4.00	0.1121	4.02	0.1033	4.02	0.0955	4.04	0.0800
2.99	0.1111	2.99	0.0964	2.99	0.0924	2.98	0.0753
2.03	0.1097	1.98	0.0929	2.00	0.0875	2.01	0.0720
1.02	0.1078	1.01	0.0872	1.04	0.0826	1.06	0.0624

Table B.7: Pressure-composition data for the absorption/desorption of CO_2 in the binary mixture [C_2C_1im][OAc] + [C_2C_1im][$EtSO_4$], at 298.2 K and as a function of the composition ratio of the two ionic liquids (ω'_1 stands for the mass fraction of [C_2C_1im][OAc] in a CO_2-free basis). The solubility of CO_2 is expressed as mass fraction (ω_{CO2}).

[C_2C_1im][OAc] (1) + [C_2C_1im][$EtSO_4$] (2) + CO_2									
ω'_1 = 0.0000		ω'_1 = 0.1949		ω'_1 = 0.4108		ω'_1 = 0.6840		ω'_1 = 1.0000	
P / bar	ω_{CO2}	P / bar	ω_{CO2}	P / bar	ω_{CO2}	P / bar	ω_{CO2}	P / bar	ω_{CO2}
Absorption									
1.00	0.0006	0.99	0.0169	0.98	0.0325	0.98	0.0542	0.94	0.0835
2.00	0.0034	2.03	0.0228	1.98	0.0407	1.99	0.0614	2.00	0.0962
3.10	0.0044	3.02	0.0258	2.91	0.0459	3.03	0.0677	2.96	0.1030
3.99	0.0069	4.04	0.0289	3.93	0.0493	4.06	0.0723	4.00	0.1090
5.05	0.0079	5.00	0.0306	4.91	0.0523	5.00	0.0742	5.00	0.1123
6.04	0.0094	5.99	0.0348	6.00	0.0541	5.98	0.0792	6.04	0.1109
6.98	0.0109	6.97	0.0373	6.74	0.0588	7.05	0.0838	7.02	0.1117
9.03	0.0146	8.95	0.0424	8.71	0.0640	8.96	0.0899	9.04	0.1134
10.98	0.0181	10.98	0.0468	10.89	0.0685	10.98	0.0947	11.04	0.1151
13.04	0.0237	12.95	0.0518	12.46	0.0743	12.90	0.0999	12.89	0.1171
14.87	0.0290	15.04	0.0560	14.39	0.0797	15.03	0.1070	14.86	0.1190
16.46	0.0309	16.02	0.0596	16.02	0.0837	16.39	0.1107	16.39	0.1174
Desorption									
14.05	0.0305	13.97	0.0595	13.04	0.0795	13.98	0.1094	14.03	0.1207
12.02	0.0293	12.03	0.0554	11.98	0.0789	12.10	0.1057	12.00	0.1191
9.82	0.0244	10.04	0.0507	9.78	0.0733	10.05	0.0994	10.03	0.1174
8.03	0.0207	8.01	0.0465	7.90	0.0708	8.06	0.0972	8.01	0.1158
6.08	0.0168	6.03	0.0422	5.70	0.0622	6.00	0.0883	6.00	0.1141
5.00	0.0150	5.00	0.0396	4.97	0.0601	5.01	0.0850	4.98	0.1131
4.00	0.0130	4.02	0.0353	3.98	0.0584	3.99	0.0836	4.00	0.1121
3.00	0.0106	2.97	0.0341	2.98	0.0538	2.99	0.0792	2.99	0.1111
2.01	0.0080	2.00	0.0322	2.01	0.0509	2.00	0.0783	2.03	0.1097
1.02	0.0069	1.02	0.0278	1.04	0.0482	1.05	0.0726	1.02	0.1078

Table B.8: Pressure-composition data for the absorption/desorption of CO_2 in the binary mixture $[C_2C_1im][OAc]$ + $[C_2C_1im][EtSO_4]$, at 358.2 K and as a function of the composition ratio of the two ionic liquids (ω'_1 stands for the mass fraction of $[C_2C_1im][OAc]$ in a CO_2-free basis). The solubility of CO_2 is expressed as mass fraction (ω_{CO2}).

$[C_2C_1im][OAc]$ (1) + $[C_2C_1im][EtSO_4]$ (2) + CO_2									
ω'_1 = 0.0000		ω'_1 = 0.1949		ω'_1 = 0.4108		ω'_1 = 0.6840		ω'_1 = 1.0000	
P / bar	ω_{CO2}	P / bar	ω_{CO2}	P / bar	ω_{CO2}	P / bar	ω_{CO2}	P / bar	ω_{CO2}
Absorption									
1.04	0.0001	1.06	0.0082	1.01	0.0193	1.00	0.0242	0.98	0.0477
2.05	0.0004	2.06	0.0118	2.02	0.0252	1.99	0.0329	1.96	0.0609
3.08	0.0010	3.01	0.0142	3.04	0.0289	3.08	0.0381	3.11	0.0686
4.00	0.0016	4.01	0.0165	4.02	0.0315	4.07	0.0411	4.00	0.0726
5.01	0.0027	5.02	0.0179	5.03	0.0339	5.02	0.0440	5.01	0.0773
6.00	0.0032	5.99	0.0192	5.99	0.0361	6.03	0.0469	5.97	0.0804
7.03	0.0036	7.02	0.0213	7.03	0.0380	7.03	0.0490	7.02	0.0829
8.98	0.0051	9.02	0.0228	8.98	0.0410	8.97	0.0529	9.10	0.0881
11.00	0.0073	10.93	0.0257	10.95	0.0439	11.05	0.0566	11.02	0.0927
12.98	0.0079	12.98	0.0280	13.02	0.0467	12.94	0.0599	13.01	0.0965
15.00	0.0095	15.00	0.0308	14.93	0.0494	15.00	0.0624	14.98	0.0998
16.36	0.0098	16.37	0.0311	16.48	0.0511	16.14	0.0641	16.30	0.1019
Desorption									
14.01	0.0100	14.01	0.0301	13.99	0.0506	14.00	0.0635	13.99	0.1009
12.01	0.0094	11.98	0.0281	12.03	0.0477	11.94	0.0605	11.97	0.0978
9.94	0.0082	9.97	0.0259	9.99	0.0448	10.04	0.0577	10.04	0.0953
7.99	0.0064	7.99	0.0238	8.01	0.0421	8.02	0.0558	7.95	0.0902
6.02	0.0047	6.02	0.0214	6.00	0.0392	5.95	0.0503	6.00	0.0854
5.00	0.0039	5.00	0.0198	4.98	0.0369	5.02	0.0484	5.00	0.0843
4.02	0.0033	4.02	0.0187	3.92	0.0341	4.00	0.0454	4.04	0.0800
2.99	0.0026	2.99	0.0171	2.98	0.0316	3.00	0.0417	2.98	0.0753
2.01	0.0019	1.99	0.0147	1.99	0.0292	2.00	0.0379	2.01	0.0720
1.01	0.0009	1.02	0.0124	1.04	0.0240	1.04	0.0328	1.06	0.0624

APPENDIX C:

DSC and TGA thermograms

Appendix C:

DSC and TGA thermograms

The heating ramps of the last cycle of the DSC thermograms for all samples in the mixtures of ionic liquids are reported in the first part of this Appendix. Later, the corresponding TGA thermograms are also presented.

To facilitate the visualisation of the TGA thermograms, solid and dashed lines have been alternatively chosen to plot the curves corresponding to the different concentrations.

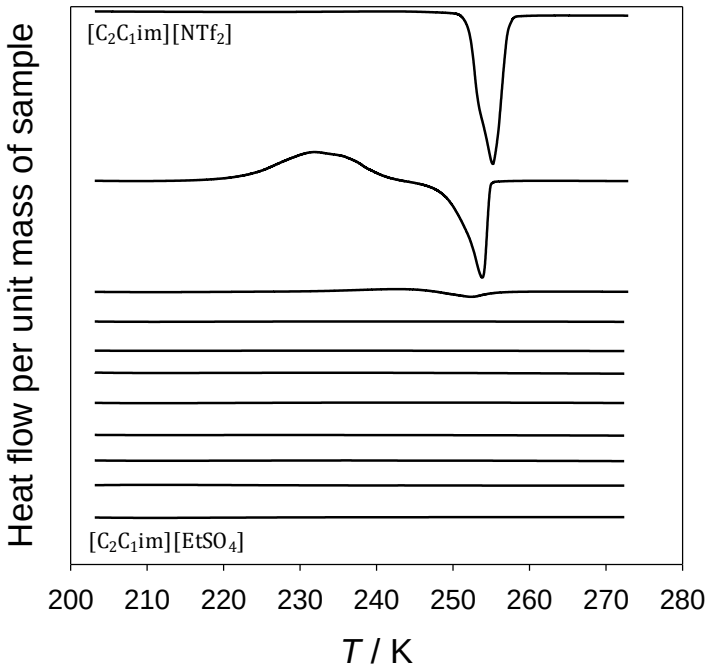

Fig C.1: DSC heating ramps of thermograms for $[C_2C_1im][NTf_2]$ + $[C_2C_1im][EtSO_4]$ mixtures, from pure $[C_2C_1im][NTf_2]$ (top) to pure $[C_2C_1im][EtSO_4]$ (bottom) with a step of 0.10 in molar fraction.

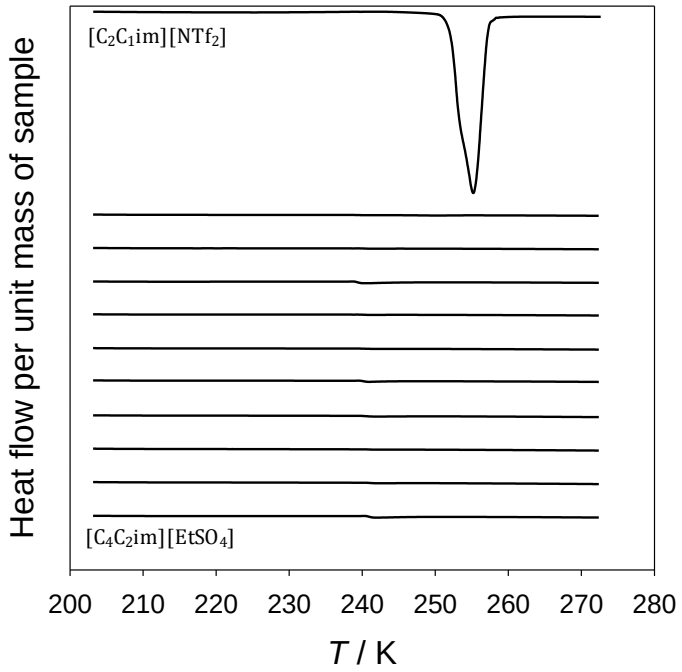

Fig C.2: DSC heating ramps of thermograms for $[C_2C_1im][NTf_2]$ + $[C_4C_2im][EtSO_4]$ mixtures, from pure $[C_2C_1im][NTf_2]$ (top) to pure $[C_4C_2im][EtSO_4]$ (bottom) with a step of 0.10 in molar fraction.

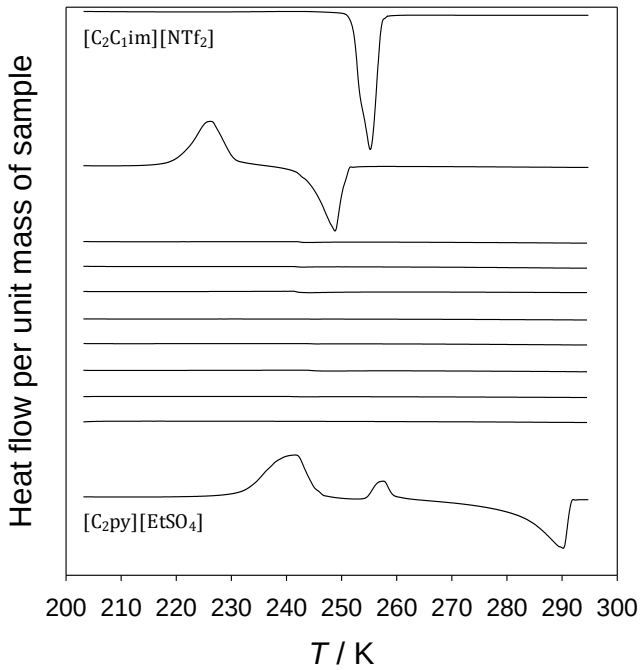

Fig C.3: DSC heating ramps of thermograms for $[C_2C_1im][NTf_2]$ + $[C_2py][EtSO_4]$ mixtures, from pure $[C_2C_1im][NTf_2]$ (top) to pure $[C_2py][EtSO_4]$ (bottom) with a step of 0.10 in molar fraction.

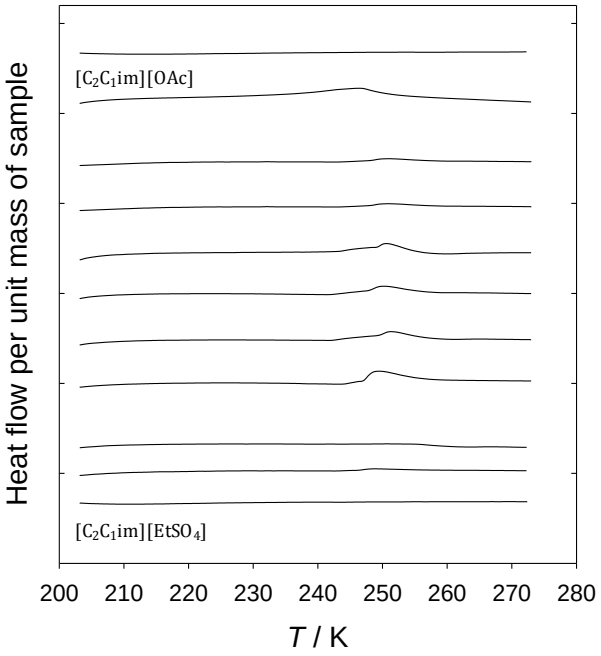

Fig C.4: DSC heating ramps of thermograms for $[C_2C_1im][OAc]$ + $[C_2C_1im][EtSO_4]$ mixtures, from pure $[C_2C_1im][OAc]$ (top) to pure $[C_2C_1im][EtSO_4]$ (bottom) with a step of 0.10 in molar fraction.

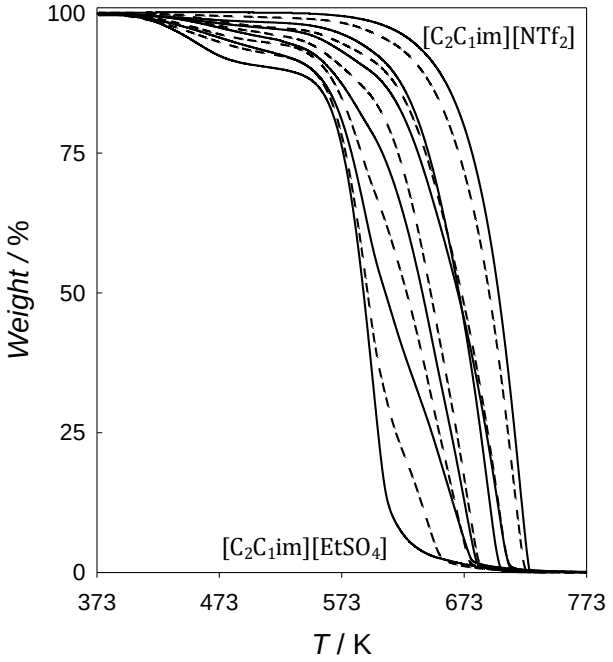

Fig C.5: TGA thermograms for $[C_2C_1im][NTf_2]$ + $[C_2C_1im][EtSO_4]$ mixtures, from pure $[C_2C_1im][NTf_2]$ (top/right) to pure $[C_2C_1im][EtSO_4]$ (bottom/left) with a step of 0.10 in molar fraction.

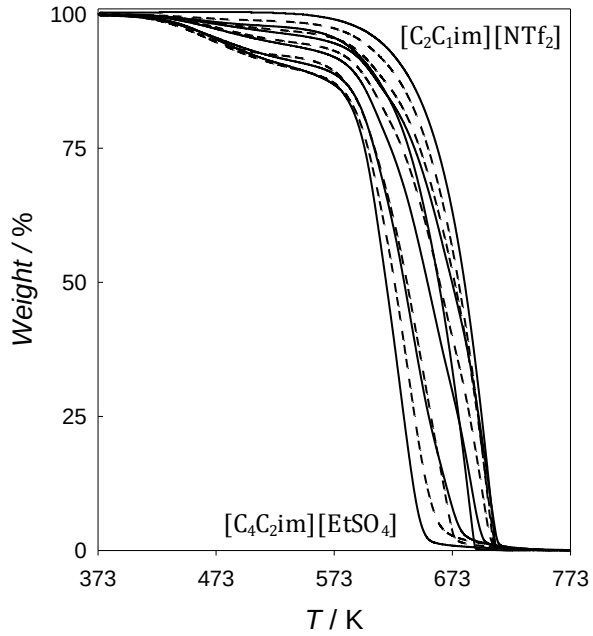

Fig C.6: TGA thermograms for $[C_2C_1im][NTf_2]$ + $[C_4C_2im][EtSO_4]$ mixtures, from pure $[C_2C_1im][NTf_2]$ (top/right) to pure $[C_4C_2im][EtSO_4]$ (bottom/left) with a step of 0.10 in molar fraction.

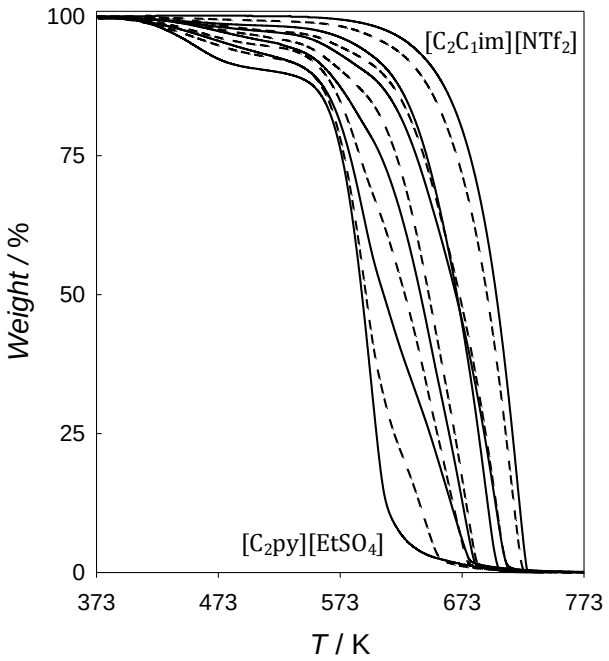

Fig C.7: TGA thermograms for $[C_2C_1im][NTf_2]$ + $[C_2py][EtSO_4]$ mixtures, from pure $[C_2C_1im][NTf_2]$ (top/right) to pure $[C_2py][EtSO_4]$ (bottom/left) with a step of 0.10 in molar fraction.

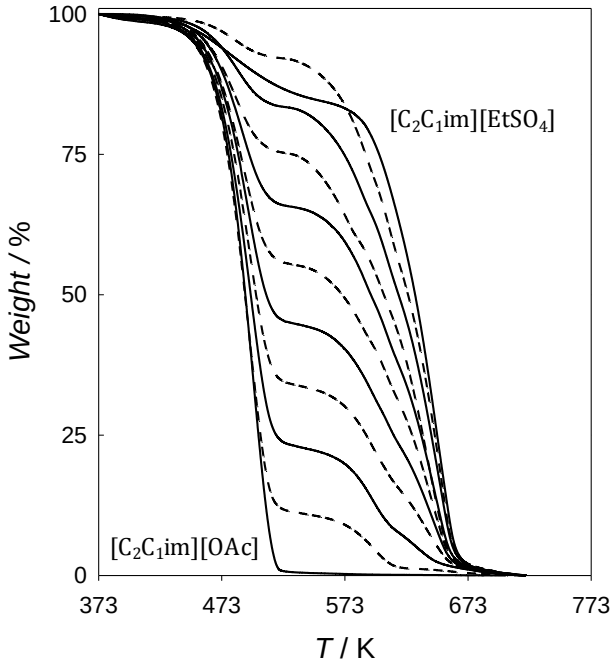

Fig C.8: TGA thermograms for $[C_2C_1im][OAc]$ + $[C_2C_1im][EtSO_4]$ mixtures, from pure $[C_2C_1im][EtSO_4]$ (top/right) to pure $[C_2C_1im][OAc]$ (bottom/left) with a step of 0.10 in molar fraction.

APPENDIX D:

Publications

Appendix D:

Publications

- Pinto, A. M.; Rodríguez, H.; Colón, Y. J.; Arce Jr., A.; Arce, A.; Soto, A. **2013**. Absorption of Carbon Dioxide in Two Binary Mixtures of Ionic Liquids. *Ind. Eng. Chem. Res.*, 52, 5975.

- Pinto, A. M.; Rodríguez, H.; Arce, A.; Soto, A. **2013**. Carbon dioxide absorption in the ionic liquid 1-ethylpyridinium ethylsulfate and in its mixtures with another ionic liquid. *Int. J.Greehouse Gas Control*, 18, 296.

- Pinto, A. M.; Rodríguez, H.; Arce, A.; Soto, A. **2013**. Combined physical and chemical absorption of carbon dioxide in a mixture of ionic liquids. *J. Chem. Thermodyn.* http://dx.doi.org/10.1016/j.jct.2013.10.023

APPENDIX E:

“Resumen” (Summary, in Spanish)

Appendix E:

"Resumen" (Summary, in Spanish)

Introducción

El objetivo central de la presente Tesis consiste en analizar la capacidad de absorción de algunos líquidos iónicos, así como sus combinaciones binarias, para su posible aplicación en procesos de absorción de dióxido de carbono (CO_2).

La idea nace a partir de la necesidad de buscar nuevas tecnologías más eficientes para la captura reversible de CO_2 en corrientes gaseosas emitidas a la atmósfera por actividades antropogénicas. El CO_2 emitido en las actividades industriales actualmente, causa una grave afección al medioambiente dado su carácter de gas de efecto invernadero. En los últimos años, son numerosos los convenios y tratados establecidos a nivel internacional con el fin de controlar sus niveles, lo cual se ve reflejado en la disminución de las emisiones. Sin embargo esta reducción dista de ser suficiente.

El CO_2 representa más del 80 % del total de emisiones de gases de efecto invernadero, y proviene principalmente de la quema de combustibles fósiles para la generación de energía. La tecnología existente en estas plantas de producción energética, desafortunadamente, no permite por sí misma satisfacer las necesidades actuales con un bajo nivel de emisiones. Por ello, la mejora de la eficiencia de los procesos industriales y de captación y almacenamiento de CO_2 es absolutamente necesaria.

Las tecnologías de captura de CO_2 se pueden clasificar en tres tipos: oxy-combustión, pre-combustión y post-combustión; siendo este último el más empleado. Dentro de los procesos de post-combustión, el de absorción de CO_2 por medio de disoluciones acuosas de aminas es el más común a escala industrial. Se basa en hacer pasar la corriente gaseosa con el CO_2 en contracorriente por la disolución acuosa de amina. Esto genera un carbamato, en una reacción exotérmica y reversible,

capturando el CO_2. No obstante, el uso de las disoluciones acuosas de aminas como absorbentes presenta varios inconvenientes, como por ejemplo: altos gastos de operación, energéticos, baja estabilidad y alta volatilidad. Debido a esto, la búsqueda de nuevos disolventes más económicos y eficientes se ha convertido en una prioridad.

Una posible alternativa es el uso de líquidos iónicos. Estas sustancias han generado gran expectación en la comunidad científica e industrial en los últimos años. Sus atractivas características permiten poder adaptarlos a procesos existentes, haciéndolos más eficientes y sostenibles. Los líquidos iónicos son sustancias constituidas por iones y con un punto de fusión bajo; considerándose normalmente un valor inferior a los 373 K. Aunque esta familia agrupa a muy diferentes compuestos y cualquier generalización es difícil, se puede decir que entre las propiedades más comunes a muchos líquidos iónicos se encuentran: su baja volatilidad, el amplio rango de temperaturas en que se encuentran en estado líquido, y que sus propiedades pueden ser modeladas para una aplicación particular mediante la variación controlada de su estructura. De aquí que se acuñase el término "disolventes de diseño" para referirse a ellos.

La aplicación de líquidos iónicos en la captura de CO_2 se comenzó a investigar cuando Brennecke y colaboradores (Blanchard *et al.*, 1999) comprobaron que el gas podía ser absorbido en un líquido iónico y luego ser completamente recuperado por simple disminución de la presión de trabajo. A partir de ahí se han publicado numerosos trabajos que analizan la solubilidad, selectividad e interacciones entre el CO_2 y diferentes líquidos iónicos.

Se ha comprobado que los líquidos iónicos presentan dos posibles mecanismos de absorción de CO_2. La absorción física es un mecanismo sencillo basado en interacciones débiles. El gas llena los espacios libres a medida que aumenta la presión, interactuando con los iones pero sin afectar a la estructura química del líquido iónico. Su principal ventaja es la baja energía requerida para recuperar el gas, lo cual puede hacerse por disminución de la presión o por un ligero incremento de la temperatura. Los iones constituyentes del líquido iónico determinan la capacidad de éste para absorber más o menos CO_2 por fisisorción. En general, las mayores capacidades de absorción se han obtenido con líquidos iónicos conteniendo un anión fluorado, dada la alta electronegatividad que presentan los átomos de flúor que les

permite una mayor interacción con los átomos de oxígeno del CO_2. Sin embargo dichos aniones fluorados suelen presentar una serie de desventajas, entre las que típicamente se encuentra su alto coste o toxicidad. Los cationes parecen tener una influencia menor, si bien la longitud de cadena de sus sustituyentes alquílicos también puede mejorar la capacidad de absorción.

El segundo mecanismo identificado es la absorción química. En este caso, el CO_2 reacciona con el líquido iónico para formar un complejo químico. Debido a ello, se requiere de mayor cantidad de energía para romper los enlaces y poder desorber el gas. Este mecanismo puede observarse, principalmente, en líquidos iónicos que se han funcionalizado con aminas o aminoácidos, o en líquidos iónicos convencionales con anión básico. La principal ventaja de este mecanismo es la alta capacidad de absorción. Con él se han conseguido rendimientos comparables al obtenido con disoluciones acuosas de aminas, pero además con la ventaja de su mayor estabilidad y la disminución de la pérdida de disolventes a la atmósfera por evaporación.

Si bien los resultados obtenidos hasta la fecha pueden considerarse prometedores, también son insuficientemente satisfactorios y se requiere de más investigaciones para mejorar el rendimiento en estos sistemas. Con ese objetivo, se han intentado diferentes estrategias para mejorar la capacidad de absorción. Aparte de la no siempre viable opción de cambiar las condiciones del proceso (temperatura y presión), una posibilidad que va más allá de la simple modificación de la estructura química del catión y el anión de un líquido iónico es la utilización de mezclas de líquidos iónicos. En mezclas binarias de dos líquidos iónicos 'puros' habrá hasta cuatro iones diferentes (dos cationes y dos aniones), en proporciones variables; o solamente tres iones diferentes si los líquidos iónicos constitutivos tienen bien el catión o bien el anión comunes. En cualquier caso, se producirán nuevas interacciones en un fluido con propiedades particulares y diferentes a las que se podrían obtener con líquidos iónicos sencillos. Los estudios disponibles acerca de mezclas de líquidos iónicos aún son escasos, centrándose principalmente en el estudio del efecto de la composición sobre las propiedades físicas. En esta Tesis se investigarán tanto la capacidad de absorción de CO_2 de las mezclas como propiedades térmicas y físicas de importancia para el diseño de un proceso, utilizando esas mezclas como fluidos de trabajo.

Otra alternativa novedosa para mejorar la absorción de CO_2 por parte de líquidos iónicos, en particular aquellos con propiedades de transporte desfavorable (como por ejemplo una muy elevada viscosidad), es el uso de soportes sólidos de alta área superficial. Los líquidos iónicos soportados (SILPs) consisten en líquidos iónicos adsorbidos en la superficie de la estructura porosa de un soporte sólido, como puede ser el caso de sílica o alúmina. De los estudios realizados en SILPs, son escasos los que se centran en su uso para la absorción del CO_2. Sin embargo se ha podido comprobar que el uso de los soportes permite reacciones más rápidas y reversibles, sin pérdida significativa de la capacidad de absorción después de numerosos ciclos sucesivos de absorción y desorción. En esta Tesis también se explorará un SILP construido a partir de un líquido iónico muy viscoso con un anión derivado de aminoácido, utilizando sílice como soporte.

Experimental

Se seleccionó un conjunto de líquidos iónicos con diferentes cationes y aniones. Se eligió algún líquido iónico previamente estudiado en la bibliografía con el objetivo de verificar la validez de la puesta en marcha del dispositivo experimental. El resto se seleccionó con idea de cubrir ambos mecanismos de absorción (físico y químico), y en general permitiendo un análisis de la influencia de distintos elementos de la estructura de los iones constitutivos de los líquidos iónicos en su capacidad de absorción de CO_2 y propiedades térmicas y físicas.

Los líquidos iónicos fueron sintetizados en su mayoría en el laboratorio, a excepción del acetato de 1-etil-3-metilimidazolio, que fue comprado a la empresa Iolitec, GmbH (Heilbronn, Alemania) y posteriormente purificado en el laboratorio. La pureza final de todos los lotes de líquido iónico se verificó mediante confirmación de su estructura química y ausencia de cantidades relevantes de impurezas por espectrometría de resonancia magnética nuclear de carbono-13 y protón (^{13}C NMR y ^{1}H NMR, respectivamente), y mediante la determinación de su contenido en agua por valoración usando el método de Karl-Fischer. Este último aspecto es importante, dado que el agua es una impureza omnipresente en líquidos iónicos dado el carácter higroscópico de estos, y las propiedades y comportamiento del líquido iónico se

pueden ver afectadas de manera importante si no se mantienen los valores de contenido en agua lo más bajos posible.

Las mezclas de líquidos iónicos se prepararon por pesada de cada componente, agitando posteriormente al menos 4 h a 333.2 K para asegurar su homogeneidad.

Para determinar la capacidad de absorción de CO_2 de los líquidos iónicos puros y sus mezclas binarias, se realizaron curvas isotérmicas hasta 16 bar en una balanza de suspensión magnética Rubotherm (modelo Metal). La masa de CO_2 absorbida por la muestra fue determinada por el incremento de las fuerzas electromagnéticas necesarias para que la muestra se mantenga en suspensión. En el caso del SILP, los primeros experimentos fueron realizados a temperatura ambiente y presión atmosférica en un analizador termogravimétrico Mettler Toledo TGA/DSC 1, con el cual se determinó la masa de CO_2 absorbida por simple diferencia entre la masa inicial y final de la muestra. Posteriormente, se hizo la isoterma a la misma temperatura pero variando la presión hasta los 16 bar, con la balanza de suspensión magnética Rubotherm.

Para determinar las condiciones térmicas a las que sería posible la utilización de cada líquido iónico y de las mezclas de éstos, se determinaron en cada caso las correspondientes propiedades térmicas. Las temperaturas de descomposición se determinaron en un analizador termogravimétrico (TGA) TA instrument Q500; y las temperaturas de fusión y cristalización se investigaron en un calorímetro diferencial de barrido (DSC) TA instrument Q2000. Los resultados obtenidos con ambos equipos se han analizado a través del software TA Universal Analysis 2000 versión 4.5A. Para la temperatura de descomposición se utilizó el *onset* a un 5 % de descomposición, que es una medida más conservativa y a la vez más realista de la estabilidad térmica de una muestra que el *onset* simple que normalmente se utiliza.

Además, la caracterización de las muestras se completó con la determinación de propiedades físicas críticas para el diseño de procesos en los que se utilicen los fluidos investigados. Concretamente, las propiedades determinadas fueron: densidad, viscosidad y tensión superficial. Las medidas se realizaron en un densímetro Anton Paar DMA 5000, micro-viscosímetros capilares tipo Ubbelohde de diferentes diámetros, y un tensiómetro Krüss K11 equipado con una placa de platino cilíndrica

que permite la medición en muestras pequeñas. Todos estos aparatos están equipados con los correspondientes accesorios de termostatación para efectuar las mediciones con control preciso de la temperatura de la muestra.

Resultados

Líquidos iónicos puros

Para validar la instalación y puesta en marcha de la balanza de suspensión magnética, así como la técnica en que se basa, se determinó en primer lugar la absorción de CO_2 por parte del líquido iónico bis(trifluorometilsulfonil)amiduro de 1-etil-3-metilimidazolium ($[C_2C_1im][NTf_2]$). Este líquido iónico ha sido ampliamente estudiado en la bibliografía, a través de diferentes metodologías, por lo que se ha considerado apto para confirmar la metodología experimental aquí utilizada. Además, su capacidad de absorción es elevada dentro de los líquidos iónicos que absorben CO_2 mediante un mecanismo de absorción física, por lo que simultáneamente se puede utilizar como referencia frente a la absorción obtenida por otros líquidos iónicos.

Además, se determinaron las isotermas de absorción de CO_2 para los siguientes líquidos iónicos puros, a 298.2 K y a presiones hasta *ca.* 16 bar:

- Etilsulfato de 1-etilpiridinio ($[C_2py][EtSO_4]$).
- Etilsulfato de 1-etil-3-metilimidazolio ($[C_2C_1im][EtSO_4]$).
- Etilsulfato de 1-butil-3-etilimidazolio ($[C_4C_2im][EtSO_4]$).
- Acetato de 1-etil-3-metilimidazolio ($[C_2C_1im][OAc]$).

Los líquidos iónicos con anión etilsulfato absorben CO_2 mediante fisisorción. Sus valores no consiguieron superar la capacidad de absorción del $[C_2C_1im][NTf_2]$, lo cual demuestra la fuerte influencia de los átomos fluorados en la misma.

Por comparación de los resultados obtenidos con los líquidos iónicos con anión etilsulfato, se puede observar el efecto del catión y de la longitud de las cadenas alquílicas. Ordenando los cationes de mayor a menor absorción de los líquidos iónicos de los que forman parte, se tiene: $[C_4C_2im]^+ > [C_2C_1im]^+ \approx [C_2py]$; lo cual coincide con el orden decreciente de la extensión o número de sus sustituyentes alquílicos. A su vez,

se comprueba que al variar el catión imidazolio por un piridinio no se aprecia un efecto importante.

Al comparar las curvas de los líquidos iónicos anteriores con la del $[C_2C_1im][OAc]$ se aprecia una clara diferencia en su forma y en su capacidad de absorción, debido al cambio en el mecanismo de absorción. Dada la alta basicidad del anión acetato, el $[C_2C_1im][OAc]$ reacciona químicamente con el CO_2, por lo que el primer mecanismo de importancia en su isoterma es una quimisorción. El resultado que se obtuvo para este líquido iónico a altas presiones difiere de lo publicado anteriormente por otros investigadores. Esto puede deberse a la diferencia en el contenido de agua de cada muestra, ya que un contenido suficientemente elevado puede dar lugar a la no obtención del producto sólido de reacción entre $[C_2C_1im][OAc]$ y CO_2, tal como indican Gurau *et al.* (2011).

Mezclas con absorción física

En una primera exploración de mezclas de líquidos iónicos, se decidió combinar pares de líquidos iónicos absorbiendo CO_2 meramente por un mecanismo físico. Se analizó así la capacidad de absorción, junto con las propiedades térmicas y físicas, de mezclas de $[C_2C_1im][NTf_2]$ con los diferentes etilsulfatos antes mencionados. En concreto, las tres mezclas exploradas fueron:

- $[C_2C_1im][NTf_2]$ + $[C_2C_1im][EtSO_4]$
- $[C_2C_1im][NTf_2]$ + $[C_4C_2im][EtSO_4]$
- $[C_2C_1im][NTf_2]$ + $[C_2py][EtSO_4]$

En las tres mezclas realizadas los resultados obtenidos para la absorción de CO_2 no consiguieron superar la capacidad del líquido iónico $[C_2C_1im][NTf_2]$ en estado puro. Esto se vio reflejado en las constantes de Henry obtenidas, las cuales disminuyen a medida que la fracción molar del $[C_2C_1im][NTf_2]$ aumenta. Sin embargo, se observó un ligero efecto sinérgico en composiciones intermedias, con una capacidad de absorción superior a la que correspondería a la media ponderada de las absorciones de los líquidos iónicos constituyentes de la muestra acorde a la composición molar de la misma.

Se realizaron las curvas de desorción para todos los casos. Se observó que se consigue desorber el CO_2 por simple descenso de la presión, aunque siempre con un

cierto grado de histéresis, en el que la concentración de CO_2 a una determinada presión es siempre más elevada en el proceso de desorción que en el de absorción. Al disminuir la longitud de los sustituyentes catiónicos alquílicos del líquido iónico con anión etilsulfato, el grado de histéresis también se reduce.

Todas las curvas fueron correlacionadas adecuadamente con el modelo termodinámico NRTL (siglas a partir del original en inglés "Non-Random Two-Liquid"). Los parámetros de interacción binaria necesarios para el ajuste se obtuvieron mediante un programa que ejecuta un método de regresión no lineal (Sørensen and Arlt, 1980) para la minimización de los desvíos entre presiones experimentales y correlacionadas, tratando a las mezclas como sistemas pseudo-binarios (el CO_2 como un componente y la mezcla de líquidos iónicos como el otro). Como los líquidos iónicos presentan una presión de vapor despreciable en las condiciones de operación estudiadas, se consideró un comportamiento ideal para la fase gas, íntegramente formada por CO_2 gaseoso.

Con respecto a las propiedades térmicas, el líquido iónico $[C_2py][EtSO_4]$ es el que muestra una mayor temperatura de fusión, cercana a las temperaturas ambientales habituales. Esto es probablemente debido al grado de simetría de su catión, en contraste a los cationes más asimétricos de los otros líquidos iónicos. No obstante, al mezclarlo con $[C_2C_1im][NTf_2]$ se produce una fuerte reducción de la temperatura de fusión, evitando riesgos de que se produzca solidificación del fluido de trabajo. Este peligro tampoco está presente en los otros dos sistemas, en los que únicamente se detectaron temperaturas de fusión superiores a 200 K en mezclas con alta concentración de $[C_2C_1im][NTf_2]$, que en cualquier caso es líquido a temperaturas superiores a 257 K.

En el estudio de la temperatura de descomposición, se observó que tanto los líquidos iónicos puros como sus mezclas presentan temperaturas de descomposición moderadamente altas. No obstante, el anión $[NTf_2]^-$ da más estabilidad al líquido iónico comparado con el $[EtSO_4]^-$, requiriéndose concentraciones molares de $[C_2C_1im][NTf_2]$ superiores a *ca.* 0.50 para generar un efecto importante en la temperatura de descomposición.

Con respecto a las propiedades físicas de las mezclas, se determinaron la densidad, viscosidad y tensión superficial a 298.2 K y presión atmosférica en todo el

rango de composición. Se observó que la densidad del $[C_2C_1im][NTf_2]$ es superior a la de los líquidos iónicos de etilsulfato, por lo que las densidades de las mezclas son ascendentes a medida que la concentración del $[C_2C_1im][NTf_2]$ aumenta. Por el contrario, los valores de viscosidad y tensión superficial son descendentes, observándose un mayor descenso en la viscosidad debido a la mayor diferencia entre los valores de los líquidos iónicos puros constitutivos de la mezcla.

Se obtuvo una perspectiva más detallada al analizar las propiedades de exceso y efecto de mezcla. Con respecto al volumen molar de exceso, los valores obtenidos fueron positivos sobre todo el rango estudiado. Esto demuestra que hay una disminución de las interacciones de atracción, lo cual se refleja en un aumento del volumen libre de las mezclas y puede explicar parcialmente el efecto sinérgico observado en el caso de la absorción de CO_2 por parte de las mezclas de líquidos iónicos.

Con respecto al cambio de propiedad por efecto de mezcla en la viscosidad, se puede ver que las mezclas $[C_2py][EtSO_4] + [C_2C_1im][NTf_2]$ y $[C_2C_1im][EtSO_4] + [C_2C_1im][NTf_2]$ muestran un comportamiento similar, apreciándose un cambio de desviación positiva a desviación negativa al aumentar la concentración de $[C_2C_1im][NTf_2]$. Sin embargo, la magnitud de estos valores es mucho menor que la de los obtenidos para la mezcla de $[C_4C_2im][EtSO_4] + [C_2C_1im][NTf_2]$. En esta mezcla, la desviación de viscosidad obtenida es negativa sobre todo el rango de concentración, con un máximo en las proximidades de la mezcla equimolar.

El cambio de tensión superficial por efecto de mezcla presenta un comportamiento diferente. En este caso, todos los valores obtenidos fueron negativos. Esto es indicativo de un enriquecimiento de la superficie de la mezcla en el componente más tensioactivo, en relación a la composición global del total de la mezcla fluida. No obstante, la magnitud de los valores obtenidos para el sistema con $[C_4C_2im][EtSO_4]$ fue mucho menor a la de los otros dos sistemas. A partir de estos resultados se postula que la longitud de las cadenas alquílicas en el catión tiene un efecto importante en la tensión superficial.

Las propiedades de exceso y de efecto de mezcla fueron correlacionadas por medio de expansiones polinómicas de Redlich-Kister (Redlich y Kister, 1948), obteniéndose resultados aceptables con expansiones de segundo y tercer orden.

Se evaluó la capacidad de algunos modelos simples para la predicción de las propiedades físicas de las mezclas a partir de información únicamente de las propiedades de los componentes puros. Teniendo en cuenta que la magnitud de los volúmenes de exceso es muy inferior a la de los volúmenes molares, una primera estimación para la densidad podría venir dada de obviar ese volumen de exceso y considerar una variación lineal (ideal) del volumen molar. No obstante, es importante tener presente que esto implicaría denostar el volumen de exceso existente, y la consiguiente información al respecto del comportamiento termodinámico a nivel molecular de las mezclas.

Para el caso de la viscosidad y la tensión superficial se exploraron dos reglas de mezcla (Grunberg y Nissan, 1949; Katti y Chaudhri, 1964). Los resultados obtenidos son bastante similares entre sí, aunque las mejores predicciones se obtuvieron para el sistema con $[C_4C_2im][EtSO_4]$. Sin embargo, los resultados no describen con suficiente exactitud (para propósitos ingenieriles típicos) las propiedades buscadas, ni suministran una buena descripción de la variación de estas propiedades con la composición de la mezcla.

Combinación de absorción física y química

En esta sección se determinó el efecto de la temperatura sobre capacidad de absorción y las propiedades de la mezcla $[C_2C_1im][EtSO_4]$ +$[C_2C_1im][OAc]$.

Las isotermas de los líquidos puros se determinaron en el rango entre 298.2 K y 358.2 K con una variación de la presión hasta 16 bar. Tal como se explicó en la sección de líquidos iónicos puros, la afinidad observada para el líquido iónico $[C_2C_1im][OAc]$ es mucho mayor que la del $[C_2C_1im][EtSO_4]$, por la diferencia en sus mecanismos de absorción. Sin embargo, en el caso del primero de ellos se obtuvieron resultados diferentes a los que se esperaban. Es sabido que un aumento en la temperatura disminuye normalmente la afinidad del líquido iónico por el CO_2. Pero en el caso del $[C_2C_1im][OAc]$ esto no se cumple estrictamente, en concreto si se comparan las isotermas a altas presiones para las temperaturas 298.2 y 318.2 K. La variación se debe a que el aumento en la temperatura impide en este caso la formación del sólido resultante de la reacción química de $[C_2C_1im][OAc]$ y CO_2, y que limita la posibilidad de continuar absorbiendo CO_2 por medio de un mecanismo físico a 298.2 K.

Para el caso de esta mezcla, se observa que la adición de un 25 mol% de $[C_2C_1im][EtSO_4]$ en la mezcla impide a 298.2 K la formación del referido sólido, consiguiéndose una absorción máxima similar a la del $[C_2C_1im][OAc]$ puro. A 358.2 K, el comportamiento es el esperado, con disminución de la capacidad de absorción como resultado del aumento de la temperatura. Con mayores aumentos de concentración de $[C_2C_1im][EtSO_4]$ en la mezcla de líquidos iónicos, la capacidad de absorción del CO_2 disminuye, tal como se esperaría.

En relación a las propiedades térmicas, no se observan temperaturas de fusión ni cristalizaciones de los líquidos iónicos puros. Pese a esto, se detectaron picos de cristalización fría a las concentraciones intermedias, aunque muy por debajo de las temperaturas utilizadas en el trabajo experimental. La estabilidad térmica de la mezcla mejora a medida que disminuye la concentración del anión acetato, pudiéndose observar claramente el cambio en las curvas de descomposición.

También se determinaron densidad y viscosidad en el mismo rango de temperaturas y cubriendo todo el rango de composición. Se vio que la densidad disminuye con el aumento de la temperatura y con el aumento en la concentración de $[C_2C_1im][OAc]$. Los volúmenes molares de exceso que se obtuvieron son positivos en todos los casos, siendo esto representativo del mayor grado de disrupción de las fuerzas interiónicas en la mezcla, comparadas a las de cada uno de los líquidos iónicos puros. Con respecto a la viscosidad, ésta disminuye a medida que la concentración de $[C_2C_1im][EtSO_4]$ aumenta, y también con un aumento de la temperatura. La evolución de las series de viscosidad con la temperatura se correlacionó adecuadamente mediante la ecuación de Vogel-Fulcher-Tamman.

Al igual que en el caso de las mezclas físicas, el volumen molar de exceso y la desviación de la viscosidad fueron satisfactoriamente correlacionadas en función de la composición mediante expansiones polinomiales de Redlich-Kister.

Líquidos iónicos soportados (SILP)

El líquido iónico isoleucinato de tetrahexylamonio ($[N_{6666}][Ile]$) contiene un anión de aminoácido que puede ser de gran interés para la absorción de CO_2 mediante quimisorción. Sin embargo su viscosidad en estado líquido puro es muy elevada, condicionando los procesos de transporte necesarios para un adecuado desarrollo de la absorción. Una alternativa para vencer estas dificultades en la transferencia de

materia puede ser su utilización en combinación con un soporte poroso, configurando un SILP.

En primer lugar se determinó la isoterma de absorción de $[N_{6666}][Ile]$ en estado puro, como líquido, a 298.2 K y hasta una presión de 16 bar. El resultado fue inferior al teórico estequiométrico, probablemente debido a problemas de transferencia de materia. Una vez inmovilizado sobre el soporte de sílica, se consiguió una mejora sustancial en la afinidad por el CO_2, lo cual fue comprobado a través de dos metodologías diferentes. Además, se verificó que el soporte también provoca un aumento de la estabilidad térmica del líquido iónico.

Conclusiones

En esta Tesis se han investigado una serie de líquidos iónicos de diferente naturaleza, y mezclas binarias de varios de ellos, para su potencial utilización como absorbentes en procesos de captura de CO_2. En el desarrollo del trabajo se buscaron diversas estrategias de optimización, variando las condiciones de operación del sistema, la estructura de los líquidos iónicos, la configuración de las mezclas y la utilización de soportes sólidos mesoporosos. Se prestó atención tanto a la propia capacidad de absorción del gas como a las propiedades térmicas y físicas de los absorbentes.

En el empleo de mezclas de líquidos iónicos que absorben CO_2 exclusivamente por mecanismos físicos, se observó un efecto sinérgico en la capacidad de absorción, pudiendo preferir la mezcla en vez del líquido iónico puro con mayor absorción si las propiedades térmicas, físicas y de otro tipo (coste, toxicidad...) así lo confirmasen.

En la combinación de un líquido iónico fisisorbente y otro quimisorbente también se ha visto algún beneficio respecto a la utilización del líquido iónico quimisorbente en estado puro. En este caso, se observó que el segundo líquido iónico podía prevenir la solidificación del producto de la reacción de absorción química, favoreciendo la continuación de la absorción de CO_2 mediante fisisorción; además de permitir una mayor flexibilidad en el control de las propiedades físicas del absorbente líquido.

Como última estrategia, se evalúo la utilización de un soporte para mejorar la capacidad de absorción de un líquido altamente viscoso. Los resultados muestran un

claro aumento en la capacidad de absorción de CO_2 y en la estabilidad térmica del líquido iónico.

El trabajo aquí realizado pretende unir el conocimiento precedente en este campo con la utilización de estrategias alternativas de reciente actualidad, para el caso particular de la aplicación a procesos de captura de CO_2 con tecnología basada en líquidos iónicos. Se espera que sea un trabajo de apoyo para el desarrollo futuro de nuevas investigaciones en este ámbito, en el camino hacia la aplicación práctica real.